

CYCLOADDITION MECHANISMS/ELECTRON CORRELATION & LOCALIZATION

THEORETICAL STUDIES OF THE SPIN AND CHARGE DISTRIBUTIONS IN MOLECULES

PART A

REACTION MECHANISMS OF THE CYCLOADDITION OF SINGLET AND TRIPLET ATOMIC
OXYGEN TO OLEFINS

PART B

ELECTRON CORRELATION AND LOCALIZATION

By

MICHAEL EDWIN STEPHENS, B.Sc.

A Thesis

Submitted to the School of Graduate Studies
in Partial Fulfilment of the Requirements

for the Degree

Doctor of Philosophy

McMaster University

March 1975

DOCTOR OF PHILOSOPHY (1975)
(Chemistry)

McMASTER UNIVERSITY
Hamilton, Ontario

TITLE: Theoretical Studies of the Spin and Charge Distributions in
Molecules.

Part A: Reaction Mechanisms of the Cycloaddition of Singlet
and Triplet Atomic Oxygen to Olefins

Part B: Electron Correlation and Localization

AUTHOR: Michael Edwin Stephens, B.Sc. (University of Waterloo)

SUPERVISOR: Professor R. F. W. Bader

NUMBER OF PAGES: xv, 199

ACKNOWLEDGEMENTS

The author wishes to express his appreciation to those who were of instrumental assistance, academic and otherwise, to the completion of these studies:

Dr. Ray Gangi, for access to his results on the $H_2 + O$ mechanism, many discussions on potential surface computations and quantum chemistry in general;

Dr. Jon Duke, for providing a sophisticated version of the PØLYATØM/2 system;

my comrades-in-arms, Bob Messer, Gord Runtz, Peter Beddall and Joc. Pelletier for many discussions (technical, philosophical, and otherwise) and access to their results and programmes;

Dr. Richard Bader, for unfailing enthusiasm and concrete suggestions;

Mrs. Jan Gallo, for uncomplaining conversion of very rough drafts into this typed manuscript;

my several friends in Hamilton and Toronto, especially

Dr. Bill and Judy Hall, Dave Potter and John Holloway, for moral support when it was most needed; and,

the people of Canada, through the generous N.R.C. support I have received while at McMaster.

This thesis is Dedicated

TO MY PARENTS,

who didn't request it,

but for whom it was written.

ABSTRACT

Potential surfaces for the cycloaddition of singlet and triplet atomic oxygen to ethylene to form ethylene oxide were constructed. The singlet species was found to energetically favour a symmetric attack on the ethylene along the right bisector of the carbon-carbon axis in a plane perpendicular to the plane of the nuclei, with an activation energy of the order of 10 kcal/mole. The triplet species was found to prefer an asymmetric attack yielding an open-ring transition state geometry of energy 36 kcal/mole above the energy of the separated reactants. From this geometry, spin inversion and subsequent ring closure result in the formation of the singlet ethylene oxide product.

Experimentally observed retention/loss of cis-trans stereochemistry of olefins added to by singlet/triplet oxygen are attributed to the concerted formation of ring bonds in the singlet case, and non-concerted ring bond formation in the triplet case with free rotation around the carbon-carbon axis in the intermediate transition state.

Spin "uncoupling" and "transfer" mechanisms (originally developed elsewhere in a study of the varying tendencies of singlet and triplet oxygen to insert into or abstract a proton from hydrocarbon CH bonds) are also shown to explain the observed triplet asymmetric attack, non-concerted bond formation, and loss in product stereospecificity.

The formalism of two statistical measures of the information content of a quantum mechanical wavefunction, the "missing information function", I , and "population fluctuation", Λ , are developed. The formal coordinate-space quantum description of the distribution of "event probabilities" of observing various numbers of electrons in various spatial regions of a molecule is shown to be related to intuitive concepts of the localizability of primarily intra-correlated groups of electrons within non-overlapping volumes.

The effects of the Fermi correlation described by a Hartree-Fock wavefunction were studied. Several small hydride molecules, LiH^+ , LiH , BeH(X) , BH , BeH_2 , BH_3 , BH_4^- , and CH_4 , were found to be partitionable (by criteria based on I and on Λ) into volumes corresponding to intuitive notions of "core", "bonding", and "non-bonding" regions of a molecule, each containing a population of two primarily intra-correlated electrons. For several other molecules, BeH(A) , NH_3 , H_2O , N_2 , and F_2 , only core pair populations were found to be well-localized. The valence density in these cases was found to be unpartitionable.

The formalisms developed here provide a useful method of computing the effects of correlation on particle localizability described by any form of wavefunction. The techniques also permit evaluation of the likelihood of accurate wavefunction decomposition into a product of wavefunctions each incorporating a description of the internal group particle correlation. Finally, one can assess the probability of an accurate partitioning of a quantum system into nearly independent subsystems.

TABLE OF CONTENTS

	<u>Page</u>
ACKNOWLEDGEMENTS	iii
DEDICATION	iv
ABSTRACT	v
TABLE OF CONTENTS	vii
LIST OF FIGURES	viii
LIST OF TABLES	x
INTRODUCTION	1
CHAPTER I -- PREVIOUS STUDIES	3
CHAPTER II -- POTENTIAL SURFACE THEORY	11
CHAPTER III -- CALCULATIONS ON THE POTENTIAL ENERGY SURFACES	16
1. C_{2v} Approach	24
2. C_s Approach	31
3. Methylene Rotation Barrier	36
4. Ring Closure	40
5. Miscellaneous Data	40
CHAPTER IV -- INTERPRETATION	46
The Insertion/Abstraction Reactions	51
Insertion Reactions	52
Abstraction Reactions	56
Cycloaddition Reactions	61
C_{2v} Oxygen Approach	61
C_s Oxygen Approach	66
CONCLUSIONS	75
APPENDIX A-1	77
REFERENCES	79
PART B -- ELECTRON CORRELATION AND LOCALIZATION	83

LIST OF FIGURES

<u>Figure</u>		<u>Page</u>
1	Nuclear Geometry Parameters Varied	23
2	C_{2v} Singlet and Triplet Surfaces	26
3	Optimization of C_{2v} Surface with Respect to R2	29
4	C_s Singlet and Triplet Surfaces	35
5	Optimization of Triplet C_s Surface with Respect to R1 and α	37
6	C_s Triplet Energy Versus γ	39
7	Singlet and Triplet Energies Versus α	42
8	Variation of Crossing Energy and Crossing Angle with R2	42
9	Total Charge and Spin Density Distributions for Planar ${}^3B_{3u}$ Ethylene	49
10	Total Charge Distributions for C_{2v} $H_2 + O$ Singlet and Triplet Insertion	54
11	Spin Density Distributions for C_{2v} $H_2 + O$ Triplet Insertion	55
12	Total Charge Distributions for $H_2 + O$ Singlet and Triplet Abstraction	58
13	Spin Distributions for Triplet Abstraction Reaction	60
14	Total Singlet and Triplet Charge Distributions for C_{2v} Oxygen Attack on C_2H_4	63
15	Triplet Spin Distributions for C_{2v} Oxygen Attach on C_2H_4	64
16	1A_1 Minus 3B_1 Charge Density Difference at $C_2H_4O(X)$ Equilibrium Geometry	67
17	Total Singlet and Triplet Charge Distributions for C_s Oxygen Attack on C_2H_4	69

<u>Figure</u>		<u>Page</u>
18	Triplet Spin Distributions for C_s Oxygen Attack on C_2H_4	70
19	Total Charge and Spin Density Distributions for $C_2H_4O(^3A'')$ State	72

LIST OF TABLES

<u>Table</u>		<u>Page</u>
1	Final Atomic Orbital Basis Set	20
2	Experimental Ground State Ethylene Oxide Equilibrium Geometry	21
3	Total Energy Changes of Low-Lying States of Ethylene Oxide on Basis Set Expansion	22
4	Experimental Bond Lengths and Bond Angles of Ground State Ethylene and Ethylene Oxide	25
5	Singlet and Triplet Energy Variations for C_{2v} Oxygen Approach	27
6	Terminal Methylene Geometry Variation for C_{2v} Attack	28
7	Singlet and Triplet Energy Variations for C_s Oxygen Approach	33-34
8	Ethylene Oxide Triplet Energy Versus γ	38
9	Lowest Singlet-Triplet Crossing Energy and Corresponding α Value Versus R_2	41
10	Miscellaneous Surface Points	44

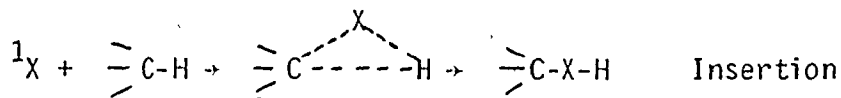
PART A

REACTION MECHANISMS OF THE CYCLOADDITION OF SINGLET AND TRIPLET
ATOMIC OXYGEN TO OLEFINS

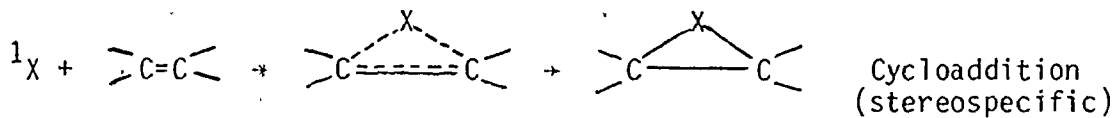
INTRODUCTION

It has long been known that the spin multiplicity of a reagent can affect its chemical properties. For instance, $O(^1D)$, $CH_2(^1A_1)$ and $S(^1D)$ are observed to insert into saturated hydrocarbon CH bonds. In contrast, $O(^3P)$ and $CH_2(^3\Sigma_g^-)$ only abstract H atoms under the same conditions and $S(^3P)$ will not react with paraffins at all. As well, these species when in the singlet state add across olefin double bonds stereospecifically, whereas in the triplet state they yield a mixture of geometrical isomers of the three-membered ring products.

A consistent explanation of these observations can be derived from consideration of the electron configuration of the open-shell reactant. In the singlet state of these species, all the electrons are paired. Simultaneous formation of two bonds to a closed-shell reactant is spin allowed and facile. Thus, insertion into a CH bond results from the concerted formation of two bonds between the attacking species and the carbon and hydrogen of the substrate bond.

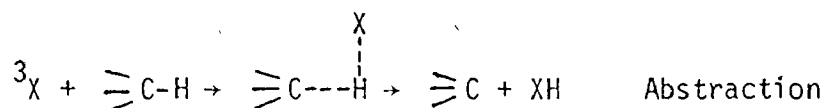


Similarly, cycloaddition to olefins can be visualized as involving the simultaneous formation of two bonds to the unsaturated carbon nuclei.

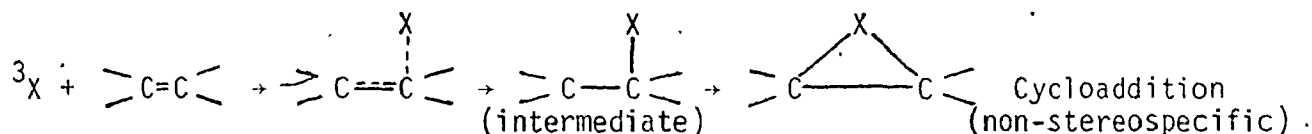


The triplet species contain two unpaired electrons. Simultaneous

formation of two bonds is thus spin disallowed. Triplet species attack on a bonded hydrogen may be expected to lead to abstraction. Formation of a second bond would require a spin inversion which occurs more slowly than separation of the attacking species (with its abstracted H) from the molecular residue. Thus abstraction is preferred to insertion.



Triplet species attack on olefins may be pictured similarly. Initially, formation of only one bond is spin-allowed. If the species formed is a metastable intermediate (rather than a transition state) then relaxation of the initial CC bond from double to single may permit relatively unrestricted rotation around it. When eventual spin inversion and ring closure does occur, the products are expected to show some loss of reactant stereoisomeric purity.



A more detailed description of the mechanisms of these reactions requires computation of the potential surfaces on which the nuclei move. Interpretation of the effects of spin on the mechanism can be obtained from the distribution of electronic charge and unpaired spin density of the reacting species. Such a study of the abstraction and insertion reactions has previously been reported. Here are presented the results of an analogous investigation into the addition reaction.

CHAPTER I

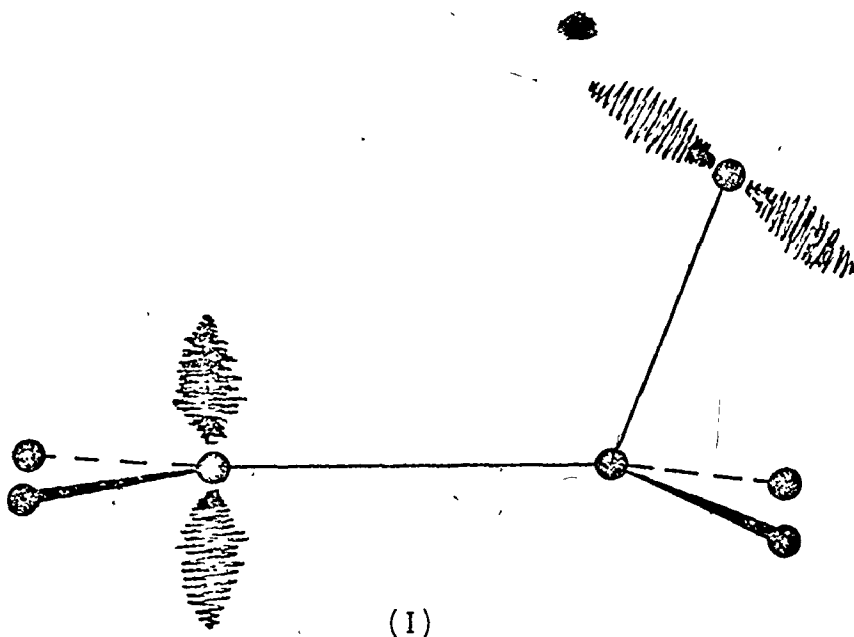
PREVIOUS STUDIES

In the 1950's, Skell and coworkers¹ studied the possibility that the mechanisms and products of reactions with methylene and its derivatives may depend on their spin states. It was postulated that singlet carbenes should add stereospecifically, since in that case a concerted addition is spin-allowed. On the other hand, triplet carbenes might be expected to add in two adiabatic steps, with spin inversion occurring as a distinct process in the intermediate. Such an intermediate is likely to have an open-ring geometry and permit loss of product stereospecificity through low-energy rotation around the ring bonds.

The suggested mechanisms and the fundamental question they raise, that of a possible spin dependence of the course of a chemical reaction, were the centre of a controversy for several years. The original proposals were questioned on several grounds: there was no firm basis for the assumption that rotation around single bonds was significantly faster than spin inversion; singlet addition of methylene need not be a concerted process simply because it might be without violating conservation of spin; and finally, any ring product formed in an adiabatic reaction would be "hot" enough to undergo isomerization.² De More and Benson³ proposed a different solution to the question of the spin-dependence of stereochemistry and distribution of structural isomeric products. They postulated that an open-ring diradical is

formed in both singlet and triplet cases. Faster ring closure than rotation around the ring bonds leads to stereospecific singlet cycloaddition. This proposal has been criticized² since the barrier to methylene rotation is unlikely to be more than 3 kcal/mole. Hence the rate of rotation should at least equal the rate of cyclization in an excited biradical. Part of the controversy was settled by Bader and Generosa,⁴ who showed unequivocally that singlet methylene does add stereospecifically to olefins, and triplet methylene does not.

Analogous studies have been performed on the reaction we consider, oxygen addition to olefins, by R. J. Cvetanović and coworkers⁵⁻¹⁴ and others. The gas phase data consistently suggest an electrophilic^{5,8} attack of triplet oxygen on the alkene π density. This is indicated by the decreased reactivity of halosubstituted olefins¹⁵⁻²⁰ and increased reactivity of alkylsubstituted⁵ olefins. Triplet cycloaddition products can exhibit temperature-dependent stereospecificity. $O(^3P)$ adds to cis-2-butene non-stereospecifically at 77°K and 300°K, but with trans-2-butene, trans- and cis-1,2-dimethyloxirane are produced in the ratio 17/1 at 77°K (condensed phase) but 2/1 at 300°K (gas phase).²¹ There has been speculation^{8,21-24} on the nature of a "triplet biradical" intermediate presumed to be involved. Such a metastable intermediate may close to form the epoxide products, it may fragment to radicals (which then react to form products of higher molecular weight), or it may rearrange to form aldehyde and/or ketone products.⁶ It has been proposed that this intermediate, if it exists, may have an open-ring⁵ geometry (I) with unpaired electronic charge localized at both the oxygen and terminal methylene carbon.



Such a structure would permit the molecule several possible further processes: H atom and/or alkyl migration, ring closure and formation of a second CO bond (if associated with an available triplet-singlet surface crossing), or fragmentation into radicals. Rotation of the terminal methylene group around the formally single bond is expected to require only a few kcal/mole and potentially allow loss of reactant stereospecificity.

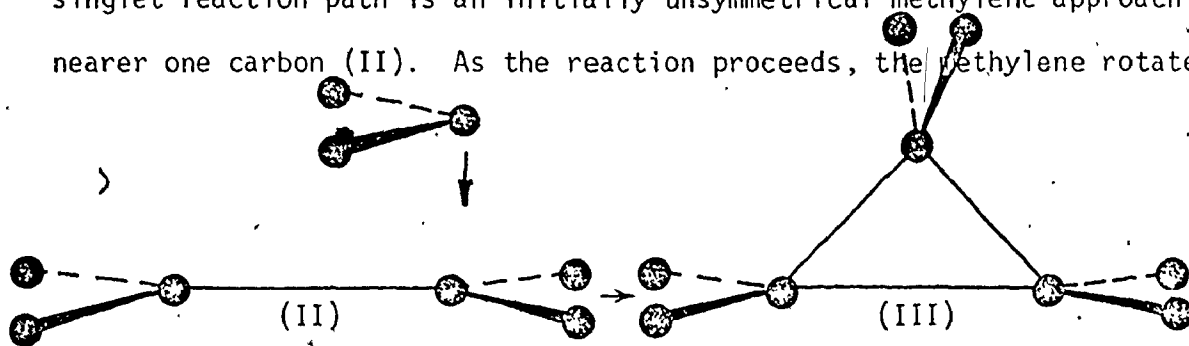
It has been observed that the larger the alkyl groups substituted on the olefin are, the greater is the ratio of epoxide to fragmentation products.^{6,25,26} Thus, addition of triplet oxygen to ethylene forms fragmentation products for the most part at room temperatures. In liquid nitrogen at 77°K, primarily ethylene oxide and acetaldehyde are produced.¹⁰ Involvement of a vibrationally "hot" intermediate of geometry (I) would be consistent with these observations, as the extra degrees of freedom of a substituted ethylene would increase the lifetime of the intermediate and hence reduce the fragmentation products. Similar observations have been made in the reaction of triplet oxygen with solid ethylene.^{27,28}

Gunning, Strausz and coworkers²⁹ discovered that atomic sulphur adds to olefins stereospecifically in both its lowest singlet and triplet states. Both reactions have a low activation energy as they proceed to a significant extent at even -196°C . As for atomic oxygen addition, reaction rates increase as alkyl substitution on the olefins is increased, indicating atomic sulphur electrophilicity. The stereospecificity of the triplet addition is suggested to be due to the nature of a relatively long-lived intermediate diradical of geometry (I). CC bond rotation may be slowed down by the heavy sulphur atom which also enhances the triplet-singlet conversion.²⁹ Alternately, there may be partial bonding between the sulphur non-bonding p orbital and methylene p orbital.

A final case is the liquid phase addition of singlet and triplet forms of carbethoxynitrene (EtO_2CN) to cis- and trans-4-methyl-2-pentene, which yields³³ products consistent with a stereospecific triplet mechanism.

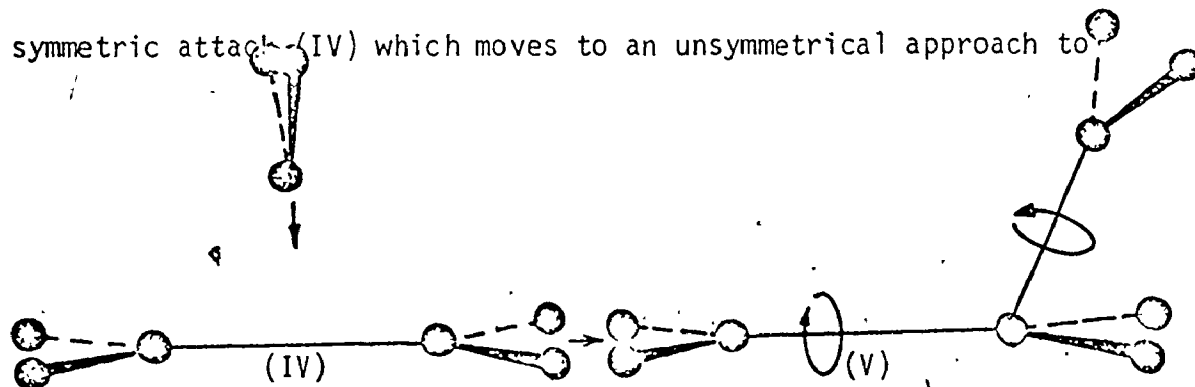
There have been several theoretical studies of these systems at various levels of approximation.

A partial potential surface for the singlet CH_2 cycloaddition has been computed by Hoffmann³⁴ at the extended Hückel level. He concluded from the qualitative features of the surface that the favoured singlet reaction path is an initially unsymmetrical methylene approach nearer one carbon (II). As the reaction proceeds, the methylene rotates



and the system approaches the symmetric geometry of the product cyclopropane (III). The attack is termed concerted in that the path is energetically downhill throughout with almost simultaneous formation of the two ring bonds.

Triplet methylene, however, is predicted to prefer an initially symmetric attack (IV) which moves to an unsymmetrical approach to

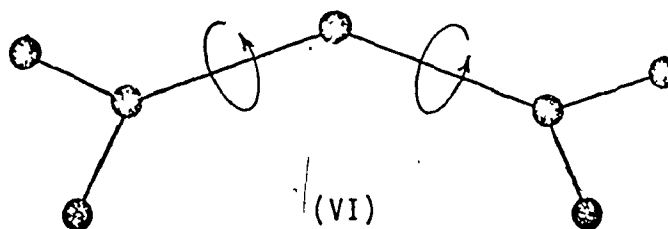


produce a stable open-ring intermediate (V). This geometry has a low rotation barrier around the original CC axis. Thus, loss of substrate stereospecificity is to be expected in the singlet products it forms on transition to the singlet state and ring closure.

Hoffmann *et al.*³⁵ have also used extended Hückel theory to compute potential surfaces for the lowest singlet and triplet states for the addition of sulphur. Singlet cycloaddition was found to be downhill to the thiirane product via a C_{2v} path (c.f. IV). A singlet intermediate was found which was planar and had the CC bond broken (c.f. V). Singlet stereospecificity was attributed to preferred conrotary ring closure. No singlet open-ring geometry with a broken CS bond was found.

Triplet sulphur was calculated to undergo addition via a C_{2v} path which is energetically downhill from the separated reactants, maintaining significant CC bonding throughout. However, two minima

in the triplet surface were found, each a ring-open geometry. One had the carbon-carbon bond broken in a completely planar structure (VI)



with higher barriers to CH_2 rotation than for the trimethylene case. The second structure had one C-S bond broken and a 5 kcal/mole terminal methylene rotation barrier.

Strausz and coworkers³¹ have computed fragments of the lowest singlet and triplet potential surfaces for the addition of sulphur to ethylene in an SCF calculation. They predict the preferred triplet path to be a C_{2v} attack at long range changing to a C_s unsymmetrical geometry at closer distances. The result is an intermediate with one C-S bond broken.

A binding interaction between the sulphur and terminal methylene yields a 23.0 kcal/mole barrier to rotation of the terminal methylene. This barrier is sufficient to be stable to the 20 kcal/mole excess vibrational energy estimated to be available to the molecule. The predicted height of this barrier is of sufficient magnitude to account for the observed stereospecificity found for the addition reactions of $\text{S}(^3\text{P})$.

Leppin and Gollnick³⁶ had previously suggested that the stereospecific triplet sulphur addition could be rationalized on the assumption of a symmetrical C_{2v} approach. The reaction is symmetry allowed for both $\text{S}(^3\text{P})$ and $\text{S}(^1\text{D})$ states in that case. The triplet stereospecificity was attributed to an energy barrier postulated to exist via Walsh's

rules for the lowest triplet state. Although Hoffmann³⁵ agrees with this analysis, it appears to be inconsistent with the high barrier to C_{2v} triplet sulphur addition computed by Strausz et al.³¹

Haines and Csizmadia³⁷ have performed limited calculations on the nitrene cycloaddition system. In agreement with the Strausz et al.³¹ results on the sulphur system, they found that the lowest triplet and lowest excited singlet state molecules had lower total energy for ring-opened geometries with one CN bond broken.

Atomic oxygen-olefin addition, while receiving much experimental attention, has had little quantitative treatment from a theoretical standpoint. A recent³⁸ CNDO/2 sketch of a small portion of the lowest singlet and triplet surfaces indicates the possibility of there existing an open-ring triplet intermediate. However, the results are inconclusive and no attempt was made at specifying any details of the reaction mechanism because of the approximations inherent in the method.

It appeared to us that a useful study of the singlet and triplet oxygen-olefin reactions could be made using relatively accurate ab initio methods. Calculation of the complete singlet and triplet potential hypersurfaces for the cycloaddition, fragmentation, radical migration and insertion/abstraction reactions is far beyond all but the most simplified theoretical models. Accordingly, this study concentrated on more restrictive questions for which at least semi-quantitative answers are obtainable.

Specifically, it was hoped to determine whether or not the preferred singlet and triplet attacks are symmetric with respect to

the olefin double bond. An alternate possible approach is an initial attachment to one of the carbon atoms. In the former case, a symmetric ring product would be expected; in the latter, an open-ring product or intermediate. If an open-ring intermediate is found, is there the expected⁵ almost free rotation of the terminal methylene? What is the activation energy required to produce a ring-opened triplet structure?

Previous studies⁴⁰ of the insertion/abstraction reactions of singlet and triplet species interpreted the computed differences in potential surface features in terms of spin "uncoupling" and "transfer" mechanisms. We hoped to find an analogous rationale for the differences between singlet and triplet cycloaddition mechanisms.

CHAPTER II

POTENTIAL SURFACE THEORY

In the quantum description of molecular dynamics, the idea of a potential surface is based on the separability of nuclear and electronic motion first suggested by Born and Oppenheimer.⁴¹ The electronic energy is computed for all static nuclear geometries. The nuclei are treated as moving in a potential due to their mutual electrostatic repulsions and the total electronic energy.

The potential surface concept is intimately connected with the description of the preferred paths of molecular reactions. Indeed, the very definitions of equilibrium nuclear geometry, transition state, reaction intermediate and activation energy all relate to the energy changes accompanying nuclear motion on a potential energy hypersurface.

The potential operator for a system of electrons and nuclei under no applied external electromagnetic fields contains no explicit time dependence. In that case, the total system wavefunction for the v^{th} stationary state of energy E_v can be written as a product of a time-dependent function, $e^{-E_v t / \hbar}$, and a spatial function, $\psi_v(\underline{r}, \underline{R})$, where $\{\underline{r}\}$ and $\{\underline{R}\}$ are the electronic and nuclear coordinates (including spin). Thus, the molecular eigenstate problem becomes the solution of the time-independent Schrödinger equation of the system:

$$H\psi_v(\underline{r}, \underline{R}) = E_v \psi_v(\underline{r}, \underline{R}) \quad (1)$$

for the possible eigenstates $\psi_v(\underline{r}, \underline{R})$ associated with each eigenenergy E_v .

The total non-relativistic "spinless" Hamiltonian for a system of M nuclei (masses $\{M_j\}$, charges $\{Z_j e\}$) and N electrons (masses m_e , charges $-e$) can be written as

$$H(\underline{r}, \underline{R}) = -\frac{\hbar^2}{2} \sum_{j=1}^M \frac{\nabla_j^2}{M_j} - \frac{\hbar^2}{2} \sum_{i=1}^N \frac{\nabla_i^2}{m_e} - \sum_{j=1}^M \sum_{i=1}^N \frac{e^2 Z_j}{r_{ij}} + \sum_{j<\ell}^M \frac{e^2 Z_j Z_\ell}{R_{j\ell}} + \sum_{i<k}^N \frac{e^2}{r_{ik}} \quad (2A)$$

or, in atomic units*

$$H(\underline{r}, \underline{R}) = -\frac{1}{2} \sum_{j=1}^M \frac{\nabla_j^2}{M_j} - \frac{1}{2} \sum_{i=1}^N \nabla_i^2 - \sum_{j=1}^M \sum_{i=1}^N \frac{Z_j}{r_{ij}} + \sum_{j<\ell}^M \frac{Z_j Z_\ell}{R_{j\ell}} + \sum_{i<k}^N \frac{1}{r_{ik}} \quad (2B)$$

The respective terms are the operators for the nuclear and electronic kinetic energy and electronic-nuclear, internuclear and interelectronic potential energy.

The mass and hence kinetic energy of the nuclei and electrons differ by three orders of magnitude. Hence, the nuclear motion can be treated as occurring in a potential due to the nuclear repulsions and negatively charged cloud of electron density. To a good approximation it is possible to express the total molecular eigenfunction, $\Psi_{v,n}(\underline{r}, \underline{R})$ as a simple product of an electronic and a nuclear function:

$$\Psi_{v,n}(\underline{r}, \underline{R}) = \psi_{v,B}(\underline{r}) \phi_{v,n}(\underline{R}) \quad (3)$$

The electronic and nuclear wavefunctions are now treated separately in two steps.

* The atomic unit (a.u.) of length is the first Bohr radius of the hydrogen atom, $a_0 = 0.52917 \text{ \AA}$; 1 a.u. of energy = 627.71 kcal/mole = 27.210 eV = $2.1947 \times 10^5 \text{ cm}^{-1}$.

Defining the electronic Hamiltonian, H_{el} , as

$$H_{el} = -\frac{1}{2} \sum_{i=1}^N \nabla_i^2 - \sum_{j=1}^M \sum_{i=1}^N \frac{Z_j}{r_{ij}} + \sum_{j<\ell}^M \frac{Z_j Z_\ell}{R_{j\ell}} + \sum_{i<k}^N \frac{1}{r_{ik}} \quad (4)$$

we first solve the electronic Schrödinger equation for the so-called "clamped nucleus" approximation:

$$H_{el} \psi_{v,R}(r) = E_v(R) \psi_{v,R}(r) \quad (5)$$

for various nuclear geometries.

Secondly, defining the nuclear kinetic operator, T_N , as

$$T_N = -\frac{1}{2} \sum_{j=1}^M \frac{\nabla_j^2}{M_j} \quad (6)$$

we then proceed to solve the nuclear Schrödinger equation

$$[T_N + E_v(R)] \phi_{v,n}(R) = E_{v,n} \phi_{v,n}(R) \quad (7)$$

Thus, we find the nuclear eigenstates $\phi_{v,n}(R)$ for the v^{th} system eigenstate, using $E_v(R)$, the parametrically defined electronic energy of the v^{th} state as the nuclear potential. This is the Born-Oppenheimer approximation.⁴¹

One can improve the molecular description by redefining each molecular eigenstate in terms of the complete set of exact solutions to the electronic Schrödinger equation, $\psi_{\mu,R}(r)$. The expansion coefficients are then taken to be a set of nuclear wavefunctions $\phi_{\mu}(R)$. Thus,

$$\Psi_{\mu,n}(r,R) = \sum_{\mu} \psi_{\mu,R}(r) \phi_{\mu}(R) \quad (8)$$

This method leads⁴² to a revised infinite set of coupled equations for

the nuclear functions $\phi_\mu(\underline{R})$:

$$[T_N + E_\mu(\underline{R}) + \langle \psi_\mu | T_N | \psi_\mu \rangle - E_{\mu\eta}] \phi_\mu(\underline{R}) = - \sum_{\mu \neq \nu} \langle \psi_\mu | T_N | \psi_\nu \rangle \phi_\nu(\underline{R}) \quad (9)$$

This is another exact statement of the Schrödinger equation for the system (equation 2) and as difficult to solve.

Exact solution of equations (5) and (9) constitute the "non-adiabatic" approximation to the original problem (equation 1).

We see that the approximation made in equation (7) is to assume that $\langle \psi_\mu | T_N | \psi_\nu \rangle = 0$. If one uses the single product form of the approximate eigenfunction, one obtains the eigenvalue equation:

$$[T_N + E_\mu(\underline{R}) + \langle \psi_\mu | T_N | \psi_\mu \rangle] \phi_\mu(\underline{R}) = E_{\mu\eta} \phi_\mu(\underline{R}) \quad (10)$$

The difference between this and the Born-Oppenheimer nuclear equation (7) is the presence of the term $\langle \psi_\mu | T_N | \psi_\mu \rangle$, the so-called "adiabatic correction". As mentioned above, its value should be only $\sim .0005$ the value of $E_\mu(\underline{R})$.

The Born-Oppenheimer approximation may fail in cases where there is degeneracy or near-degeneracy in the electronic states $\{\psi_{\nu,R}(\underline{r})\}$. In this case, there may be a strong coupling of the electronic states and nuclear motion, as in the Jahn-Teller and Renner distortions of nuclear geometry for non-linear and linear molecules⁴³ respectively.

A thermal reaction of ground state reactants can be analyzed through the features of the lowest potential surface. However, a photochemical reaction as studied here must be described by the properties of several such surfaces.⁴⁴ The intersections of these surfaces calculated within the Born-Oppenheimer approximation will correspond to

the most probable geometries for radiationless transition between the electronic states.

Solutions to the electronic Schrödinger equation (5) may in principle be determined to any degree of accuracy required. However, the capabilities of current computational techniques limit the calculation of potential energy surfaces to chemical accuracy (1 kcal/mole or less) to only a few two- and three-electron systems. Two recent reviews of potential surface calculations^{45,46} discuss the difficulties encountered.

Even within the current technical constraints, useful studies of the nuclear dynamics of chemical reactions are possible by solution of nuclear Schrödinger equation (7) via classical and quantum methods.⁴⁷ As well, a computation of the general features of a potential surface permits prediction of the general nature of the reaction paths, activation energies and products of a chemical reaction.

We have taken the latter approach. Approximate electronic functions of several low-lying states of a model cycloaddition system were calculated for chosen nuclear geometries. From the variation in electronic energies of the various states with changes in the nuclear geometry, the preferred reaction paths for the lowest singlet and triplet states are predicted. An explanation of the computed differences in singlet and triplet paths is proposed based on the associated total electronic charge and spin density distributions for the various geometries. Finally, these results are reconciled with the observed experimental data.

CHAPTER III

CALCULATIONS OF THE POTENTIAL ENERGY SURFACES

The model olefin-oxygen system chosen for computational study is the simplest possible, ethylene (C_2H_4) in its $^1A_{1g}$ ground state plus atomic oxygen in its lowest 3P and 1D states. This choice of system allows us to calculate the potential energy surfaces at a level of accuracy sufficient to predict their major features. The reaction paths deduced from the surfaces should hold for the whole class of reactions.

The electronic wavefunctions generated here are of the LCAO-MO-SCF type. That is, each of the molecular orbitals (MO) used in the construction of a single determinantal wavefunction is expressed in a linear combination of atomic orbitals (LCAO) or basis functions. Our basis set size limitations preclude reaching the Hartree-Fock limit.

Self-consistent-field (SCF) calculations of the required determinantal wavefunctions were carried out primarily using the PØLYATØM/2⁴⁸ system of programmes (locally upgraded by Dr. A. J. Duke). For some of the geometries studied, the PØLYATØM SCF calculations exhibited oscillatory non-convergence. When this occurred, the programmes PREP, RØPEN and ØPEN (kindly supplied by Dr. R. A. Gangi) were used instead. These programmes are based on McWeeny's⁴⁹ method of steepest descent and solved the oscillation problem satisfactorily.

Triplet wavefunctions were taken to be single determinantal wavefunctions of the unrestricted Hartree-Fock (UHF) type. Since the

space orbitals associated with the α and β spin functions are allowed to differ, the resultant wavefunction is not necessarily an eigenfunction of S^2 . Contamination of the desired triplet by states of higher multiplicity is thus possible. The extent of contamination in our calculations was monitored through calculation of $\langle S^2 \rangle$ for each triplet wavefunction. The most serious contamination is expected to arise from the state of next highest multiplicity.⁵⁰ In the triplet case, contamination arises primarily from a quintet state ($\langle S^2 \rangle = 6$). The computed $\langle S^2 \rangle$ values were greater than the pure triplet value of 2 by .4 at most and .03 \rightarrow .2 on average. Hence contamination of the lowest triplet state by states of higher multiplicity was found to be minimal.

As a first approximation, the lowest singlet state wavefunctions were taken to be single restricted Hartree-Fock (RHF) determinants. Considering the valence shell configurations of oxygen, the atomic oxygen 1D state wavefunction must consist of a linear combination of three determinants (see Appendix A-1). This was taken into account by performing a three-state configuration interaction (CI) using the virtual orbitals (VO) generated with each ground state (GS) wavefunction. The occupied and virtual orbital sets were used to construct two excited state determinantal functions. The three (orthogonal) states were mixed using the one- and two-electron integral evaluation package in PØLYATØM, plus a configuration interaction programme written by the author.

A more accurate CI method was employed where possible. This requires use of reconverged SCF wavefunctions as the three-component

CI basis and thus avoided the use of virtual orbitals. Since such determinantal functions are not orthogonal, recourse was made to the corresponding orbital procedures of Amos and Hall.⁵¹ Calculations of this type could be performed only for a separated oxygen atom due to basis set size. This gave the limiting description of the separated reactants in our basis set. It also yielded an estimate of the error involved in the virtual orbital method when later applied to several surface points.

The atomic basis set used was taken from the Gaussian type orbital (GTO) sp set constructed by Basch, Robin and Keubler⁵² for their studies of the electronic states of several small molecules. They state that the set is of best-atom double zeta (BADZ) quality, and is sufficient to describe the ground and excited state molecular orbitals of first-row-containing molecules.

Our preliminary studies included computation of ethylene oxide wavefunctions for the three triplet states expected to be of lowest energy (based on ground state orbital energies). The highest energy molecular orbitals for all three triplets showed heavy use of the most diffuse basis functions of the Basch double zeta (BDZ) set. Hence this basis did not satisfactorily span the required orbital space. We supplemented the set by adding three s- and one p-type functions per first row atom. The orbital exponents of the added functions were fixed by continuing the trend in the ratio of the BDZ exponents. The contraction of the BDZ set suggested by Basch et al. was retained, and the added functions were left uncontracted. The contraction of the final basis set was (13,6/4) + [7,3/2]. The orbital exponents and contraction coefficients

of the final basis set are listed in Table 1. The three triplet and lowest closed-shell singlet wavefunctions were recomputed at the experimental ground state equilibrium geometry⁵⁴ (Table 2). Total energy changes for the four states on expanding the basis set are reported in Table 3. The ground state energy was essentially unaffected. The energies of two of the three triplets decreased significantly. The added basis functions contribute significantly to the description of the most diffuse MO in all three triplet states. In each case, the most diffuse basis function of each type is not the most heavily used; thus, the basis now spans the MO space satisfactorily.

A basis set of this size may be expected to predict rotational barriers to within 1 kcal/mole.⁴⁵

A potential energy hypersurface for a seven-nucleus non-linear system is a function of 15 dimensions. Only a small portion of such a surface can and need be searched to establish minimum energy reaction paths. Each of the questions we wished to answer necessitated finding the changes in total energy with variation of one or more of four nuclear geometry parameters (Figure 1): R_1 , the carbon-carbon distance; R_2 , the shorter of the two carbon-oxygen distances; α , the angle between R_1 and R_2 ; and γ , the torsion angle of the terminal methylene group. For a symmetric oxygen approach (along the bisector of the carbon-carbon bond), it is useful to define R_3 , the distance between the oxygen nucleus and midpoint of the carbon-carbon bond. R_3 is then more convenient to use than the related parameters R_2 and α .

The geometries of the two methylene groups were also varied in each search. These variations are not large because the two limiting

TABLE 1

Final Atomic Orbital Basis Set

Atom	Type	Basis Function ^a
H	S	0.817238(0.65341)+0.231208(2.89915)+0.032828(19.24060)
	S	1.000000(0.17758)
C	S	0.243311(17.18930)+0.453799(7.05910)+0.269832(2.52690)+0.153480(41.84270)
	S	0.904751(159.62740)+0.121599(781.64950)+0.029314(2548.72600)
	S	1.053375(0.47350)-0.146302(4.93440)
	S	1.000000(0.14800)
	S	1.000000(0.045)
	S	1.000000(0.014)
	S	1.000000(0.00426)
	P _x , P _y , P _z	0.640080(0.35945)+0.386200(1.14293)+0.115440(3.98040)+0.018533(18.15570)
O	P _x , P _y , P _z	1.000000(0.037)
	S	0.243991(31.31660)+0.458240(12.86070)+0.264438(4.60370)+0.152763(76.23200)
	S	0.904785(290.78500)+0.121603(1424.06430)+0.029225(4643.44850)
	S	1.051534(0.92110)-0.140314(9.70440)
	S	1.000000(0.28250)
	S	1.000000(0.089)
	S	1.000000(0.028)
	S	1.000000(0.00882)
	P _x , P _y , P _z	0.627380(0.71706)+0.394730(2.30512)+0.124190(7.90403)+0.019580(35.18320)
	P _x , P _y , P _z	1.000000(0.064)

^a Each basis expansion is written as $C_1(\alpha_1) + C_2(\alpha_2) + \dots + C_N(\alpha_N)$ where C_i is the expansion coefficient of the Gaussian $e^{-\alpha_i R^2}$.

TABLE 2

Experimental⁶⁰ Ground State Ethylene Oxide Equilibrium Geometry

Atom	x(a.u.)	y(a.u.)	z(a.u.)
H1	0.0	-1.74031707	2.39572547
H2	0.0	1.74031707	2.39572547
H3	0.0	-1.74031707	-2.39572547
H4	0.0	1.74031707	-2.39572547
C1	0.37730991	0.0	1.39085
C2	0.37730991	0.0	-1.39085
O	2.7106700	0.0	0.0

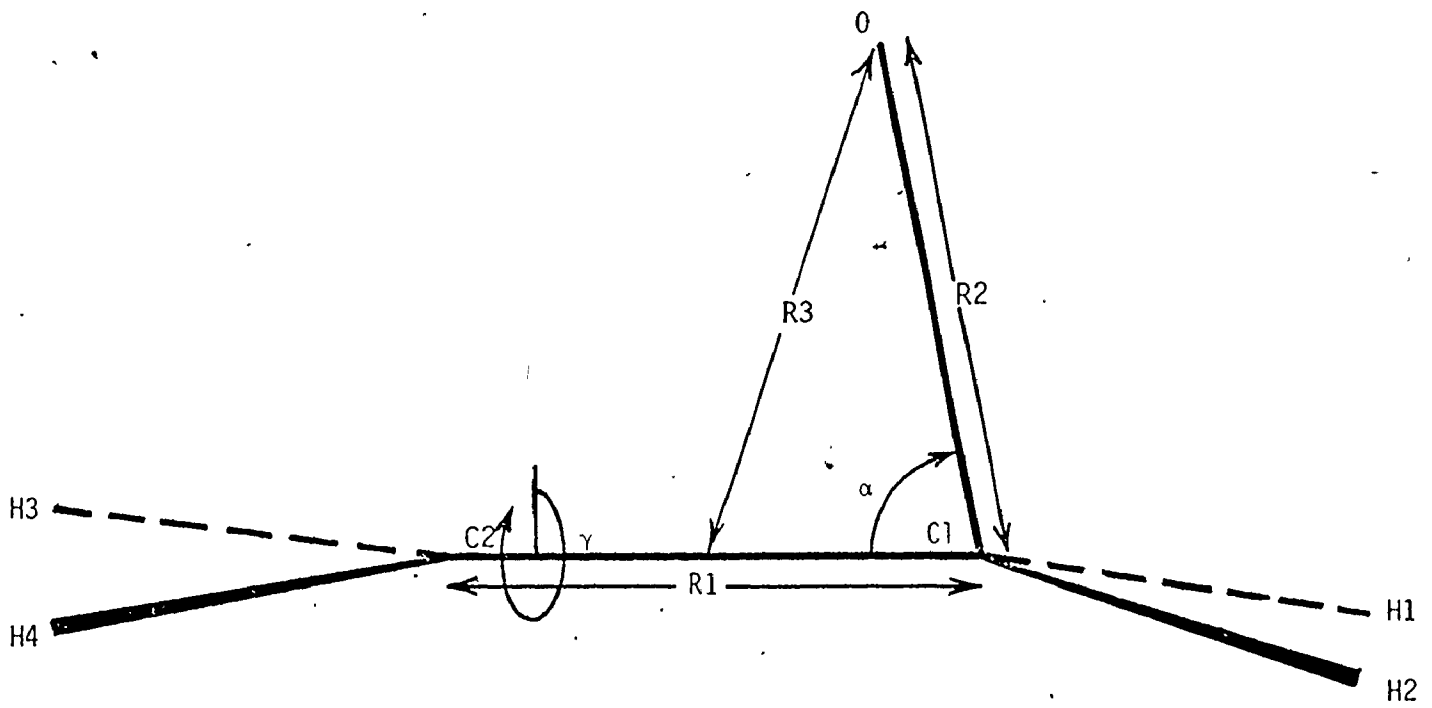
TABLE 3

Total Energy Changes of Several Low-Lying States of Ethylene Oxide
on Basis Set Expansion (at the ground state equilibrium geometry)

State	Energy (a.u.) [†] (BDZ basis)	Energy (a.u.) [†] (Extended BDZ basis)	Energy Change (a.u./kcal/mole)
¹ A ₁	-152.80027	-152.80403	-0.00376/-2.36
³ B ₁	-152.53685	-152.57574	-0.03889/-24.4
³ A ₂	-152.522	-152.55448	-0.032/-20.2
³ B ₂	-152.4942	-152.50235	-0.0082/-5.15

[†] S.C.F. energies converged to last digit quoted.

Figure 1. Nuclear Geometry Parameters Varied



geometries, of reactant ethylene⁵³ and product ethylene oxide⁵⁴ are very similar (Table 4). The energy changes introduced are less than 5 kcal/mole, as comparison of points 8 and 10 of Table 5 indicate.

1. C_{2v} Approach

We first studied the variation in total singlet and triplet state energies for oxygen approaching the ethylene along the x-axis (Figure 2), equidistant from the two carbons. The two lowest surfaces for this C_{2v} approach are presented in Table 5 and Figure 2.

The singlet surface is strongly "downhill attractive" for such a symmetric attack, leading to the potential well around the ground state equilibrium geometry.

For $R_3 < 4$ a.u., the methylene geometries were taken to be those in the equilibrium geometry of ground state ethylene oxide. For $R_3 \geq 5$ a.u., the methylenes were fixed to be in the planar geometry of ground state ethylene. For $R_3 = 4$ a.u., an intermediate geometry was chosen (Table 6). The singlet energy for several values of R_3 was optimized with respect to R_1 . These results are included in Table 5 and illustrated in Figure 3. The optimum value of R_1 increases with decreasing R_3 , reflecting the weakening of the carbon-carbon bond with approach of the oxygen. The lowest energy path is accurate to better than 5 kcal/mole with respect to R_1 variation along the complete range of R_3 values.

The magnitude of the correlation error changes are illustrated in Figure 2. For the very extended C_{2v} geometry where $R_3 = 10$ a.u., wavefunctions for the lowest singlet state were computed by three methods.

TABLE 4

Experimental Bond Lengths and Bond Angles of Ground State Ethylene⁶¹
and Ethylene Oxide⁶⁰

Parameters (a.u./deg.)	Ethylene	Ethylene Oxide
R(CO)	---	2.7164
R(CC)	2.5304	2.7817
R(CH)	2.052	2.045
$\hat{C}OH$	---	61.5
$\hat{H}CH$	117.6	116.7

Figure 2. C_{2v} Singlet and Triplet Surfaces

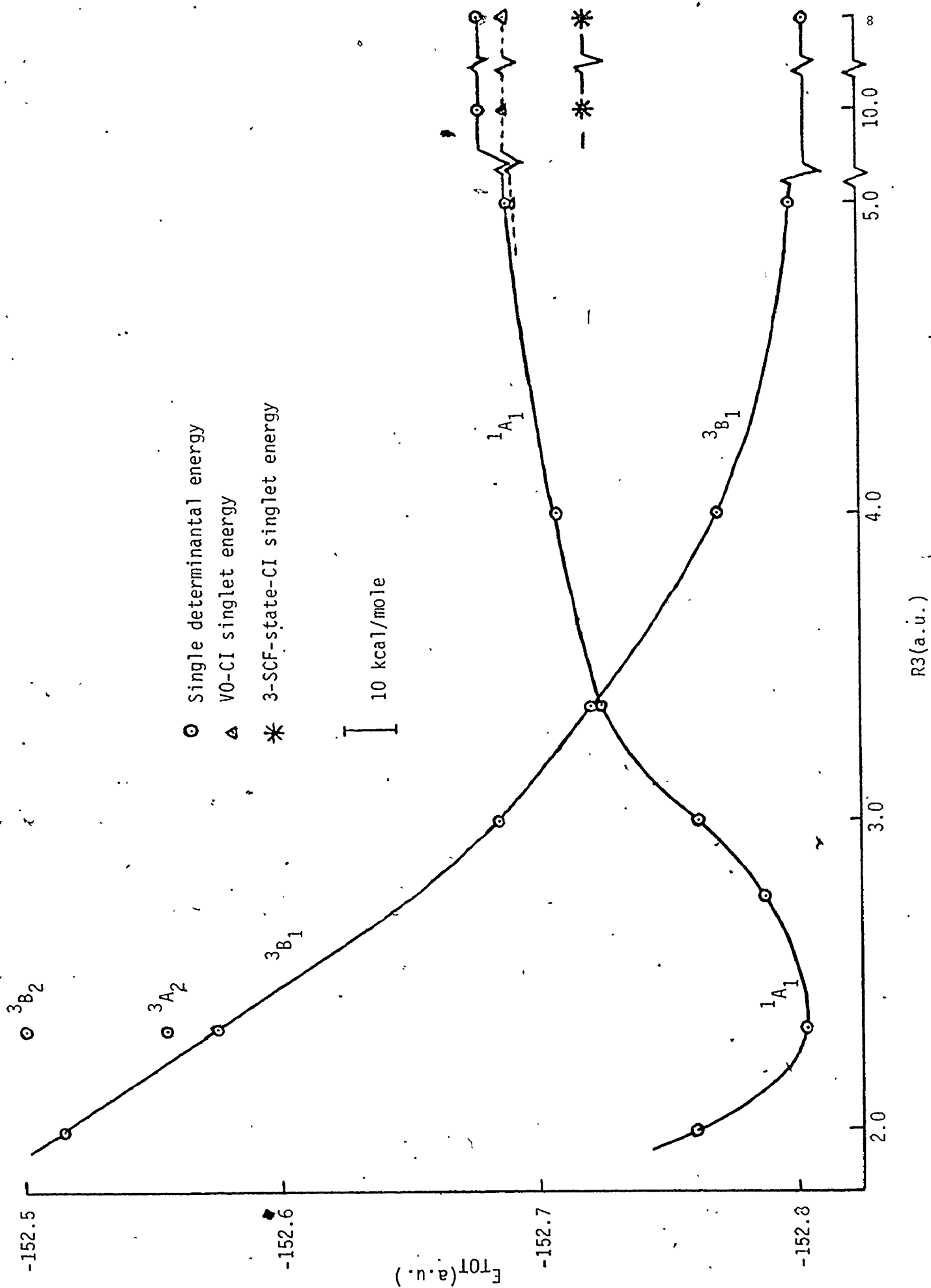


TABLE 5

Singlet and Triplet Energy Variations for C_{2v} Oxygen Approach

Point	Geometry ^a	R3(a.u.)	R1(a.u.)	R2(a.u.)	1A_1 Energy ^b (a.u.)	3B_1 Energy ^{b,c} (a.u.)	$\langle S^2 \rangle^c$
14	2 ^d	10.000	2.530	10.08	-152.68075	-152.80483	2.006
5	2 ^d	5.000	2.530	5.158	-152.69035	-152.79915	2.009
6	2 ^d	5.000	2.600	5.166	-152.68912	----	---
11	3	4.000	2.782	4.235	-152.694	----	---
12	3 ^d	4.000	2.700	4.222	-152.7017	----	---
13	3 ^d	4.000	2.600	4.206	-152.7071	-152.7718	---
2	1 ^d	3.373	2.782	3.649	-152.7188	----	---
3	1 ^d	3.373	2.700	3.630	-152.72132	-152.7223	2.023
4	1 ^d	3.373	2.600	3.612	-152.728	----	---
7	1 ^d	3.000	2.782	3.307	-152.76116	----	---
8	1 ^d	3.000	2.700	3.290	-152.76342	-152.68643	2.019
9	1 ^d	3.000	2.600	3.270	-152.76202	----	---
10	1 ^{d,e}	3.000	2.700	3.290	-152.75421	----	---
15	1 ^d	2.750	2.782	3.082	-152.78647	----	---
16	1 ^d	2.750	2.700	3.063	-152.78750	----	---
1	1	2.331	2.782	2.714	-152.80403	-152.57574	2.014
15	1 ^d	2.000	2.782	2.436	-152.76207	-152.51601	---

^a geometries 1, 2 and 3 defined in Table 6.^b SCF energy converged to last digit shown.^c UHF state.^d geometry based on 1, 2 or 3 as indicated but R1 and/or R3 changed to values given.^e geometry as for point 8, except the methylenes are coplanar.

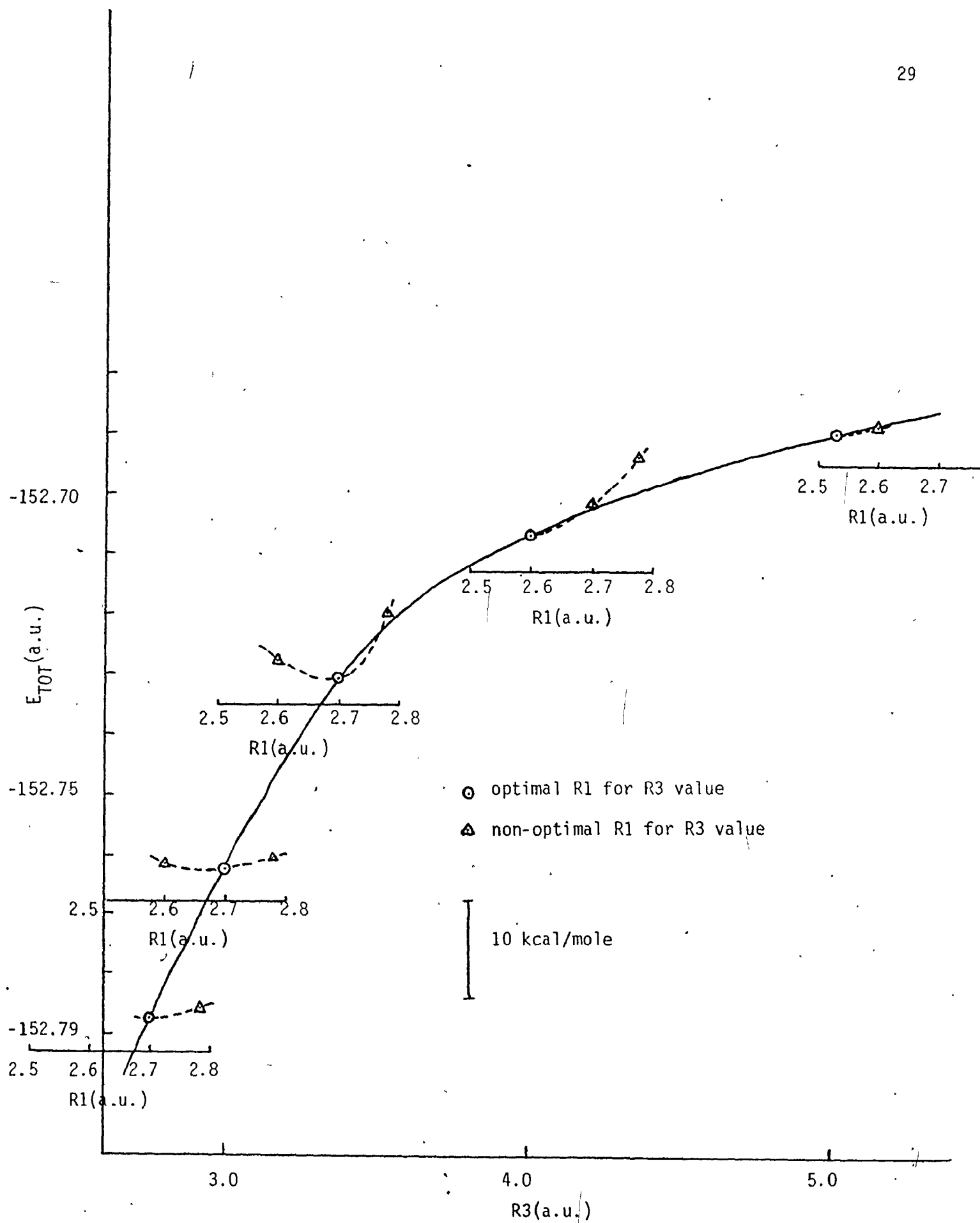
TABLE 6

Terminal Methylene Geometry Variation for C_{2v} Attack

- 1 Ethylene oxide ground state experimental⁵⁴ equilibrium geometry
- 2 Ethylene oxide geometry chosen intermediate to 1 and 3.
- 3 Ethylene ground state experimental⁵³ equilibrium geometry (plus oxygen).

	CH (a.u.)	HCH (degrees)	R1 (a.u.)	R3 (a.u.)
1	2.045	117.6	2.782	2.708
3	2.052	116.7	2.782	4.187
2	2.052	116.7	2.530	5.000

Figure 3. Optimization of Singlet C_{2v} Surface with Respect to R2



First, we employed a three-state CI using a basis set of individually converged SCF ethylene oxide functions. The lowest singlet energy was -152.72013 a.u., only 0.08 kcal/mole less than the sum of the energies of separated $C_2H_4(^1A_{1g})$ (-78.00643 a.u.) and $O(^1D)$ (-74.71357 a.u.) in this basis.

A second calculation was performed using a virtual orbital description of the interacting determinants. This yielded a lowest singlet energy of -152.68888 a.u., 18 kcal/mole above the previous CI result. The lowest single determinantal singlet energy is -152.68075, a further 6 kcal/mole higher than the V0-CI result. Thus, the V0-CI recovered only 6 kcal/mole of the 24 kcal/mole error incurred by attempting to describe the open-shell oxygen by a single determinantal function.

For surface points near the 1A_1 equilibrium geometry, a single determinant is expected to suffice to describe the closed-shell product state to the accuracy we require. This was found to be the case for the singlet ground state of H_2O in the insertion/abstraction study.⁴⁰

At intermediate R3 values, some determinantal mixing can be expected to occur. Accordingly, a V0-CI was performed for point 5 (R3 = 5 a.u.). The lowest singlet energy decreased only 1.3 kcal/mole. This strongly suggests the possibility of there being an energy barrier to the singlet reaction for this geometry of approach of about 10 kcal/mole.

The triplet surface for C_{2v} approach is strongly repulsive at all values of R3. Unlike the singlet case, the single determinantal UHF wavefunction correctly describes the dissociated reactants. Changes

in correlation energy are not expected to be as important since the next lowest triplet states are of different symmetry and hence non-interacting. Smooth energy increase on transition from separated reactants to the lowest excited product triplet state was observed.

The results of this search may be briefly summarized by saying that the singlet surface is "downhill attractive" for a C_{2v} attack and leads to the ring product in its ground state. There may be a moderate barrier at large distances; however, this is not unambiguously shown in these calculations due to problems in overcoming correlation effects. The triplet surface, on the other hand, is strongly repulsive for the C_{2v} approach.

2. C_s Approach

The second series of calculations was carried out to evaluate the energy changes accompanying an unsymmetric oxygen attack on the olefin. Thus, sequences of runs were performed wherein the oxygen was constrained to remain in the plane both perpendicular to the ethylene molecular plane and containing the olefinic bond. The terminal methylene was fixed in the planar ethylene geometry. The internal methylene was given the more tetrahedral geometry of the ground state ethylene oxide equilibrium geometry.

In the C_s point group, the lowest closed-shell singlet state is designated $^1A'$, the lowest triplet $^3A''$, and the second lowest triplet $^3A'$. The lowest open-shell singlet states with configurations corresponding to those of the open-shell triplets are labelled $^1A''_{o.s.}$ and $^1A'_{o.s.}$.

The first set of computations was carried out for $\alpha = 109.47^\circ$ and varying R2. The results are included in Table 7 and illustrated in Figure 4.

The closed-shell singlet surface is slightly repulsive. To estimate the correlation error, we performed a three-state V0-CI on points 4 and 23. The lowest singlet energy decreased 7 kcal/mole and 6 kcal/mole, respectively.

In open-ring geometries, there may exist low-lying open-shell singlet states related to the lowest triplet states. To check this, we computed the lowest energy RHF $^3A''$ and $^3A'$ states, then generated the corresponding singlet energy from those functions. On transferring from UHF to RHF wavefunctions, the lowest $^3A''$ and $^3A'$ states increased in energy (for C_s point 4) by 5 kcal/mole each. The calculated $^1A'_{o.s.}$ energy was found to be -152.636 a.u., 18 kcal/mole above the lowest closed-shell singlet. Thus, the lowest singlet state at that geometry was still a closed-shell configuration.

Mixing of the $^1A'_{o.s.}$ and closed-shell $^1A'$ states was considered possible. Accordingly, the V0-CI calculations were repeated for points 4 and 23 with the open-shell configuration added to the basis. Mixing was found to be minimal, the lowest singlet state energy being respectively less than 10 kcal/mole and 6 kcal/mole lower than the single closed-shell determinantal result. Thus, the singlet curve is predicted to be repulsive.

The triplet surface is also repulsive, though much less so than for a symmetric attack.

A slight dip was noted in the triplet surface for $R2 \approx 3$ a.u.

TABLE 7

Singlet and Triplet Energy Variations for C_s Oxygen Approach

Point	R2 (a.u.)	α (degrees)	R1 (a.u.)	$1A'$ Energy ^a (a.u.)	$3A''$ Energy ^{a,b} (a.u.)	$\langle S^2 \rangle$	$3A'$ Energy ^{a,b} (a.u.)
12	4.000	103.00	2.782	-----	-152.78336	2.426	-----
23	4.000	109.47	2.782	-152.6738	-152.78373	2.433	-152.78338
24	4.000	118.00	2.782	-----	-152.78233	---	-----
15	3.300	109.47	2.782	-----	-152.77742	2.210	-----
37	3.250	70.00	2.782	-152.75614	-152.70941	---	-----
36	3.250	90.00	2.782	-152.71198	-152.7698	---	-----
18	3.250	100.00	2.782	-----	-152.77819	2.178	-----
17	3.250	105.00	2.782	-----	-152.77865	2.185	-----
16	3.250	109.47	2.782	-152.6768	-152.77727	2.197	-----
19	3.250	105.00	2.650	-----	-152.77857	2.175	-----
27	3.250	105.00	2.718	-----	-152.77948	2.177	-----
21	3.250	105.00	2.950	-----	-152.77059	2.191	-----
14	3.200	109.47	2.782	-----	-152.77740	---	-----
20	3.100	109.47	2.782	-----	-152.77760	---	-----
13	3.050	109.47	2.782	-----	-152.77766	2.089	-----
11	3.014	100.00	2.782	-----	-152.77915	2.075	-----
25	2.014	103.00	2.782	-----	-152.77972	2.076	-----
10	3.013	106.00	2.782	-----	-152.77929	2.076	-----
7	3.014	109.47	2.782	-152.67288	-152.77763	2.074	-152.7732
22	3.014	103.00	2.650	-----	-152.77690	2.078	-----
28	3.014	103.00	2.750	-----	-152.77970	1.074	-----
26	3.014	103.00	2.950	-----	-152.77401	2.076	-----

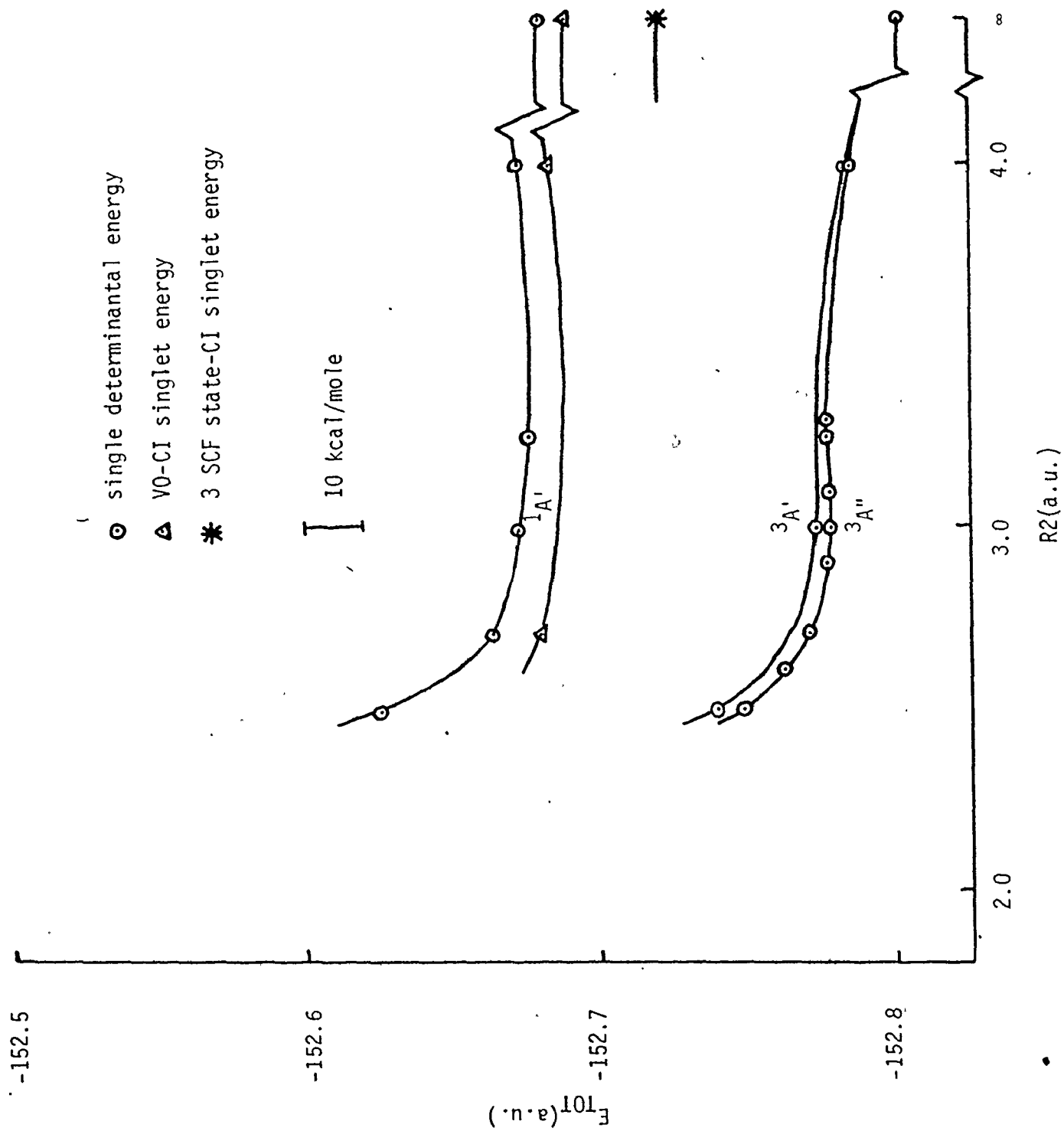
5	2.914	109.47	2.782	----	-152.77697	2.076	----
38	2.900	83.00	2.782	-152.74537	-152.74963	---	----
35	2.714	70.00	2.782	-152.78802	-152.66214	2.034	----
34	2.714	90.00	2.782	----	-152.75906	2.033	----
9	2.714	100.00	2.782	----	-152.77214	2.030	----
8	2.714	104.47	2.782	----	-152.77283	2.030	----
4	2.814	109.47	2.782	-152.66529	-152.77481	2.037	-152.76060(RHF)
3	2.714	109.47	2.720	----	-152.76909	2.030	----
1	2.714	109.47	2.782	----	-152.77030	2.029	----
2	2.714	109.47	2.840	----	-152.77009	2.030	----
6	2.614	109.47	2.782	----	-152.76242	2.027	----
0	2.500	109.47	2.782	-152.6259	-152.74779	---	-152.73700

All geometries are based on that of point 1 (see Fig. 1) with the indicated changes in α , R1 and R2.

a SCF energy converged to last digit given

b UHF wavefunction

Figure 4. C_S Singlet and Triplet Surfaces



To define the surface more accurately in this region, we optimized the triplet energy with respect to both α and R1 for several R3 values. The results of this search are included in Table 7 and Figure 5.

The originally observed dip, less than 1 kcal/mole, is not meaningful in itself. However, the α - and R1-optimizations show that the preferred angle of attack is a consistent $104 \pm 2^\circ$ and carbon-carbon distance $2.75 \pm .05$ a.u. for carbon-oxygen distances in the 3 a.u. range. Hence the full triplet C_s attack curve (Figure 4) is quite possibly within 2 kcal/mole, and certainly 10 kcal/mole of the lowest energy path.

3. Methylene Rotation Barrier

One of the primary questions of interest was the non-stereospecificity of the triplet reaction. As previously mentioned, one explanation of this observation is the existence of a low energy barrier to rotation of the terminal methylene of an asymmetric triplet intermediate. Accordingly, we studied the variation in total triplet state energy with γ , the terminal methylene rotation angle (Figure 1). The results are reported in Table 8 and Figure 6. Unless explicitly stated otherwise, the geometric parameters are those of the ground state equilibrium geometry.

The rotation barrier is only 5.9 kcal/mole for $R2 = 2.714$ a.u. and $\alpha = 109.47^\circ$. The barrier height is relatively insensitive to the value of α in this range of α values, being 5.0 kcal/mole for $\alpha = 90^\circ$. We computed the rotation barrier for ethylene in its lowest triplet (3T) state to be 15 kcal/mole (for $R1 = 2.916$ a.u. and using our basis). In this case, however, the perpendicular geometry is lower

Figure 5. Optimization of Triplet C_S Surface with Respect to R_1 and α

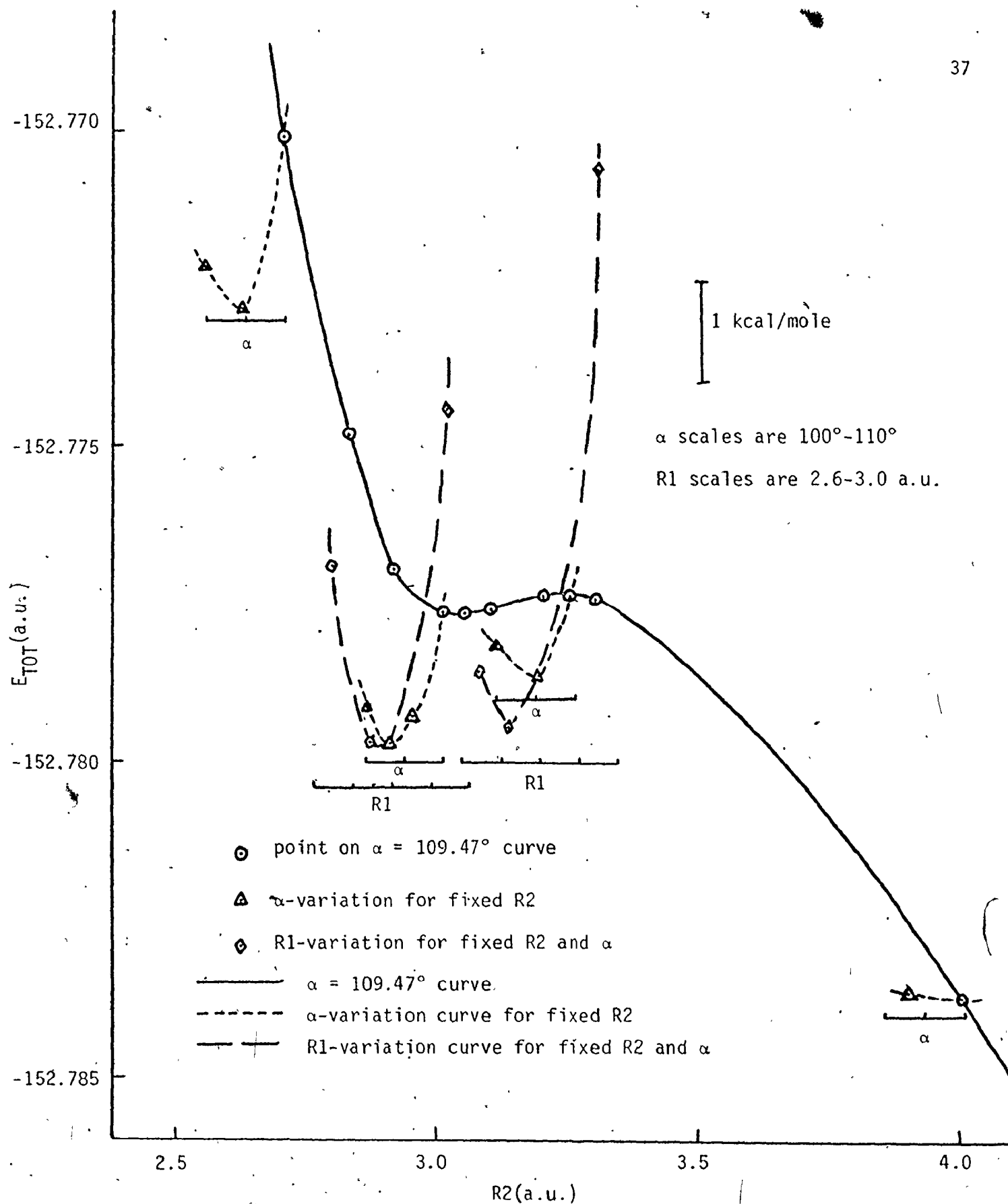


TABLE 8

Ethylene Oxide Triplet Energy Versus γ

Point ^a	Geometry ^b	α (degrees)	γ (degrees)	Energy (³ A) ^{c,e} (a.u.)	$\langle S^2 \rangle^c$	Energy Above Point 1(C _s) (kcal/mole)
1(C _s)	1	109.47	0.0	-152.77030	2.029	0.0
3(C ₁)	1 ^d	109.47	45.0	-152.76891	2.082	0.9
1(C _s)	1 ^d	109.47	90.0	-152.76096	2.025	5.9
32(C _s)	1 ^d	90.00	90.0	-152.76230	2.025	5.0

a Point group indicated in brackets.

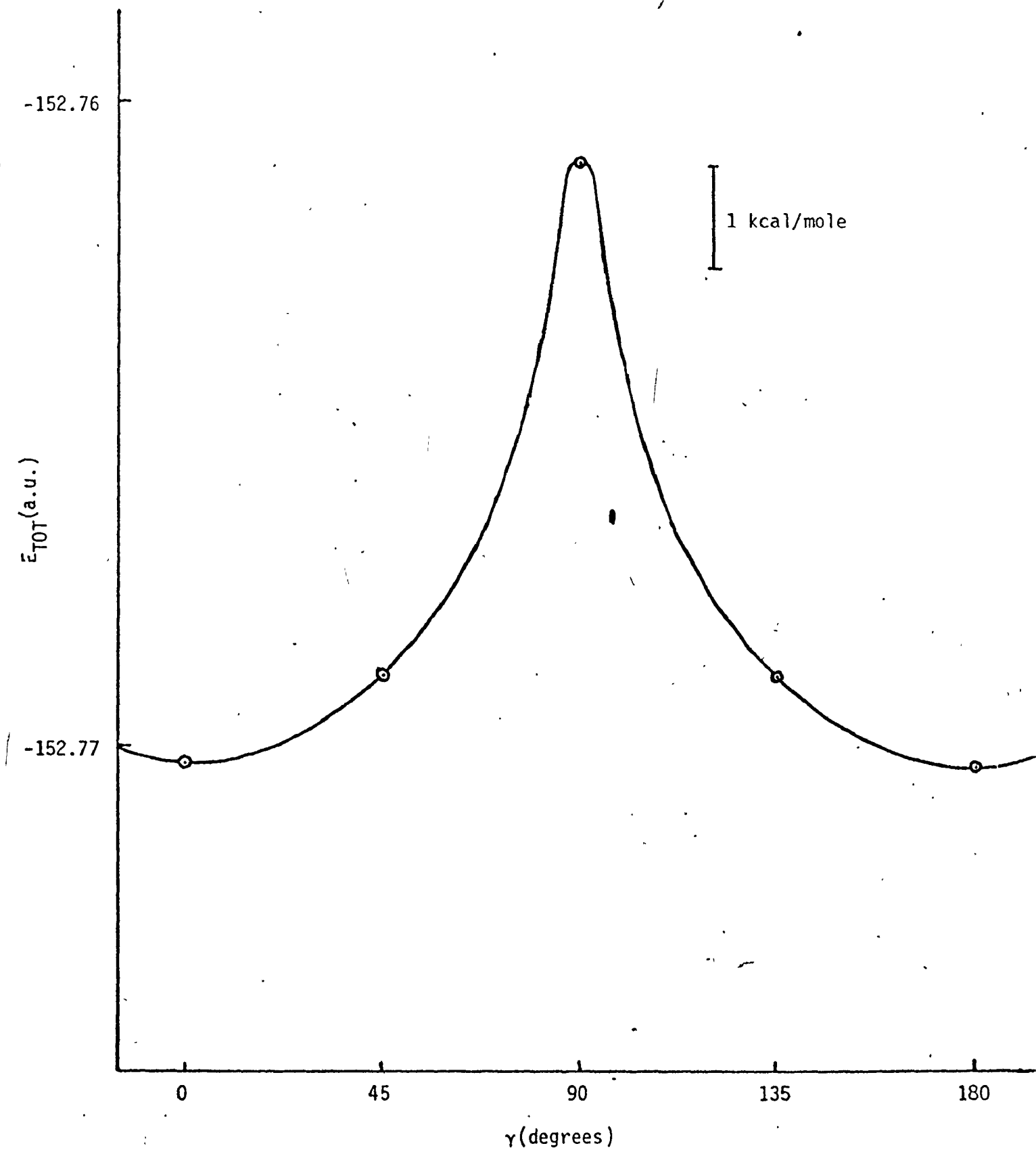
b All geometries based on that of Point 1(C_s).

c UHF wavefunction.

d Geometrical parameters indicated differ from those of Point 1(C_s) (see Table 7 for geometry of 1(C_s)).

e SCF energy converged to last digit included.

Figure 6. C_s Triplet Energy versus γ ($R_1 = 2.782$ a.u.; $R_2 = 2.714$ a.u.;
 $\alpha = 109.47^\circ$)



in energy. In comparison, the experimental rotation barrier of singlet ethylene is 65 kcal/mole.⁵³

4. Ring Closure

We next considered the energy required for closure of an opening triplet state to form the singlet product. This required calculation of the associated intersection of the singlet and triplet surfaces.

The singlet state lies below the triplet for C_{2v} geometries with internuclear distances typical of normal bonds (Figure 2). The relative positions of the surfaces are reversed for ring-open C_s geometries (Figure 4). Thus, the surfaces must cross at intermediate α values for $R_2 < 3.6$ a.u. Accordingly, we optimized the singlet-triplet crossing energy with respect to α and R_2 . All surface points used are included in Tables 5 and 7. The results are summarized in Table 9 and Figures 7 and 8.

The minimum energy required to reach a singlet-triplet surface intersection was found for $R_2 = 2.9$ a.u. and $\alpha = 83^\circ$. The energy barrier is 36 kcal/mole above the sum of the energies of the separated reactants, $C_2H_2(^1A_{1g})$ and $O(^3P)$. This is the lowest barrier found for addition in the triplet state yielding the ground state singlet product. In comparison, in the C_{2v} approach the triplet state encounters an energy barrier of 49 ± 5 kcal/mole (Figure 2) before intersecting the singlet surface.

5. Miscellaneous Data

During the course of the preceeding searches, it appeared useful to calculate the energies of several assorted surface points. These

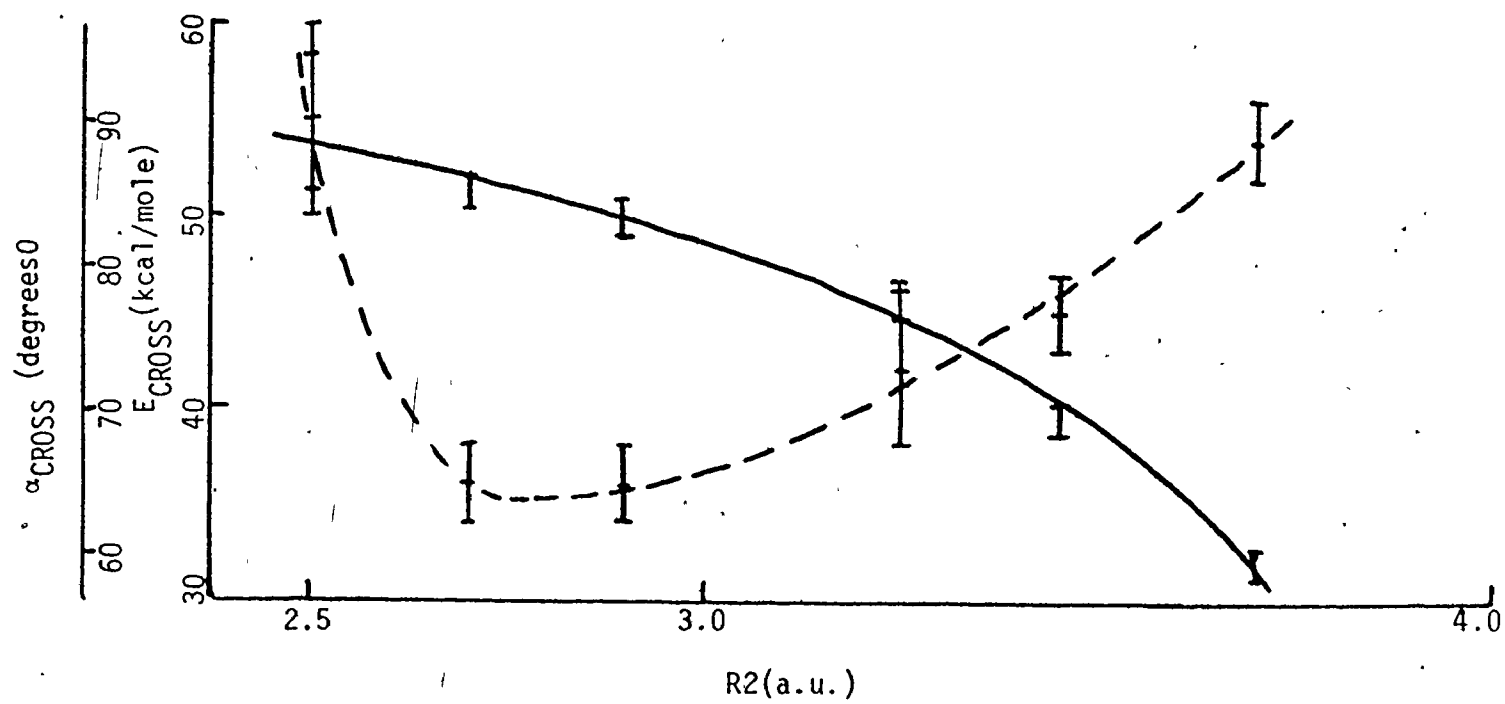
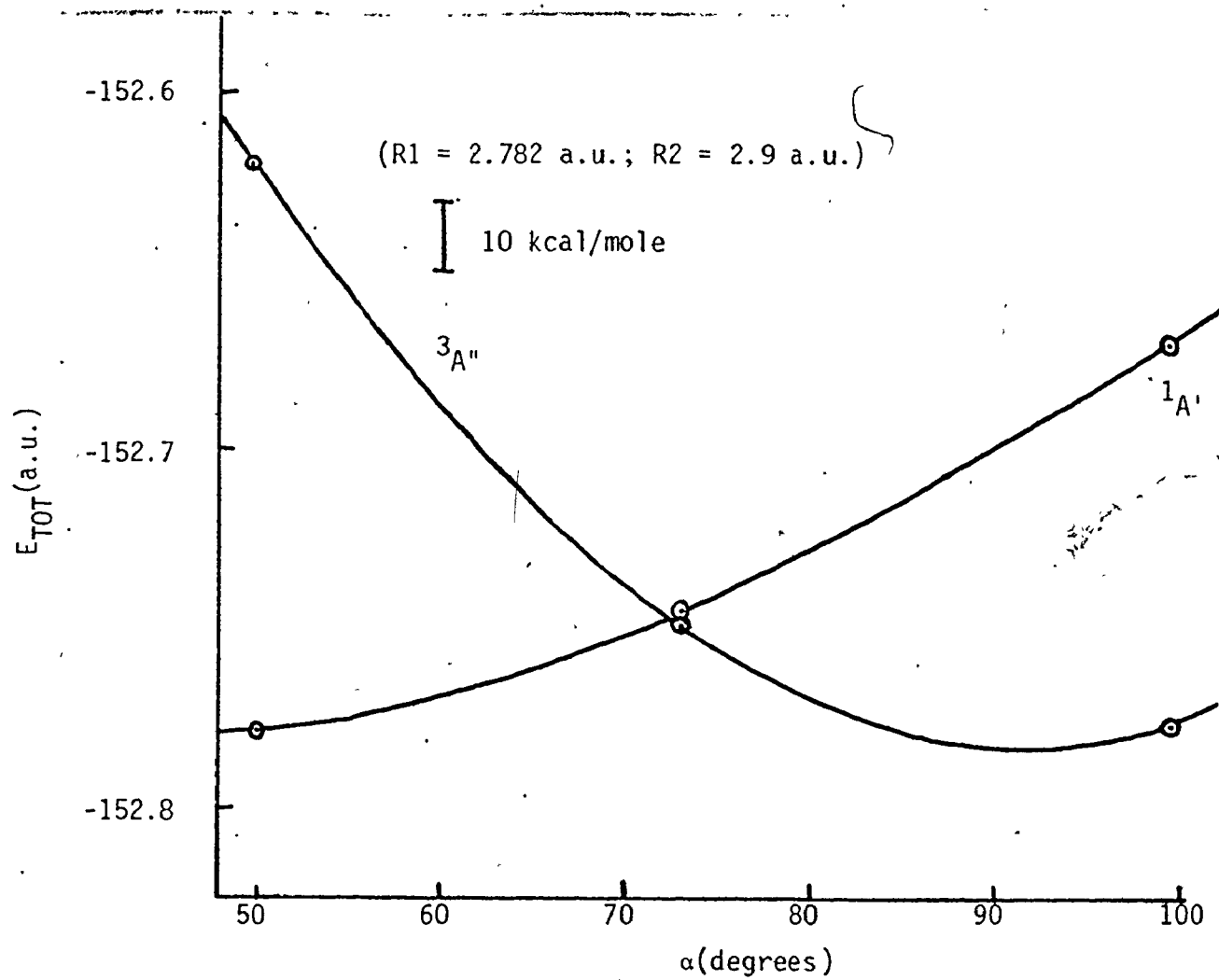
TABLE 9
Lowest Singlet-Triplet Crossing Energy (E_{CROSS}) and
Corresponding α Value (α_{CROSS}) Versus R_2

R_2 (a.u.)	E_{CROSS}^+ (a.u.)	α_{CROSS}^+ (degrees)
2.50	55 ± 5	90 ± 5
2.71	36 ± 2	85 ± 1
2.90	36 ± 2	85.5 ± 1
3.25	42 ± 4	77 ± 1
3.45	45 ± 2	69 ± 1
3.70	49 ± 2	59.5 ± 1

⁺ Uncertainty due to data interpolation.

Figure 7. Singlet and Triplet Energies Versus α ($R_1 = 2.782$ a.u.;
 $R_2 = 2.9$ a.u.)

Figure 8. Variation of Crossing Energy (---) and Crossing Angle α (—)
with R_2



are summarized in Table 10.

Point A was computed to observe the effect of pyramidalizing the terminal methylene carbon. This permits the non-bonding methylene spin density to occupy that region of space farthest from the oxygen density. This geometry change increased the lowest $^3A''$ state energy by 8 kcal/mole, and the lowest closed-shell $^1A'$ energy by 18 kcal/mole.

Point B was calculated to establish the effect of a $\gamma = 120^\circ$ rotation of the pyramidal methylene defined in point A. The triplet energy increased a further 3 kcal/mole, and the singlet 29 kcal/mole.

Point C was computed to obtain the methylene rotation barrier for the lowest singlet state in a C_{2v} geometry. A $\gamma = 90^\circ$ rotation increased the singlet energy 200 kcal/mole.

Point D was calculated to test the energy changes accompanying simultaneous symmetrical oxygen approach and opposed $\gamma = 45^\circ$ rotations of both methylenes. The triplet energy was found to lie 248 kcal/mole above the energy of the separated reactants. Such geometries of triplet attack are highly improbable.

In summary, we have computed enough of the lowest singlet and triplet surfaces to predict the respective preferred reaction paths. The singlet surface is slightly repulsive for asymmetric oxygen approach, and highly attractive for a symmetric C_{2v} approach after an initial energy barrier of about 10 kcal/mole is surmounted. Triplet attack was found to be repulsive; no stable intermediate was found. However, unsymmetrical C_s oxygen approach is much less repulsive than a C_{2v} attack. The energy barrier to terminal methylene rotation for the ring-opened geometry is only 6 kcal/mole for the triplet state. The

TABLE 10

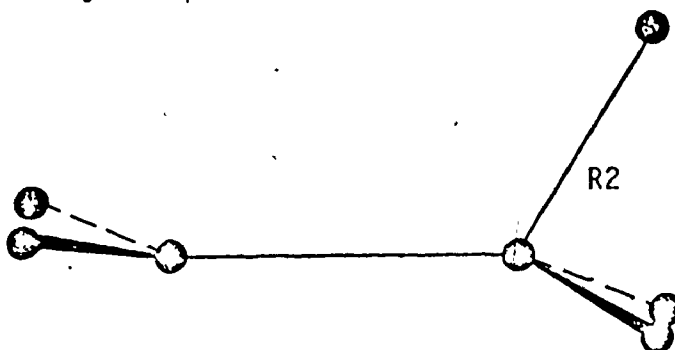
Miscellaneous Surface Points

Point	Geometry	Singlet Energy ^a (a.u.)	Triplet Energy ^{a,b} (a.u.)	$\langle S^2 \rangle^b$
29(C _s)	A	-152.63700	-152.76219	2.032
1(C ₁)	B	-152.5902	-152.75767	2.026
39(C _s)	C	-152.48169	----	---
1(C ₂)	D	----	-152.4088	2.022

^a SCF convergence to last digit included.

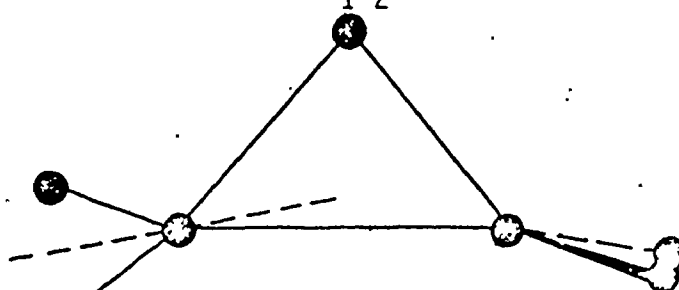
^b UHF wavefunction.

A Point 1(C_s) geometry except R2 = 2.810 a.u. and terminal methylene pyramidalized and inverted:

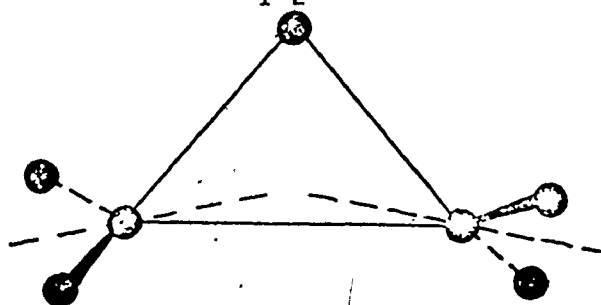


B As in A, only terminal methylene rotated 120°.

C Point 2(C_{2v}) geometry except terminal methylene is rotated around its group symmetry axis to be coplanar with C₁C₂O plane:



D Point 2(C_{2v}) geometry except methylenes rotated to be mutually perpendicular and each rotated to be 45° from C₁C₂O plane:



minimum energy barrier found for production of the ground state ethylene product from triplet reactant is 36 kcal/mole.

CHAPTER IV

INTERPRETATION

The potential surfaces presented in the previous chapter show how the electronic energies of the singlet and triplet cycloaddition species change with nuclear geometry. We can relate the observed differences in singlet and triplet chemistry to the general features of the surfaces. However, a description of the energy changes accompanying a reaction does not constitute a rationale for the underlying mechanism. We shall seek a consistent explanation by an interpretation of the changes in the total charge spin density distributions accompanying the variations in nuclear geometry.

For a system of N electrons, described by a wavefunction ψ , the total electronic charge density function, $\rho(\underline{r})$, is given by:

$$\rho(\underline{r}) = N \int_{\infty} \psi^*(\underline{x}_1, \underline{x}_2, \dots, \underline{x}_N) \psi(\underline{x}_1, \underline{x}_2, \dots, \underline{x}_N) d\underline{s}_1, d\underline{s}_2, \dots, d\underline{s}_N d\underline{r}_2, d\underline{r}_3, \dots, d\underline{r}_N \quad (9)$$

where \underline{x}_i denotes the space and spin coordinates of the i^{th} electron. The quantity $\rho(\underline{r})d\underline{r}$ gives the total amount of electronic charge in the volume element $d\underline{r}$. Integration of $\rho(\underline{r})$ over all space gives the total number of electrons in the system, N . That is,

$$\int_{\infty} \rho(\underline{r}) d\underline{r} = N \quad (10)$$

In an orbital approximation to ψ , equation (9) may be rewritten as

$$\rho(\underline{r}) = \sum_i n_i \phi_i^*(\underline{r}) \phi_i(\underline{r}) \quad (11)$$

where n_i is the occupation number of the i^{th} space orbital, ϕ_i . If one allows distinct space orbitals for α - and β -spin components of ψ (ϕ_j^α and ϕ_k^β , respectively), then $\rho(\underline{r})$ may be split into contributions from α - and β -orbital densities:

$$\begin{aligned}\rho(\underline{r}) &= \sum_j n_j \phi_j^{*\alpha}(\underline{r}) \phi_j^\alpha(\underline{r}) + \sum_k n_k \phi_k^{*\beta}(\underline{r}) \phi_k^\beta(\underline{r}) \\ &= \rho^\alpha(\underline{r}) + \rho^\beta(\underline{r}).\end{aligned}\quad (12)$$

The spin density distribution function, $\sigma(\underline{r})$, is defined as

$$\sigma(\underline{r}) = \rho^\alpha(\underline{r}) - \rho^\beta(\underline{r}) \quad (13)$$

whence $\sigma(\underline{r})d\underline{r}$ is the number of excess α -over β -electrons in the volume element $d\underline{r}$. Integration of $\sigma(\underline{r})$ over all space yields the total number of unpaired electrons in the system:

$$\int \sigma(\underline{r}) d\underline{r} = N^\alpha \quad (\text{or } -N^\beta),$$

where N^α and N^β are the net number of excess α - or β -electrons, respectively.

In general, a molecular charge distribution generated from a Hartree-Fock wavefunction is found to differ from that obtainable by fully correlated wavefunctions by less than 2% at all points.⁵⁵ Our LCAO-MO wavefunctions are not of Hartree-Fock accuracy. A double-zeta basis set such as we use may underestimate changes in charge distribution accompanying a chemical reaction by as much as 10%.⁵⁵ However, we are interested in the qualitative features of the charge and spin distributions and for this our wavefunctions are quite sufficient.

As an illustration of the features of typical charge, $\rho(\underline{r})$, and

spin, $\sigma(r)$, density maps, we include here the contour plots for the ${}^3B_{3u}$ states of ethylene in a planar nuclear geometry. Figure 9 contains the charge and spin density maps for two planes through the molecule: the plane containing the six nuclei, and the plane perpendicular to it which contains the carbons.

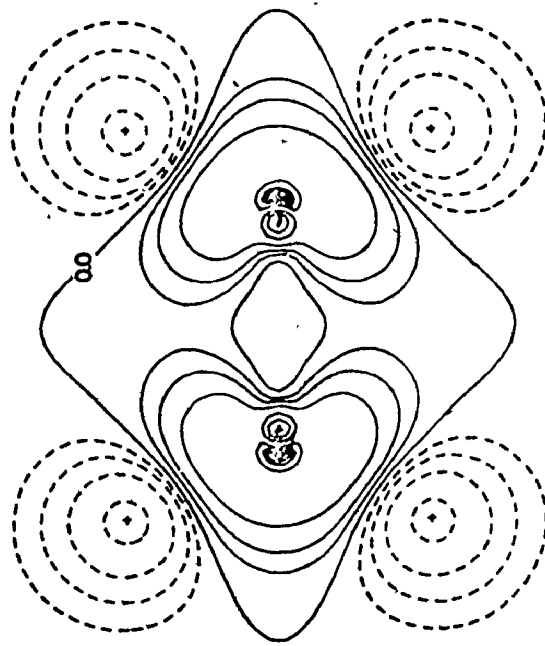
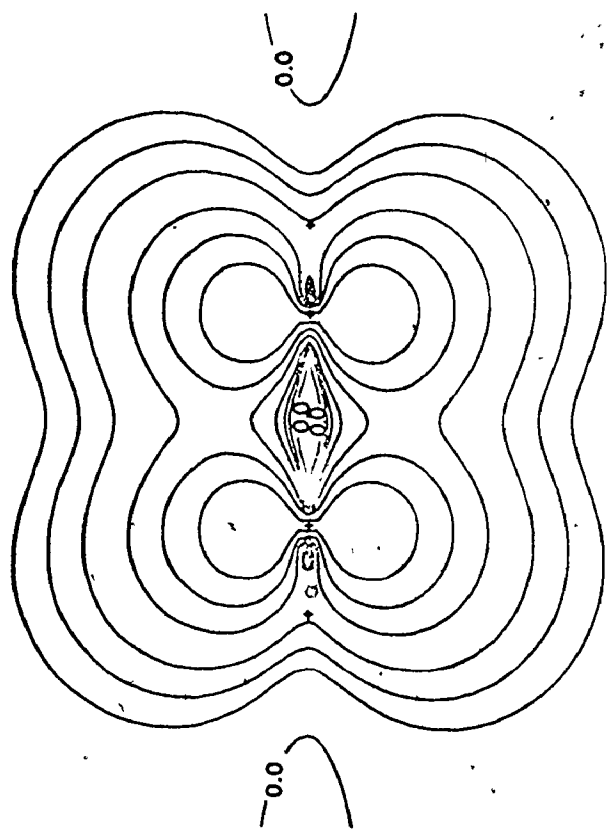
In this, and all the charge density maps presented in this work, the density contours plotted are in increasing value in the order 2×10^{-n} , 4×10^{-n} , 8×10^{-n} (a.u.) for n decreasing from 3. Thus, the outermost contour corresponds to a density of .002 a.u. It has previously been shown⁵⁶ that in general, the .002 contour encompasses over 95% of the electronic charge in a molecule.

The charge distribution is well-characterized by the two planes shown. The compact core density on the two carbons is quite evident, as indicated by the closely spaced nearly spherical contours surrounding these two nuclei. The chemical binding appears as the accumulation of charge between the nuclei, as indicated by the 0.2 contour surrounding all six nuclei. Whether or not the 0.2 contour encompasses two or more nuclei has been found⁴⁰ a useful indicator of the presence of charge accumulation sufficient to create a chemical "bond".

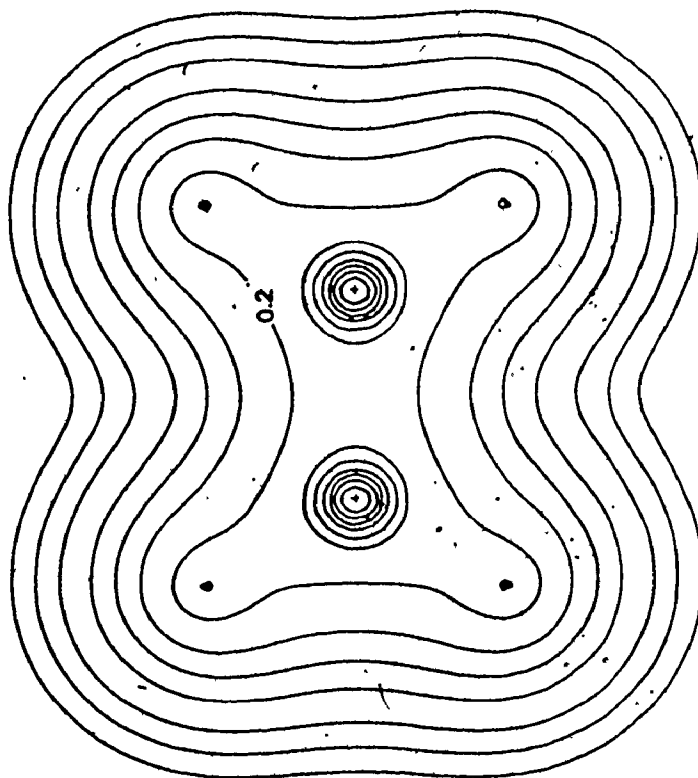
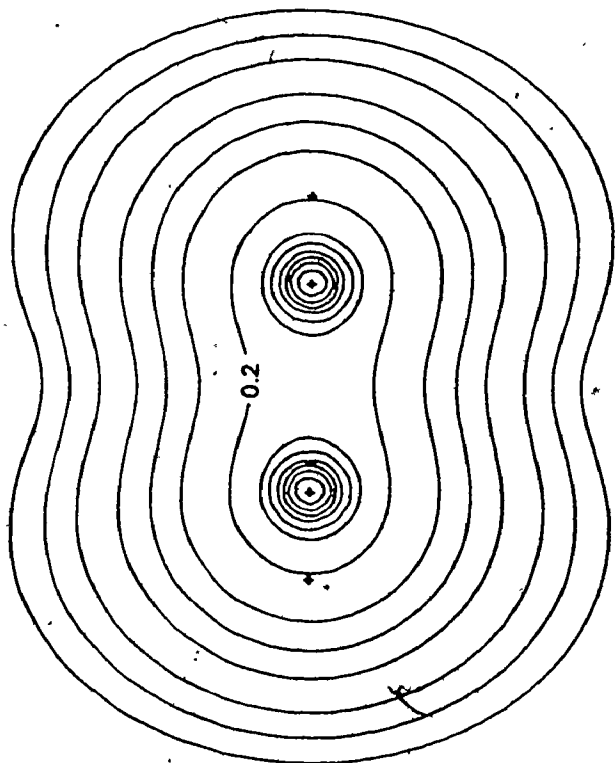
Consider now the two spin density plots for ${}^3B_{3u}$ ethylene. In both of these and all of the spin density contour maps presented here, the contours of excess α -or β -spin densities are indicated by solid or dashed curves, respectively. The solid line adjacent to a region of β -density indicates the zero contour (equal density of α -and β -spin). Both α -and β -density contours increase in the same increments as do the total charge density contours.

Figure 9. Total charge and spin density distributions for planar ${}^3B_{3u}$ ethylene. In all charge density maps, the contours increase in value from the outer boundary in steps of 2×10^n , 4×10^n , 8×10^n a.u. for increasing n , starting at $n = -3$. In all spin density maps, the contours increase from the 0.0 a.u. contour in steps of 2×10^n , 4×10^n , 8×10^n a.u. for increasing n , starting at $n = -3$. Regions of excess α density are indicated by solid contours, and excess β density by dashed contours. The top diagrams are in the plane perpendicular to the plane of the nuclei which contains the two carbon nuclei. The bottom diagrams are in the plane containing all the nuclei.

SPIN DENSITY



CHARGE DENSITY



The ${}^3B_{3u}$ ethylene spin density distributions of Figure 9 contain several prominent features.

In the plane perpendicular to the plane of the nuclei, one sees only contours of excess α density. The distribution is strongly reminiscent of the simplest molecular orbital description of this state of ethylene. Consider, for a moment, the ${}^3B_{3u}$ state as being obtained via a simple $\pi^* + \pi$ excitation from the ground ${}^1A_{1g}$ state. To a first approximation, the unpaired spin density is due to the occupation of the π and π^* orbitals by one α -electron each. Equally, one can consider there being one α -electron in the two mathematically equivalent localized orbitals corresponding to $(\pi \pm \pi^*)$. These localized orbitals are simply the two carbon p- π orbitals. Considering only the one spin density map, one sees a distribution which is an apparent sum of such orbital densities. Hence, the simple theoretical description given above seems quite adequate to this point. This model can be described by a RHF determinantal wavefunction wherein the spin density distribution for a triplet is calculated as the sum of the densities of two orbitals each containing one α -spin. All other spatial orbitals contain paired α and β density and contribute zero unpaired density everywhere.

However, these maps were generated from an UHF wavefunction. If one now considers the second spin density plot (in the plane of the nuclei), another feature is apparent. Surrounding each hydrogen nucleus is a region of excess β density, and this in a molecule constrained to have a net spin excess of 2α electrons. If one were to integrate over the regions of excess alpha density, one would find a total of

more than 2α -electrons. Thus, there has been a polarization of the molecular spin density, with excess α -density being localized on the two carbons, and excess β -density induced on the four hydrogens.

Spin densities are experimentally measured (through the associated magnetic moment distribution) by neutron diffraction.⁵⁹ Spin distributions for all states of a term differ only by a proportionality constant.⁶⁰

By definition, an UHF wavefunction permits different molecular orbitals for different spins (DODS). Each orbital is singly occupied, and all orbital densities contribute to $\sigma(r)$ at all points in space. Thus, polarization of the spin density into localized regions of excess α - and β -density may be described. The net spin density distribution results from a combination of both excess α -spin redistribution and α, β -spin uncoupling. UHF wavefunctions can be expected to reproduce in detail the pattern of spin distribution in molecules calculated using more extensive functions.⁴⁰

The Insertion/Abstraction Reactions

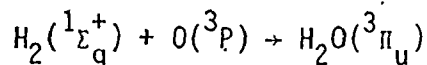
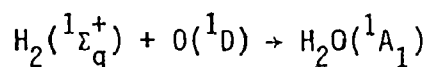
We now discuss a proposed rationale of the insertion/abstraction reaction mechanisms based on the concepts of spin transfer and polarization. This will serve to illustrate more fully the changes in charge and spin density accompanying a specific chemical reaction. Furthermore, as we shall see, the insertion/abstraction and cycloaddition reactions have closely related mechanisms in terms of the spin distributions.

The insertion/abstraction studies⁴⁰ were carried out on the model system of $H_2(^1\Sigma_g^+)$ plus $O(^3P)$ or $O(^1D)$. To completely specify such a three-nucleus potential surface, one requires three independent internal coordinates. Those chosen were r_H , the H-H distance; r_O ,

the distance from O to the midpoint of r_H ; and α , the angle between r_O and r_H .

Insertion Reactions

The minimum energy paths for $\alpha = 90^\circ$ (fixed) were found by optimization with respect to r_H for several values of r_O from infinity (isolated reactants) to zero (linear H-O-H). The reactants were thereby constrained to a C_{2v} geometry ($D_{\infty h}$ for the linear cases). The overall reactions corresponding to the insertion reaction paths thus defined may be written as:



The singlet potential surface, after less than a 10 kcal/mole barrier at long range, is downhill attractive to the ground state (triangular) equilibrium geometry with an OH bond length of 1.80784 a.u. and bond angle of $111^\circ 42'$. The linear geometry has an energy 33 kcal/mole above that of the equilibrium configuration.

The triplet C_{2v} surface is strongly repulsive to a maximum of 80 kcal/mole above the energy of the separated reactants, then drops to an energy minimum for a linear geometry (still 67 kcal/mole above the energy of the separated reactants). At each value of r_O , the optimum value of r_H is larger than for the singlet. The triplet intermediate is unstable with respect to unsymmetrical motion of the nuclei leading to the abstraction products $OH(^2\Pi) + H(^2S)$ for all values of r_O . Note that the general behaviour of these surfaces, i.e., singlet attractive and triplet repulsive, is identical to the corresponding surfaces for

the C_{2v} cycloaddition reactions.

Total charge density plots for four r_0 values on the singlet and triplet paths are shown in Figure 10. At $r_0 = 2.00$ a.u. both singlet and triplet distributions show a pinching of the 0.2 a.u. contour surrounding the hydrogen nuclei due to the increasing r_H value. However, at shorter r_0 values, the singlet and triplet distributions take on distinctly different character corresponding to the energy decreasing for the singlet case and increasing for the triplet case. The charge density of the singlet species becomes increasingly more compact, with high density (0.2 a.u.) contours encircling all three nuclei (an indication of a high accumulation of charge density between the nuclei) in the ground state and linear geometries. In contrast, the triplet distribution is very diffuse, and the charge density is largely localized on the individual nuclei (rather than between them), an effect most pronounced in the linear geometry, where all three nuclei are individually encompassed by a 0.2 a.u. contour.

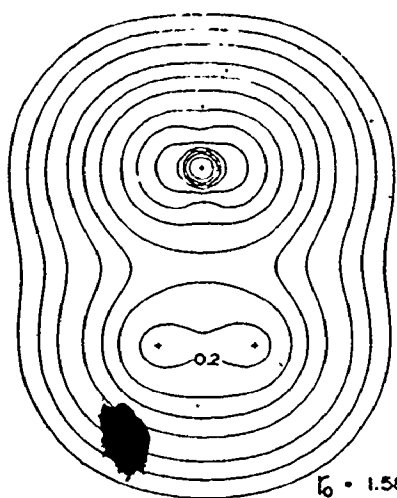
We can correlate the differences in optimum r_H value and charge distributions for singlet and triplet states directly with the associated spin density distributions. The plots are for the $M_S = 1$ component. One spin is localized in a distribution near the oxygen nucleus with maximum values in a plane perpendicular to that shown. Figure 11 contains the spin density distributions for five points on the triplet path. Even at $r_0 = 4.00$ a.u., one can see a polarization of the spin density, as evidenced by the regions of α -density localized on the two protons. Both effects increase as r_0 is decreased, the increasing α -density in the region of each proton also becoming more localized in

Figure 10. Total charge distributions in the plane of the nuclei for the symmetrical $H_2 + O$ singlet and triplet insertion reactions.

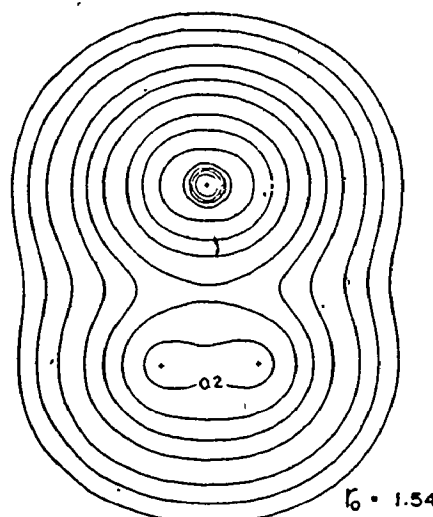
SINGLET

TRIPLET

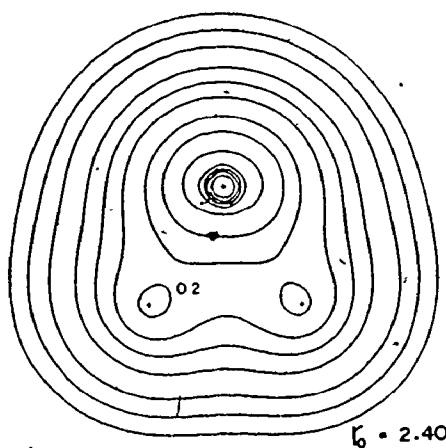
54



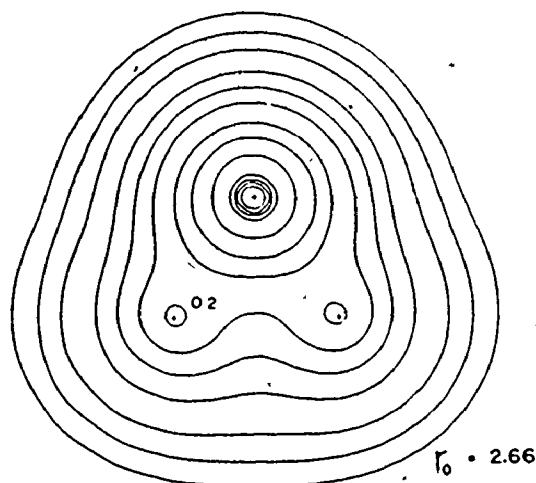
$l_0 = 3.00$



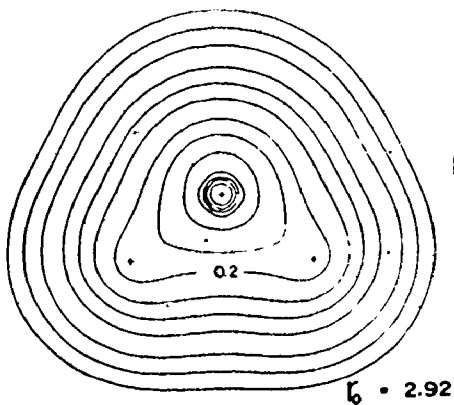
$l_0 = 1.54$



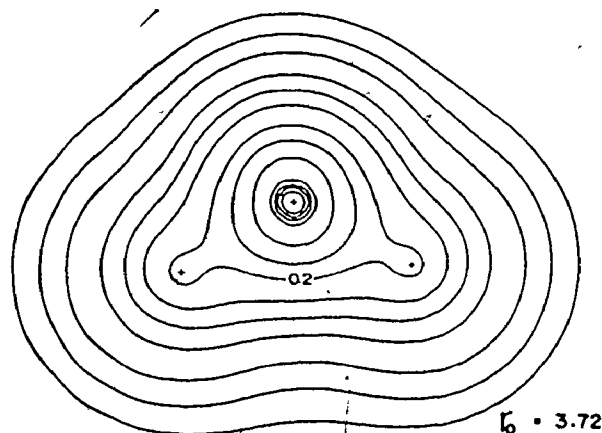
$l_0 = 2.00$



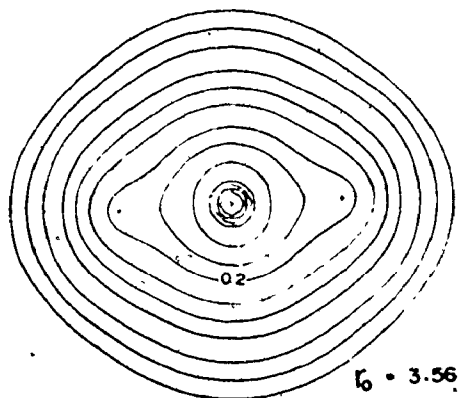
$l_0 = 2.66$



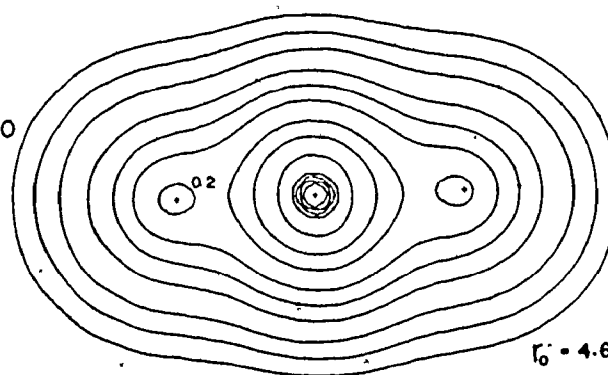
$l_0 = 1.11$



$l_0 = 3.72$

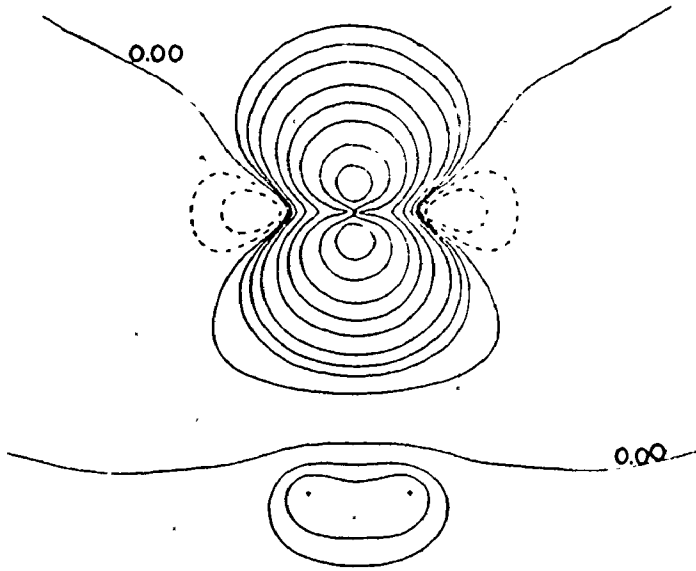
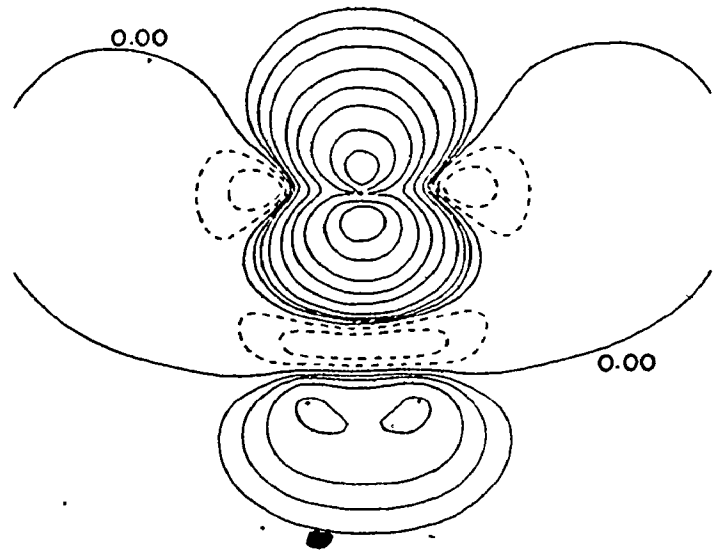
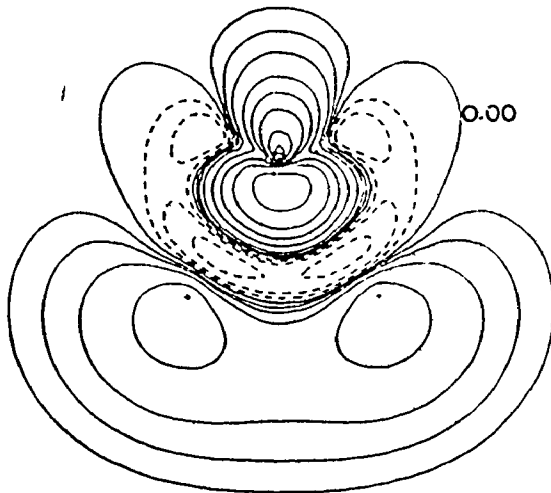
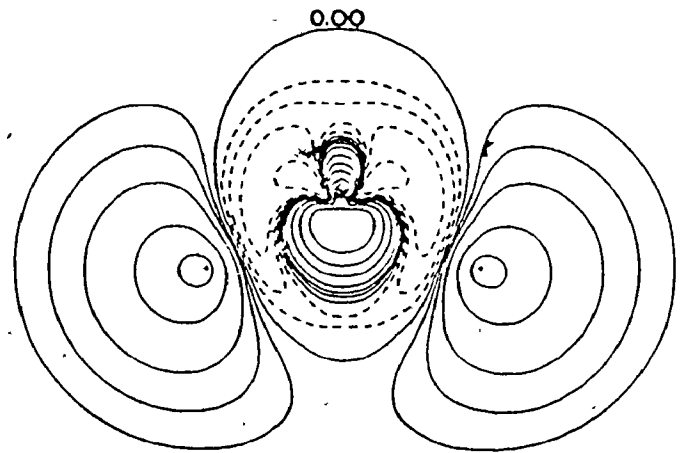
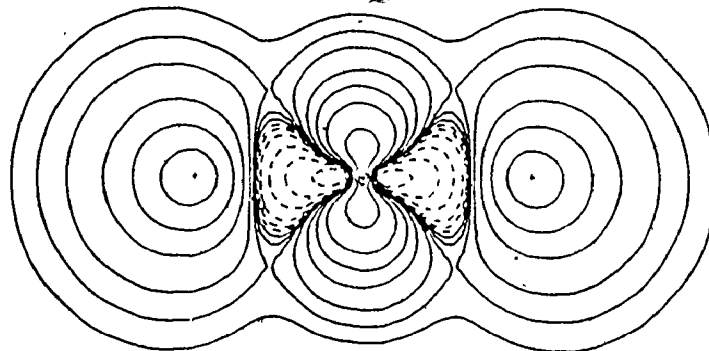


$l_0 = 0.00$



$l_0 = 4.61$

Figure 11. Spin density distributions for the symmetrical $\text{H}_2 + \text{O}$ triplet insertion reaction.


 $r_0 = 4.00$

 $r_0 = 3.00$

 $r_0 = 2.00$

 $r_0 = 1.11$

 $r_0 = 0.00$

the non-bonding region. Comparison of the charge and spin density distributions for the linear geometry indicate that 80-100% of the charge density near each proton is of α -spin.

These observations lead to a simple interpretation of the mechanism of triplet addition. The transfer of α density to the region of each proton constitutes a quasi-excitation of H_2 to its unbound $^3\Sigma_u^+$ state, which is characterized by localized distributions of α density near each proton and polarized into the non-bonding regions.

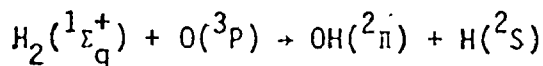
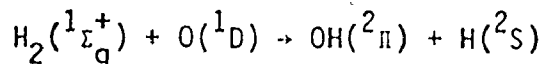
The weakening of the H_2 binding may be attributed directly to the restrictions the Pauli principle imposes on the (primarily α -spin) charge distribution near each proton. That is, the Pauli principle requires⁵⁷ that

$$\lim_{r_1 \rightarrow r_2} \rho(r_1, r_2) = 0$$

Thus, significant compact accumulation of charge density in the internuclear regions of the incipient molecule is precluded for a charge density composed primarily of α -spin. Hence, the triplet surface is strongly repulsive. At the minimum energy linear geometry, the α -spin distributions on the protons are most widely separated and regions of β density accompanying the oxygen nucleus permit some charge accumulation in the binding regions between the nuclei (but much less than for the singlet state).

Abstraction Reactions

The minimum energy singlet and triplet paths were also studied for $\alpha = 0^\circ$ (fixed). The abstraction reactions thus defined may be written



Both singlet and triplet potential surfaces were found to contain double minima for $r_0 \geq 2.7$ a.u., for the energy taken as a function of r_H . The minima correspond to the central proton being bonded to the end proton ($\text{H} - \text{H} + \text{O}$) or to the oxygen ($\text{H} + \text{H} - \text{O}$). The triplet geometry of maximum energy is predicted to be 35.2 kcal/mole above the energy of the separated reactants, and the singlet maximum 24.7 kcal/mole above the sum of the energies of its isolated reactants.

Comparison of these surfaces with those for the C_{2v} approach shows that the singlet species prefers a symmetric C_{2v} insertion (with essentially no activation energy), while the triplet prefers the less repulsive linear abstraction reaction.

We can find a consistent description of the differing singlet and triplet tendencies for abstraction through the associated charge and spin density distributions, Figures 12 and 13. The total charge distributions show that up to the transition state ($r_0 = r_t = 3.125$ a.u. (singlet) and 3.150 a.u. (triplet)), the singlet oxygen perturbs the hydrogen molecule more than does the triplet. The singlet surface shows charge localization around the hydrogens, corresponding to significant weakening of the H_2 bond. In contrast, the triplet maps indicate that the H_2 binding density remains substantial. The transition state of the singlet shows marked loss of density near the end proton, whereas the triplet transition state charge density shows a separation of the H_2 reactants into an H atom plus a proton partially bonded to the oxygen.

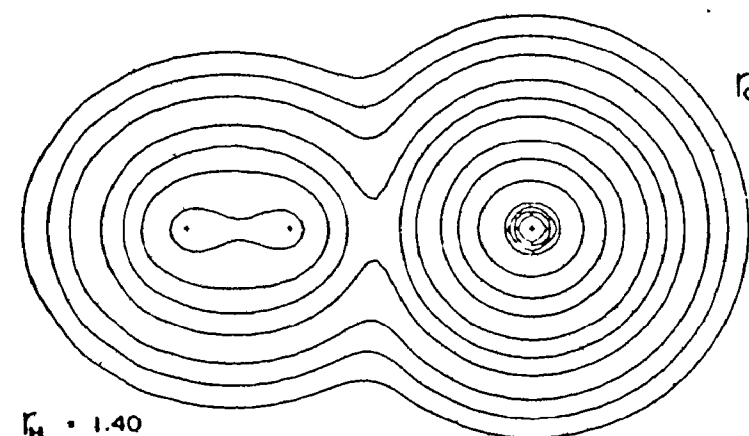
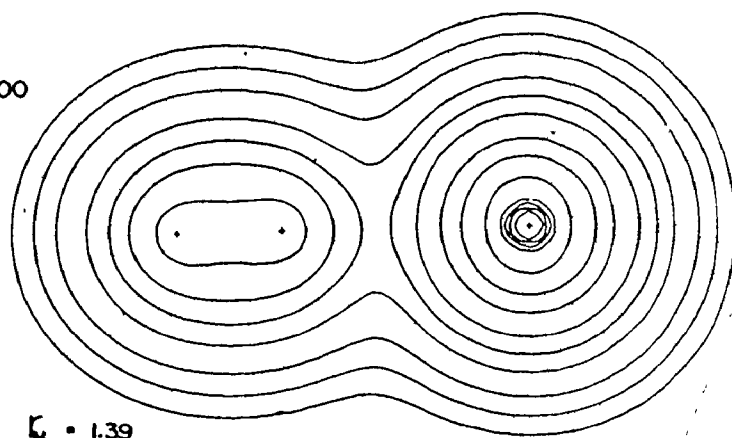
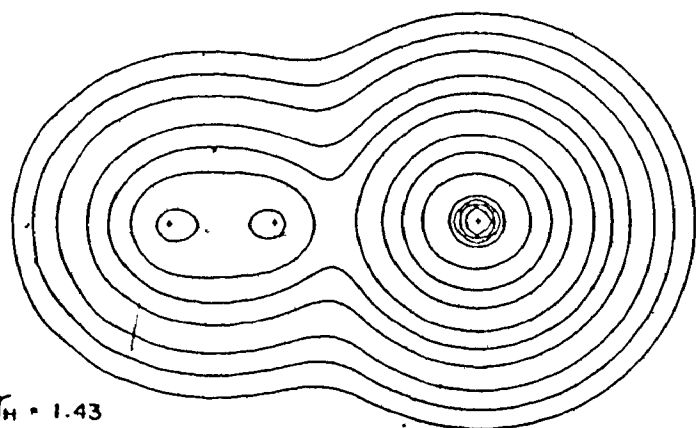
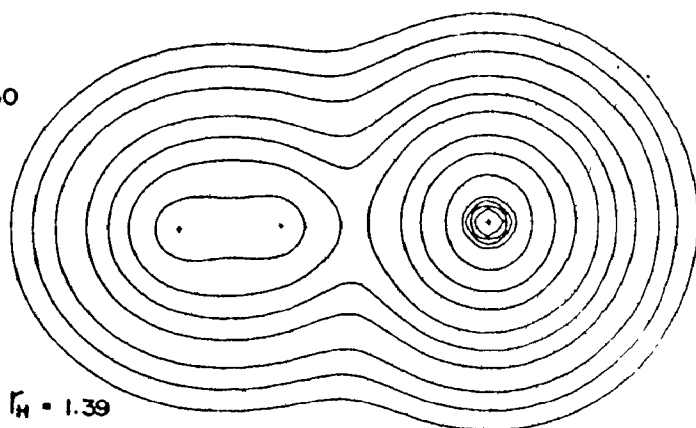
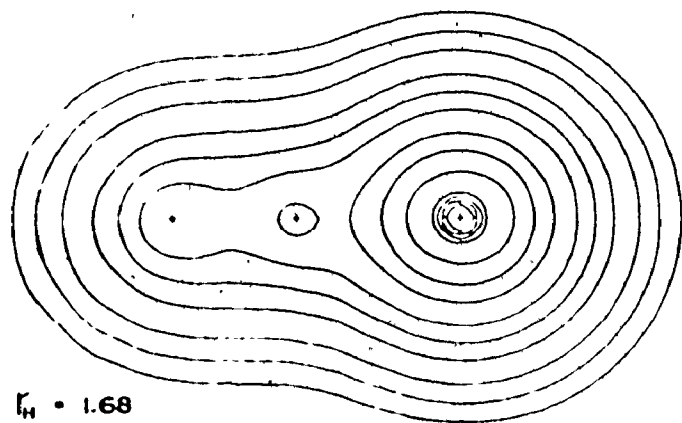
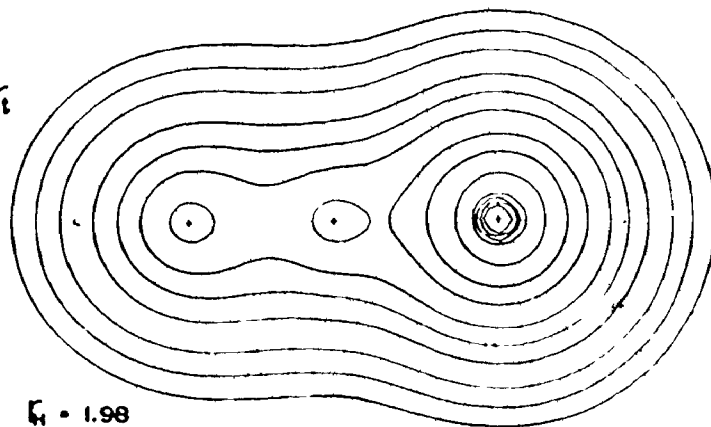
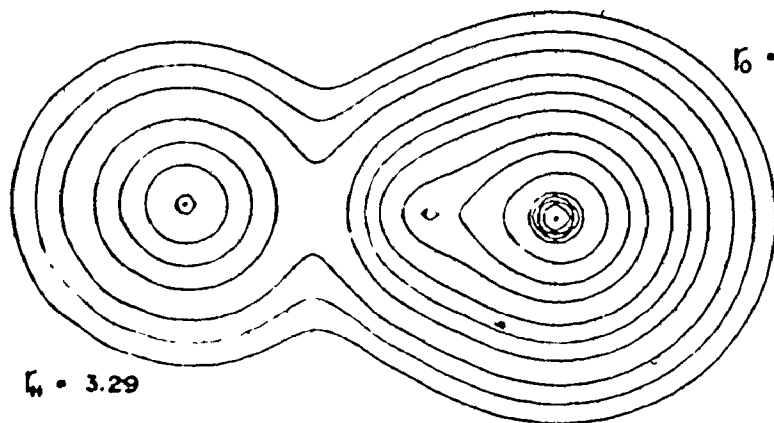
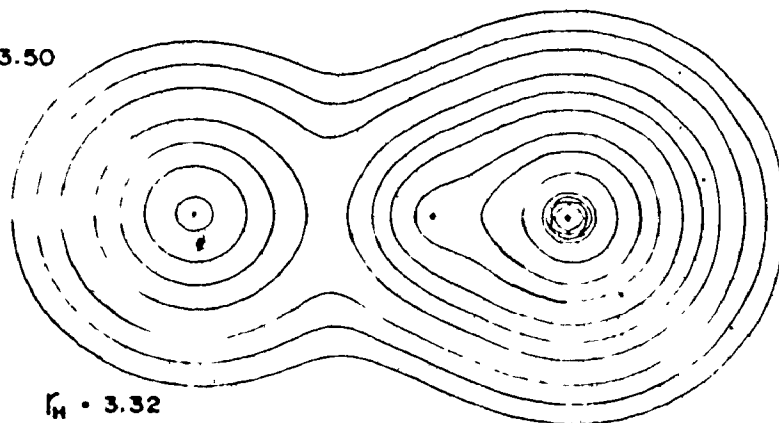
Figure 12. Total charge distributions for the singlet and triplet
 $\text{H}_2 + \text{O}$ abstraction reactions.

>

SINGLET

TRIPLET

58

 $r_H = 1.40$  $r_H = 1.39$  $r_H = 1.43$ $r_0 = 3.50$  $r_H = 1.39$  $r_H = 1.68$ $r_0 = r_c$  $r_H = 1.98$  $r_H = 3.29$ $r_0 = 3.50$  $r_H = 3.32$

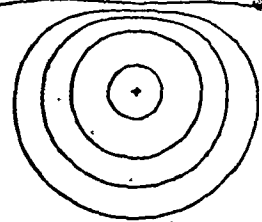
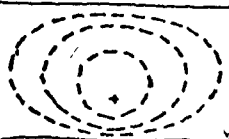
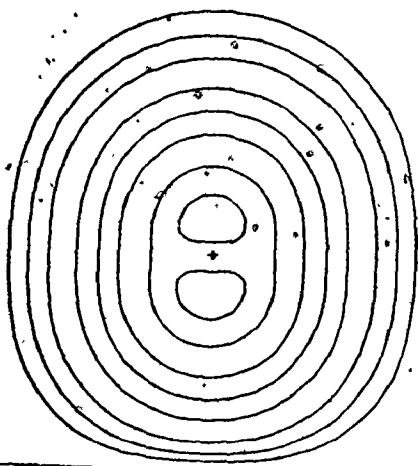
After passing through the transition state, both singlet and triplet distributions have the characteristics of a separating H atom and hydroxyl radical.

The spin density maps in Figure 13 show the reason why the triplet energy path is lower for linear abstraction than symmetric insertion. The maps are again of the $M_S = 1$ triplet component and are axially symmetric. The end-on approach of the triplet oxygen induces an uncoupling of the initially paired α - and β -spin distributions of the hydrogen molecule. Thus, $\sigma(r)$ (which is everywhere zero for the isolated H_2 molecule) shows a migration of α -density to the end proton and a counter-migration of a lesser amount of β -density to the central proton. Since less β -than α -density is induced, there has been a net migration of α density from the oxygen to H_2 . The transition state density shows equal accumulation of excess α -density on the oxygen and terminal proton, as required for the production of two doublet state products. Comparison of the charge and spin density maps in the triplet transition state geometry shows that about 90% of the charge density on the end proton is of α -spin.

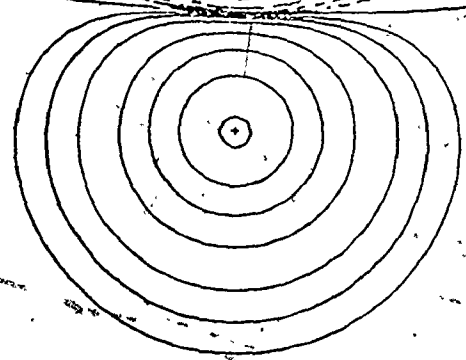
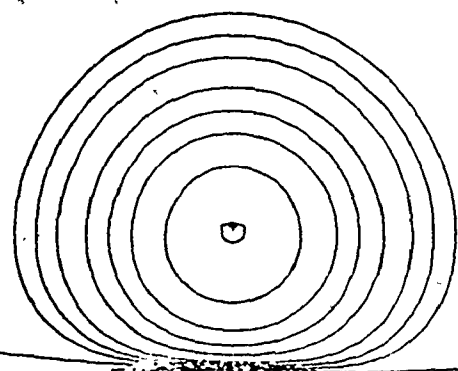
These results may be generalized to the whole class of insertion/abstraction reactions. For the symmetrical C_{2v} approach of a triplet reactant to singlet substrate, there are equal localizations of excess spin density of one type on both substrate nuclei. This weakens the bond between them and forces an increase in their optimum separation distance along the reaction path. Furthermore, the spin polarization precludes strong bonding between the substrate and insertion species. For a linear attack, the induction of α - and β -migrations in

Figure 13. Spin density distributions for the triplet abstraction reaction.

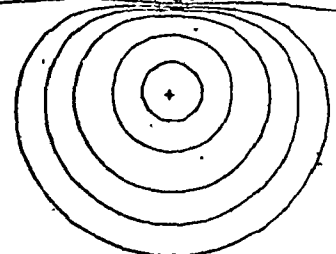
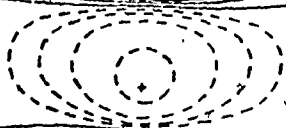
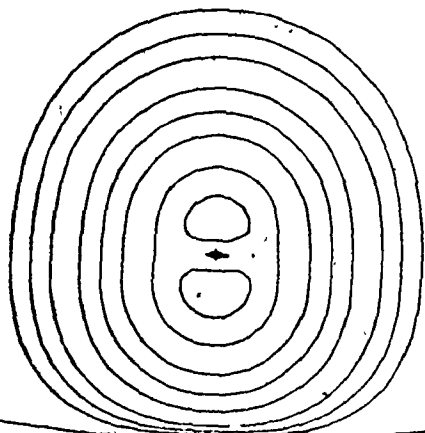
The map in the upper right corner is for the initial stage of the reaction, and that in the lower left-hand corner for the separating products $H + OH$.



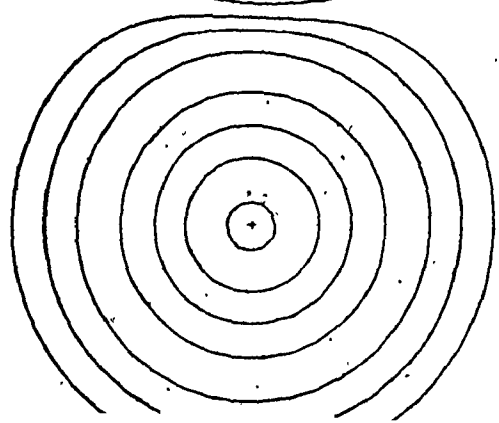
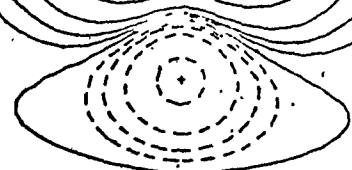
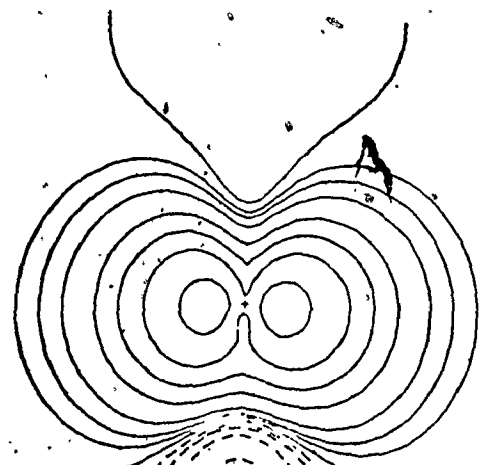
$r_0 = 4.00$
 $r_H = 1.39$



$r_0 = 3.23$
 $r_H = 1.98$



$r_0 = 3.50$
 $r_H = 1.39$



$r_0 = 3.50$
 $r_H = 3.29$

opposite directions accomplishes an uncoupling of the spins of the substrate bond. This allows simultaneous formation of the product bond to occur during the breaking of the substrate bond. Thus the activation energy is reduced over that required for symmetrical insertion where the substrate bond is broken and no new bonds between O and H are formed. As the angle α is decreased from 90° to 0° , there will be a smooth transition from the spin polarization characteristic of insertion to that of abstraction. Correspondingly, the energy will show a decrease as more oxygen bonding is permitted to one of the hydrogens.

Cycloaddition Reactions

We are now in a position to correlate the features of the singlet and triplet cycloaddition potential surfaces of our model system to the accompanying changes in the charge and spin density distributions.

We shall also deduce reaction mechanisms explaining the experimentally observed differences in the singlet and triplet product stereochemistries and see the close parallel to the insertion/abstraction reactions.

1. C_{2v} Oxygen Approach

Consider first the C_{2v} mode of attack, wherein the oxygen approaches along the bisector of the ethylene carbon-carbon bond perpendicular to the plane of the six nuclei.

The singlet reaction encounters a barrier of 10 kcal/mole for oxygen about 4 a.u. away and proceeds downhill to the ground state

ethylene oxide product geometry. In contrast, the triplet energy remains low until R_2 (oxygen to midpoint of C-C separation) = 4.0 a.u.; it then faces a rapidly increasing energy barrier and crosses the singlet surface at $R_2 = 3.25$ a.u. The barrier is 75 kcal/mole at $R_2 = 3.0$ a.u. and 145 kcal/mole at $R_2 = 2.31$ a.u. away. As previously noted, the overall nature of these surfaces parallels that of the $H_2 + O$ C_{2v} approach.

Figure 14 contains the singlet and triplet charge distributions for three points on the symmetric surfaces. For $R_3 = 4.0$ a.u., both charge distributions show the initial significant overlap of the reactant densities. At $R_3 = 3.0$ a.u., the distributions for the two states are still almost superposable. However, for $R_3 = 2.31$ a.u., the singlet distributions contain wide belts of high (0.2 a.u.) density between all three heavy nuclei, indicative of the strong ring binding of the ground state equilibrium geometry. In contrast, the triplet density while very similar to the singlet in the non-bonded regions exhibits much lower charge accumulation between the nuclei. The 0.2 contour is still localized around the ethylene and oxygen fragments. Thus the incipient carbon-oxygen binding in the triplet state is much weaker than that of the singlet at this geometry, corresponding to the high triplet energy calculated.

An explanation for this weak bonding along the triplet path can be found in the associated spin density distribution. Plots of $\sigma(r)$ in the plane of the heavy nuclei are given in Figure 15. The UHF wavefunctions used are those presented in Chapter III and are for the $M_S = 1$ component of the triplet. One of the two unpaired

Figure 14.. Total singlet and triplet charge distributions (in the plane of the heavy nuclei) for C_{2v} oxygen approach to C_2H_4 . The oxygen is at the top of each map.

SINGLET

TRIPLET

R3 = 4.0

R3 = 3.0

R3 = 2.31

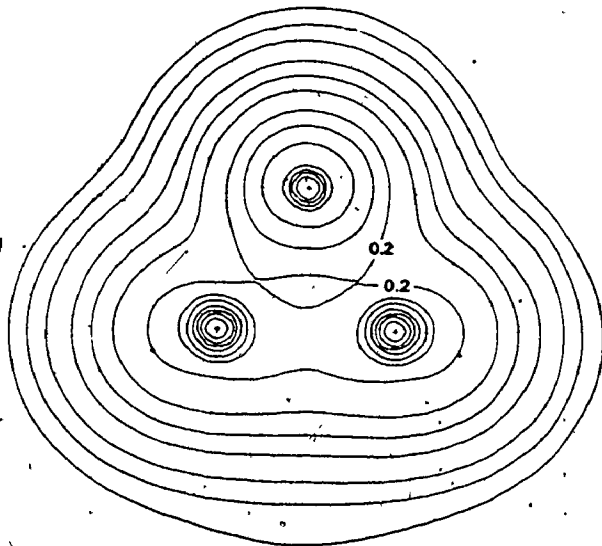
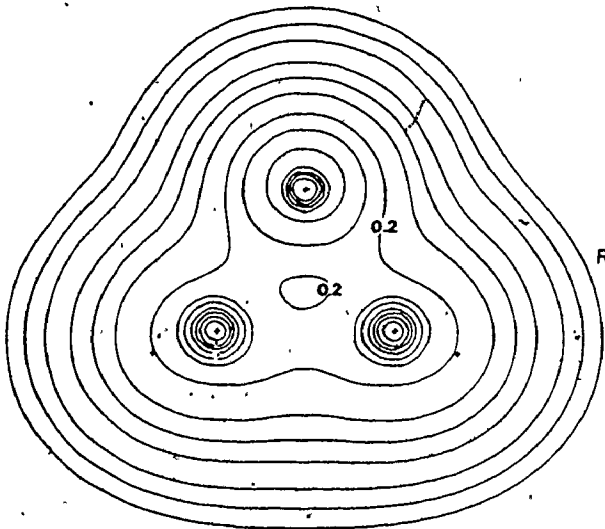
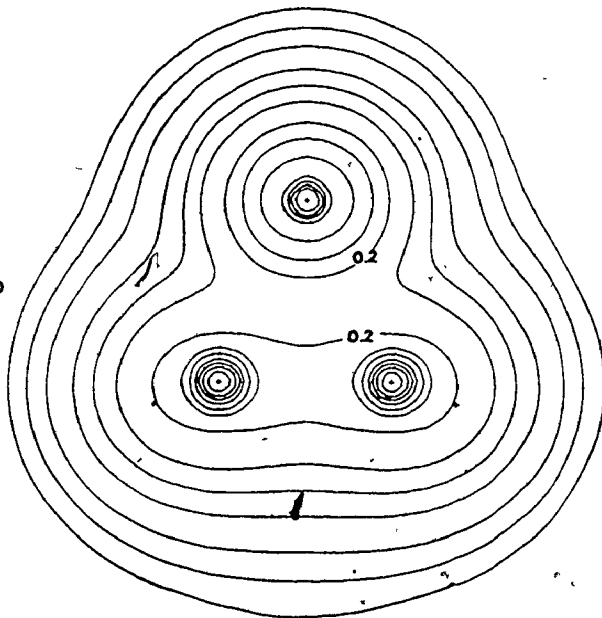
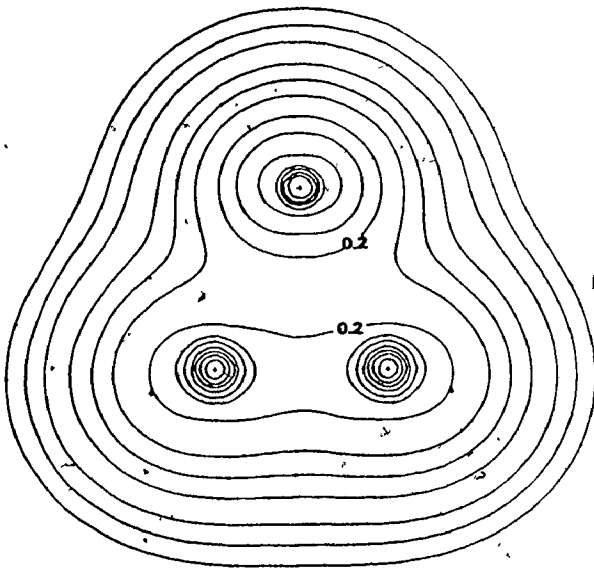
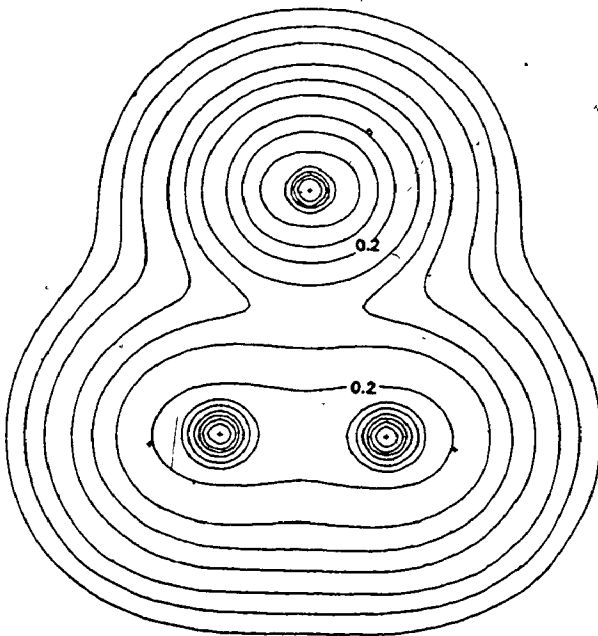
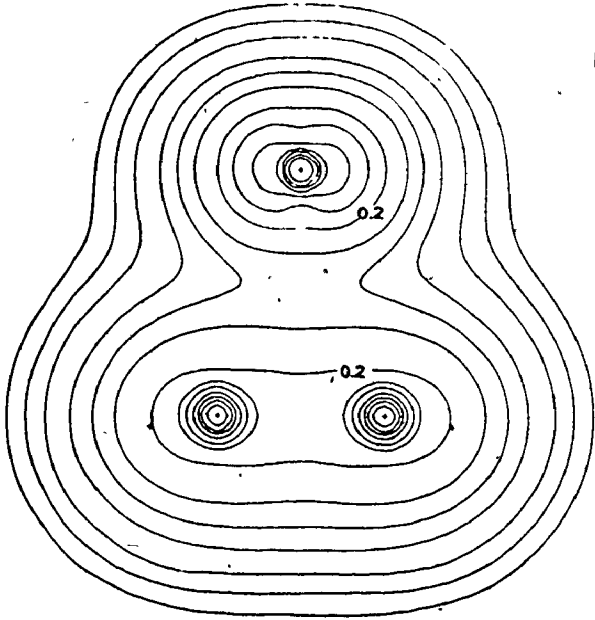
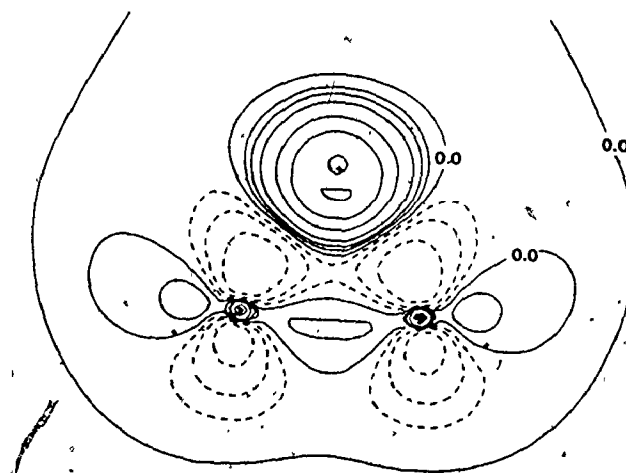
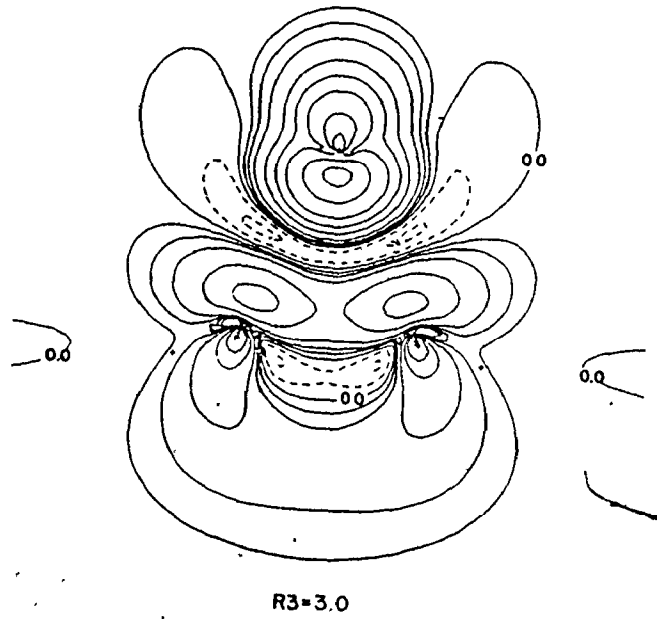
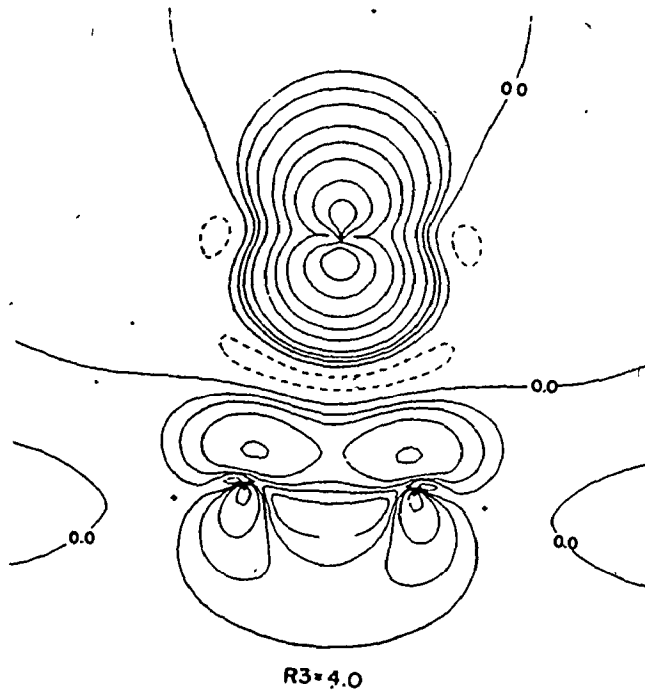


Figure 15. Triplet spin distributions (in the plane of the heavy nuclei) for C_{2v} oxygen approach to C_2H_4 . The oxygen is at the top of each map.



electrons remains localized largely on the oxygen in the plane containing R3 and perpendicular to the plane of the heavy nuclei. At $R3 = 4.0$ a.u., spin polarization is already apparent. There is a π -like distribution of α -density on the ethylene carbons, and small regions of excess β -density near the oxygen. For $R3 = 3.0$ a.u., these effects are more pronounced, and additionally a small region of excess β -density appears between the carbons. A large excess of α -density has been localized in the π -region of the two carbons. The pattern of spin polarizations (including small regions of β -density on each proton not shown here) is strongly reminiscent of that of the triplet ethylene molecule (Figure 9) modified, of course, by the increased carbon-carbon distance and presence of oxygen spin density. This polarization suggests the simple interpretation that the transfer of α -density from oxygen to the π -region of both carbons is inducing a quasi-excitation of the ethylene to its lowest triplet (T) state. This rationale is consistent with the energy of this geometry being 45 kcal/mole above the separated reactants. (The T + N excitation energy of ethylene was computed to be 75 kcal/mole in our basis set.)

The spin distribution for oxygen approach to $R3 = 2.31$ a.u. shows marked variation from the preceeding plots. The π -distribution of α -density near the carbons has been completely supplanted by an excess of β -density. What excess α -density remains near the carbons is localized in a σ -distribution along the carbon-carbon axis. The total system energy is now 145 kcal/mole above that of the separated reactants, far more than that needed to effect the previously hypothesized T + N ethylene excitation. The qualitative divergence of

spin distribution from its previous characteristics is therefore to be expected.

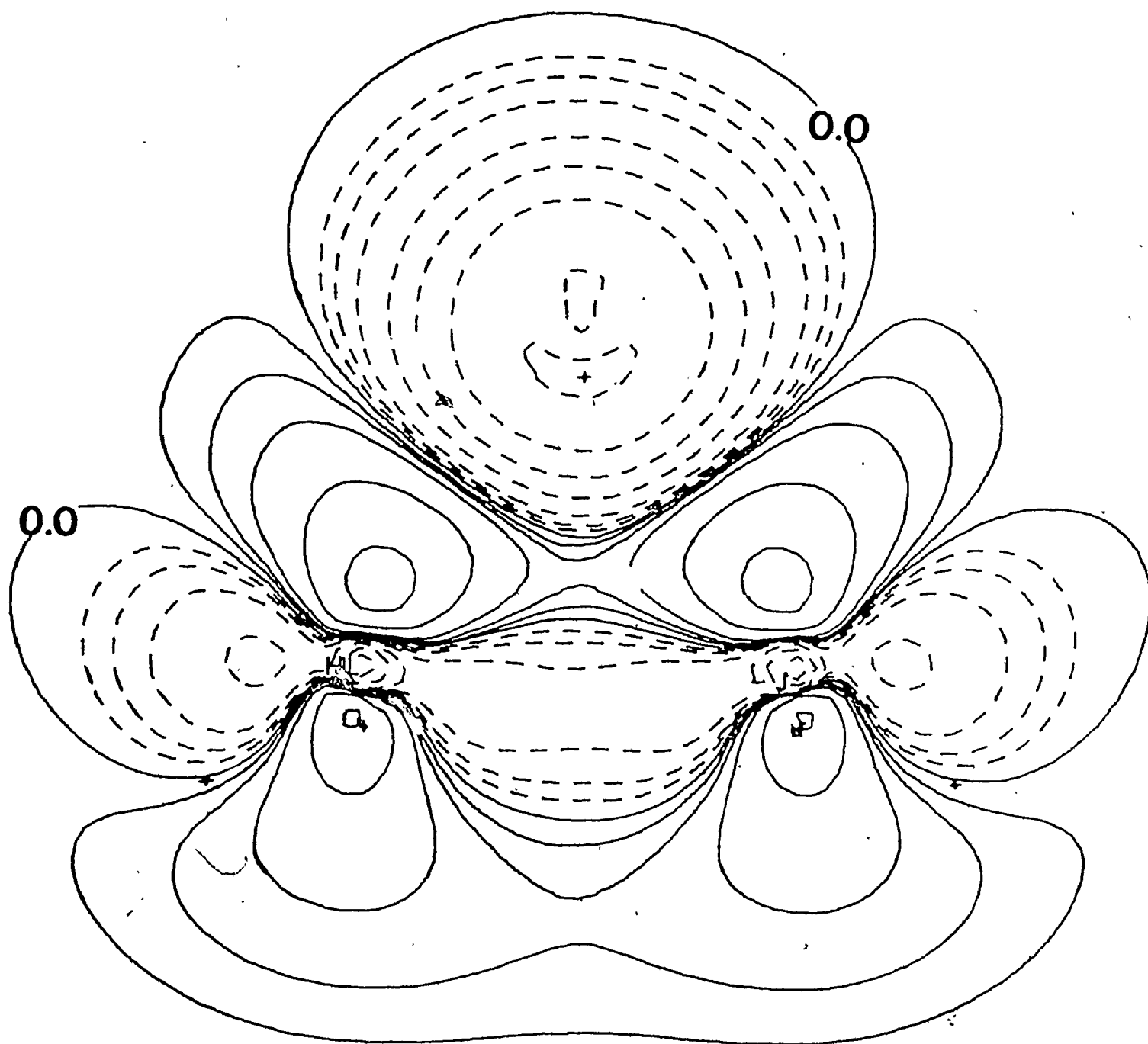
The difference in total charge distributions for the lowest singlet and triplet states at the 1A_1 equilibrium geometry are shown in Figure 16. An excitation from the lowest singlet to triplet state transfers large amounts of charge density from the bonding regions between the three-ring nuclei to the anti-bonding regions of those centres.

The C_{2v} insertion and cycloaddition mechanisms are seen to be fundamentally identical. In both cases, excess α -spin density is transferred from the oxygen atom to the substrate causing localization of the bond density on the substrate nuclei rather than between them. In the insertion reaction, sufficient density is removed to rupture the original substrate σ -bond, whereas in the cycloaddition case, the disruptive spin polarization effectively breaks the olefin π -bond, leaving the σ -bond intact. The result in the hydrogen case is the monotonic increase in H-H separation and eventual formation of a linear (asymmetrically unstable) H-O-H intermediate. The symmetrical triplet cycloaddition reaction is simply energetically highly unfavourable.

2. C_s Oxygen Approach

For an unsymmetrical oxygen approach ($\alpha \approx 105^\circ$ - 110°) both singlet and triplet surfaces are purely repulsive, each to the extent of 20-30 kcal/mole for R_2 (the shorter carbon-oxygen distance) equal to 2.71 a.u. The singlet C_s surface is energetically downhill to the C_{2v} geometry for all $R_2 \lesssim 4.0$ a.u. In contrast, the triplet surface is uphill for α both higher and lower than about 105° . The singlet and triplet total

Figure 16. 1A_1 minus 3B_1 charge density difference at the ground state ethylene oxide equilibrium geometry. Contour values are the same as for spin density maps.



charge distributions for three points on the unsymmetrical path are shown in Figure 17. For $R_2 = 4.0$ a.u., the reactant charge distributions have begun to overlap significantly for both states. In the singlet case, there has been some migration of charge from the terminal methylene into the interior of the molecule. Substantial C-O bonding for $R_2 = 2.81$ a.u. is indicated by the charge accumulation between oxygen and internal methylene.

For $R_2 = 4.0$ a.u., the triplet charge distribution appears quite similar to that of the singlet, except that the charge near the terminal methylene is not as severely disturbed. At $R_2 = 2.81$ a.u., accumulation of charge between the oxygen and internal methylene shows C-O bonding similar to that in the singlet state. The charge distribution near the terminal methylene is essentially superposable on that of the isolated triplet ethylene molecule all along the path.

The variation in the spin density distribution of the triplet on this path provides an explanation of the observed changes in the charge distribution. The spin distributions are shown in Figure 18. As in the C_{2v} triplet case, one of the spins remains localized in a plane perpendicular to that shown.

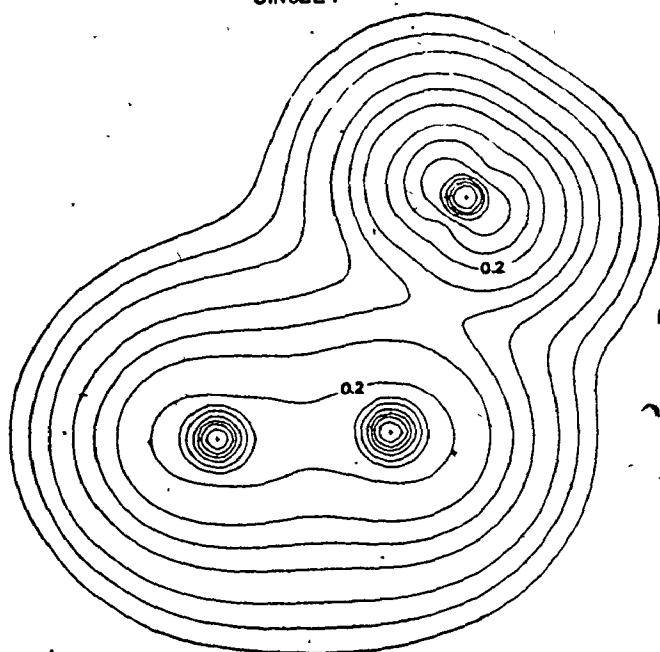
Even for $R_2 = 4.0$ a.u., the primary mechanism of the unsymmetrical triplet attack is strongly in evidence. Associated with the excess α -density near the oxygen are large $p\pi$ -like accumulations of excess α - and β -density on the terminal and internal methylene carbon nuclei, respectively. The oxygen has induced an uncoupling of the α - and β -density in the π region of the ethylene. Even for this value of α , the pattern of spin polarization is strongly reminiscent of that for

Figure 17. Total singlet and triplet charge distributions (in the plane of the heavy nuclei) for C_s oxygen attack on C_2H_4 . The oxygen is in the upper right portion of each map.

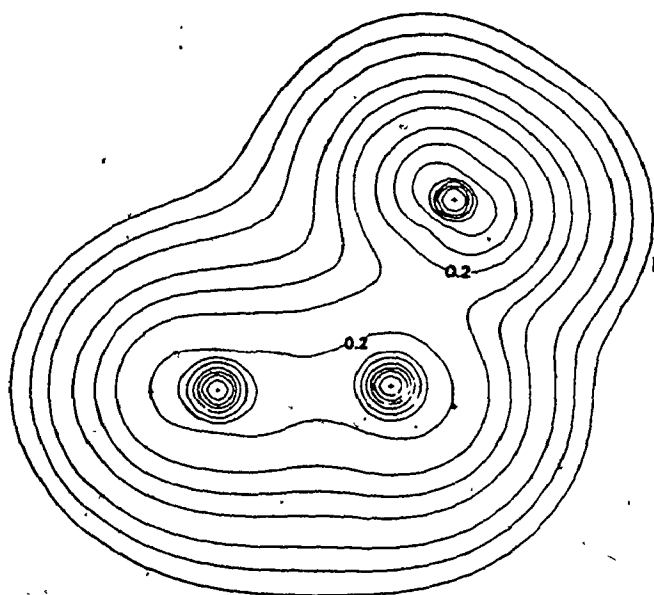
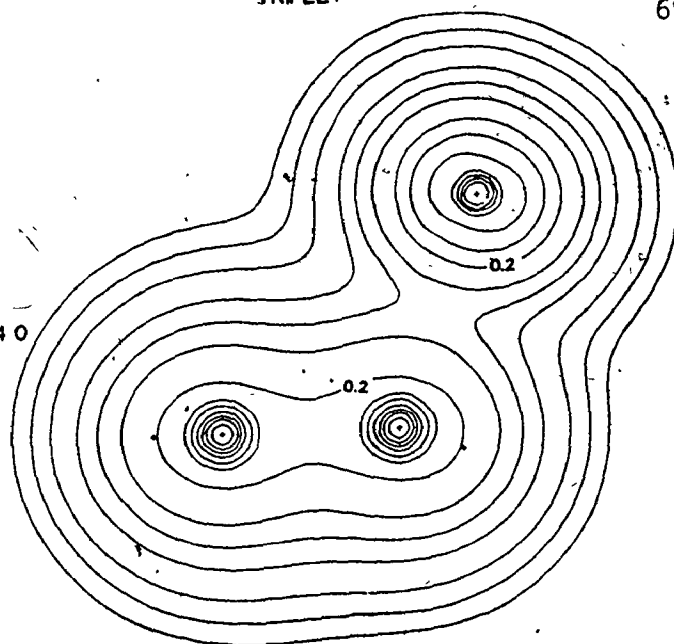
SINGLET

TRIPLET

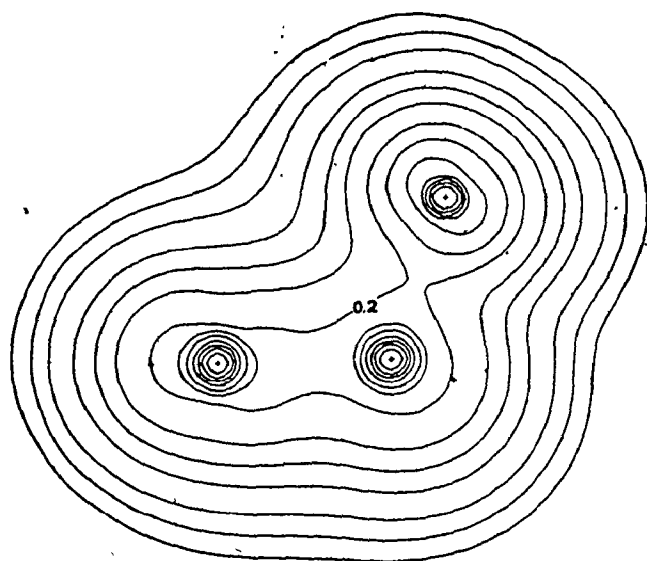
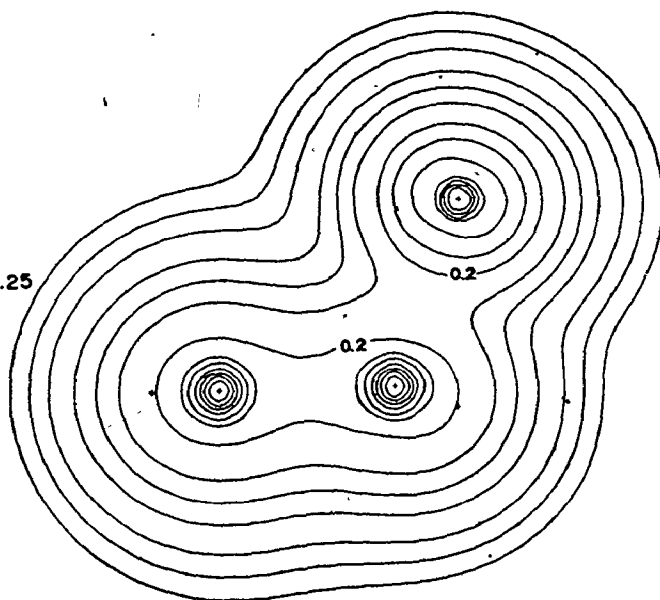
69



$R2=4.0$



$R2=3.25$



$R2=2.81$

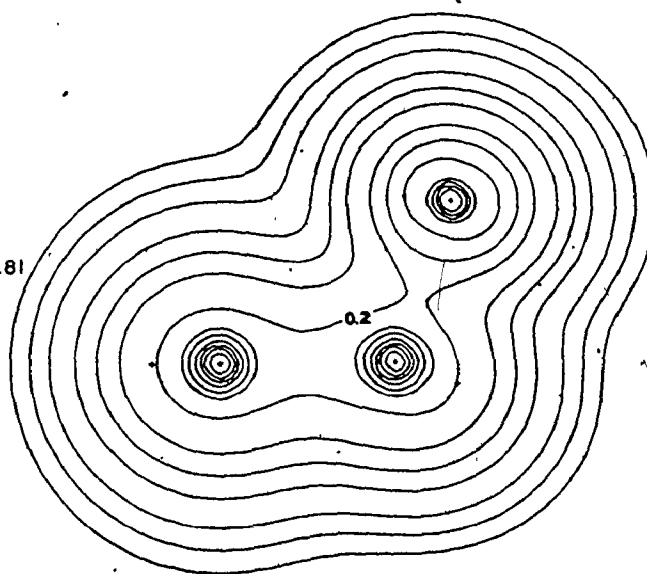
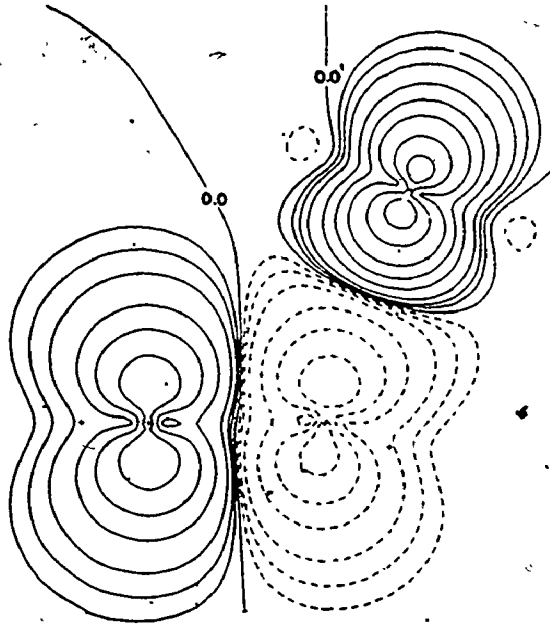
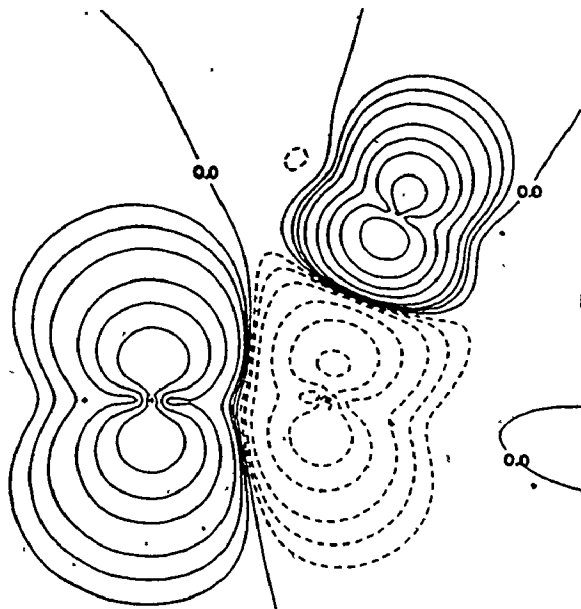
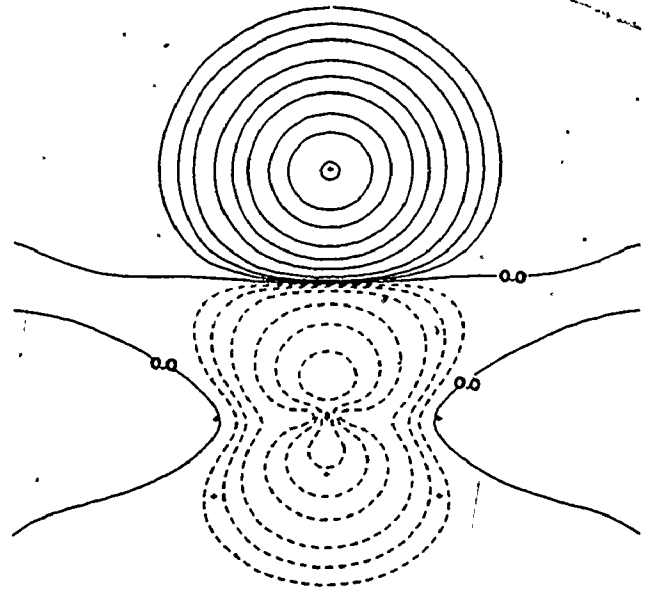
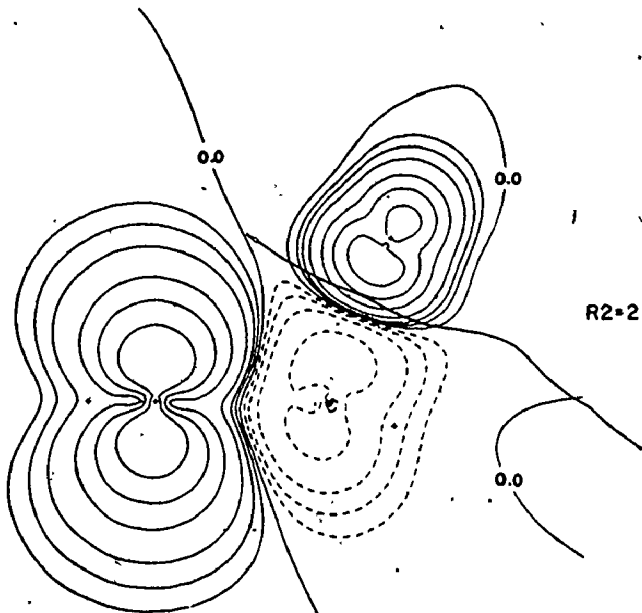
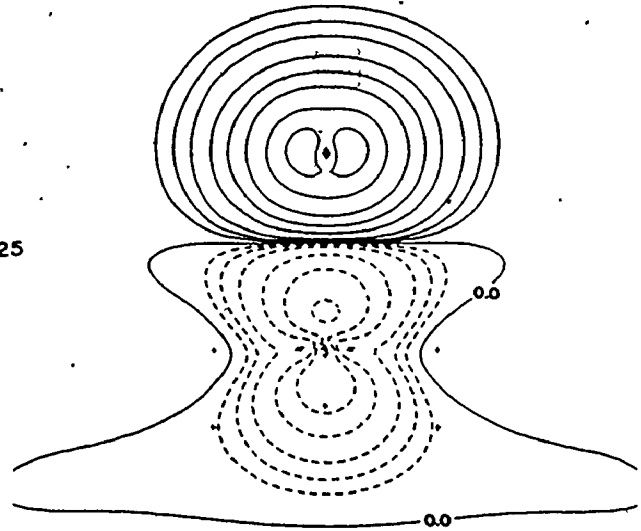
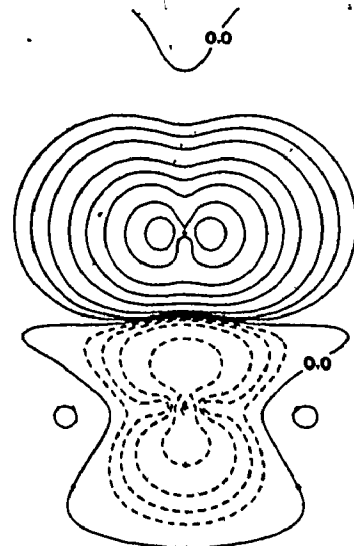


Figure 18. Triplet spin distributions (in the plane of the heavy nuclei in the left column, and in the plane perpendicular to that plane also containing the CO axis on the right) for C_5 oxygen approach to C_2H_4 . The oxygen is in the upper right portion of each map.

 $R2=4.0$  $R2=3.25$  $R2=2.81$ 

the linear abstraction reaction. There is always less β -density induced on the internal methylene than α -density on the terminal methylene. Thus there has also been a net transfer of α spin from oxygen to terminal methylene. The uncoupling and transfer effects increase along the path until for $R_2 = 2.81$ a.u., the excess α -spin distribution on the terminal methylene is essentially superposable on that of the ethylene T state (Figure 9).

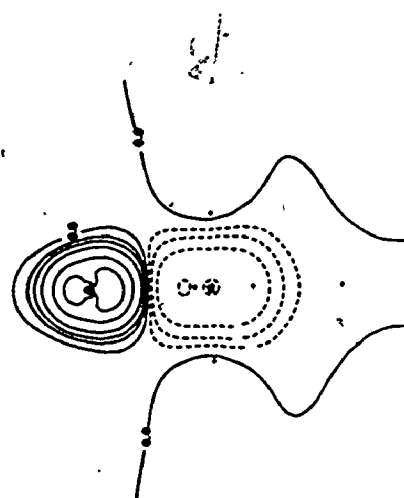
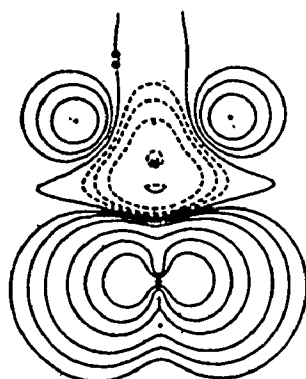
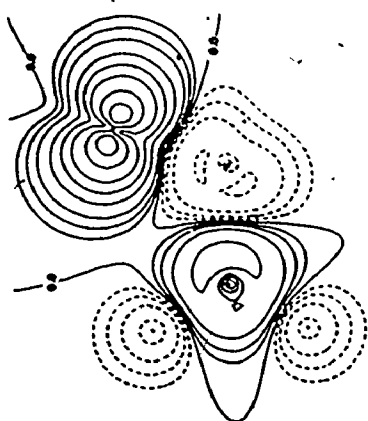
To more fully describe the spin polarization effects on the triplet charge and spin densities, we include the charge and spin density maps in three planes for C_s geometry with $R_2 = 2.71$ a.u. (Figure 19). At this distance, the asymmetrical triplet has an energy only 22 kcal/mole above that of the separated reactants, compared to 148 kcal/mole for the corresponding symmetrical geometry.

The three charge distribution plots show that there is a charge accumulation between the oxygen and internal methylene almost as great as in the singlet equilibrium geometry (Figure 14). This is indicative of the formation of a strong C-O bond. (In contrast, the triplet C_{2v} charge density indicates no formation of CO bonds.) The three planes through the spin density distribution illustrate the localization of alternating regions of excess α -or β -density on all the nuclei in the molecule.

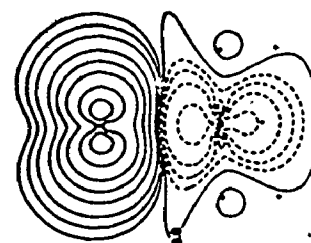
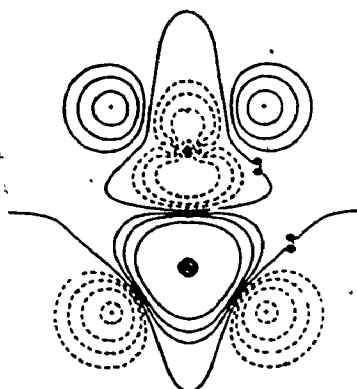
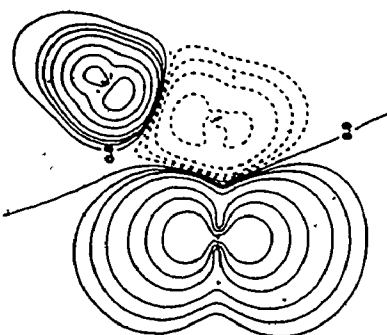
These alternating α -and β -excesses show a spin polarization of the σ -bonding density of the molecule. In addition, there are distributions of excess α -spin localized in the π -region of the terminal methylene and non-bonding region of the oxygen nucleus. These distributions have maxima in mutually perpendicular planes. These are precisely the features

Figure 19. Total charge and spin density distributions for ethylene oxide $^3A''$ state, $R_2 = 2.71$ a.u. The first column contains the charge distributions for (from top to bottom) the plane containing both carbon nuclei and the oxygen nucleus, the plane containing both carbon nuclei and terminal hydrogen nuclei, and the plane containing the internal carbon-oxygen bond also perpendicular to the first plane. The second column contains the corresponding spin density distributions. The third column contains the spin density distributions in the same three planes for a wavefunction generated for the same state and geometry, except that the terminal methylene group is rotated into the plane containing both carbon nuclei and the oxygen nuclei.

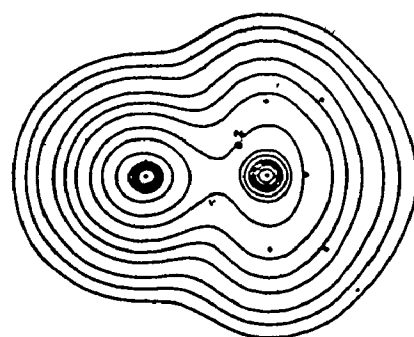
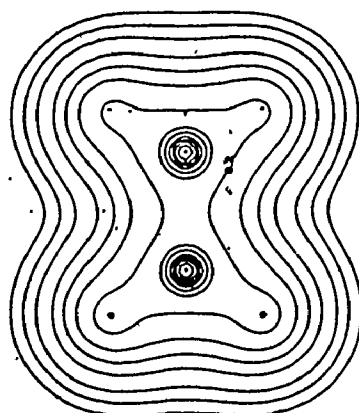
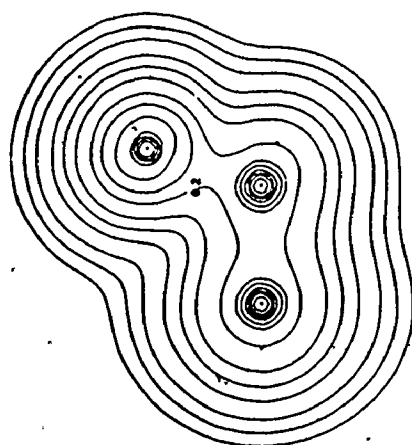
SPIN DENSITY



SPIN DENSITY



CHARGE DENSITY



one associates with a triplet diradical.

Thus, the spin polarization occurring for an unsymmetrical triplet attack geometry is composed of several simultaneous processes:

- (i) uncoupling of the olefin π -bonding density and counter-migrations of the α - and β -components to the two carbon nuclei;
- (ii) due to the uncoupling, weakening of the carbon-carbon bonding;
- (iii) steadily increasing binding between the oxygen and its neighbouring carbon atom;
- (iv) polarization of the σ -bonding density throughout the resultant open-chain molecule similar to that for the triplet state of ethylene itself; and,
- (v) localization of the excess 2α -spins into distributions of one α -spin each at opposite ends of the molecule.

The simultaneous weakening of the carbon-carbon bonding and increase in carbon-oxygen bonding accounts for the much lower energy increase for unsymmetrical than symmetrical attack.

The parallels between the triplet abstraction and cycloaddition processes are striking. Abstraction of a hydrogen atom occurs since the spin polarization causes sufficient removal of the density binding it to the substrate molecule to force scission of the original bond. Asymmetrical triplet attack on an olefin has an accompanying spin polarization which forces transfer of charge density from the carbon-carbon binding region to a carbon-oxygen binding region. However, the charge decrease is insufficient to lead to complete fracture of the carbon-carbon bonding. Hence, one obtains an open-ring transition state rather than separated radicals.

We have computed several other characteristics of the diradical geometry of Figure 19. There is a mere 6 kcal/mole barrier to rotation of the terminal methylene. (Recall that the experimental barrier to rotation is 65 kcal/mole for ground state ethylene⁵³ and 3 kcal/mole for ethane.⁵⁸) The carbon-carbon double bond has in effect been reduced from double to single. Our spin density contour maps for this process indicate that as the terminal methylene and its $p\pi$ -localized excess α -spin distribution is rotated, so does the unpaired α -density on the oxygen. This maintains the perpendicularity, hence minimal overlap, of the two α -distributions. As well, a pyramidalizing of the terminal methylene increases the energy and indicates that the preferred geometry of the H_2C-C group is planar.

CONCLUSIONS

The potential surfaces we have computed confirm the suggestion of Cvetanović⁷ that singlet oxygen undergoes a C_{2v} symmetric concerted reaction to form an ethylene oxide ring product. Triplet ethylene, on the other hand, faces a (36 kcal/mole) barrier to the formation of an open-ring triplet biradical intermediate, which is not stable to all nuclear motions. Concurrent hindered terminal methylene rotation and ring-closing adiabatic triplet-singlet surface crossing lead to the formation of non-stereospecific substituted ethylene oxide product. The spin uncoupling and transfer polarization mechanisms governing the asymmetrical triplet addition accord well with the previous results on the insertion and abstraction systems.

That both the singlet and triplet prefer addition rather than insertion or abstraction can be explained by the greater strength of olefin carbon binding. The separation of the substrate nuclei required for both insertion and abstraction is precluded thereby in both cases.

We did not find the stable "triplet biradical"¹⁴ or " π -complex"¹¹ intermediates previously suggested by others. However, an open-ring geometry with $\alpha = 83^\circ$ and $R_2 = 2.9$ a.u. has the characteristics of a diradical and is the lowest energy transition state found.

The concerted symmetrical singlet cycloaddition path and asymmetrical triplet diradical transition state we predict follow the same pattern as the previous calculated methylene,³⁴ sulphur,³⁵ and nitrene³⁷ addition surfaces.

The spin-density transfer and uncoupling mechanisms have now been shown to explain the differences in singlet and triplet chemistry for the insertion, abstraction and cycloaddition reactions. The application of these concepts should provide a useful tool for the prediction of the paths of photolytic chemical reactions.

APPENDIX A-1

When using the PØLYATØM system of programmes, one is restricted to the RHF or UHF formalism of the use of single determinantal electronic wavefunctions composed of real basis functions. The Hamiltonian assumed for the system is the spinless electronic Hamiltonian mentioned in Chapter II. At this degree of approximation, the levels of each term generated for an electronic configuration are degenerate. Certain real wavefunctions are usually able to be constructed for at least one level per term.

If the valence electronic configuration is p^4 , as in the oxygen atom case, then there are fifteen possible determinantal wavefunctions corresponding to the five degenerate 1D functions, three triply degenerate 3P functions, and one 1S function:

	Irreducible Representation in C_{2v} Field
$\psi_1 = x^2y^2 $	A_1
$\psi_2 = x^2z^2 $	A_1
$\psi_3 = y^2z^2 $	A_1
$\psi_4 = x^{2\alpha\beta}yz \pm x^{2\alpha\beta}zy , x^{2\alpha\alpha}zy , x^{2\beta\beta}zy $	B_1
$\psi_5 = y^{2\alpha\beta}xz \pm y^{2\alpha\beta}zx , y^{2\alpha\alpha}xz , y^{2\beta\beta}xz $	B_2
$\psi_6 = z^{2\alpha\beta}xy \pm z^{2\alpha\beta}yx , z^{2\alpha\alpha}xy , z^{2\beta\beta}xy $	B_3

These functions may be assigned to the different irreducible representations of the C_{2v} point group when in an external field of that symmetry. This is the case on the symmetric C_{2v} cycloaddition

path. Only those wavefunctions belonging to the same irreducible representation have non-zero interaction between them. Thus, only the three singlet A_1 wavefunctions (degenerate at long range) interact, to a degree varying with the oxygen-ethylene separation. At the ground state ethylene oxide geometry, two of the three A_1 determinants increase significantly in energy and the description of the lowest state by one determinant is quite accurate. At long range, the three determinants can be shown to represent two states of the 1D term and the lone 1S state. The complete list of states appears as:

$$^1D: \phi_1, \phi_2, \psi_4^+, \psi_5^+, \psi_6^+$$

$$^3P: \psi_4^-, \psi_5^-, \psi_6^-, \psi_4^{\alpha\alpha}, \psi_4^{\beta\beta}, \psi_5^{\alpha\alpha}, \psi_5^{\beta\beta}, \psi_6^{\alpha\alpha}, \psi_6^{\beta\beta}$$

$$^1S: \phi_3$$

$$\text{where } \phi_1 = \frac{1}{\sqrt{6}}[2\psi_1 - \psi_2 - \psi_3]$$

$$\phi_2 = \frac{1}{\sqrt{2}}[\psi_2 - \psi_3]$$

$$\phi_3 = \frac{1}{\sqrt{3}}[\psi_1 + \psi_2 + \psi_3].$$

REFERENCES

1. R. C. Woodworth and P. S. Skell, J. Am. Chem. Soc. 81, 3383 (1953) and references therein.
2. W. Kirmse, "Carbene Chemistry", (Chapter 12 by P. G. Gaspar and G. S. Hammond), Academic Press, New York (1964).
3. W. B. DeMore and S. W. Benson, Advan. Photochem. 2, 219 (1964).
4. R. F. W. Bader and J. I. Generosa, Can. J. Chem. 43, 1631 (1965).
5. R. J. Cvetanović, Advan. Photochem. 1, 115 (1963).
6. R. J. Cvetanović, Can. J. Chem. 36, 623 (1958).
7. S. Sato and R. J. Cvetanović, Can. J. Chem. 36, 1668 (1958).
8. R. Cvetanović, Can. J. Chem. 38, 1678 (1960).
9. R. Atkinson and R. J. Cvetanović, J. Chem. Phys. 56, 432 (1972).
10. S. Hirokami and R. J. Cvetanović, Can. J. Chem. 51, 373 (1973).
11. S. Hirokami and R. J. Cvetanović, J. Am. Chem. Soc. 96, 3738 (1974).
12. R. J. Cvetanović, J. Chem. Phys. 30, 19 (1959).
13. R. J. Cvetanović, J. Chem. Phys. 33, 1063 (1960).
14. R. J. Cvetanović, J. Phys. Chem. 74, 2730 (1970).
15. R. Huie, Int. J. Chem. Kinet. 4, 521 (1972).
16. R. Huie, J. Phys. Chem. 76, 3311 (1972).
17. W. B. DeMore, Chem. Phys. Lett. 16, 608 (1972).
18. W. B. DeMore and O. F. Raper, J. Chem. Phys. 37, 2048 (1962).
19. W. B. DeMore, J. Phys. Chem. 73, 391 (1969).
20. D. Saunders and J. Heicklen, J. Phys. Chem. 70, 1950 (1966).
21. M. D. Scheer and R. Klein, J. Phys. Chem. 73, 597 (1969).
22. R. Klein and M. D. Scheer, J. Phys. Chem. 73, 1598 (1969).

23. A. P. Stefain and M. Szwarc, J. Am. Chem. Soc. 84, 3661 (1962).
24. G. E. Owen, J. M. Pearson and M. Szwarc, Trans. Farad. Soc. 61, 1722 (1965).
25. R. Klein and M. D. Scheer, J. Phys. Chem. 72, 616 (1968).
26. R. Klein and M. D. Scheer, J. Phys. Chem. 74, 613 (1970).
27. A. N. Ponomarev, Kinet. Katal. 7, (1966).
28. E. E. Kasimovskaya and A. N. Ponomarev, Kinet. Katal. 9, 687 (1968).
29. H. E. Gunning and O. P. Strausz, Advan. Photochem. 4, 143 (1966).
30. E. M. Lown, H. S. Sandhu, H. E. Gunning and O. P. Strausz, J. Am. Chem. Soc. 90, 7164 (1968).
31. O. P. Strausz, H. E. Gunning and I. G. Csizmadia, J. Am. Chem. Soc. 94, 8317 (1972).
32. O. P. Strausz, R. K. Gasavi, A. S. Denes and I. G. Csizmadia, Theor. Chim. Acta (Berl.) 26, 367 (1972).
33. W. Lwowski and J. S. McConaghy Jr., J. Am. Chem. Soc. 87, 5490, 5491 (1965).
34. R. Hoffmann, J. Am. Chem. Soc. 90, 1475 (1968).
35. R. Hoffmann, C. C. Wan and V. Neagu, Mol. Phys. 19, 113 (1970).
36. E. Leppin and K. Gollnick, Tet. Lett. 43, 3819 (1969).
37. W. J. Haines and I. G. Csizmadia, Theoret. Chim. Acta (Berl.) 31, 283 (1973).
38. S. Koda, Can. J. Chem. 52, 287 (1974).
39. S. Sato and R. J. Cvetanović, J. Am. Chem. Soc. 81, 3223 (1959).
40. R. F. W. Bader and R. A. Gangi, J. Am. Chem. Soc. 93, 1831 (1971).
41. M. Born and R. Oppenheimer, Ann. Phys. 84, 457 (1927).
42. C. W. Kern and M. Karplus, "Water -- A Comprehensive Treatise", Vol. I, F. Franks, Ed., Plenum, New York, New York, 1974, p. 21.
43. G. W. King, "Spectroscopy and Molecular Structure", Holt, Rinehart and Winston, Inc., Toronto, 1964, p. 410.

44. J. McKenna, "M.T.P. International Review of Science. Series I, Organic Chemistry, Vol. I", W. D. Ollis, Ed., Butterworths, London, 1973.
45. R. F. W. Bader and R. A. Gangi, "Ab Initio Calculation of Potential Energy Surfaces", R. N. Dixon, Ed., Specialist Reports of the Chemical Society, Theoretical Chemistry, Vol. I, 1975.
46. J. Hinze, Advan. Chem. Phys. 26, 213 (1974).
47. J. C. Polanyi and J. L. Schreiber, "Physical Chemistry -- An Advanced Treatise. Vol. VI, Kinetics of Gas Reactions", H. Eyring, W. Jost and D. Henderson, Editors, Academic Press, New York,
48. POLYATOM/2, Quantum Chemistry Program Exchange, Program 199.
49. R. McWeeny, "Molecular Orbitals in Chemistry, Physics, and Biology", P.-O. Löwdin and B. Pullman, Academic Press, New York, 1965, p. 305.
50. A. T. Amos and L. C. Snyder, J. Chem. Phys. 41, 1773 (1964).
51. A. T. Amos and G. G. Hall, Proc. Roy. Soc. (London) A263, 483 (1961).
52. H. Basch, M. B. Robin and N. A. Keubler, J. Chem. Phys. 47, 1201 (1967); ibid., 49, 5007 (1968); J. R. Lombardi, W. Klemperer, M. B. Robin, H. Basch and N. A. Keubler, J. Chem. Phys. 51, 33 (1969).
53. M. H. Wood, Chem. Phys. Lett. 24, 239 (1974).
54. G. L. Cunningham Jr., A. W. Boyd, R. J. Meyers, W. D. Gwinn and W. I. Le Van, J. Chem. Phys. 19, 676 (1951).
55. R. F. W. Bader, "Molecular Charge Distributions, Their Display and Use", C. A. Coulson and D. A. Buckingham, Editors, M.T.P. International Series on Science, Theoretical Chemistry, Vol. II, Butterworths, 1975.
56. R. F. W. Bader, W. H. Henneker and P. E. Cade, J. Chem. Phys. 46, 3341 (1967).
57. R. McWeeny and B. T. Sutcliffe, "Methods of Molecular Quantum Mechanics", Vol. II, Academic Press, New York, New York, 1969.

58. S. Weiss and G. E. Leroi, J. Chem. Phys. 48, 962 (1968).
59. R. M. Moon, Trans. Am. Cryst. Ass'n. 8, 59 (1972).
60. R. McWeeny and B. T. Sutcliffe, "Methods of Molecular Quantum Mechanics", Vol. II, Academic Press, New York, New York, 1969, p. 104.

.. PART B
ELECTRON CORRELATION AND LOCALIZATION

TABLE OF CONTENTS

	<u>Page</u>
TABLE OF CONTENTS	xi
LIST OF FIGURES	xiii
LIST OF TABLES	xv
INTRODUCTION	83
CHAPTER I -- HISTORY OF THE CORRELATION PROBLEM	86
CORRELATION	86
ELECTRON PAIRING	89
ELECTRON LOCALIZATION	96
MOLECULAR PARTITIONING	97
CHAPTER II -- THE LOGE CONCEPT, THE MISSING INFORMATION FUNCTION AND THE ELECTRON PAIR	100
THE LOGE CONCEPT	100
THE MISSING INFORMATION FUNCTION	103
THE ELECTRON PAIR	104
NUMERICAL TECHNIQUES	109
THE DIATOMIC MOLECULES LiH^+ , LiH , BeH^+ , BeH , BH	109
Core Loges	110
Valence Density Partitioning	116
THE TRIATOMIC MOLECULE BeH_2	122
CHAPTER III -- ELECTRON FLUCTUATION AND CORRELATION	129
CORRELATION FUNCTIONS	131
FLUCTUATION AND LOCALIZATION FOR HARTREE-FOCK WAVE- FUNCTIONS	143
ARGON	145
THE 10-ELECTRON ISOELECTRONIC SERIES Ne , HF , H_2O , NH_3 , CH_4	150

	<u>Page</u>
Heavy Atom Cores	151
Valence "Bonding" and Non-Bonding" Loges	155
Neon	155
CH ₄	161
NH ₃ , H ₂ O, HF	170
LiH, BH, BeH ₂	171
BH, BH ₃ , BH ₄ ⁻	178
F ₂ and N ₂	184
CONCLUSIONS	187
FUTURE WORK	188
APPENDIX B-1 PROGRAMME DIALØGE	190
REFERENCES	196

LIST OF FIGURES

<u>Figure</u>		<u>Page</u>
1	Electronic Charge Distributions for LiH^+ , LiH , BeH^+ , BeH(X) , BH , and BeH(A)	106
2	Variation in the $P_n(\Omega)$, $I(P,\Omega)$ and $\Lambda(\bar{N},\Omega)$ for BH Spherical Cores	111
3	Electronic Charge Distributions in BH , BeH(X) and BeH_2	120
4A	Fluctuation and Related Properties Versus R for Argon Spherical Cores	146
4B	Electronic Charge Distribution for $\text{Ar}(1s)$	148
5	Electronic Charge Distributions for CH_4 , NH_3 , H_2O , HF , Ne	153
6	Fluctuation and Related Properties Versus R for Neon Spherical Cores	154
7	Fluctuation Versus R for Spherical Cores of 10-Electron Molecules	156
8	Fluctuation and Related Properties Versus R_2 for Neon Shells	158
9	Fluctuation Versus Population for Various Shapes of Neon Valence Fragments	160
10	Fluctuation and Related Properties Versus θ_0 for CH_4 " C_{3v} " Valence Fragments	163
11	Fluctuation and Related Properties Versus R for CH_4 Tetrahedral Valence Fragments	164
12	Fluctuation Versus Population for "Bond" Fragments in 10-Electron Molecules	168
13	Fluctuation Versus Population for "Non-Bonded" Fragments in 10-Electron Molecules	169

<u>Figure</u>		<u>Page</u>
14	Fluctuation Versus R/\bar{N} for LiH Core/Non-Bonded Fragments	174
15	Fluctuation Versus R/\bar{N} for BH Core/Non-Bonded Fragments	175
16	Fluctuation Versus R/\bar{N} for BeH ₂ Core/Bond Fragments	177
17	Electronic Charge Distributions for BH ₃ and BH ₄ ⁻	179
18	Fluctuation Versus R for BH, BH ₃ , BH ₄ ⁻ Spherical Cores	180
19	Fluctuation and Related Properties Versus Population for BH ₃ Valence Wedges	182
20	Fluctuation and Related Properties Versus θ_0 for BH ₄ ⁻ "C _{3v} " Valence Fragments	183

LIST OF TABLES

<u>Table</u>		<u>Page</u>
1	Characteristics of the Charge Distributions	108
2	Properties of Best Spherical Core Loges in AH	112
3	Properties of Virially Defined (A) Fragments	115
4	(a) Three-Loge Partitioning in BH	117
	(b) Three-Loge Partitioning in BeH(X)	117
5	(a) Three-Loge Partitioning of BeH(A)	123
	(b) Bond-Loge Properties for BeH(A)	123
6	Three-Loge Partitioning in BeH ₂	125
	(a) Symmetrical Partitioning (σ_h plane)	125
	(b) Symmetrical Partitioning (σ_v plane)	125
	(c) Virial Partitioning	126
7	Wavefunctions for Ne, HF, H ₂ O, NH ₃ , and CH ₄	152
8	Properties of the "Best" Cores for Ne, HF, H ₂ O, NH ₃ , and CH ₄	157
9	Total Partitionings of CH ₄	166
10	Fluctuation and Related Properties for Core and Valence Loges in Simple Hydrides	172

INTRODUCTION

Chemistry is devoted to the microscopic explanation of the observed macroscopic properties and reactions of common substances. The basic building blocks which are stable in the range of energy changes involved are the elemental nuclei. The study of a molecular structure thus involves the description of the equilibrium geometry of the nuclei and their rotation and vibration states. Chemical reactions involve the reclustered of nuclei into new groupings from old. In both cases, there is a rearrangement of the highly labile electronic charge within the system from eigenstates in the original molecule(s) to new states in the product molecule(s).

The classical description of chemical reactions involves the visualization of three-dimensional nuclear geometries with variable amounts of electronic charge, hence net charge, associated with each nuclear centre. Shifts of electronic density from one internuclear region to another are associated with changes in the degree of bonding between the various nuclei. Usually, one can consistently explain such mechanics by invoking the picture of almost independent rearrangements of charge and nuclei each localized to one portion of the nuclear framework, the remainder of the molecule remaining largely unchanged (except for minor polarizations of the charge density and slight adjustments in nuclear geometry).

The quantum mechanical description of such localized changes in bonding has long been a challenge to theorists. Knowing the electro-

static forces, quantum mechanical restrictions of indeterminacy and spin, one can in principle calculate exactly all the properties of a stable molecule and the changes occurring in a chemical reaction, in a relativistic or non-relativistic scheme.

Such precise descriptions have several drawbacks, however. First of all, the calculations required are totally impractical due to their complexity. Secondly, even if the exact solutions were obtained, they would contain far more information than required to answer the chemist's questions. Furthermore, most of the information would be redundant, i.e., there would be near transferability of the descriptions of the reactive chemical "groups" between molecules.

Thus there has arisen in the past few years systematic theoretical studies of the problem of obtaining the simplest possible description of the localizability of electron properties and localized changes in chemical bonding consistent with more accurate calculations. Intimately associated with these goals is the question of the extent to which one can partition a molecule or reacting system into fragments. If the fragments are well-defined, changes in various of their properties may explain the forces driving a chemical reaction, and the underlying reason one can consistently describe molecules in terms of identifiable components ("groups") at all.

There have been studies of electron localization and molecular fragmentation from several points of view. We shall briefly describe some of these. We then shall consider in more detail one of the schemes, that of "loge" partitioning. We shall show that partitionings of electronic properties on several criteria proposed for this method can

be related to the information content of the total electronic wavefunction retained in the "event probabilities" one can calculate. We relate this to the long held picture of electron pairs. A second approach to the loge partitioning method involving the definition of loge "fluctuations" is shown to be related to the separability of electrons into strongly intracorrelated and weakly intercorrelated groups, and the resultant localizability of electron properties. We finally apply the fluctuation criterion to a 10-electron series of isoelectronic molecules plus several other small molecules. This provides a comparison of the predictions of the fluctuation partitioning with more common descriptions of chemical bonding in these systems via the concepts of quasi-independent core, bonding (σ - and π -type) and non-bonding electron pairs.

CHAPTER I

HISTORY OF THE CORRELATION PROBLEM

CORRELATION

In classical mechanics, the exact description of a system of N particles is possible in principle. However, no general methods leading to direct solutions in all cases are known. This is the well-known "N-body problem".¹

The same difficulty arises in a new guise in quantum mechanics. One is faced in this case with finding the conditions constraining the allowable form of the N^{th} -order density matrix (which contains all the knowable information for the system). This quantum analogue of the "N-body problem" is termed the "N-representability problem".

Now, the description of the stationary states of a molecular system requires that one find the eigenfunctions for the non-relativistic spinless Hamiltonian operator mentioned in Part A, Chapter II:

$$H(\underline{r}, \underline{R}) = -\frac{1}{2} \sum_{\alpha} \frac{1}{M_{\alpha}} \nabla_{\alpha}^2 - \frac{1}{2} \sum_i \nabla_i^2 + \sum_{\alpha < \beta} \frac{Z_{\alpha} Z_{\beta}}{R_{\alpha\beta}} - \sum_{i, \alpha} \frac{Z_{\alpha}}{r_{i\alpha}} + \sum_{i < j} \frac{1}{r_{ij}} \quad (1)$$

This operator explicitly omits the effects of orbital and spin angular momentum interaction ("coupling") and external fields. Fortunately, the omitted operators do not change the gross features of the electronic charge distribution for molecular stationary states.

We assume the Born-Oppenheimer approximation decouples the electronic and nuclear motion accurately. The electronic states then

are represented by the eigenfunctions of the electronic Hamiltonian:

$$H_{el,R}(r) = -\sum_i \nabla_i^2 - \sum_{i,\alpha} \frac{Z_\alpha}{r_{i\alpha}} + \sum_{i<j} \frac{1}{r_{ij}} \left(+ \sum_{\alpha<\beta} \frac{Z_\alpha Z_\beta}{R_{\alpha\beta}} \right) \quad (2)$$

($\sum_{\alpha<\beta} \frac{Z_\alpha Z_\beta}{R_{\alpha\beta}}$ is constant for any fixed nuclear geometry.)

The difficulties encountered in attempting to accurately take into account the $\sum_{i<j} \frac{1}{r_{ij}}$ term in H_{el} using wavefunctions constructed of one-particle orbitals are the source of the so-called "Coulomb correlation". That is, the electronic electrostatic repulsion operator will in part determine the system eigenstate hence the distribution and localization of electron event probability throughout the system coordinate space. An approximate wavefunction not taking this into account will suffer from a "correlation energy" error in the total system energy predicted.

This "Coulomb correlation" is an effect distinct from the "Fermi correlation" introduced by the antisymmetry required of a multi-fermion wavefunction. Either correlation effect can affect the qualitative as well as quantitative predictions of calculations on a system. Thus, a Hartree-Fock calculation (which includes Fermi, but not Coulomb correlation) of the formation of F_2 from two F atoms yields the incorrect sign for the binding energy.²

Formal treatments of the general correlation problem, such as Sinanoglu's "cluster function" development³ attempt a dissection of the N^{th} order density matrix for the system in terms of correlation operators dependent on various numbers of electron coordinates. He has found, for instance, that the energy for a molecular ground state (describable to zeroth order by a single determinantal function) can be

obtained correct to second order by accounting for the Coulomb correlation in terms of $\frac{N(N-1)}{2}$ decoupled pair contributions.

In a system with few electrons (such as the helium atom), highly accurate solutions have long been known.⁴ Such wavefunctions explicitly include the interelectronic variables r_{ij} as wavefunction parameters. However, the calculations rapidly become intractable for even simple molecules.

Practical methods of including the important correlation effects in accurate system wavefunctions of large molecular systems are still under development. One avenue of approach is based on refinement of the electronic wavefunction composed of products of one-particle functions. It has been specifically shown⁵ that an exact N-fermion wavefunction can, in principle, be expressed in terms of an expansion over a basis set of N^{th} order determinants built from any complete set of one-particle functions. Practical problems arise when one actually attempts to use this technique. There is no completely satisfactory method of construction of one-particle functions (all potential basis sets suffer from such problems as improper cusp behaviour, difficulty of integration or the like). The apparently simplest method, direct expansion of the determinantal basis functions in terms of the sets of occupied and virtual orbitals generated from a Hartree-Fock self-consistent field calculation is only slowly convergent. (This problem can be alleviated somewhat through the use of "natural orbitals", the eigenvectors of the first order density matrix of the system.⁶)

In evaluating the accuracy of such calculations, a convenient standard is provided by the Hartree-Fock wavefunction. In fact, the

"correlation energy" is defined² in terms of the difference between the "true" non-relativistic energy and the "true" Hartree-Fock energy. (Actual calculation of self-consistent field wavefunctions almost of necessity involves defining the one-particle molecular orbitals arrived at as an expansion over some convenient set of "primitive" atomic orbitals. Thus, with such a calculation, one can only hope to approach the true Hartree-Fock "limit".)

ELECTRON PAIRING

The concept of an electron "pair" has had a long and tortuous history. Rationales for even considering chemical bonding in terms of a preferred sharing of two electrons between nuclei have been arrived at from several starting points. The concept is also commonly misunderstood.

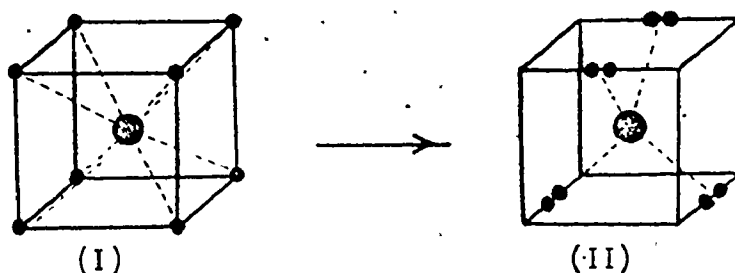
We give here a brief recounting of some of these theories, devised both before and after the development of quantum mechanics. This will give a better picture of what we shall see to be a rather slippery notion.

The conceptual development of the nature of chemical bonding has its origin in the theories of valence developed in the third quarter of the nineteenth century.⁷ Direct attempts to correlate chemical properties of substances to the electrical structure of their constituent atoms and molecules were carried out around the turn of the century by J. J. Thomson (the "plum-pudding atom"), I. Langmuir (the "cubical" atom) and W. Kossel (the "concentric ring atom").⁸ These descriptions suffered from two problems: the fact that nuclei in molecules are es-

essentially positively charged point masses (in the atomic scale) had yet to be discovered (Rutherford, 1911) and the electrons were assumed to be at rest. Even in classical mechanics, this latter assumption is a direct contradiction of Earnshaw's theorem (the unavoidable instability of a static collection of charged particles).

In his famous paper of 1916, "The Atom and the Molecule", G. N. Lewis⁹ attempted a significant pre-quantum era explanation of the observed properties of polar and non-polar molecules. His analysis was based on several postulates about the electronic structure of molecules. The origins of the concepts of relatively unchanging core density, valence shells and stability of valence electron octets are found in this work.

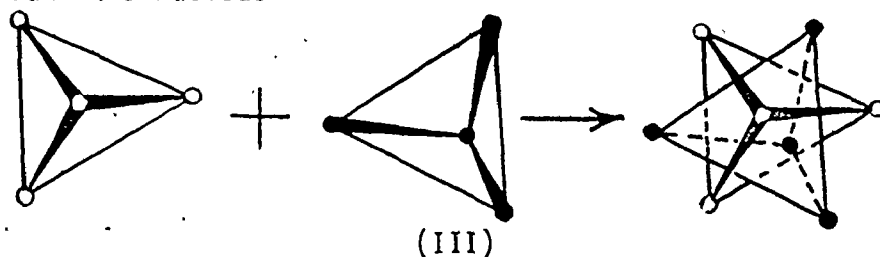
In that article, Lewis first suggested that the electron pair (rather than valence octet) might be the electron group of fundamental importance. Such a scheme implied the regrouping of electron octets (which he had previously assumed cubically arranged around a kernel of nucleus and core electrons (I)) into a tetrahedron of four pairs (II).



This description permitted a straightforward explanation of multiple bonding (including the observed limit of three bonds) as the sharing of more than one pair. The concept also could account for observed rotation around single bonds and provided the "tetrahedral"

carbon atom required for consistent nuclear structures of organic compounds. The forces invoked to hold electrons into pairs were unspecified, and suggested to be perhaps magnetic. As a final note, in the paper the use of the colon or two dots, to represent the electron pair identified with a chemical bond was first suggested. Lewis "dot" diagrams still provide a favoured introduction to formal study of chemical structure.

The electron pair has since been reclothed in the garments provided by quantum mechanics. Thus, Linnett¹⁰ has proposed that one consider the valence shell octet of a first or second row atom as two quartets, one of four α -spin and the other of four β -spin electrons. The Pauli exclusion or antisymmetry principle¹¹ is invoked to suggest that the system wavefunction will be forced to constrain each quartet into a preferred tetrahedral shape around the nucleus. That is, the square of the wavefunction will have its highest value, for a tetrahedral electronic configuration. Furthermore, for a lone atom (e.g., Ne) coulomb inter-electronic repulsion is assumed to cause interlacing of the two tetrahedra (III) around the nucleus.



In the presence of nuclei surrounding the central nucleus (e.g., CH_4), the lowered potential for electrons lying in the region between the central and terminal nuclei is assumed to align the two tetrahedra somewhat, so that one arrives at a stable molecule containing a pair of electrons (one α -spin and one β -spin) in each bonding

region. We have arrived again at a preferred tetrahedral orientation of four bonding pairs, with the added feature of predicting less "pairing" of non-bonding α - and β -density.

Application of the Pauli principle to the general problem of n -valence electrons where n may or may not be an octet has been shown to lead to a Valence Shell Electron Pair Repulsion (VSEPR) theory.^{8,12-14} The fundamental basis of the theory is that the Pauli principle restricts the accumulation of electrons in the low potential binding regions of molecules to at most two, one of α -spin and the other of β -spin. The geometry of molecules containing centres known to be surrounded by several ligands can be predicted, including effects of "larger" valence shell lone pairs. Because the geometrical predictions of this model can be (to a first approximation) equated to the electrostatically least repulsive distribution of n point charges on a sphere, it has commonly been misunderstood that the model is based on an electronic coulomb repulsion argument. This latter interpretation of electron pair separation has been clearly disclaimed by the originators,¹² but the continued use of the term "Pauli repulsion" in the descriptions of this and other related theories is, we think, unfortunate.

The VSEPR interpretation of the effect of the Pauli principle on molecular geometries has been vigorously challenged^{15,16} and defended.^{12,17} Of the simplified models of chemical binding it has had a consistently satisfactory predictive record. One recent study¹⁸ shows a direct correlation between the VSEPR and molecular orbital explanations^{19,20} of preferred molecular geometries. Thus, the concept of electron pair separation and a delocalized molecular orbital picture (based on the changes in the energies of one-particle delocalized molecular orbitals) yield the same geometrical predictions.

Active research is still being carried on in attempts to refine the electron pair model in a manner consistent with the more accurately known quantum mechanical description. Thus, a recent study²¹ has proposed a precise definition of the "size" of a delocalized electron pair and its use in the interpretation of molecular stereochemistries.

Briefly, the hypothesis of electron "pairing" can be summarized as being an attempt to correlate the effect that the Pauli principle has on the system electronic wavefunction with observed chemical properties.

All of the theories mentioned above are consistent with the more accurate description of molecular bonding in terms of the accumulation of charge in the low potential energy internuclear binding regions. The Pauli principle actually constrains the form of the wavefunction in a non-trivial manner. That is, it does not explicitly restrict electrons to different regions of real space. Rather, it alters the form of the associated reduced density matrix kernels in a $(4N)$ -dimension coordinate-space representation (for an N -electron system). That these restrictions are consistent with an interpretation in terms of the effects of the Pauli Principle in real space is the problem we consider.

To do so, one requires a method of actually calculating the effect of the Pauli principle on real space electron distributions, and of assessing the suitability of descriptions of these distributions in terms of the concept of separable electron pairs.

By definition, a Hartree-Fock wavefunction provides the best description of a molecular system (based on a single determinant of one-particle functions) incorporating the Pauli principle. More accurate descriptions of a system wavefunction are needed to describe the Coulomb correlation (non-averaged electron charge repulsion) also known to exist.

However, such wavefunctions which incorporate more correlation would tend to separate the α and β electrons of any localized pair. If one cannot identify a localized pair of electrons (via some criterion) using a Hartree-Fock wavefunction, then the electron pair cannot be a true entity described by a completely correlated wavefunction.

The methodology of evaluating the effects of electron correlation we consider here is based on the probabilistic interpretation of the wavefunction for a system. Thus, for an N-particle quantum system describable by the exact wavefunction ψ dependent on the $4N$ space and spin coordinates $\{r_i, \sigma_i\} \equiv \{\underline{x}_i\}$, one can associate

$$\psi(\{\underline{x}_i\})\psi^*(\{\underline{x}_i\})d\underline{x}_1, d\underline{x}_2, \dots, d\underline{x}_N \quad (1)$$

with the probability of simultaneously locating particle 1 in $d\underline{x}_1$, particle 2 in $d\underline{x}_2$, and so on.²²

If one wishes to find the most likely configuration of electrons in the system configuration space, then one should seek the set of electronic coordinates which maximizes the value of $|\psi\psi^*|$. This approach, in fact, forms the basis of the "Linnett double quartet" model described earlier. Thus, Linnett and Poë²³ computed that the most probable configuration for the 5S state of atomic carbon consists of two electrons (α and β spin) at the nucleus and four electrons (of identical spin) situated 2.35 a.u. from the nucleus at the corners of a tetrahedron situated at the nucleus. This result, as previously noted is directly attributed to Fermi correlation. For the ground state of the neon atom using a single determinantal wavefunction, one predicts two electrons at the nucleus and eight on a nucleus-centred sphere, four α spin electrons and four β spin

electrons each forming a separate tetrahedron. In this approximation, the relation of the two tetrahedra does not affect $|\psi\psi^*|$ at all (probably because coulomb correlation is represented only through a spatially averaged value). A full calculation might predict an alignment of the valence tetrahedra such that the eight electrons would fall at the corners of a cube.

The "most probable configuration" approach suffers from a defect similar to that of the classical pictures of Langmuir and Lewis.²⁵ One is considering only a single configuration of electrons. Hence, one ignores the bulk of the information contained in the wavefunction about even the average distribution of electrons in real space, let alone any numerical assessment of the possibility of partitioning of the system into weakly correlated subsystems.

The criterion of localizability we shall adopt is couched in terms of the "loge" partitioning concept of Daudel and coworkers.²⁶ The partitioning of a molecule into its best "loges" (Fr. lodge, cell, booth, (theatre) box) is defined as yielding the most probable division of the real space charge density of a molecule into localized groups of electrons.¹⁷ Specifically, we shall consider the variation of a "missing information" function with variation in the partitioning of real molecular space. This function provides a measure of the information available from the system wavefunction preserved by describing the molecule in fragments rather than pointwise. Such a technique was first suggested by C. Aslangul.²⁷ We shall discuss the basis of this criterion and show its direct relation to the probabilistic interpretation of quantum mechanics. We shall then attempt identification of electron

pairs in several small molecules according to the above concepts.

ELECTRON LOCALIZATION

The chemist's concept of electron "pairing" is only one example of attempts to interpret the mathematical predictions of quantum mechanics in more easily visualized quasi-classical models. We also consider the more general problem of the visualization of the effects of electron correlation involved in the non-relativistic quantum description of molecules. The localizability of electronic charge (i.e., fragmentation of real space into regions containing groups of electrons exhibiting little interregional correlation) can be related to the variation of a statistical "fluctuation function". We shall show the direct relation of this function to the evaluation of the electron correlation effects described above and hence derive a criterion of electron localization consistent with the concepts of quantum mechanics. We then show how the fluctuation function can be applied directly to localization of groups of electrons in the 10-electron isoelectronic series CH_4 , NH_3 , H_2O , HF , Ne and attempt partitionings of several other small atoms and molecules. We shall use Hartree-Fock wavefunctions in all of this work, and hence will be directly analyzing the effect of Fermi correlation on the localizability of electron groups. Coulomb correlation, ignored in our wavefunctions, will tend to destroy any spatial localization of groups of electrons. Hence, as in the study of electron pairs, we shall determine if such localization of electron groups for the true system wavefunction is possible, but not if in fact the effect is still present for a totally correlated wavefunction.

MOLECULAR PARTITIONING

If, in fact, one can find such divisions of electrons into strongly intracorrelated and weakly intercorrelated groups in distinct regions of real space, then one will be on more solid ground if one attempts a description of a correlated wavefunction for a system in terms of spatially localized group wavefunctions. Such techniques as those of "localized orbitals (LO)",²⁸ "strongly orthogonal geminals (SOG)",²⁹ or "completely loge localized (function) model (CLLM)",³⁰ all propose consideration of such spatially localized electron groups (α and β -spin pairs in the LO and SOG case, and in principle, groups of any number in the CLLM case). As well, the question of the constancy of correlation energy for fragments of a molecule is important for the understanding of variation (or lack of it) in the properties of molecules with substitution. Finally, any attempt to build large molecules from fragments of accurately computed smaller molecules, of whatever form one chooses,^{31,32} must address themselves at some stage to the question of localization of correlation. Thus, the results we obtain are of value for several practical reasons as well as being of intrinsic theoretical interest.

The problem of partitioning a quantum mechanical system into independent or almost independent subsystems has been approached from several viewpoints. Essential criteria for any partitioning scheme are that the chosen fragments be well-defined (i.e., unique) and that the method be independent of the explicit form of the wavefunction (which is, of practical necessity, approximate).

One attempt at associating the intuitive picture of nearly independent chemical bonds with the quantum reality is that employing localized orbitals. Briefly, this method involves application of a unitary transformation³³ to the set of completely delocalized canonical molecular orbitals, $\{u_n\}$, obtainable from a Hartree-Fock calculation. One chooses the transformation (which may not be unique) which simultaneously²⁸ maximizes the "localization sum", $\sum_n \langle u_n | \frac{1}{r_{ij}} | u_n \rangle$, minimizes the "interorbital exchange repulsions", $\sum_{n \neq m} \langle u_n | \frac{1}{r_{ij}} | u_m \rangle$, and minimizes the "interorbital Coulomb repulsions", $\sum_{n \neq m} \langle u_n | \frac{1}{r_{ij}} | u_m \rangle$. This transformation concentrates and separates the molecular orbitals. This makes the quantum mechanical description behave as closely as possible to a classical electrostatic interaction between electron pairs.¹⁸ However, the technique does not satisfy either of the criteria previously mentioned as being crucial: the partitioning is not necessarily unique²⁸ and is dependent on assuming a single determinantal orbital form of approximate wavefunction.

Several possible partitioning schemes which do satisfy both partitioning criteria are currently being investigated. They involve the division of a molecular system into mononuclear fragments rather than internuclear bond regions. Thus, Mazziotti, Parr and Simons³⁴ have proposed a "regional" partitioning of molecules satisfying a regional virial theorem. However, their derivation has been shown³⁵ to be incomplete. Srebrenik, Weinstein and Pauncz³⁶ have proposed but not developed two possible fragment definitions. One is based on the path of lowest rate of descent from internuclear electron density cols,

and the other employs partitioning surfaces constructed in the direction of the gradient of the total electrostatic potential of the molecule. The latter definition has the particularly useful feature of defining fragments containing equal and integral amounts of positive and negative charge. Construction of molecules from such fragments guarantees generation of neutral species of integrally quantized electronic charge, unlike some other proposals.

The most highly developed proposal along these lines is the "virial" partitioning technique of Bader and coworkers.^{37,35,38} Virial and hypervirial theorems for the "zero flux" fragments they proposed^{35,39} and additivity of the fragment energies to yield the total system energy³⁷ have been established. We shall compare the results of our "loge" partitionings to the predictions of the virial partitioning method allowing quantum mechanical evaluation of our interpretations from this second viewpoint.

CHAPTER II
THE LOGE CONCEPT, THE MISSING INFORMATION FUNCTION
AND THE ELECTRON PAIR

THE LOGE CONCEPT

In this chapter, we attempt to relate the predictions of quantum calculations to the chemist's intuitive concept of electron core, bonded and non-bonded pairs. As previously noted, one faces a very real problem in attempting to devise a precise definition of the "volume" occupied by a pair, as all nuclei of a molecule interact with all others directly (internuclear repulsion) and through the electronic charge (electron-nuclear attraction).

R. Daudel has proposed⁴⁰ a "loge" partitioning theory which bases a proposed definition of chemical bonds on the localizability of groups of electrons. A loge is defined⁴¹ as a part of the (three-dimensional) space of a molecule in which there is a high probability of finding a given number, n , of electrons with a certain orientation of their spins. The best decomposition into space-filling non-overlapping loges is that which gives the "minimum amount of indetermination" about the atom or molecule.

A complete derivation of the requisite formalism is available in the recent literature.^{41,30} We summarize here only the crucial features.⁴¹ We use the coordinate representation and Schrödinger picture.

Consider a pure system state describable by the eigenket $|\psi\rangle$. For an N -fermion system, such a state tensor is describable in a $4N$ -

dimensional coordinate-spin space built as the tensor product of N single particle spaces. Each of these is itself the product of a continuous space (generated by $|q\rangle$ for $q \in \mathbb{R}^3$) and a two-dimensional space (for which a basis is $|w\rangle$ where $w = \pm \frac{1}{2}$); q and w are the space and spin coordinates for one particle. The basis for the N -fermion system is thus $|q_1 w_1 q_2 w_2 \dots q_N w_N\rangle = |q_1 w_1\rangle \otimes |q_2 w_2\rangle \otimes \dots \otimes |q_N w_N\rangle$.

We can express $|\psi\rangle$ in this basis as:

$$\begin{aligned} |\psi\rangle &= \sum_{w_1} \int_{q_1} \sum_{w_2} \int_{q_2} \dots \sum_{w_N} \int_{q_N} |q_1 w_1 q_2 w_2 \dots q_N w_N\rangle \langle q_1 w_1 q_2 w_2 \dots q_N w_N | \psi \rangle dq_1 dq_2 \dots dq_N \\ &= \sum_{\{w_n\}} \int_{\{q_n\}} |\{q_n w_n\}\rangle \langle \{q_n w_n\} | \psi \rangle d\{q_n w_n\} \end{aligned}$$

where $\langle \{q_n w_n\} | \psi \rangle \equiv \psi(\{q_n w_n\})$ is the wavefunction for the system.

We can define a partitioning of the physical space \mathbb{R}^3 into v non-overlapping volumes, V_λ ($\lambda = 1, v$), which sum to \mathbb{R}^3 . The probability of finding n_1 particles in V_1 , n_2 particles in V_2 , etc., termed an "event", is then given by⁴⁴

$$\begin{aligned} P_\mu \equiv P(\{V_\lambda^{n_\lambda}\}) &\equiv P(\{V_1^{n_1}, V_2^{n_2}, \dots, V_v^{n_v}\}) = \frac{N!}{\prod_{\lambda=1,v} n_\lambda!} \int_{V_1} dx_1 \dots \int_{V_{n_1}} dx_{n_1} \int_{V_{n_1+1}} dx_{n_1+1} \dots \\ &\quad \times \int_{V_{n_1+n_2}} dx_{n_1+n_2} \dots \int_{V_v} dx_N \cdot r^{(N)}(\{q_n\}) \end{aligned}$$

where

$$r^{(N)}(\{q_n\}) = \sum_{\{w_n\}} \psi^*(\{q_n w_n\}) \psi(\{q_n w_n\})$$

As well,

$$\sum_\mu P_\mu = 1 \quad \text{and} \quad \sum_{\lambda=1}^v n_\lambda = N$$

If one partitions real space into two loge volumes, Ω and Ω' , then one can⁴² calculate the probability of the event localizing n electrons in Ω and the remaining $(N-n)$ in Ω' as

$$P_n(\Omega) = \frac{N!}{n!(N-n)!} \int_{\Omega} dx_1 \dots \int_{\Omega} dx_n \int_{\Omega'} dx_{n+1} \dots \int_{\Omega'} dx_N \Gamma^{(N)}$$

We now have a formal definition of a probability for various partitionings of groups of electrons within subspaces of \mathbb{R}^3 .

Several criteria to evaluate various loge partitionings have been suggested. In the preliminary studies of these concepts,^{25,26} it was suggested that one establish separate partitionings of the α -spin and β -spin electrons into loges "of order 1" (partitionings with the constraint that all $n_\lambda = 1$). For any trial partitioning one will then obtain a set of loge probabilities, $\{P_\lambda\}$, representing the probability of encountering one and only one particle per assumed loge volume. One then computes $\Omega = \sum_{\lambda} P_\lambda$ ($\leq \nu$) and η , the "localization defect":

$$\eta = \frac{P - \Omega}{P} \quad (n \geq 0)$$

The smaller the value of η is, then the better the partitioning is said to be. This methodology has been applied to partitioning of atoms.⁴³ The computed loge volumes are suggestive of the intuitively expected shell structure and preferred angular separation of valence electrons (from Fermi correlated approximate functions). The results based on this new criterion of localizability strongly parallel the predictions of localized orbital, equivalent orbital, and hybrid orbital formalisms.

The "localization defect" criterion is not really satisfactory in that it considers only partitionings of order one. Even searching

for the (non-trivial) partitioning which yields the absolute maximum value of any of the P_μ will not suffice as a satisfactory criterion of partitioning.⁴¹ One could not distinguish between partitionings yielding equally probable "leading" (i.e., most probable) events but different "satellite" (less but still highly probable) events. One is really interested in localization of groups of two or more electrons of either spin (to find an electron "pair", "three-electron bond" or delocalized electron sextet in aromatic molecules, for instance). As well, as noted above, one must consider all the loge probabilities for various spatial groupings of electrons (some of which one may predict or find to be negligible) to create a pedagogically satisfactory criterion of localizability.

THE MISSING INFORMATION FUNCTION

A function which satisfies all of these requirements has long been in use in information theory. This is the "missing information function",^{44,27} $I(P)$:

$$I(P) = -\sum_{\mu} P_{\mu} \log_2 P_{\mu}$$

(where $P \equiv \{P_{\mu}\}$).

The limiting values of $I(P)$ are

$$0 \leq I(P) \leq \log_2 N$$

where N is the number of possible events (of placing N particles in v loges, where $1 \leq v \leq N$ and for each value of v , one considers all spatial partitions). $I = 0$ only for the trivial partitioning of performing no partitioning at all. $I = \log_2 N$ for all events equally probable (random)

in which case $P_\mu = \frac{1}{N}$. In general, "good" partitionings of a molecule into loges thus correspond to obtaining values of $I(P)$ closer to zero than the upper limit.

In the case of a two-loge partitioning into regions Ω and Ω' , the formula for $I(P)$ reduces to

$$I(P) \equiv I(P_n, \Omega) = -\sum_n P_n(\Omega) \log_2 P_n(\Omega)$$

This proposal has several advantages.²⁷ The partitioning is in no way subjective. It is consistent with the postulates of non-relativistic quantum mechanics. It potentially provides a direct link between quantum predictions of electron localizability and the intuitive classical picture of almost isolated groups of electrons. Since it incorporates the probabilities of all the events, it permits an accurate assessment of the reality of any dominant localization. Finally, it provides an objective basis for the assessment of any proposed wavefunction construction in terms of spatially localized, strongly intra-correlated, and weakly intercorrelated "group" wavefunctions.

THE ELECTRON PAIR

We have performed loge partitionings of several small molecules using the criterion of minimization of $I(P)$. These calculations⁴² were performed for several reasons. We attempted an evaluation of the reality of electron localization due to Fermi correlation, into core, bonding, and non-bonding pairs in these systems. We assessed the practicality of the methodology required for use of the missing information criterion. We tried to determine what properties of a system may be used to predict loge shapes. In particular, our results indicate that loge boundaries

may, in some cases, be determined by the topological features of the electronic charge distribution.

The virial partitioning method of Bader and coworkers proposes a partitioning of molecular systems based on just such properties of the charge distribution. Partitioning surfaces in this technique are defined by the sets of paths of steepest descent through the charge distribution starting from the internuclear minima. The resultant fragments contain spatially localized electron populations in the sense that the fragments are separated by the minima in the charge distribution. A natural question to ask is whether or not there is any correlation between virial fragments and loges for a molecule. This would require that the essential information contained in the many-electron probabilities is retained in the charge density, $\rho(\underline{x})$, a one-particle probability function. Accordingly, we also compared the predictions of the loge and virial partitioning schemes for the systems studied.

The molecules chosen were $\text{LiH}^+(\text{X } ^2\Sigma^+)$, $\text{LiH}(\text{X } ^1\Sigma^+)$, $\text{BeH}^+(\text{X } ^1\Sigma^+)$, $\text{BeH}(\text{X } ^2\Sigma^+)$, $\text{BeH}(\text{A } ^2\Pi_r)$, $\text{BH}(\text{X } ^1\Sigma^+)$ ⁴⁵ and BeH_2 .⁴⁶ The charge distributions are given in Figure 1, and the important features summarized in terms of the virial fragment electron populations, $\bar{N}(\text{X})$ (for fragment X) and heavy-atom non-bonded populations in Table 1.

Virial partitioning of LiH^+ and LiH yields Li fragment populations near two, and hydrogen fragment populations near one and two, respectively. This suggests a likely loge partitioning to be one yielding a two-electron Li core plus, respectively, a one- and two-electron bonding loge. Similar observations hold for the other molecules. In each case, one finds a hydrogen fragment with a population

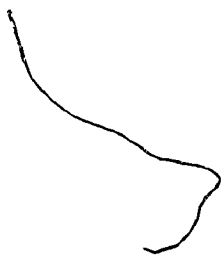
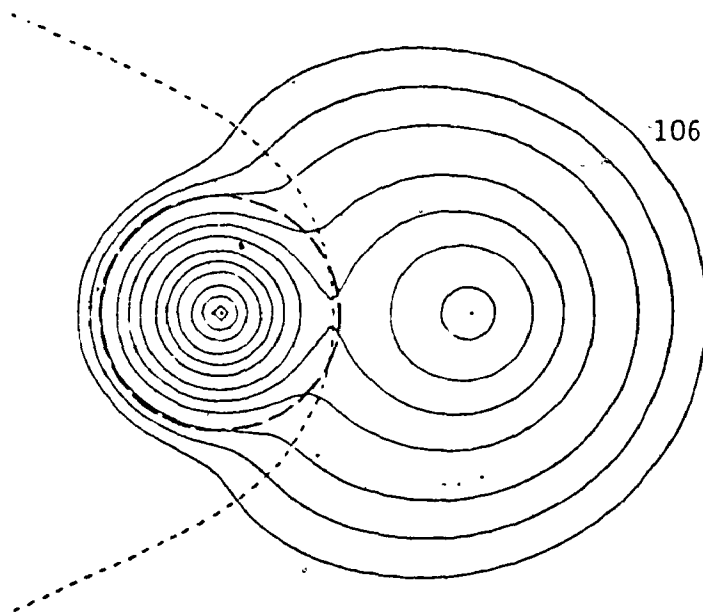
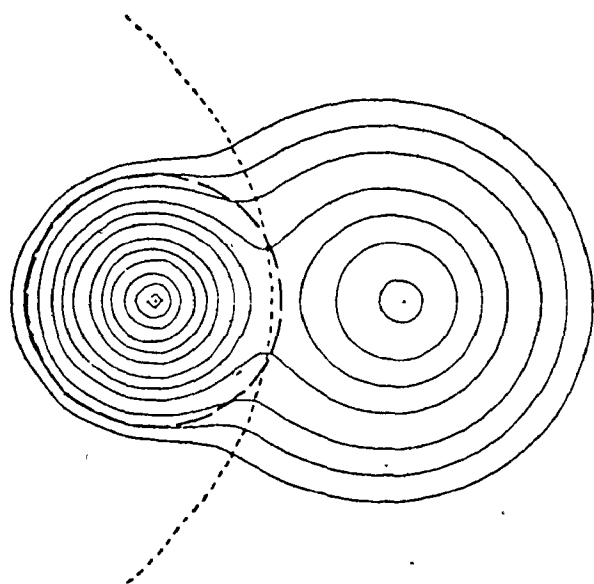
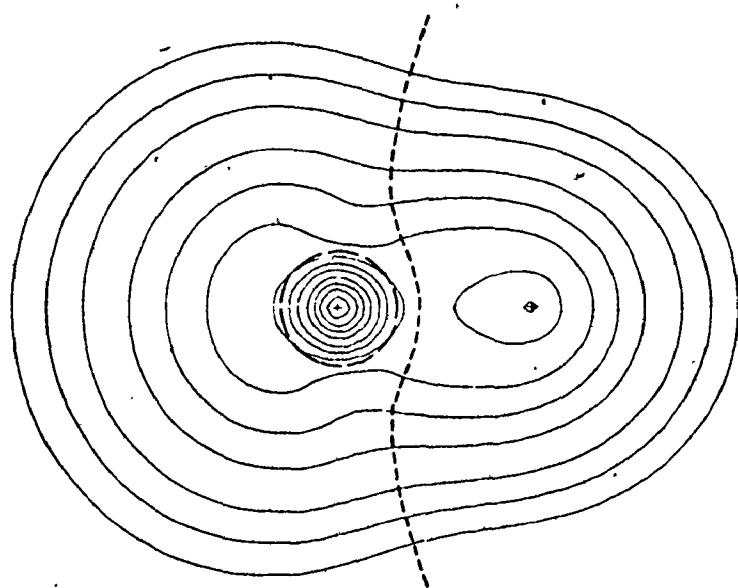
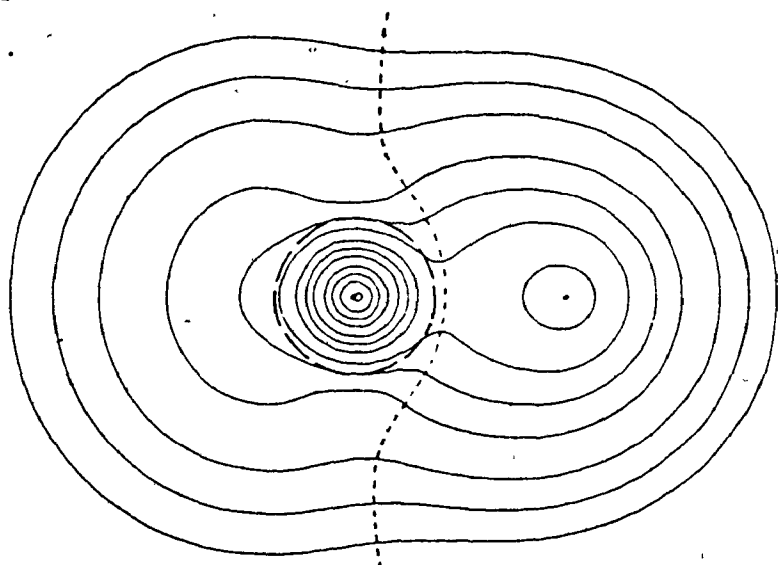
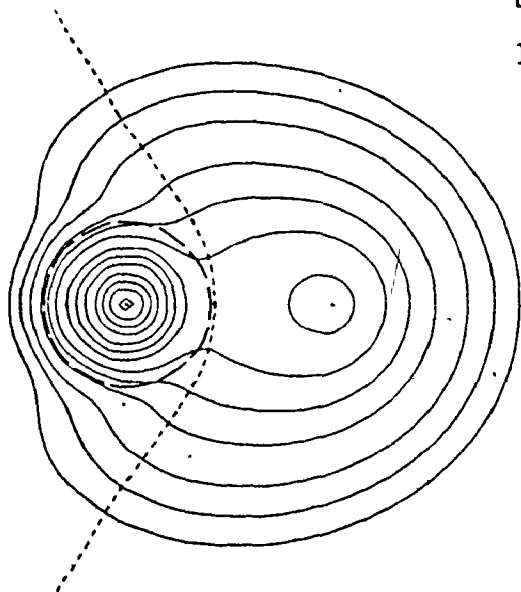


Figure 1. Contour maps of the electronic charge distribution for (displayed from left to right on succeeding rows) $\text{LiH}^+(\chi^2_\Sigma^+)$, $\text{LiH}(\chi^1_\Sigma^+)$, $\text{BeH}^+(\chi^1_\Sigma^+)$, $\text{BeH}(\chi^2_\Sigma^+)$, $\text{BH}(\chi^1_\Sigma^+)$ and $\text{BeH}(\text{A}^2_{\pi_r})$. In each diagram the curve indicated by short dashes denotes the virial partitioning surface defining the (A) and (H) fragments. The circle denoted by longer dashes defines the boundary of the "best" spherical lobe centred on the A nucleus. The density contours increase from the outermost, 0.002, to a maximum of 20, in steps of 2×10^n , 4×10^n , and 8×10^n for n integral and increasing from -3.



1 a.u.



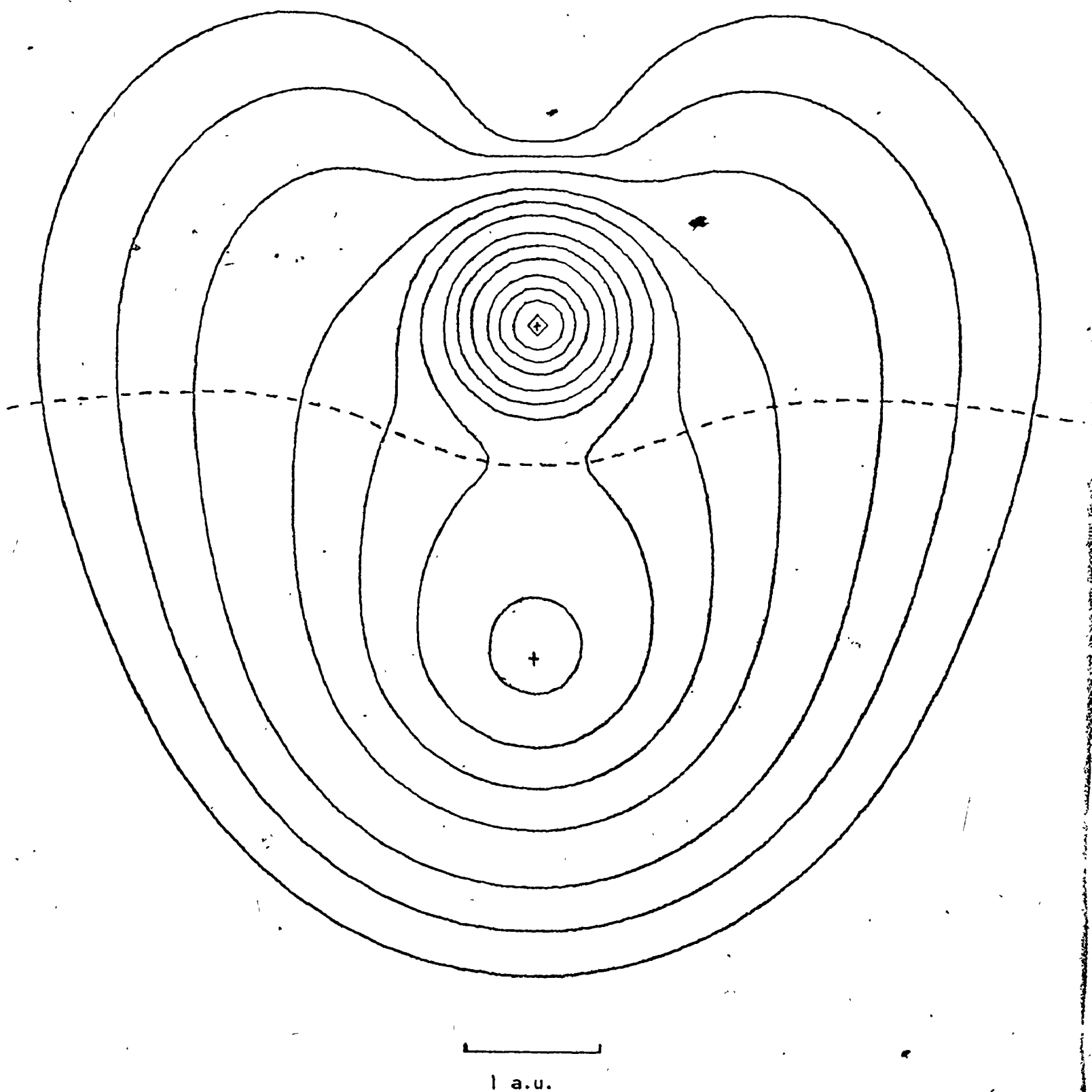


TABLE 1
Characteristics of the Charge Distributions

AH	Bond Lengths (a.u.)	$\bar{N}(A)$	$\bar{N}(H)$	Nonbonded Charge on (A)
$LiH^+(X \ ^2\Sigma^+)$	3.015	2.037	0.963	1.006
$LiH(X \ ^1\Sigma^+)$	3.015	2.089	1.911	1.065
$BeH^+(X \ ^1\Sigma^+)$	2.479	2.257	1.743	1.141
$BeH(X \ ^2\Sigma^+)$	2.538	3.132	1.868	1.964
$BeH(A \ ^2\Pi_r)$	2.519	3.073	1.928	1.692
$BH(X \ ^1\Sigma^+)$	2.336	4.246	1.754	2.748
$BeH_2(X \ ^1\Sigma_g^+)$	2.540	2.278	1.861	---

in the range 1.743 to 1.928. The non-bonded charge on a nucleus is defined as the charge contained on the non-bonded side by a plane through the nucleus. Such a plane almost halves a core density and shows that 96% and 88% of the unshared valence density is located in the heavy atom non-bonded regions in BeH(X) and BH, respectively.

The above analysis suggests that the leading event for loge partitioning of these systems would place two electrons in the heavy-atom core, two in a bonding loge (except for LiH, where one would obtain one), and the remaining electrons (if any) in a non-bonding loge on the heavy atom.

NUMERICAL TECHNIQUES

The calculation of event probabilities and missing information function values involved several steps. The Hartree-Fock wavefunctions were taken from the literature.^{45,46} They approach the Hartree-Fock limit in accuracy. The overlap integrals between all possible pairs of orbitals over all the loges in a system were evaluated by numerical integration using Gaussian quadrature techniques. The computer programme DIALØGE (Appendix B-1) was written for the $v = 2$ (two-loge) partitioning case by the author to perform the construction of the P_μ 's and $I(P)$ from the list of orbital loge overlaps. An extension to the three-loge partitioning case was made by D. S. Borrett (programme TRILØGE).

THE DIATOMIC MOLECULES LiH⁺, LiH, BeH⁺, BeH, BH

The six-electron molecule, BH(X ¹ Σ^+), is one of the simplest molecules which should exhibit electron localization into all three types of pair loges; core, bonding and non-bonding. Accordingly, we

shall discuss it as a representative system.

Core Loges

We found it most convenient to search first for the core loge expected of a heavy atom. These fragments in general were found to be the most strikingly localized.

Figure 2 summarizes the results of a search for the best spherical core loge (in a two-loge partitioning) of BH. Plotted are the values of $P_n(\Omega)$ and $I(P_n, \Omega)$ versus r , where Ω is a spherical loge centred on the heavy atom of radius r . Also plotted is the fluctuation in core fragment population, $\Lambda(\bar{N}, \Omega) = \overline{N^2}(\Omega) - (\bar{N}(\Omega))^2 = \sum_n n^2 P_n(\Omega) - (\sum_n n P_n)^2$. (We shall consider Λ in detail in the next chapter. It is sufficient to note here that Λ represents a measure of the statistical dispersion of measured fragment populations around the average.)

The single most probable event (ignoring the trivial cases of $P_0(\Omega) = 1$ for $r = 0$ and $P_6(\Omega) = 1$ for $r = \infty$) is obtained for $r = 0.7$ a.u. This volume simultaneously maximizes $P_2(\Omega)$ and minimizes $I(P_n, \Omega)$. For this partitioning there is an 85% probability of finding two electrons in the core loge and four in the remainder of the system. The largest satellite event probabilities $P_1(\Omega)$ and $P_3(\Omega)$ are small and almost equal (see Table 2). Hence the most probable core population is two, and the average population is 2.002.

Note that the decisive criterion is not simply the maximization of a single event. Thus, the missing information function has a maximum for $P_1(\Omega)$ a maximum because the satellite event probabilities $P_0(\Omega)$ and $P_2(\Omega)$ are also large. In general, $\Lambda(\bar{N}, \Omega)$ exhibits behaviour parallel to

Figure 2. The variation in the probabilities, $P_n(\Omega)$, the missing information function, $I(P, \Omega)$, and the fluctuation in $N(\Omega)$, $\Lambda(\bar{N}, \Omega)$, for a spherical loge of variable radius r (in a.u.) centred on the boron nucleus in $BH(X^{1\Sigma^+})$. The positions of the maxima in the $P_n(\Omega)$ values for each value of r are indicated on the plot showing the variation in $I(P, \Omega)$ and $\Lambda(\bar{N}, \Omega)$.

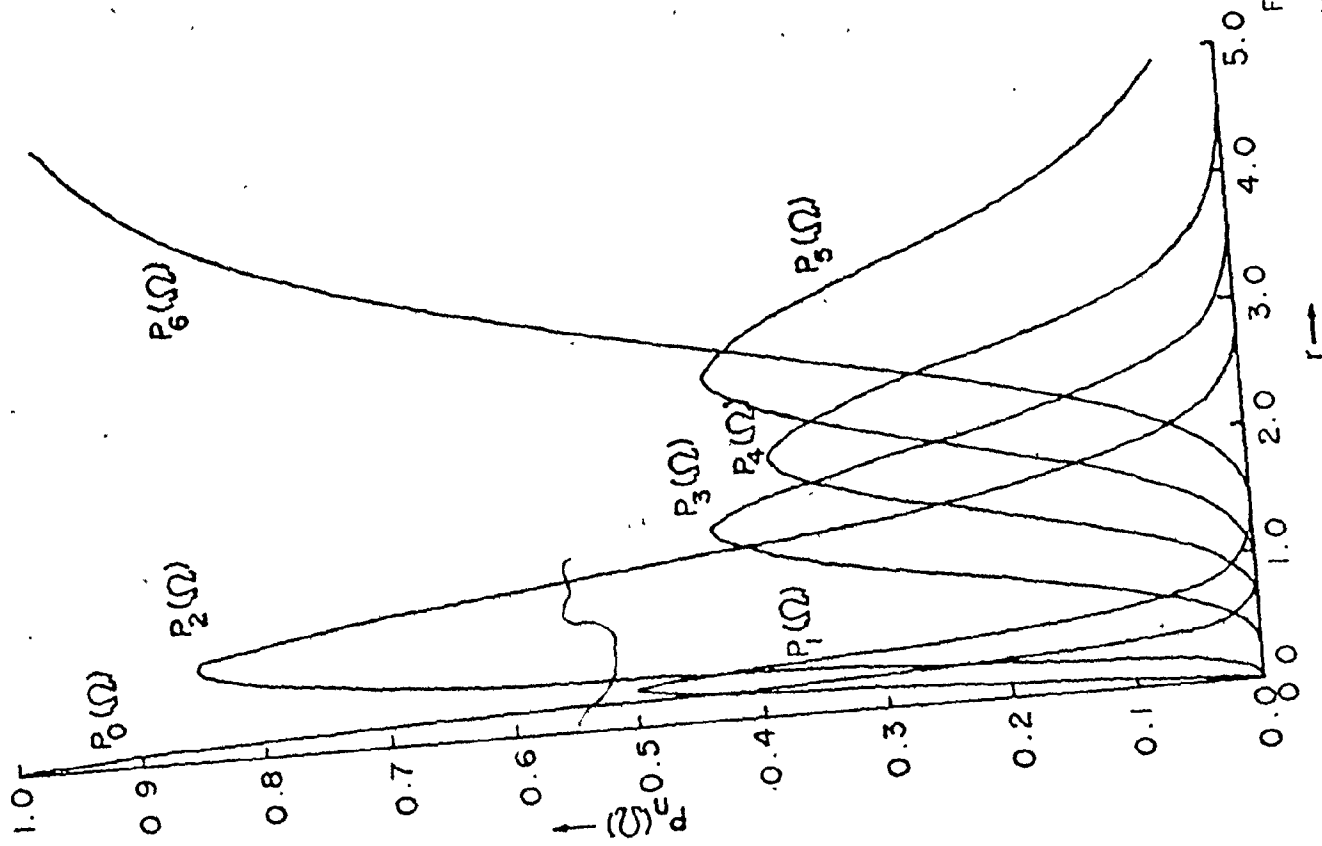


Figure 2

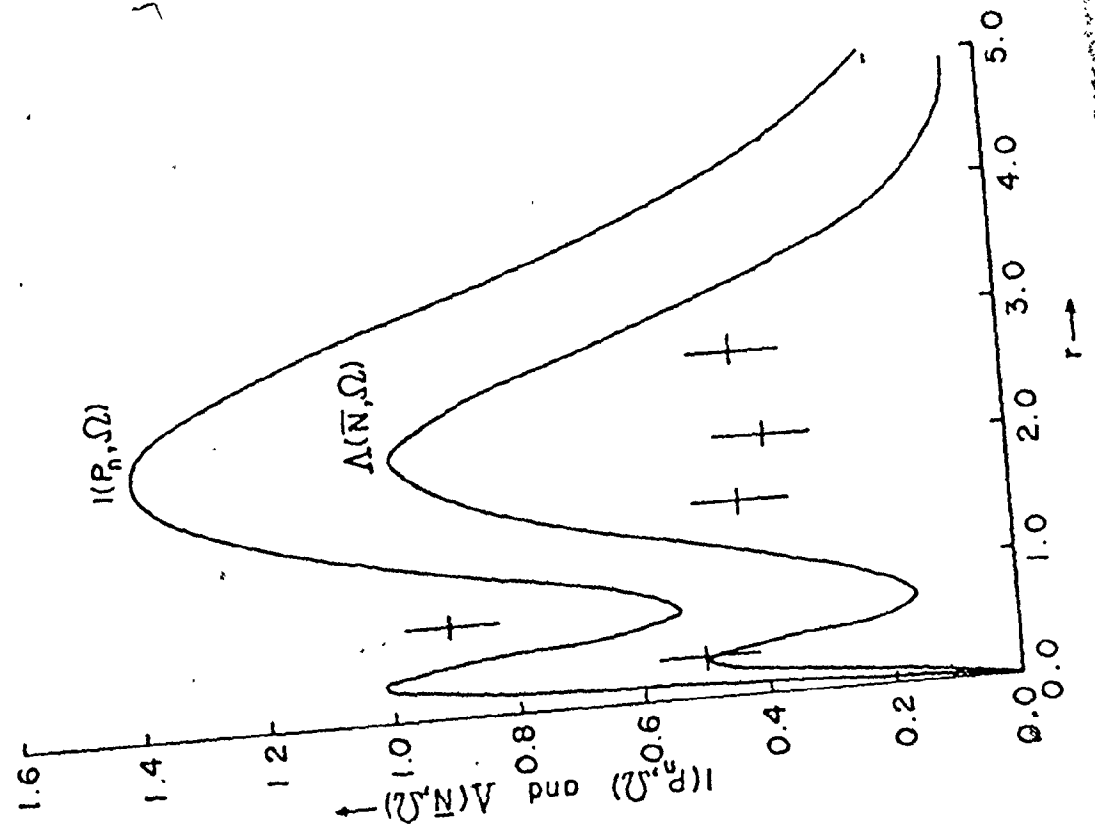


TABLE 2

Properties of Best Spherical Core Loges in AH

AH	r_c	$P_1(\Omega)$	$P_2(\Omega)$	$P_3(\Omega)$	$\bar{N}(\Omega)$	$I(P, \Omega)$	$\Lambda(\bar{N}, \Omega)$
LiH^+	1.55	0.0286	0.9427	0.0285	1.999	0.2604	0.0599
LiH	1.42	0.0438	0.9123	0.0428	1.999	0.3635	0.0902
BeH^+	1.00	0.0455	0.8969	0.0561	2.011	0.4103	0.1076
$\text{BeH}(X)$	0.95	0.0584	0.8804	0.0589	2.001	0.4602	0.1264
$\text{BeH}(A)$	1.00	0.0459	0.8764	0.0750	2.032	0.4690	0.1659
BH	0.70	0.0714	0.8532	0.0716	2.002	0.5364	0.1582

that of $I(P_n, \Omega)$ suggesting the importance of a criterion based on fragment dispersion.

Table 2 contains a summary of the optimum spherical cores obtained for the diatomic systems considered. Only the leading and two largest satellite event probabilities are listed, as they sum to greater than 99% of the total probability. $I(P_n, \Omega)$ is, in all cases, minimized for a sphere which maximizes the pair occupation probability. The satellite probabilities are small and approximately equal. Thus, $\bar{N}(\Omega) = 2.00 (\pm .011)$ in all cases. Note the decreasing $P_2(\Omega)$ values and increasing $I(P_n, \Omega)$ values as the number of electrons increases and degree of isolation or localization of the core density decreases. This is illustrated also in the variation of $\Lambda(\bar{N}, \Omega)$ which is only 0.06 for the well-localized core in LiH^+ but 0.16 in BH. (One also notes a steady decrease in core radius with increase in charge of the heavy nucleus.)

Table 3 contains the two-loge virial partitionings of these molecules. In those cases where the virial fragment contains a near-integral population (LiH^+ and LiH where the (Li) fragment is essentially an Li^+ ion), then the virial fragments correspond to the best loges. However, in general, virial fragments feature a non-integral population and both core and valence density. The missing information function correspondingly has a higher value for virial fragments than for a spherical core containing an electron pair.

In two molecules (LiH^+ and LiH) the radius of the best spherical core is greater than the distance from the heavy nucleus to the charge density minimum on the internuclear axis. The best spherical core loge thus crosses the virial surface. In those two cases, the virial parti-

tioning yields the lowest value of $I(P)$. This suggests that the virial surfaces define limiting boundaries for the definition of optimum spherical core loges. This is plausible since if one passes the density minimum then one is attempting to combine density from two core density peaks into one localized core pair.

The best core loges for the systems studied are listed in Tables 2 and 3. Loges of other shapes and populations were computed for the systems. For instance, the charge density in core regions is often slightly ellipsoidal reflecting a slight quadrupolar polarization along the internuclear axis. We defined a core loge for (B) in BH with boundary surface consisting of a constant density contour. For such core loges, $I(P)$ was again minimized (0.5748) for $P_2(\Omega)$ a maximum (0.8384). However, this type of core did not surpass the best spherical core for this system (Table 2). However, the optimal loges obtained always corresponded to minimal fragment population dispersion ($\Delta(\bar{N}, \Omega)$ value). Even if $P_2(\Omega)$ was not maximal (e.g., LiH) for the best loge (as defined by $I(P_n, \Omega)$), the dispersion was. Thus, a spherical core loge for LiH gave $P_2(\Omega) = .9123$ but also $P_1(\Omega) = .0438$ and $P_3(\Omega) = .0428$, whereas the virial fragment had a lower $P_2(\Omega) = .8995$, but $P_1(\Omega) = .0069$ and $P_3(\Omega) = .0912$. The virial fragment contains one important satellite event but the spherical core two equally important satellites.

To sum up, the most probable two-loge partitioning of these diatomics isolates a core with high $P_2(\Omega)$ value and minimal dispersion about the average population. The $P_2(\Omega)$ values indicate localization of electron core pairs to be very probable (over 95% for LiH^+ , 91% for LiH, 90% for BeH, and 85% for BH). For systems of an odd number

TABLE 3

Properties of Virially Defined (A) Fragments

AH	Bonded Radius of A (a.u.)	$P_1(A)$	$P_2(A)$	$P_3(A)$	$\bar{N}(A)$	$I(P,A)$	$\Lambda(\bar{N},\Omega)$
LiH ⁺	1.408	0.0054	0.9527	0.0418	2.036	0.2070	0.0471
LiH	1.344	0.0069	0.8995	0.0912	2.089	0.3622	0.0995
BeH ⁺	1.049	0.0034 $P_2(A)$	0.7536 $P_3(A)$	0.2261 $P_4(A)$	2.257	0.6379	0.2311
BeH(X)	1.083	0.0426 $P_3(A)$	0.7903 $P_4(A)$	0.1591 $P_5(A)$	3.132	0.6526	0.2175
BeH(A)	1.072	0.1778 $P_2(A)$	0.5901 $P_3(A)$	0.2114 $P_4(A)$	3.073	1.0301	0.4669
BH	1.001	0.0494	0.6757	0.2503	4.246	0.8549	0.3372

of electrons, core pairing is more important than for a bond loge (e.g., LiH^+). As we shall see, bond pairing is more important than for non-bonding electrons (e.g., BeH below).

Valence Density Partitioning

If electron pairing is a valid concept in interpreting valence charge distributions, then the ground state valence density in BeH and BH should be decomposable into a two-electron bond loge plus one- and two-electron non-bonding loge, respectively. The final loges for such a system one intuitively feels should be definable by the heavy atom core radius, r_c , plus an angle α between the internuclear axis and a radical partitioning surface extending from the surface of the core to infinity (see Figure 3). These latter surfaces will partition the valence density into cylindrically symmetric internuclear bonding regions and terminal non-bonding regions.

We varied both r_c and α to minimize $I(P)$ for a three-loge partitioning in both BeH and BH . An event is now defined by three fragment populations (n_c, n_n, n_b), the core, non-bonding, and bonding loge populations. We now denote an event probability by a double subscript: $P_{n_c, n_n}(\Omega_c, \Omega_n)$, where necessarily $n_b = N - n_c - n_n$.

In both BH and BeH , the optimal values of r_c were the same as that defined by the two-loge partitioning. $I(P)$ was found to be a minimum for r_c and α chosen such as to maximize the probability of the event (2,2,2). The results are summarized in Table 4. Note the dominance of event (2,2,2). There is a 69% probability of localizing the electrons into core, bonding and non-bonding pairs. The probabilities of eight

TABLE 4

(a) Three-log Partitioning in BH

(i) Probabilities of Events (n_c, n_n, n_b)*

n_c	n_n	1	2	3
1		0.0026	0.0253	0.0391
2		0.0831	0.6870	0.0781
3		0.0377	0.0302	0.0016

(ii) Maximum Two-log Probabilities, $I(P, \Omega)$ and Λ Values

	Core	Nonbonded	Bonded
$P_2(\Omega)$	0.8532	0.7431	0.7649
$I(P, \Omega)$	0.5364	0.7981	0.7491
$\Lambda(\bar{N}, \Omega)$	0.1582	0.2950	0.2648

* $r_c = 0.7$ a.u., $\alpha = 73^\circ$, $\bar{N}(\Omega_c) = 2.001$, $\bar{N}(\Omega_n) = 1.998$,
 $\bar{N}(\Omega_b) = 1.999$, $I(P, \Omega_c, \Omega_n) = 1.2328$.

(b) Three-log Partitioning in BeH

(i) Probabilities of Events (n_c, n_n, n_b)*

n_c	n_n	0	1	2
1		0.0016	0.0250	0.0301
2		0.0541	0.7744	0.0511
3		0.0250	0.0329	0.0011

(ii) Maximum Two-loge Probabilities, $I(P, \Omega)$ and Λ Values

	Core	Nonbonded	Bonded
$P_n(\Omega)$	0.8804 ($n = 2$)	0.8328 ($n = 1$)	0.8297 ($n = 2$)
$I(P, \Omega)$	0.4602	0.5800	0.5931
$\Lambda(\bar{N}, \Omega)$	0.1264	0.1760	0.1822

* $r = 0.95$ a.u., $\alpha = 85^\circ$, $\bar{N}(\Omega_c) = 2.001$, $\bar{N}(\Omega_n) = 1.007$,

$\bar{N}(\Omega_b) = 1.992$, $I(P, \Omega_c, \Omega_n) = 0.9614$.

satellite events are symmetrically distributed around $P_{2,2}(\Omega_c, \Omega_n)$. The resulting average population of each fragment is 2.00 ($\pm .002$).

Similar results were found for BeH, the dominant event being (2,1,2) (one non-bonding electron). There is a 77% probability of localizing a core and bond pair plus a lone non-bonding electron.

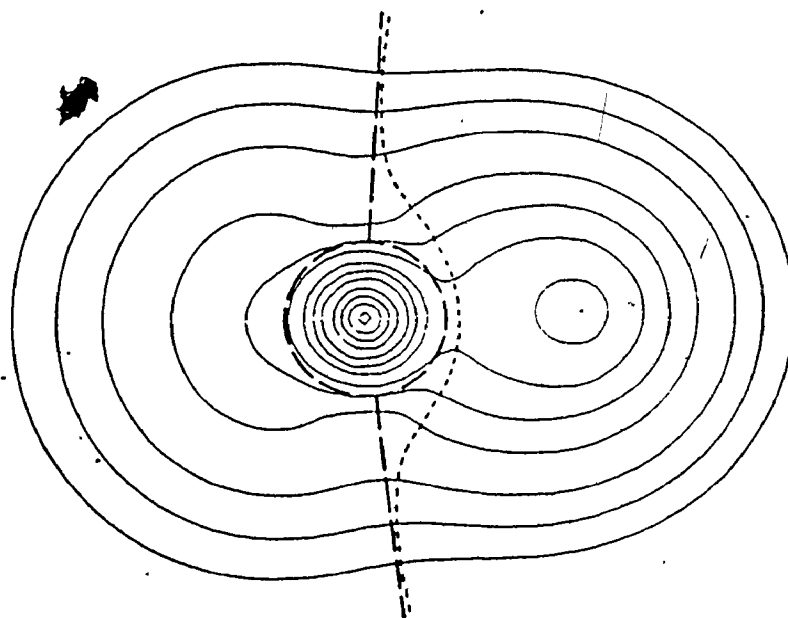
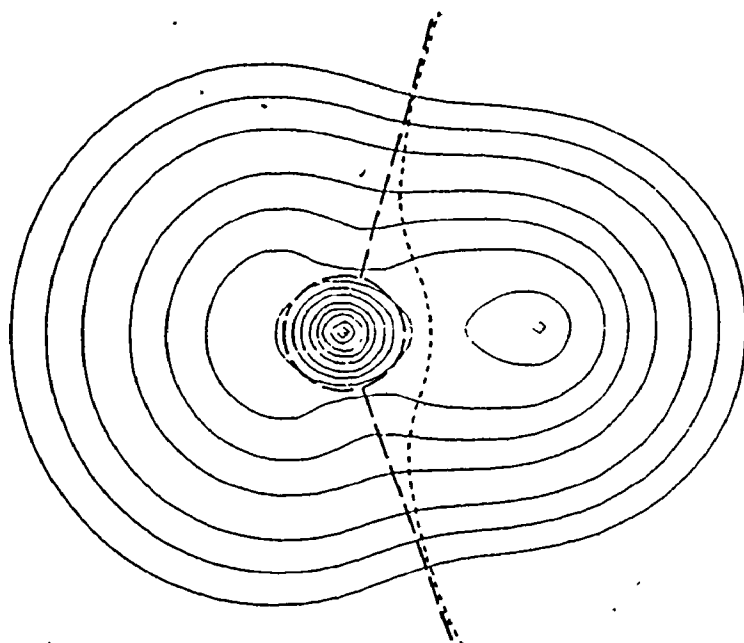
To further demonstrate the importance of the dispersion, we consider another partitioning of BH.

We halved the valence region (excluding the two-electron core sphere) by a σ_v symmetry plane containing the internuclear axis. This yields two identical valence loge volumes and all loge populations must equal 2.00. The leading event is still (2,2,2) but its probability is reduced from .6870 to .320. The satellite events (2,1,3) and (2,3,1) have equal probabilities of .213 (up from .0831 and .0781, respectively). Thus, one has replaced one very dominant event (2,2,2) by three almost equally probable events: (2,2,2), (2,1,3) and (2,3,1) which average to give the same population. For each valence region, $\Lambda = 1.0391$ (c.f. Table 4(a)(ii)).

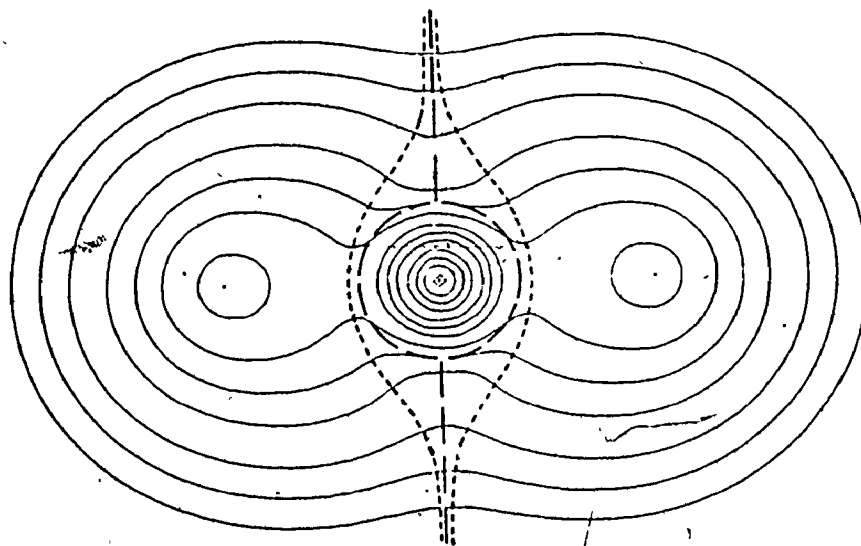
Figure 3 illustrates the striking feature that the radial valence partitioning surfaces closely approximate the virial surfaces traversing the trough in the outer valence region in each system. In this manner, a "natural" partitioning is provided by the virial surfaces.

The outer contour in Figure 3 is the .002 contour which, as previously noted, contains over 95% of the system charge density. Together with the core sphere and radial surface, this surface can be taken to define a "size" of the electron bonding and non-bonding pairs. In BH, the ratio of non-bonding to bonding pair volumes is 1.51. Even in BeH, the lone non-bonded electron occupies a volume 0.962 that of the bonded

Figure 3. Contour maps of the electronic charge distribution in $\text{BH}(X^1\Sigma^+)$, $\text{BeH}(X^2\Sigma^+)$, and $\text{BeH}_2(X^1\Sigma_g^+)$ showing the boundaries of the best three-lobe partitioning of these systems (long dashed lines) and, for comparison, the surfaces of zero-flux defining the (A) and (H) fragments (short dashed lines). The angle α is measured counterclockwise from the internuclear axis to the radial line separating the valence lobes.



1 a.u.



pair. This result is in accord with Gillespie's VSEPR postulate that non-bonding pairs occupy a larger volume than bonding pairs.

The greater the number of loges into which a system is to be partitioned, the greater is the number of event probabilities. Thus the leading event will generally have a lower probability in a three-loge partitioning than in a two-loge partitioning. One can reduce three-loge probabilities into two-loge probabilities for any of the three loges (i.e., the loge of interest plus the rest of space) by summation over the possible events for two loges being collapsed into one. For instance, $P_1(\Omega_n)$ for the non-bonded loge in BeH is given by

$$P_1(\Omega_n) = \sum_{n_c=0}^4 P_{n_c,1}(\Omega_c, \Omega_n)$$

Thus, one can define a set of probabilities for each loge.

The probabilities of the leading events and $I(P)$ values for core, non-bonded and bonded loges for BH and BeH are given in Table 4. Comparison of $I(P)$ values for various partitionings is meaningful only if the number of loges is constant. Thus, the $I(P)$ values quoted are for a two-loge partitioning (loge of interest plus remainder of molecular space).

For both BeH and BH, the core loge has highest pair probability and smallest $I(P)$ value obtained for a two-loge partition. The bonded and non-bonded loges have comparable values of leading event probabilities and $I(P)$ values and are less localized than the core.

We now consider the $A^2\Pi_r$ excited state of BeH. On excitation from the ground ($X^2\Sigma^+$) state, the changes in charge distribution occur primarily in the non-bonded region of the (Be) fragment. The diffuse

non-bonded density has changed from an axial to equatorial distribution. The core radius, population, two-loge $I(P)$ and Λ values are all slightly higher than for the ground state. Attempts to partition the valence density into a bond pair loge and non-bonded one-electron loge failed. With r_c fixed at its best two-loge value, we evaluated the three-loge $I(P)$ value for variable α . We expected that, considering the ground state results, we would obtain a minimum $I(P)$ value for α maximizing the event (2,1,2). The actual results obtained are given in Table 5. This event was maximized for $\alpha \sim 80^\circ$, giving a surface close to the virial surface as in previous cases. However, $I(P)$ was not maximized for this partition, and continued to decrease for α increasing (and thus the non-bonding loge volume decreasing). In the limit as $\alpha \rightarrow 180^\circ$, $I(P)$ approaches a minimal value for three-loge partition of 0.4690, its value for the best two-loge partitioning, separating the best spherical core from the whole valence region (the event (2,0,3) dominant). This behaviour differs from that observed in the ground state case, where a minimum $I(P)$ (relative to other three-loge partitions) was obtained for maximal probability of the event (2,1,2). Thus, the ground state valence density is partitionable into two localized distributions, but that for this excited state is apparently not. If some three-loge partition can be found, it will not correspond to the usual notions of core, bonded and non-bonded electrons.

The Triatomic Molecule BeH_2

We next partitioned the triatomic molecule BeH_2 . Considering the previous results, one anticipates the optimal loge partitioning will give a core loge and two-bond loges all with average populations

TABLE 5[†](a) Three-Loge Partitioning of BeH(A)[†]

α	$P(n_c, n_n, n_b)$			$\bar{N}(\Omega_b)$	$I(P)^*$
	(2,0,3)	(2,1,3)	(2,2,1)		
60°	0.0770	0.5322	0.2393	1.722	1.4538
80°	0.2336	0.5384	0.0996	2.109	1.3938
90°	0.3431	0.4753	0.0562	2.288	1.3570
100°	0.4627	0.3845	0.0286	2.458	1.2837
150°	0.8572	0.0191	0.0001	2.943	0.5820
179.5°	0.8764	0.0000	0.0000	2.968	0.4690

* for three-loge partition

(b) Bond Loge Properties for BeH(A)[†]

α	$P_1(\Omega_b)$	$P_2(\Omega_b)$	$P_3(\Omega_b)$	$I(P)^*$	$\Lambda(\bar{N}(\Omega_b), \Omega_b)$
60°	0.2910	0.5834	0.0868	1.0163	0.4557
80°	0.1369	0.5977	0.2524	0.9930	0.4300
90°	0.0863	0.5363	0.3646	0.9754	0.4174
100°	0.0518	0.4480	0.4849	0.9340	0.3893
150°	0.0031	0.0932	0.8616	0.5038	0.1463
179.5°	0.0021	0.0750	0.8764	0.4690	0.1308

* for two-loge partition

[†] reproduced from reference 47.+ $r = 1.00$ a.u., $\bar{N}(\Omega_c) = 2.032$

of 2.00. There are two simple ways to accomplish this. If one retains a spherical core, then by fixing $\alpha = 90^\circ$ or 0° one will obtain two identical bond loges divided by a σ_h or σ_v molecular symmetry plane, respectively. The only geometrical variable for these cases is r_c , the core radius.

Table 6(a) and 6(b) contain the results of these calculations. The optimum value of r_c was 0.93 a.u., slightly less than the 0.95 a.u. found for BeH. The difference in the event probabilities between the two proposed partitionings is striking. For the σ_h partition, the leading event is (2,2,2) ($P_{2,2} = .8028$) and all satellite events have probabilities less than 0.04. The leading event for the σ_v partition is still (2,2,2) but its probability is reduced to .3268 and the probabilities of both the two satellite events (2,1,3) and (2,3,1) are .2179. Hence, again we observe the importance of a low dispersion to an optimal partitioning, and not just a set of average populations equal to 2.00. Note also that for the σ_h case, $I(P)$ for the two-loge bond fragment partition is almost as low as for the core loge. Three pairs of electrons are thus clearly localizable.

Table 6(c) contains the results of the virial partitioning of this system into three fragments. The fragment populations all differ by more than 0.1 electron from integral values. The leading event is still (2,2,2) but its probability is more than 10% less than for the optimal (core plus σ_h plane) partition. There are now significantly probable satellite events, (3,1,2) and (3,2,1), thus increased dispersion and reduced localizability of the electron populations.

All of these molecules illustrate the possibility of finding

TABLE 6

Three-Loge Partitioning in $\text{BeH}_2(X^1\Sigma_g^+)$ (a) Symmetrical Partitioning (σ_h plane)*(i) Probability of Events ($n_c, n_b, n_{b,1}$)

$n_c \backslash n_b$	1	2	3
1	0.0012	0.0309	0.0309
2	0.0340	0.8028	0.0340
3	0.0301	0.0301	0.0006

(ii) Leading Events for Two-Loge Partitioning, $\Lambda(\bar{N}, \Omega)$ and $I(P, \Omega)$ Values

	Core	Bonded
$P_2(\Omega)$	0.8715	0.8644
$I(P; \Omega)$	0.4862	0.5061
$\Lambda(\bar{N}, \Omega)$	0.1370	0.1444

* $r_c = 0.93$ a.u., $\alpha = 90^\circ$, $\bar{N}(\Omega_c) = 1.998$, $\bar{N}(\Omega_b) = 2.001$, $\bar{N}(\Omega_{b,1}) = 2.001$,

$$I(P, \Omega_c, \Omega_b) = 0.8847.$$

(b) Symmetrical Partitioning (σ_v plane)*(i) Probability of Events ($n_c, n_b, n_{b,1}$)

$n_c \backslash n_b$	1	2	3
1	0.0100	0.0201	0.0201
2	0.2179	0.3268	0.2179
3	0.0231	0.0231	0.0077

TABLE 6 (Continued)

(ii) Leading Events for Two-Loge Partitioning, $\Lambda(\bar{N}, \Omega)$ and $I(P, \Omega)$ Values

	<u>Core</u>	<u>Bonded</u>
$P_2(\Omega)$	0.8715	0.3706
$I(P, \Omega)$	0.4862	1.4276
$\Lambda(\bar{N}, \Omega)$	0.1370	1.0347

* $r_c = 0.93$ a.u., $\alpha = 90^\circ$, $\bar{N}(\Omega_c) = 1.998$, $\bar{N}(\Omega_b) = 2.001$, $\bar{N}(\Omega_{b'}) = 2.001$,
 $I(P, \Omega_c, \Omega_b) = 1.8914$.

(c) Virial Partitioning*

(i) Probability of Events ($n_c, n_b, n_{b'}$)

$n_c \backslash n_b$	1	2	3
1	0.0001	0.0032	0.0032
2	0.0189	0.7003	0.0189
3	0.1125	0.1125	0.0015

(ii) Maximum Two-Loge Probabilities and $I(P, \Omega)$ Values

	<u>Core</u>	<u>Bonded</u>
$P_2(\Omega)$	0.7384	0.8204
$I(P, \Omega)$	0.6972	0.5702
$\Lambda(\bar{N}, \Omega)$	0.2732	0.1814

* $\bar{N}(c) = 2.277$, $\bar{N}(b) = 1.861$, $\bar{N}(b') = 1.861$, $I(P, \Omega_c, \Omega_b) = 1.0783$.

partitionings of at least some small systems into regions containing well-localized pairs of electrons as defined by minimal $I(P)$ and $\Lambda(\bar{N}, \Omega)$ values. The loge boundaries may be defined by virial boundaries in some cases. In all the cases studied, the loge boundaries lie near the virial surfaces (Figure 3). The closer the loge fragments approximate the virial fragments, the better is an interpretation of the electronic system in terms of largely self-contained electron pair quantum subsystems.³⁹

This study revealed several problems in the use of $I(P)$ as a criterion of loge partitioning. Even for a six-electron system described by a Hartree-Fock wavefunction, significant amounts of computation time are required to calculate the various event probabilities (Appendix B-1). Application to larger systems and wavefunctions sophisticated enough to properly incorporate Coulomb correlation effects will be extremely difficult if not impossible.

As well, the interpretation of $I(P)$ values for partitionings into various numbers of loges is not clearly understood. In general one can only say that the more fragments one attempts to isolate, the higher $I(P)$ must be for the partitioning as there are more events to be incorporated into it. Use of the fragment fluctuation function, $\Lambda(\bar{N}, \Omega)$, can alleviate these problems, as we shall see.

The systems studied revealed significant localization of the electron distribution into pairs. However, these systems contain at most four valence electrons. Can one find a clear-cut localizability of, for instance, four electron pairs around the carbon atom in CH_4 , a molecule

also commonly described in terms of electron pairs?

In the next chapter we consider these problems and propose several formal relationships between measures of electron group localizability and intra- versus inter-group correlation. This will provide a formal explanation of the importance of the dispersion empirically observed in the work reported in this chapter.

CHAPTER III

ELECTRON FLUCTUATION AND CORRELATION

In the previous chapter, we noted empirically the parallel behaviour of $I(P)$ and fragment fluctuations, $\Lambda(\bar{N}, \Omega)$, for molecular partitioning. Specifically, both I and the fragment fluctuations approach zero as one event becomes more and more dominant for each loge. Since we interpret the minima in I as providing the "good" choices for localizing groups of electrons in various regions of space, it is plausible that the corresponding loge population fluctuations should be small as well. This suggested that we derive the formal relation of Λ to quantum mechanical measures of the dispersion of quantum event probabilities. A further incentive was that whereas computation of $I(P)$ requires use of $\Gamma^{(N)}$, $\Lambda(\bar{N}, \Omega)$ can be calculated from $\Gamma^{(2)}$, permitting significantly simpler calculations. Finally, and most importantly, the fragment fluctuations provide direct measures of the correlation-induced intra- and inter-fragment changes in pair probability distributions from the simple product of single particle densities of the independent particle case.

For any loge volume Ω , one can calculate the fluctuation in population, $\Lambda(\bar{N}, \Omega)$, as follows:⁶⁰

$$\begin{aligned}\Lambda(\bar{N}, \Omega) &\equiv \overline{(N(\Omega) - \bar{N}(\Omega))^2} \\ &= \overline{N^2(\Omega)} - [\bar{N}(\Omega)]^2 \\ &= \sum_{n=1}^N n^2 P_n(\Omega) - \left[\sum_{n=1}^N n P_n(\Omega) \right]^2\end{aligned}$$

where $N(\Omega)$ is one of the measured populations of Ω , $P_n(\Omega)$ is the probability of finding n electrons in Ω , the remaining $(N-n)$ electrons in the rest of space, and a bar over any quantity indicates the average value of that quantity is to be taken.

But

$$\overline{N^2}(\Omega) \equiv \sum_n n^2 p_n(\Omega) \quad (1)$$

$$\begin{aligned} &= \sum_n n^2 \frac{N!}{n!(N-n)!} \int_{\Omega} dq_1 \dots \int_{\Omega} dq_n \int_{\Omega} dq_{n+1} \dots \int_{\Omega} dq_N \Gamma^{(N)}(q_1, q_2, \dots, q_N) \\ &= N(N-1) \int_{\Omega} dq_1 \int_{\Omega} dq_2 \left[\sum_{m'=0}^{N-2} \frac{(N-2)!}{m'!(N-2-m')!} \int_{\Omega} dq_3 \dots \int_{\Omega} dq_N \Gamma^{(N)}(q_1, q_2, \dots, q_N) \right] \\ &\quad + N \int_{\Omega} dq_1 \left[\sum_{m=0}^{N-1} \frac{(N-1)!}{m!(N-1-m)!} \int_{\Omega} dq_2 \dots \int_{\Omega} dq_N \Gamma^{(N)}(q_1, q_2, \dots, q_N) \right] \quad (2) \end{aligned}$$

where $m = n-1$, $m' = n-2$ and the limits of integration (Ω or Ω') are omitted after the summations, as they vary over all possible combinations of Ω and Ω' depending on the value of m and m' in the sums. If one defines the diagonal elements of the particle and pair densities as:

$$D_1(q_1) = N \sum_{w_1(s_1)=-\frac{1}{2}}^{+\frac{1}{2}} \int dx_2 \dots \int dx_N \psi^*(\{x_n\}) \psi(\{x_n\}) \quad (3)$$

$$D_2(q_1, q_2) = N(N-1) \sum_{w_1(s_1)=-\frac{1}{2}}^{+\frac{1}{2}} \sum_{w_2(s_2)=-\frac{1}{2}}^{+\frac{1}{2}} \int dx_3 \dots \int dx_N \psi^*(\{x_n\}) \psi(\{x_n\}) \quad (4)$$

then $\overline{N^2}(\Omega)$ may be written⁵² as

$$\overline{N^2}(\Omega) = \int_{\Omega} dq_1 \int_{\Omega} dq_2 D_2(q_1, q_2) + \int_{\Omega} dq_1 D_1(q_1) \quad (5)$$

Combining equations (1) and (5), we find

$$\Lambda(\overline{N}, \Omega) = \int_{\Omega} dq_1 \int_{\Omega} dq_2 D_2(q_1, q_2) + \overline{N}(\Omega) - [\overline{N}(\Omega)]^2 \quad (6)$$

where we have used the relation⁴⁹

$$\int_{\Omega} dq_1 D_1(q_1) = \overline{N}(\Omega). \quad (7)$$

CORRELATION FUNCTIONS

Now one can choose various measures of the effects of particle correlation,^{49,2} all basically involving functional comparison of the pointwise difference between $D_2(q_1, q_2)$ and $D_1(q_1)D_1(q_2)$ (which are equal for all q_1 and q_2 for non-correlated particles). We choose to use the correlation factor, $f(q_1, q_2)$, as defined by McWeeny:⁵⁰

$$D_2(q_1, q_2) = D_1(q_1)D_1(q_2)[1 + f(q_1, q_2)]. \quad (8)$$

Combining equations (6) and (8), we find

$$\begin{aligned} \Lambda(\bar{N}, \Omega) &= \int_{\Omega} dq_1 \int_{\Omega} dq_2 D_1(q_1)D_1(q_2)f(q_1, q_2) + \bar{N}(\Omega) \\ &\equiv F(\Omega) + \bar{N}(\Omega) \end{aligned} \quad (9)$$

To appreciate the meaning of this result, consider the integration of equation (8) over the coordinates of particle two; we obtain

$$(N-1)D_1(q_1) = [N + \int dq_2 D_1(q_2)f(q_1, q_2)]D_1(q_1) \quad (10)$$

Thus

$$\int dq_2 D_1(q_2)f(q_1, q_2) = -1 \quad \text{for all } q_1 \quad (11)$$

This relation is required since the pair density is normalized to $N(N-1)$ and each particle density is normalized to N . Equation (11) guarantees that one obtains the same number of pairs, $N(N-1)$, using either side of equation (8). The integrand of equation (11) is called the "correlation hole" surrounding particle one if located in the volume dq_1 at q_1 . This is another manifestation of the Pauli principle, and has the further interpretation that, if the coordinates of one particle are fixed, then the number of particles located in the system space is reduced by one.

Equation (9) can similarly be interpreted as indicating that a loge fluctuation will equal zero if the integral of the "correlation hole" for each electron over the loge reaches its limiting value of -1. In that case, the integral

$$F(\Omega) = \int_{\Omega} dq_1 \int_{\Omega} dq_2 D_1(q_1) D_2(q_2) f(q_1, q_2) \quad (12)$$

attains its limiting value, $-\bar{N}(\Omega)$. The electrons would then form a totally intra-correlated quantum subsystem in Ω . Thus, $F(\Omega)$ provides a direct measure of the total changes in particle pairing due to fragment intra-correlation.

The calculus of variations may be used to yield another result useful in the interpretation of $\Lambda(\bar{N}, \Omega)$ and $F(\Omega)$. Consider the fragment population integral

$$\bar{N}(\Omega) = \int_{\Omega} D_1(q_1) dq_1$$

We wish to assess the effects of any infinitesimal variation in the surface containing the volume Ω . With each surface element, dS , we can associate a change in the volume integral of $D_1(q_1)n(q_1)dS$ (where $n(q_1)dS$ measures the added volume associated with dS). The total change in the integral over the complete surface, $\delta[\bar{N}(\Omega)]$, is given by

$$\delta[\bar{N}(\Omega)] = \oint n(q_1) D_1(q_1) dS$$

For arbitrary $n(q_1)$ (i.e., arbitrary shifts in the position of each surface element) this integral may be zero only if $D_1(q_1) = 0$ for all q_1 on the surface of the volume.

We want Λ for a loge to be a minimum with respect to all variations in its bounding surface. Then $\delta\Lambda = 0$ for any arbitrary surface change.

Consider an infinitesimal change in $\Lambda(\bar{N}, \Omega)$ (from equation (9)):

$$\begin{aligned}\delta \Lambda(\bar{N}, \Omega) &= 2 \oint_S n(\underline{q}_1) D_1(\underline{q}_1) dS \int_{\Omega} f(\underline{q}_1, \underline{q}_2) D_1(\underline{q}_2) d\underline{q}_2 + \oint_S n(\underline{q}_1) D_1(\underline{q}_1) dS \\ &= \oint_S n(\underline{q}_1) D_1(\underline{q}_1) dS [2 \int_{\Omega} f(\underline{q}_1, \underline{q}_2) D_1(\underline{q}_2) d\underline{q}_2 + 1]\end{aligned}$$

For arbitrary $n(\underline{q}_1)$ where \underline{q}_1 is on the surface (and $D_1(\underline{q}_1) \neq 0$) $\delta\Lambda$ may equal zero (and hence $\Lambda(\bar{N}, \Omega)$ attain a stationary value) only if the quantity in square brackets itself equals zero, or

$$\int_{\Omega} f(\underline{q}_1, \underline{q}_2) D_1(\underline{q}_2) d\underline{q}_2 = -\frac{1}{2} \quad (13)$$

That is, for surface points (\underline{q}_1) of a region of (locally) minimal fluctuation, the correlation hole is divided equally between Ω and the rest of space. The surfaces partitioning a molecule into loges thus represent the boundaries of regions beyond which correlation holes for a particle at the point considered have a larger contribution from the region entered than that left. In this sense then a "best" loge partitioning yields maximally intracorrelated regions of charge density.

We can further define a relative fluctuation, $\lambda(\Omega) = \Lambda(\bar{N}, \Omega)/\bar{N}(\Omega)$, which can also be written:

$$\lambda(\Omega) = 1 + F(\Omega)/\bar{N}(\Omega) \quad (14)$$

where $-F(\Omega)/\bar{N}(\Omega)$ is the fraction of the total possible correlation of the fragment population actually contained in the loge. Surfaces defining loges for which $\Lambda(\bar{N}, \Omega)$ are relative minima thus enclose volumes of space wherein the fractions of the correlation hole for each particle are relative maxima. This implies maximization of the internal correla-

tions of the contained particles and concomitant minimization of the interactions with particles outside the loge volume.

A loge with zero population fluctuation would correspond to a totally isolated quantum system. In actual systems, one can only hope to find the "best" loges for which $\Lambda(\bar{N}, \Omega)$ is a local minimum with respect to changes in the loge surface and thereby define relatively isolated subsystems.

We have noted that the difference in normalization in the pair and particle densities forces equation (11) to hold. A more satisfactory definition would not require such an artificial restraint. Instead, a pure correlation factor should yield zero on integration over all space of its "correlation hole" expression (analogous to the integrand of equation (11)). This would better represent the rearrangement of particles and hence event probabilities due to particle correlation.

To accomplish this, we define normalized particle and pair probabilities rather than densities (c.f. equations (3) and (4)):

$$P_1(q_1) = \frac{\int_{S_1=-\frac{1}{2}}^{\frac{1}{2}} \int dx_2 \dots \int dx_N \psi^* \psi}{w_1(S_1)} \quad (15)$$

$$P_2(q_1, q_2) = \frac{\int_{S_1=-\frac{1}{2}}^{\frac{1}{2}} \int_{S_2=-\frac{1}{2}}^{\frac{1}{2}} \int dx_3 \dots \int dx_N \psi^* \psi}{w_1(S_1) w_2(S_2)} \quad (16)$$

We now define a correlation factor $\phi(q_1, q_2)$ which measures the difference between the pair probability and the product of the particle probabilities:

$$P_2(q_1, q_2) = P_1(q_1) P_2(q_2) [1 + \phi(q_1, q_2)]. \quad (17)$$

Thus, whereas $f(q_1, q_2)$ carries the burden of reproducing both

the correlation and normalization correction, $\phi(q_1, q_2)$ performs only the (desired) former function.

We can show that the loge fluctuation is related to this new measure of regional intra-correlation. Thus, by combining equations (3), (4), (9) and (16), we find that

$$\Lambda(\bar{N}, \Omega) = \bar{N}(\Omega)[1 - \bar{N}(\Omega)/N] + N(N-1)\phi(\Omega) \quad (18)$$

where

$$\phi(\Omega) = \int_{\Omega} dq_1 \int_{\Omega} dq_2 P_1(q_1) P_1(q_2) \phi(q_1, q_2). \quad (19)$$

The two measures of regional intra-correlation, $F(\Omega)$ and $\phi(\Omega)$ are related by

$$\phi(\Omega) = [F(\Omega) + \bar{N}^2(\Omega)/N]/N(N-1). \quad (20)$$

The pure correlation integral $\phi(\Omega)$ measures the total effect of the correlation-induced changes in pair probability from the product of the independent particle probabilities for all points q_1 and q_2 in the loge. $F(\Omega)$ measures the change in the number of pairs from that predicted by the integrated particle density product (hence the normalization factor $N(N-1)^{-1}$). Since $F(\Omega)$ includes also the normalization correction factor for the pair versus particle densities, one must subtract out $-\bar{N}^2(\Omega)/N$ due to the self-pairing of the population this implies.

In the limiting case of a loge having zero fluctuation, then $F(\Omega)$ and $\phi(\Omega)$ take the limiting values of

$$F_L(\Omega) = -\bar{N}(\Omega) \quad (21)$$

$$\phi_L(\Omega) = [-\bar{N}(\Omega) + \bar{N}^2(\Omega)/N]/N(N-1) \quad (22)$$

For any loge, the ratios of $F(\Omega)$ and $\phi(\Omega)$ to their limiting values provide direct measures of the fraction of the total "correlation holes" for the loge population actually contained in the loge.

To illustrate the difference between $f(q_1, q_2)$ and $\phi(q_1, q_2)$, consider a wavefunction describing a closed shell singlet state of a two-electron system:

$$\begin{aligned}\psi(\underline{x}_1, \underline{x}_2) &= \frac{1}{\sqrt{2!}} |\psi(\underline{q}_1)\bar{\psi}(\underline{q}_2)| \\ &= \frac{1}{\sqrt{2}} (\psi(\underline{q}_1)\psi(\underline{q}_2))(\alpha(s_1)\beta(s_2) - \beta(s_1)\alpha(s_2))\end{aligned}\quad (23)$$

The spinless pair and number densities are (from equations (3) and (4)):

$$D_2(\underline{q}_1, \underline{q}_2) = 2\psi^2(\underline{q}_1)\psi^2(\underline{q}_2) \quad (24)$$

$$D_1(\underline{q}_1) = 2\psi^2(\underline{q}_1) \quad (25)$$

From equation (8) we find that

$$f(\underline{q}_1, \underline{q}_2) = -\frac{1}{2} \quad (26)$$

The pair and number probabilities are (from equations (15) and (16)):

$$P_2(\underline{q}_1, \underline{q}_2) = \psi^2(\underline{q}_1)\psi^2(\underline{q}_2) \quad (27)$$

$$P_1(\underline{q}_1) = \psi^2(\underline{q}_1) \quad (28)$$

From equation (17), we find that:

$$\phi(\underline{q}_1, \underline{q}_2) = 0 \quad (29)$$

In this system, $D_2(\underline{q}_1, \underline{q}_2)$ and $D_1(\underline{q}_1)D_1(\underline{q}_2)$ differ only by a factor of 2. Thus, $f(\underline{q}_1, \underline{q}_2) = -\frac{1}{2}$ merely provides the normalization correction to subtract out the 2 "self-pairs" in the system. That there

is no particle correlation is indicated by the pure correlation factor $\phi(q_1, q_2)$ which is zero for all q_1 and q_2 . Considering any region Ω of \mathbb{R}^3 , we find that

$$F(\Omega) = -\frac{1}{2} \int_{\Omega} dq_1 \int_{\Omega} dq_2 D_1(q_1) D_1(q_2) = \frac{-\bar{N}^2(\Omega)}{2} \quad (30)$$

and

$$\phi(\Omega) = 0 \quad (31)$$

Whereas $F(\Omega)$ provides the pointwise self-pairing correction for the region, $\phi(\Omega)$ indicates the true total lack of correlation.

Use of pair distributions normalized to $N(N-1)$ (or $N(N-1)/2$) pairs will always predict a "correlation hole" when $f(q_1, q_2)$ is used as the correlation factor.

We now have two interpretations of $\Lambda(\bar{N}, \Omega)$ for fragments of any system. The first considers it to be a measure of the dispersion of event probabilities defined in the system coordinate space representation. The second relates it to the measures of intra-correlation of particles provided by $F(\Omega)$ and $\phi(\Omega)$ within any volume of real space. A (relative) minimum value in $\Lambda(\bar{N}, \Omega)$ implies both a minimal dispersion of the population localized in the fragment and a most strongly intra-correlated and weakly extra-correlated fragment. We thus have the desired interpretive link between the intuitive picture of almost independent (weakly inter-correlated) groups of system electrons and the pedagogically correct interpretation of a partition of the system into regions each having one highly probable event.

We can derive several other potentially useful properties of $\Lambda(\bar{N}, \Omega)$ in a fairly straightforward manner.

Comparison of equations (3), (4) and (8) with equations (15), (16) and (17) yields a pointwise relation for the two correlation factors $f(q_1, q_2)$ and $\phi(q_1, q_2)$:

$$\phi(q_1, q_2) = [1 + Nf(q_1, q_2)]/[N-1] \quad (32)$$

Partitioning space into two loges yields fragments of equal fluctuation (easily proven from equation (1)):

$$\Lambda(\bar{N}, \Omega_1) = \Lambda(\bar{N}, \Omega_2) \quad (33)$$

if

$$\Omega_1 + \Omega_2 = \mathbb{R}^3$$

Relations between the properties of any two loges and the properties of the loge formed from their combination may be derived as follows:

$$\begin{aligned} \Lambda(\bar{N}, \Omega_1 + \Omega_2) &= \bar{N}(\Omega_1 + \Omega_2) + F(\Omega_1 + \Omega_2) \\ &= [\bar{N}(\Omega_1) + \bar{N}(\Omega_2)] + \int_{(\Omega_1 + \Omega_2)} dq_1 \int_{(\Omega_1 + \Omega_2)} dq_2 D_1(q_1) D_1(q_2) f(q_1, q_2) \\ &= \bar{N}(\Omega_1) + \bar{N}(\Omega_2) + F(\Omega_1) + F(\Omega_2) + 2F(\Omega_1, \Omega_2) \end{aligned}$$

where

$$F(\Omega_1, \Omega_2) = \int_{\Omega_1} dq_1 \int_{\Omega_2} dq_2 D_1(q_1) D_1(q_2) f(q_1, q_2),$$

which we infer provides a measure of the inter-correlation of Ω_1 and Ω_2 . (Note that our previously defined $F(\Omega)$ correspond to $F(\Omega, \Omega)$.)

Thus,

$$\Lambda(\bar{N}, \Omega_1 + \Omega_2) = (\bar{N}(\Omega_1) + F(\Omega_1)) + (\bar{N}(\Omega_2) + F(\Omega_2)) + 2F(\Omega_1, \Omega_2)$$

or,

$$\Lambda(\bar{N}, \Omega_1 + \Omega_2) = \Lambda(\bar{N}, \Omega_1) + \Lambda(\bar{N}, \Omega_2) + 2F(\Omega_1, \Omega_2) \quad (32)$$

Similarly, we can write the relation using a "pure cross-correlation"

$$\text{factor, } \phi(\Omega_1, \Omega_2) = \int_{\Omega_1} dq_1 \int_{\Omega_2} dq_2 p_1(q_1) p_1(q_2) \phi(q_1, q_2):$$

$$\Lambda(\bar{N}, \Omega_1 + \Omega_2) = \Lambda(\bar{N}, \Omega_1) + \Lambda(\bar{N}, \Omega_2) + 2N(N-1)\phi(\Omega_1, \Omega_2) - 2 \frac{\bar{N}(\Omega_1)\bar{N}(\Omega_2)}{N} \quad (34)$$

These results can be generalized for the case of N loges:

$$\Lambda(\bar{N}, \Omega_1 + \Omega_2 + \dots + \Omega_v) = \sum_{\lambda=1}^v \Lambda(\bar{N}, \Omega_\lambda) + \sum_{\lambda \neq \mu} F(\Omega_\lambda, \Omega_\mu) \quad (35)$$

and

$$\Lambda(\bar{N}, \Omega_1 + \Omega_2 + \dots + \Omega_v) = \sum_{\lambda=1}^v \Lambda(\bar{N}, \Omega_\lambda) + N(N-1) \sum_{\lambda \neq \mu} \phi(\Omega_\lambda, \Omega_\mu) - \sum_{\lambda \neq \mu} \frac{\bar{N}(\Omega_\lambda)\bar{N}(\Omega_\mu)}{N} \quad (36)$$

This relation does not require the loges to be contiguous; however, if the loges are contiguous and they exhaust \mathbb{R}_3 , then:

$$\Lambda(\Omega_1 + \Omega_2 + \dots + \Omega_v) = \Lambda(\mathbb{R}^3) = 0 \quad (37)$$

We may then rewrite equations (35) and (36) as:

$$\sum_{\lambda=1}^v \Lambda(\bar{N}, \Omega_\lambda) = - \sum_{\lambda \neq \mu} F(\Omega_\lambda, \Omega_\mu) \quad (38)$$

or, using the "pure" correlation factors

$$\sum_{\lambda=1}^v \Lambda(\bar{N}, \Omega_\lambda) = -N(N-1) \sum_{\lambda \neq \mu} \phi(\Omega_\lambda, \Omega_\mu) + \sum_{\lambda \neq \mu} \frac{\bar{N}(\Omega_\lambda)\bar{N}(\Omega_\mu)}{N} \quad (39)$$

Thus, the sum of the fluctuations of loges exhausting \mathbb{R}^3 provides a direct measure of the "cross-correlations" of the loges. Minimizing

$\sum_{\lambda=1}^v \Lambda(\bar{N}, \Omega_\lambda)$ also minimizes the sum of the cross-correlations. This may

be used as a criterion of system partitionability, even in cases where the component fragments are not separable on the basis of minima in Λ for each loge.

To evaluate the acceptability of a partitioning, we require the limiting values of $\sum_{\lambda=1}^v \Lambda(\bar{N}, \Omega_{\lambda})$ for "best" and "worst" possible partitions. We have previously suggested that one obtains a "best" partitioning for all fragment populations if each fragment has a fluctuation of zero. Directly then, for the "best" (i.e., limiting and in practice unattainable) partition:

$$\sum_{\lambda=1}^v \Lambda(\bar{N}, \Omega_{\lambda}) = 0 \quad (40)$$

The "worst" partition of a system into two fragments will be that which results in there being an equal probability of locating all N electrons in either loge. This will yield for either loge Ω :

$$P_0(\Omega) = P_N(\Omega) = \frac{1}{2}$$

$$P_1(\Omega) = P_2(\Omega) = \dots = P_{N-1}(\Omega) = 0$$

$$\Lambda(\bar{N}, \Omega) = \sum_{n=1}^N n^2 P_n(\Omega) - \left[\sum_{n=1}^N n P_n(\Omega) \right]^2 = \frac{N^2}{2} - \left(\frac{N}{2} \right)^2 = \frac{N^2}{4} \quad (41)$$

Hence

$$\sum_{\lambda=1}^2 \Lambda(\bar{N}, \Omega_{\lambda}) = \frac{N^2}{4} + \frac{N^2}{4} = \frac{N^2}{2} \quad (42)$$

Consider the general case of a "worst" partition into v loges. One will obtain a maximum fluctuation for each loge if there is probability of locating only 0 or N particles in it. Equivalently, the "worst" delocalization of the particles will occur if there is an equal probability of locating all N particles in any one of the loges. Thus, the only non-zero

event probabilities are the v equally likely P_μ 's each placing N electrons in one of the v loges.

Hence

$$P_\mu = \frac{1}{v}$$

For any loge Ω_λ ,

$$P_N(\Omega_\lambda) = \frac{1}{v}, \quad P_0(\Omega_\lambda) = \frac{v-1}{v}$$

$$P_1(\Omega_\lambda) = P_2(\Omega_\lambda) = \dots = P_{N-1}(\Omega_\lambda) = 0$$

whence

$$\bar{N}(\Omega_\lambda) = \sum_{n=1}^N n P_n(\Omega_\lambda) = \frac{N}{v}$$

$$\begin{aligned} \Lambda(\bar{N}, \Omega_\lambda) &= \sum_{n=1}^N n^2 P_n(\Omega_\lambda) - \left[\sum_{n=1}^N n P_n(\Omega_\lambda) \right]^2 \\ &= \frac{N^2}{v} - \left(\frac{N}{v} \right)^2 = N^2 \left(\frac{v-1}{v^2} \right) \end{aligned} \quad (43)$$

And finally,

$$\sum_{\lambda=1}^v \Lambda(\bar{N}, \Omega_\lambda) = v \left[N^2 \left(\frac{v-1}{v^2} \right) \right] = N^2 \left(\frac{v-1}{v} \right) \quad \text{("worst" partitioning into } v \text{ loges).} \quad (44)$$

Note that this expression is consistent with several results derived previously. Thus, for a system considered as a whole ($v = 1$), then $\sum_\lambda \Lambda_\lambda$ has both an upper and lower limit of zero, as required if it is always to equal zero. For any v , ($1 \leq v \leq \infty$), the "worst" partitioning will always yield $\sum_\lambda \Lambda_\lambda$ less than N^2 .

Thus, for any partition of an N -electron system into any number of loges, one finds

$$0 \leq \sum_\lambda \Lambda_\lambda \leq N^2. \quad (45)$$

The effects of correlation in altering the form of the pair probability distribution (from the product of particle probabilities of the independent particle case) are measured by the correlation integrals $\Phi(\lambda, \mu)$ and $\Phi(\lambda, \lambda)$.

Now we have previously noted that

$$\Phi(R, R) = 0 \quad (46)$$

Hence

$$\sum_{\lambda} \Phi(\lambda, \lambda) + \sum_{\lambda \neq \mu} \Phi(\lambda, \mu) = 0 \quad (47)$$

and

$$\frac{\sum_{\lambda} \Phi(\lambda, \lambda)}{\sum_{\lambda \neq \mu} \Phi(\lambda, \mu)} = -1 \quad (48)$$

Thus, the total changes in pair probability within the loges must equal the negative of the total changes between the loges.

By integrating equation (17), we find that

$$\Phi(\lambda, \lambda) = \int_{\Omega_{\lambda}} dq_1 \int_{\Omega_{\lambda}} dq_2 P_2(q_1, q_2) - \int_{\Omega_{\lambda}} dq_1 P_1(q_1) \int_{\Omega_{\lambda}} dq_2 P_1(q_2) \quad (49)$$

Thus, $\Phi(\lambda, \lambda) < 0$ indicates a correlation-induced net decrease in pair probability for two particles within the loge Ω_{λ} . Similarly, $\Phi(\lambda, \mu) > 0$ indicates an increase in probability of localizing the particles of the "pair" in different loges, Ω_{λ} and Ω_{μ} . For Fermi correlation of particles, we expect to see all $\Phi(\lambda, \lambda) < 0$ and all $\Phi(\lambda, \mu) > 0$. Large values of the various $\Phi(\lambda, \lambda)$ and $\Phi(\lambda, \mu)$ indicate the existence of regions for which correlation has resulted in significant net changes in the pair probability density.

We can generate two sets of convenient measures of the changes in intrafragment correlation for any two fragments relative to the redistribution of pair density between them:

$$\frac{2F(\lambda, \mu)}{F(\lambda) + F(\mu)} \quad \text{and} \quad \frac{2\Phi(\lambda, \mu)}{\Phi(\lambda) + \Phi(\mu)}$$

For a two-loge partition of a system into two completely localized subsystems, then the F ratio has the value 0, and the ϕ ratio -1 (as it does for any two-partition of a total system).

We now have a useful set of partitioning criteria. For well-localized electron populations, we may hope to find individual loge fluctuations which are local minima with respect to all variations of their boundaries. For less localized electronic systems, we may still be able to find a minimum in $\sum_{\lambda} \Lambda_{\lambda}$ for some number of loges, v . If electron grouping in three-space is a true observable, then there will be some maximum number of well-localized loges, v , and for that v an optimal partitioning defined by a minimum in $\sum_{\lambda} \Lambda_{\lambda}$. Increasing v beyond that minimum value, no matter what the shape of the resulting fragments, will result in high $\sum_{\lambda} \Lambda_{\lambda}$ values with no local minimum.

Whether or not a partitioning has been found possible, we have measures of the degree of localizability of whatever set of loges are chosen. The F/F_L and ϕ/ϕ_L ratios indicate to what extent each loge approaches the limiting values of F and ϕ for intra-correlated fragments. The sets of ratios $\frac{2F(\lambda, \mu)}{F(\lambda) + F(\mu)}$ and $\frac{2\phi(\lambda, \mu)}{\phi(\lambda) + \phi(\mu)}$ reveal the extent to which the net correlation induced changes in pair density within any two fragments are related to the changes in pair density between them.

Fluctuation and Localization for Hartree-Fock Wavefunctions

Hartree-Fock wavefunctions are one of the simplest forms of N -particle functions built from one-particle functions including an attempt to describe correlation. Specifically, the use of a single determinantal (hence antisymmetrized) wavefunction introduces a Fermi correlation between the indistinguishable particles of like spin. This results in $F(\Omega)$ equalling -1 when Ω refers to all space, as previously mentioned.

For electrons of parallel spin, one defines an "exchange charge density"⁵¹ which yields an exchange energy cancelling the energy term due to the self-pairing, hence self-repulsion of the electrons in the Coulomb repulsion energy integrals for the system Hamiltonian. If this were the only effect of the antisymmetry, then one would expect (as in the two-electron case discussed above) that $\phi(\underline{q}_1, \underline{q}_2) = 0$ for all \underline{q}_1 and \underline{q}_2 , hence $\phi(\underline{\Omega}_1, \underline{\Omega}_2) = 0$ for all $\underline{\Omega}_1$ and $\underline{\Omega}_2$. As illustrated by the examples considered later, this is not the case. Thus, the Fermi statistical correlation is correctly accounted for, but in such a manner as to include a non-statistical correlation of electrons of parallel spin.

We derive the expression for $\Lambda(\bar{N}, \Omega)$ using a Hartree-Fock wavefunction as follows.⁵² The particle and pair densities are given by:

$$D_1'(\underline{x}_1, \underline{x}_1') = \sum_i \psi_i(\underline{x}_1) \psi_i^*(\underline{x}_1') \quad (50)$$

$$D_2'(\underline{x}_1, \underline{x}_2) = D_1'(\underline{x}_1) D_1'(\underline{x}_2) - D_1'(\underline{x}_1, \underline{x}_2) D_1'(\underline{x}_2, \underline{x}_1) \quad (51)$$

where $\psi_i(\underline{x})$ is the i^{th} spinorbital, and $D_1'(\underline{x}_1)$ and $D_2'(\underline{x}_1, \underline{x}_2)$ are not integrated over spin.

Combining equations (8), (9), (50) and (51), we find for $\Lambda(\bar{N}, \Omega)$:

$$\begin{aligned} \Lambda(\bar{N}, \Omega) &= \int_{\Omega, S_1} d\underline{x}_1 \int_{\Omega, S_2} d\underline{x}_2 \{ D_1'(\underline{x}_1) D_1'(\underline{x}_2) - D_1'(\underline{x}_1, \underline{x}_2) D_1'(\underline{x}_2, \underline{x}_1) \} \\ &\quad + \int_{\Omega, S_1} d\underline{x}_1 D_1'(\underline{x}_1) - \int_{\Omega, S_1} d\underline{x}_1 D_1'(\underline{x}_1) \int_{\Omega, S_1} d\underline{x}_1 D_1'(\underline{x}_1) \\ &= - \int_{\Omega, S_1} d\underline{x}_1 \int_{\Omega, S_2} d\underline{x}_2 \{ D_1'(\underline{x}_1, \underline{x}_2) D_1'(\underline{x}_2, \underline{x}_1) \} + \int_{\Omega, S_1} d\underline{x}_1 D_1'(\underline{x}_1) = - \sum_{i,j} S_{ij}^2(\Omega) + \bar{N}(\Omega) \end{aligned}$$

where

$$S_{ij}(\Omega) = \int_{\Omega} dx_1 \phi_i(x_1) \phi_j^*(x_1) \delta_{S_i, S_j}$$

Thus, we obtain the final form:

$$\Lambda(\bar{N}, \Omega)_{H.F.} = -\sum_i S_{ii}^2(\Omega) - \sum_{i \neq j}^{\alpha} S_{ij}^2(\Omega) - \sum_{i \neq j}^{\beta} S_{ij}^2(\Omega) + \bar{N}(\Omega) \quad (52)$$

where, in the two $\sum S_{ij}$ terms, i and j are both spinorbitals of α -spin or both of β -spin. Note that $\bar{N}(\Omega) = \sum_i S_{ii}(\Omega)$.

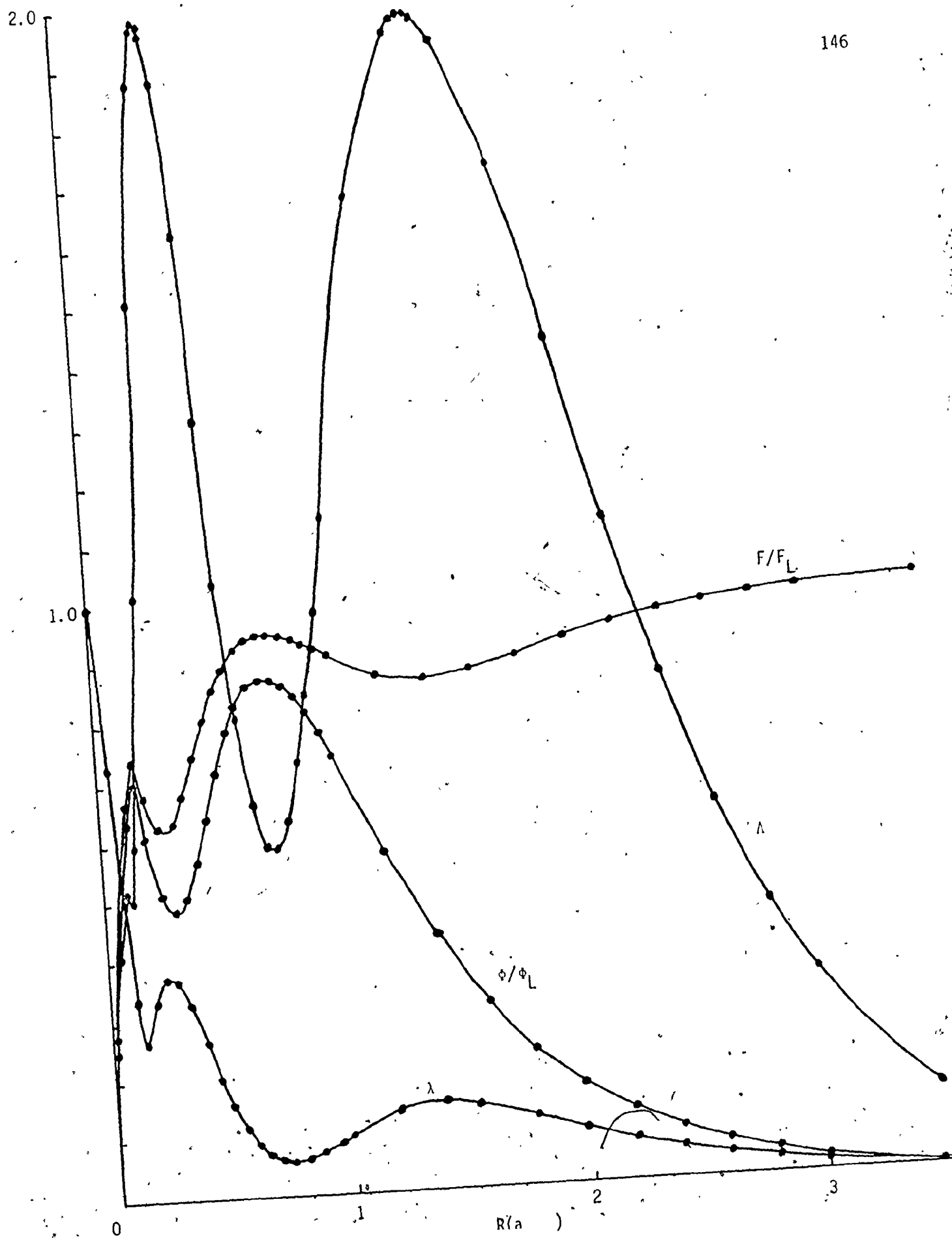
This simple expression permits facile calculation of loge fluctuations (given the requisite orbital overlaps over part of space, of course). The correlation factors and ratios may then be calculated from the fluctuations and populations.

From the form of equation (52), we see that if all occupied spinorbitals are spatially localized in Ω or the remainder of space, then all $S_{ii}(\Omega) = 1$ or 0, all $S_{ij}(\Omega) = 0$, and thus $\Lambda(\bar{N}, \Omega) = 0$ for the region. (Hence a truly "localized orbital" would satisfy this criterion of complete localizability.)

Argon

To illustrate the variations in the proposed measures of localization with spatial partitioning of an electronic wavefunction, we consider here the results we have computed for partitionings of an argon atom in its ground state. A Hartree-Fock LCAO-MO wavefunction in a Slater basis set⁵³ was partitioned into two loges, a sphere of radius R (in a.u.) centred on the nucleus plus the remainder of space. Figure 4A contains

Figure 4A. Fluctuation and Related Properties Versus R for Argon
Spherical Cores



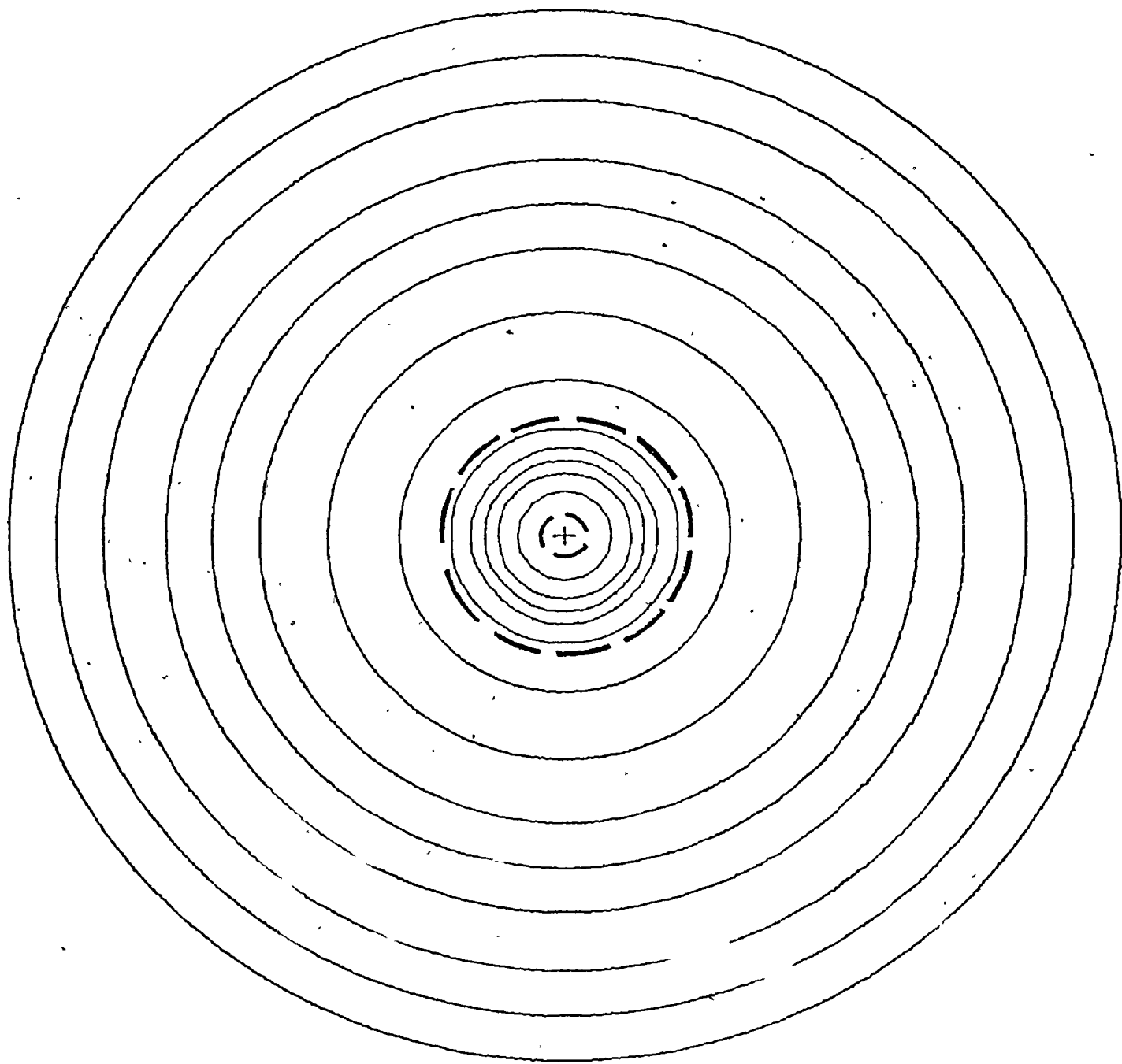
plots of Λ , λ , F/F_L , and ϕ/ϕ_L for the spherical loge as functions of R .

Λ equals zero for $R = 0$ and ∞ , i.e., for zero loge volume or the system considered as a whole. For intermediate values of R , Λ exhibits two minima, one for $R = 0.12$ a.u. ($\Lambda = 0.5012$, $\bar{N} = 1.86$) and a second at $R = 0.75$ a.u. ($\Lambda = 0.5818$, $\bar{N} = 10.13$). Λ has three maxima, one at $R = 0.08$ a.u. ($\Lambda = 0.5375$, $\bar{N} = 1.18$), a second at $R = 0.345$ a.u. ($\Lambda = 1.9836$, $\bar{N} = 6.01$) and the third at $R = 1.450$ a.u. ($\Lambda = 1.9671$, $\bar{N} = 13.80$).

These maxima and minima do not occur for integral numbers of contained electrons (R values to ± 0.01 a.u., \bar{N} values to ± 0.1 , the limit of graphical accuracy). However, there is an obvious pattern indicated. For spheres containing one or more "shells" of electrons (containing, respectively, 2, 8 and 8 electrons), one observes a minimum in Λ . For volumes containing a half-shell (plus one or more complete shells) one observes a maximum in Λ . Thus, if we interpret local minima in Λ as defining groups of intra-correlated electrons, then in this case we are picking out the largely intra-correlated shells of the atom (Figure 4B). λ shows behaviour similar to Λ , except it approaches one rather than zero as the loge volume is decreased to zero. It also has a relatively more pronounced minimum at $R = 0.15$ a.u. than the small corresponding minimum in Λ at $R = 0.12$ a.u. λ may thus provide a more definite partitioning indicator than Λ . (Note, however, that Λ and λ have minima for slightly different R values. This is a general result due, of course, to the fact that λ is equal to Λ divided by \bar{N} , a monotonically increasing function of the loge volume.)

Similarly, the ratios F/F_L and ϕ/ϕ_L exhibit parallel behaviour

Figure 4B. Contour map of the electronic charge distribution for $\text{Ar}(1s)$.
The circles denoted by the long dashes define the boundaries of the best
first and second concentric lobes.



1 a.u.

Ar

consistent with that of Λ and λ . For R values near those for which Λ and λ have minimum values, F/F_L and ϕ/ϕ_L both reach local maxima. At the first maximum ($R = 0.15$ a.u.) 71% of the limiting value of "pure" correlation is obtained. For $R = 0.70$ a.u. (second maximum), 87% of the "pure" correlation of the two inner shells (taken together) is contained within the loge. The F/F_L ratio is several percent higher than the ϕ/ϕ_L ratio for $R \leq 1$ a.u. At greater R values, the F/F_L ratio approaches its prescribed limit ($-\bar{N}/-\bar{N} = 1$), and ϕ/ϕ_L decreases to its limiting value of zero.

We established the properties of the second shell alone by searching for the volume contained between shells of radii R_1 and R_2 with $\Lambda(\bar{N}, \Omega)$ minimal w.r.t. R_1 and R_2 . A minimum Λ value of 1.0522 was found for $R_1 = 0.12$ a.u. and $R_2 = 0.75$ a.u. (± 0.02) for which $\bar{N} = 8.28 \pm .1$. The F/F_L and ϕ/ϕ_L ratios for this shell fragment were .869 and .765, respectively, indicating a satisfactory 77% containment of the pure correlation for the population of this volume.

Partitioning of the system into the three largely intra-correlated regions (K,L,M shells) also yields a minimum in $\sum_{\lambda} \Lambda_{\lambda}$. That is, altering R_1 or R_2 (hence one of the two boundary surfaces) increases the fluctuation for both the contiguous loges and thus $\sum_{\lambda} \Lambda_{\lambda}$ as well:

The pure cross-correlation integrals (between the K, L, and M shells), ϕ_{KL} , ϕ_{KM} , and ϕ_{LM} are equal to 0.00240, 0.00520, and 0.01994. These are very low values (compared to the other molecules we discuss below -- c.f. Table 10), and provide another indicator of the strong intra-correlation of the shells.

Another result of interest was obtained. A plot of the radial density, $R^2 D_1(R)$, had minima for $R = 0.14 \pm 0.01$ a.u. and 0.80 ± 0.01 a.u. These values are close to the R values for minimal Λ (0.12 a.u. and 0.85 a.u.). Radial density plots thus can serve to choose approximate spherical core boundaries. This point is reinforced by the results subsequently obtained in choosing electron cores around nuclei in molecules.

An important question remains. Can we find for an atom other than spherically-shaped loges that have well-localized populations? We consider this possibility by evaluating various partitionings of the neon atom (below).

This sample, argon, shows the utility of the fluctuation concept. Λ (or λ) provides a good indicator of the volumes containing localized populations and the F/F_L and ϕ/ϕ_L ratios provide convenient yardsticks to estimate the degree of localization for each region.

The 10-Electron Isoelectronic Series Ne, HF, H₂O, NH₃, CH₄

The ground-state electronic structures of the 10-electron molecules chosen are commonly (and approximately) described in terms of one core pair and four tetrahedrally arranged bonded and/or lone pairs. Can we establish such partitionings of the electron density using the Λ criterion? Are there detectable trends in the partitionability with changing nuclear charge of the heavy atom and increasing number of protons bonded to the heavy nucleus?

The wavefunctions used were all single-determinantal LCAO-MO

functions expanded in gaussian basis sets. Polarization "d" functions were included and the functions closely approach the Hartree-Fock limit. The important characteristics of the wavefunctions are summarized in Table 7 and Figure 5.

Heavy-Atom Cores

We first searched for evidence of spherical two-electron cores on the heavy nuclei.

Consider first the Ne atom. As for argon, we studied the variation of Λ , λ , F/F_L and ϕ/ϕ_L of a sphere centred on the nucleus with variation in its radius, R . The results are plotted in Figure 6.

The fluctuation has peaks for enclosed populations of approximately 1 ($= 2/2$) and 6 ($= 2 + 8/2$) electrons, a half-shell and one-and-a-half shells, respectively.

Choosing the "best" core by several criteria yield similar results. Thus, the minimum value of Λ ($= .3769$) is found for $R = 0.261$ a.u. and $\bar{N} = 1.963$. The minimum value of λ ($= .1857$) occurs at $R = 0.286$ a.u. and $\bar{N} = 2.096$. $\bar{N} = 2.00(1)$ for $\bar{R} = 0.268$ a.u. (where $\Lambda = .3780$).

These results agree well with the core radius of .282 a.u. predicted by Ludeña and Sanchez⁵⁴ on the basis of the maximum value of $P_2(\Omega)$. Sperber⁵⁵ predicts an optimal core radius of 0.27 a.u. arguing from the form of the first order density matrix.

On the basis of the results for the Ar and Ne atoms and the molecules studied in the preceeding chapter, it is plausible that core logs for heavy nuclei in molecules may in general be chosen spherical. On this assumption, we next searched for spherical cores in our series of

TABLE 7

Wavefunctions for the 10-Electron Isoelectronic Series Ne, HF, H₂O, NH₃, and CH₄

Molecule	Geometry	Gaussian Basis Set		Total Energy (a.u.)	Hartree-Fock ^{H,I} Limit (a.u.)	Experimental ^H Energy (a.u.)
		(uncontracted) Hydrogen	→ [contracted] Heavy Atom			
Ne(X ¹ S)	---	---	(10 6) ^E	-128.541	-128.547	-129.062
HF(X ¹ Σ^+)	FH = 1.733 ^A	(4 2)	(10 6 2) ^E	-100.063	-100.075	-100.530
H ₂ O(X ¹ A ₁)	OH = 1.796 ^B HOH = 106.14°	(4 2)	(10 6 2) ^F	- 76.060	- 76.088	- 76.483
NH ₃ (X ¹ A ₁)	NH = 1.890 ^C HNH = 107.2°	(8 2) + [4 1]	(13 8 2) ^C + [8 5 2]	- 56.222	- 56.269	- 56.818
CH ₄ (X ¹ A ₁)	CH = 2.049 ^D HCH = 109.47°	(4 1) + [2 1]	(12 6 1) ^G + [6 3 1]	- 40.211	- 40.221	- 40.525

A V. Bondybey, P. K. Pearson and H. F. Schaeffer III, J. Chem. Phys. 57, 1123 (1972).

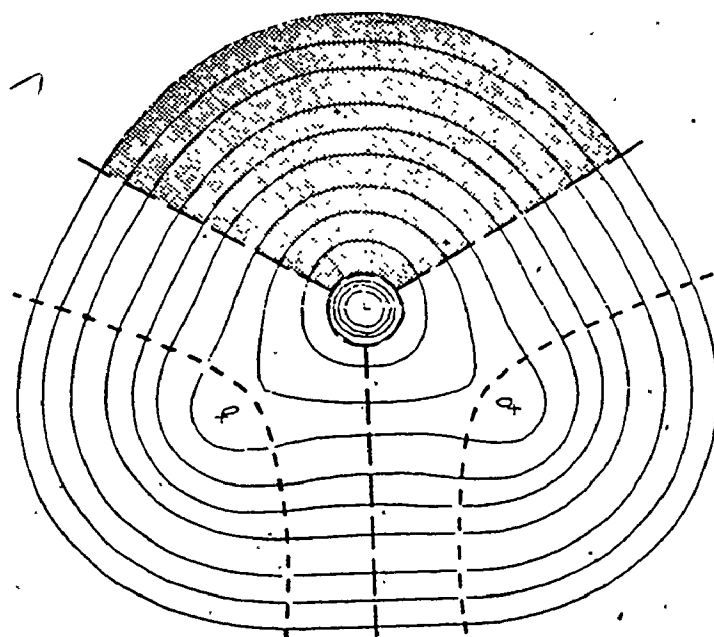
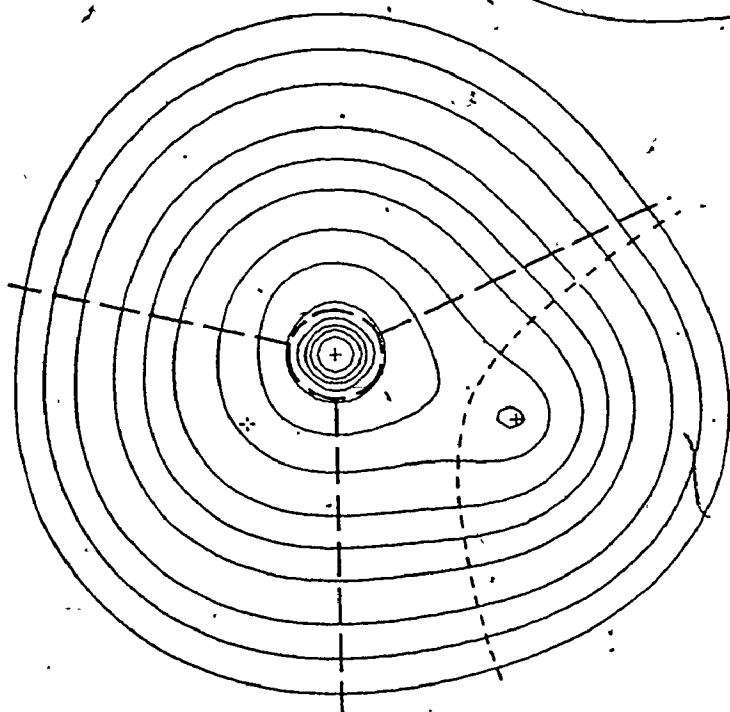
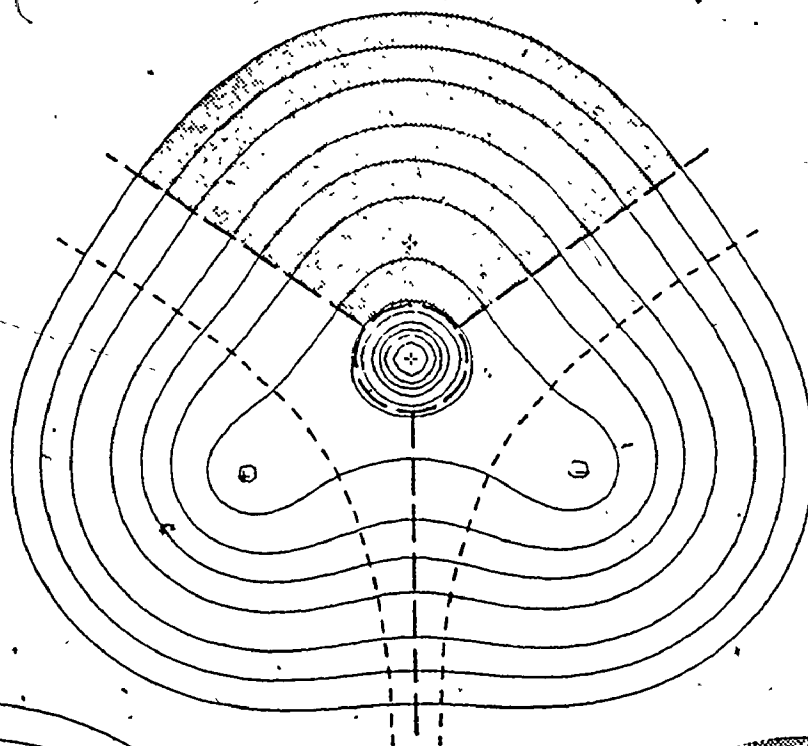
B R. Messer, unpublished results (geometry chosen to yield zero forces on protons).

C A. Rauk, L. Allen and E. Clementi, J. Chem. Phys. 52, 4133 (1970).D R. Pitzer, J. Chem. Phys. 46, 4871 (1967).E S. Huzinaga, J. Chem. Phys. 42, 1293 (1965); J. Chem. Phys. 55, 3958 (1971).F D. Newmann and J. W. Moskowitz, J. Chem. Phys. 49, 2056 (1968).

G J. Pelletier, unpublished results.

H C. Hollister and O. Sinanoğlu, J. Am. Chem. Soc. 88, 13 (1966).I J. L. Whitten, J. Chem. Phys. 44, 359 (1966).J E. Clementi, J. Chem. Phys. 38, 2248 (1963).

Figure 5. Contour maps of the electronic charge distributions for (reading from left to right on succeeding rows) $\text{CH}_4(X^1A_1)$, $\text{NH}_3(X^1A_1)$, $\text{H}_2\text{O}(X^1A_1)$, $\text{HF}(X^1\Sigma^+)$, $\text{Ne}(X^1S)$. In each diagram the curve(s) indicated by short dashes denotes the virial partitioning surface(s). The curves indicated by the longer dashes define the chosen boundary (the "best" loges for CH_4 , and the symmetrically arranged loges of population 2.00 in the remaining cases). Shading indicates a partitioning surface in that region of the plane illustrated.



| a.u.

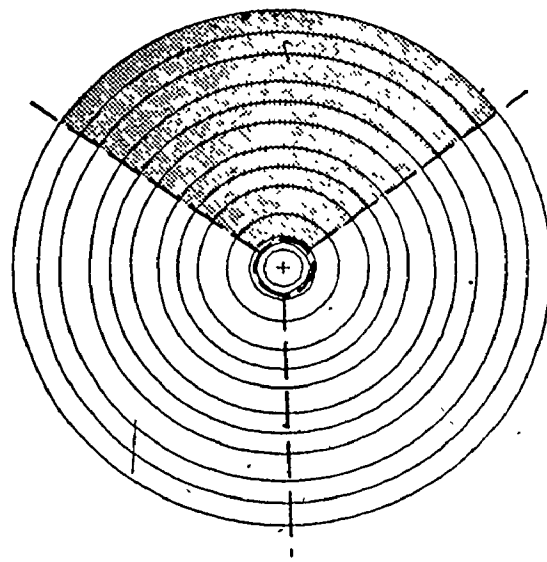
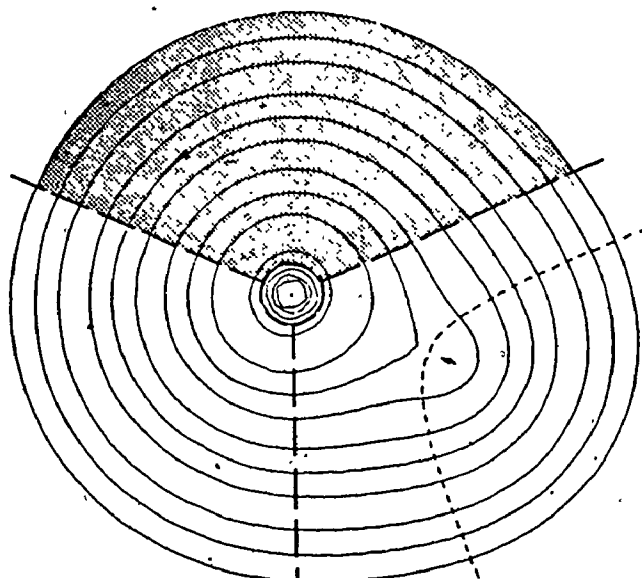
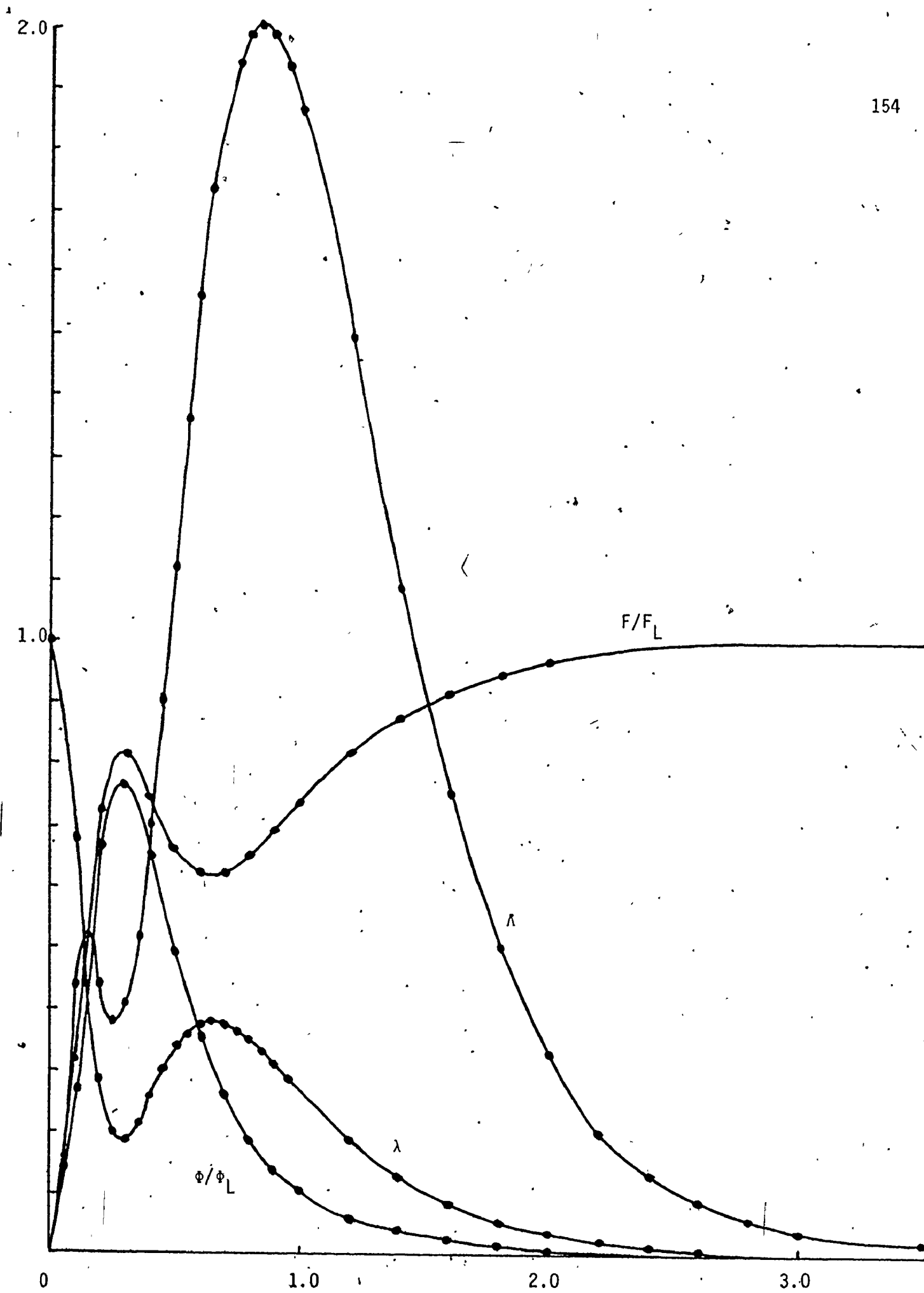


Figure 6. Fluctuation and Related Properties Versus R for Neon
Spherical Cores



molecules using the criterion of a local minimum in Λ to define the "best" loge. The results are contained in Figure 7. Readily apparent is the decreasing "best" core radius, higher minimum value in Λ , and decrease in \bar{N} for the "best" core with increasing nuclear charge. These data plus the core F/F_L and Φ/Φ_L ratios are summarized in Table 8. The results are readily understandable since a higher nuclear charge attracts the electrons into a smaller volume, hence decreasing the radius for which one observes any given population and inevitably increases the correlation of the more closely compacted electron density. In all the cases studied, a core of approximately 2 electrons was unambiguously definable. Further, the loge correlation factors F and Φ respectively attain more than 80% and 76% of their limiting values for an isolated subsystem for all the cores.

Valence "Bonding" and "Non-Bonding" Loges

We next evaluated the partitionability of the valence density in the various molecules.

Neon

Since the charge density is spherically symmetric, there are no intuitively obvious shapes of valence loge to attempt. Thus, we arbitrarily selected several shapes for trial: shells, wedges, cones and " C_{3v} wedges" (see insert on Figure 9).

Shells were defined as for Ar by two radii, R_1 and R_2 . R_1 was fixed at 0.261 a.u. (thus excluding the core of minimum Λ). Λ and λ were then calculated for variable R_2 . The results are plotted in Figure 8. Λ shows only a maximum of 2.1600 for $R_2 = 0.85$ a.u. and

Figure 7. Fluctuation Versus R for Spherical Cores of 10-Electron Molecules

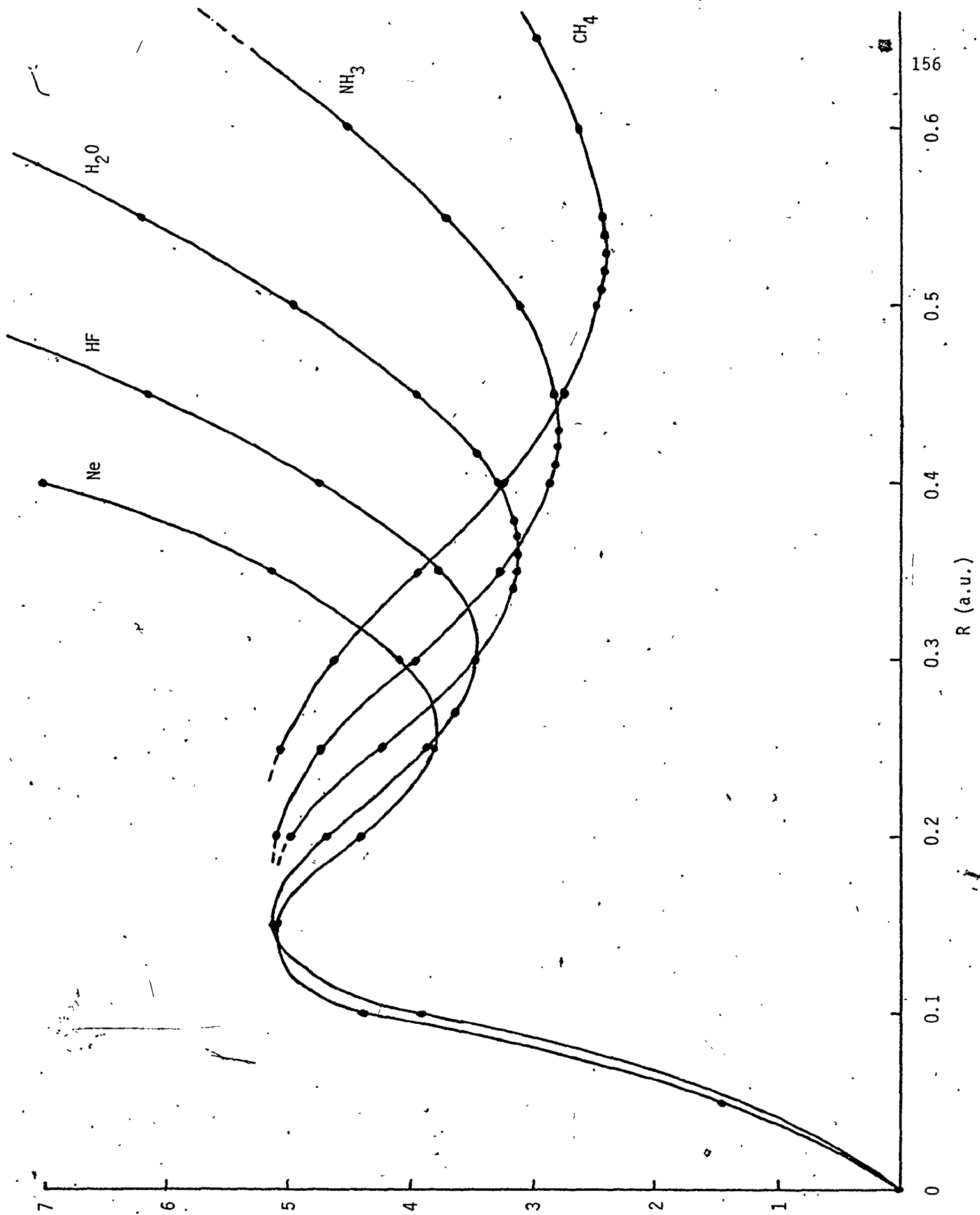


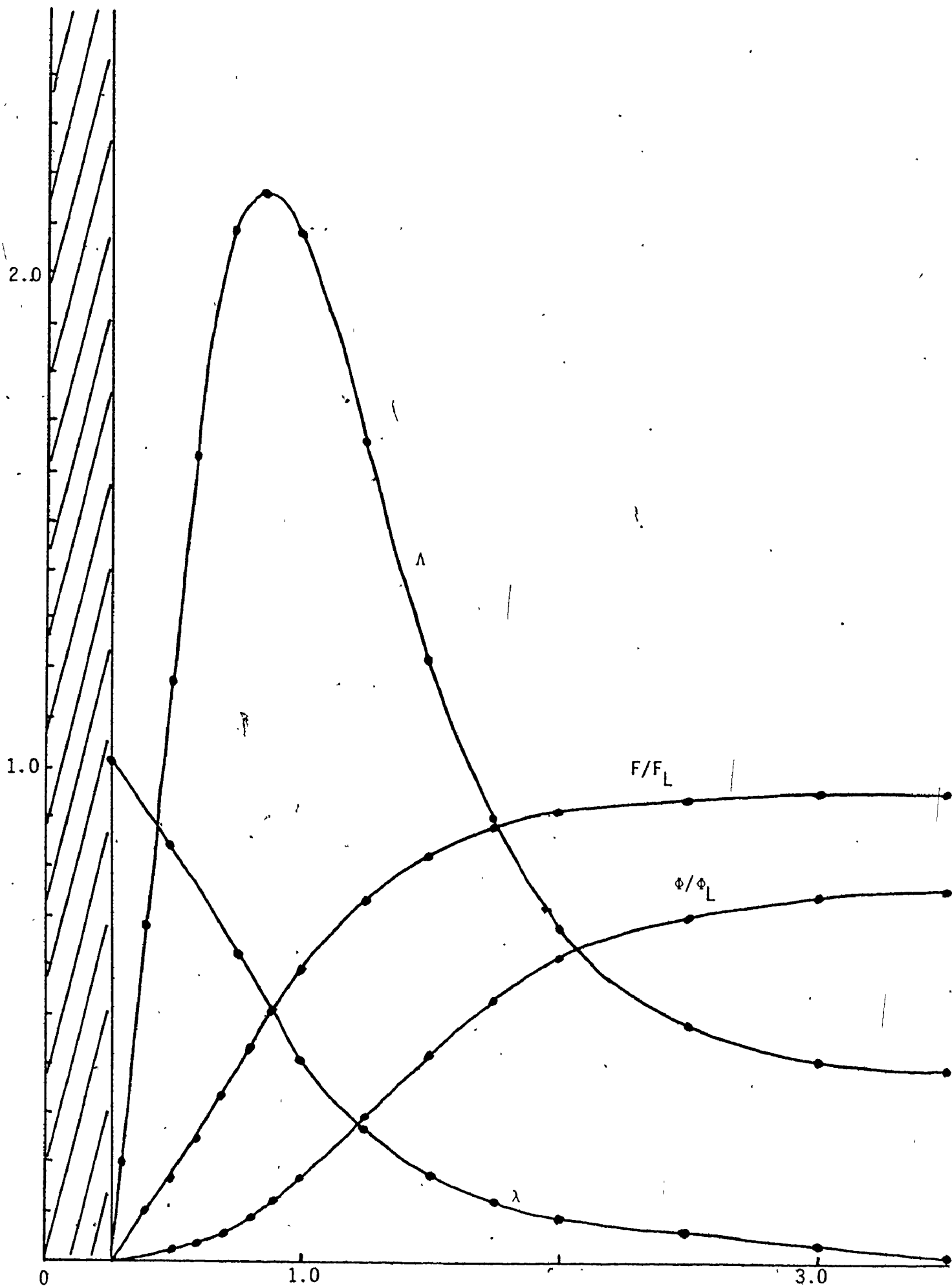
TABLE 8

Properties of the "Best" Cores for Ne, HF, H₂O, NH₃, and CH₄

Molecule	Core Radius (a.u.)	$\Lambda(\bar{N}, \Omega_{\text{core}})$	$\bar{N}(\Omega_{\text{core}})$	F/F_L	Φ/Φ_L
Ne	0.261	0.3769	1.963	.8080	.7611
HF	0.300	0.3451	1.966	.8245	.7816
H ₂ O	0.360	0.3105	2.001	.8448	.8060
NH ₃	0.430	0.2762	2.002	.8620	.8275
CH ₄	0.530	0.2386	2.005	.8810	.8510

Figure 8. Fluctuation and Related Properties Versus R_2 for Neon Shells

($R_1 = .261$ to $R_2 = \dots$)



$\bar{N} = 4.091$ between minima of zero at $R_2 = 0.261$ a.u. (i.e., zero volume) and 0.3769 and $R_2 \rightarrow \infty$ (i.e., the whole valence region). Thus, again we have found the "worst" spherical partitioning occurs for a "half-shell" population.

The wedges (shaped like apple slices -- minus the core, of course) chosen were defined by the polar angle θ between the limiting semi-disks. The search was carried out for $0 \leq \theta \leq 180^\circ$. The results (Λ vs. \bar{N}) are given in Figure 9. (Note: \bar{N} rather than R_2 was chosen for plotting as it is a monotonically increasing function permitting direct comparison of the fluctuation for regions of the same populations but varying shape.) The fluctuation steadily increases to a value of 1.3971 for $\theta = 180^\circ$ and $\bar{N} = 4.019$. For larger θ , Λ must decrease (in all probability, monotonically) to the limiting value of 0.3769 for the complete valence shell. There is no evidence of a minimum in Λ for a partial valence shell wedge.

The conical fragments (minus core) were defined by the polar angle ϕ (see insert on Figure 9). Searching was carried out over the range $0 \leq \phi \leq 90^\circ$. Again the fluctuation increases steadily for increasing population in a manner almost identical to that of the wedges. There is no evidence of a minimum. The maximum value of $\Lambda = 1.3971$ again occurs for $\phi = 90^\circ$ (a half-shell) and must decrease to 0.3769 for ϕ increasing to 180° for the whole valence region.

A final type of region was considered, a " C_{3v} wedge" of trigonal pyramidal shape with one tip pointed at the nucleus, and cut off by the surface of the core. The size of the wedge is defined by the core radius and angle (θ_0) between the central axis of the bond and a ray aligned on


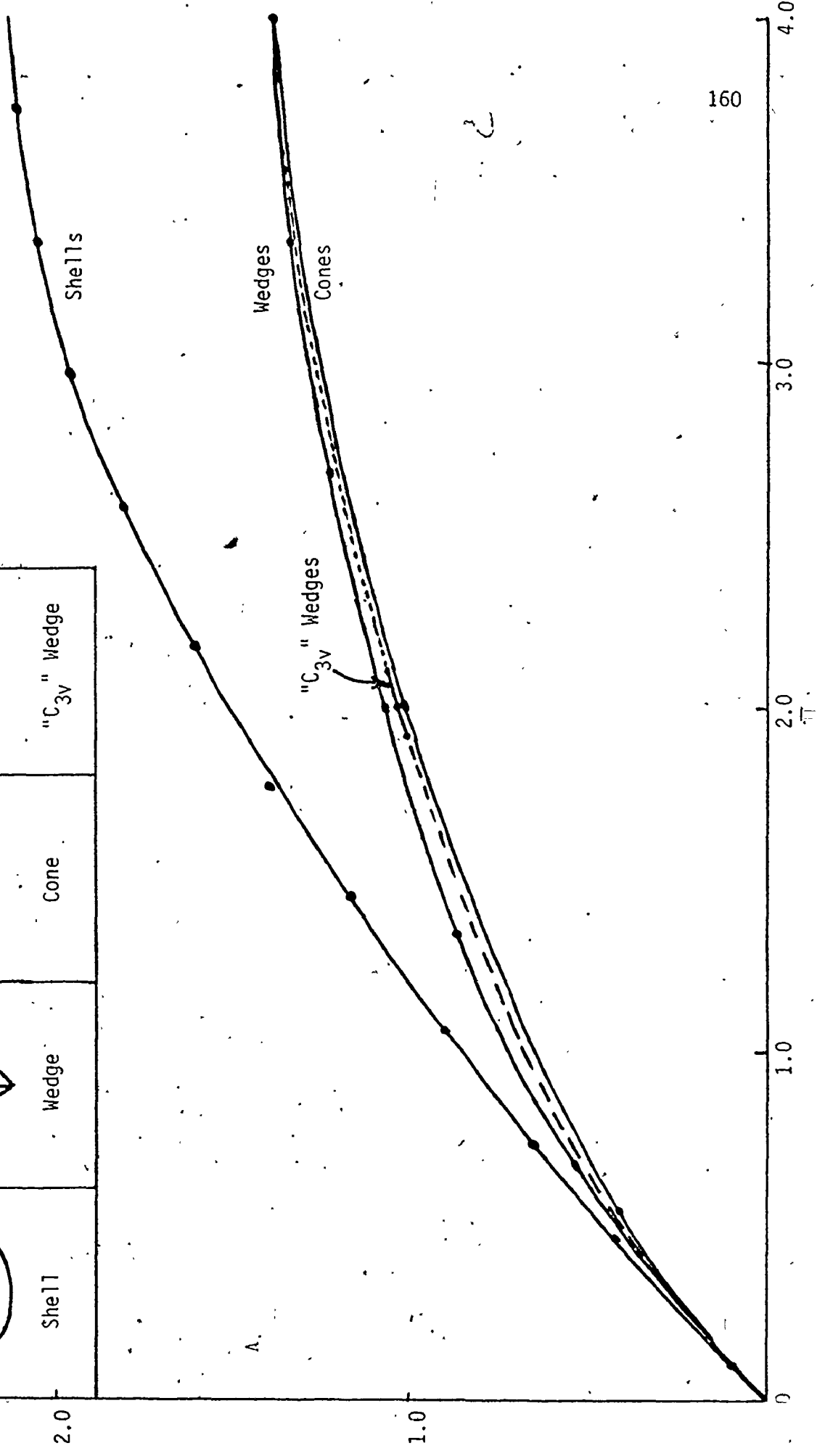
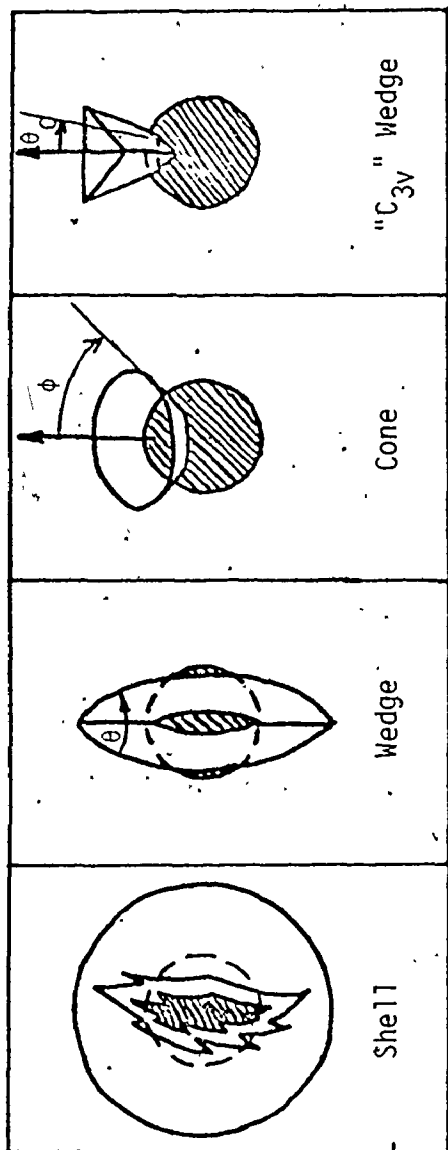


Figure 9., Fluctuation Versus Population for Various Shapes of Neon
Valence Fragments



the centre of each plane (see inset on Figure 9). (This forms a model for the volume occupied by σ -bonding pairs and lone pairs in the rest of the series.) Three values of θ_0 were chosen, 53° , 54.7° , and 57° to reveal the variation in Λ for a population near 2.00 (i.e., a "pair"). Λ monotonically increases with population and is in the range of the wedge and cone fluctuations. Thus, a minimum in Λ is unlikely, certainly not for $\bar{N} = 2.00$.

The shell fluctuations are also replotted vs. \bar{N} in Figure 9. For fragments of identical population, the fluctuation decreases as the fragment shape is changed from shell, to wedge, to C_{3v} fragment, to cone. This corresponds to the decrease in the "angular extent" of the fragment. One might infer that "radial" correlation is less important than angular correlation in this case, as a fragment of least symmetric solid angle (for a given population) has lowest fluctuation, hence greatest intra-correlation. However, no successful localization of part of the valence shell was observed for any of the shapes.

CH₄

Having discovered non-partitionability of the Ne atom valence region, it seemed prudent to next attempt a dissection of CH₄, as the valence localizability of the molecules almost certainly follows a monotonic trend between the limiting cases of Ne and CH₄.

The first type of bond tested was of " C_{3v} wedge" shape centred on one of the CH axes and symmetrically arranged with respect to the three nearest CH bonds (see insert on Figure 10). The fragment dimensions are defined by the core radius, R , and angle (θ_0) between the CH bond

axis and a vector along the centreline of one of the three limiting side-planes.

The first search was conducted for variable θ_0 and fixed $R = 0.53$ a.u. Figure 10 contains the values of Λ , λ , F/F_L and ϕ/ϕ_L obtained for $0 \leq \theta_0 \leq 90^\circ$. Although Λ does not show a minimum for $\theta_0 = 54.7^\circ$ (where $\bar{N} = 2.00$), there is a minimum in λ for that angle. Furthermore, ϕ/ϕ_L and F/F_L do have definite maxima, and the maximum in ϕ/ϕ_L occurs for $\bar{N} = 2.00$.

We next fixed $\theta_0 = 54.7^\circ$ and varied R over the range 0.25 to 0.75 a.u. This permits a check of the importance of core radius to valence loges. The results are plotted in Figure 11. (Note that the fragment population is decreasing for increasing R .) Λ attains a minimum for $R = .65$ a.u., but λ has a more pronounced minimum for R closer to .55 a.u. F/F_L and ϕ/ϕ_L both peak for $R = .60 (\pm .02)$. Hence by these criteria this valence fragment is clearly separable from the carbon core, and from the rest of the valence region as well.

This type of fragment approaches most closely one's intuitive definition of the volume occupied by an electron pair. Thus, further effort was put into clarification of the variation in the sum of the fluctuations with partitioning. The variation of this property was studied as a function of R and θ_0 . Several constraints on the partitionings naturally arise. For one fragment having θ_0 greater than 54.7° , the valence fragments (assumed to be four in number) cannot all be equivalent; one or more must be smaller than one-quarter of the valence volume. For two valence fragments of $\theta_0 > 54.7^\circ$, then these two fragments (necessarily adjacent) are either not centred on the CH bonds, or

Figure 10. Fluctuation and Related Properties Versus θ_0 for CH_4

" C_{3v} " Valence Fragments

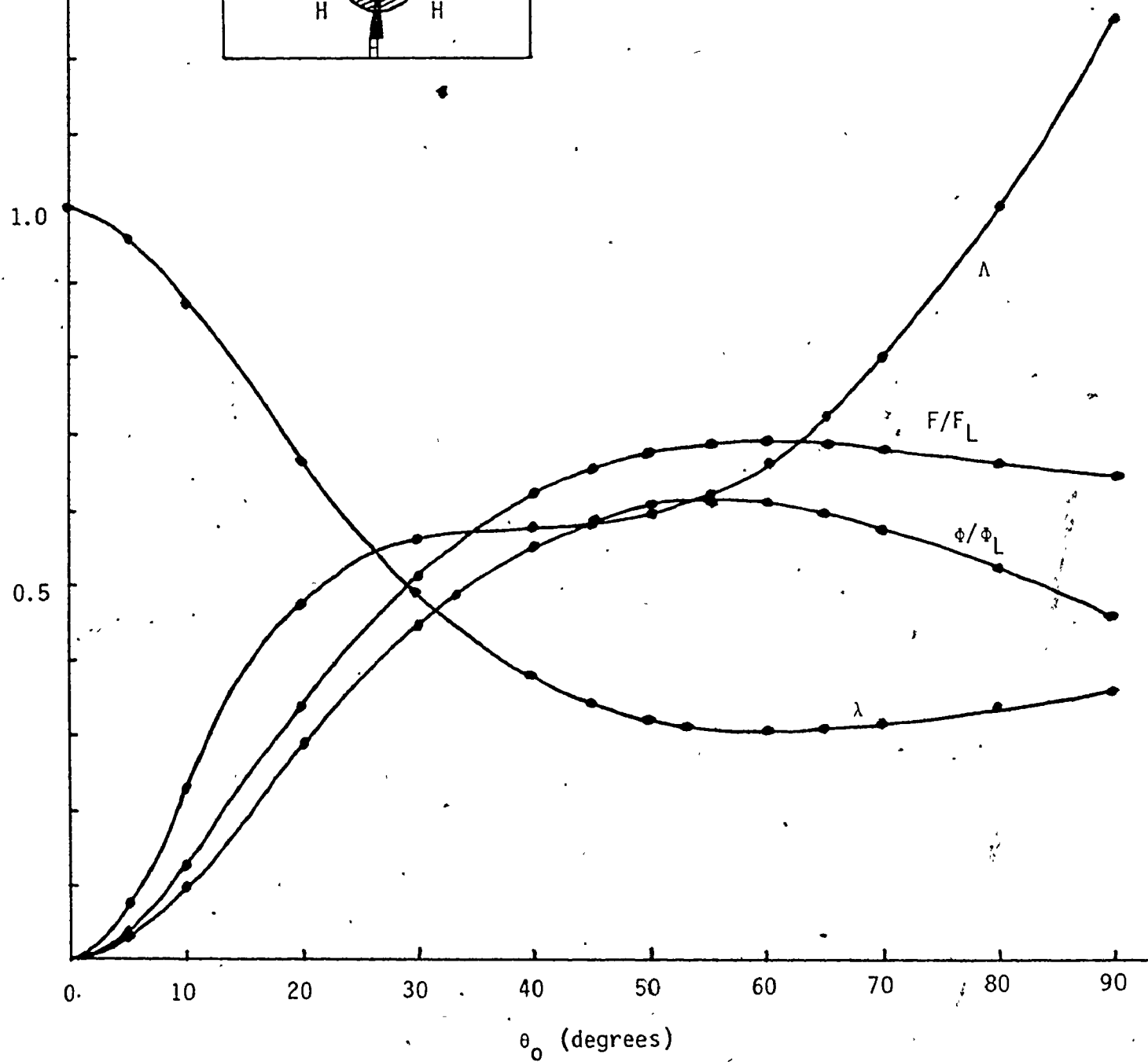
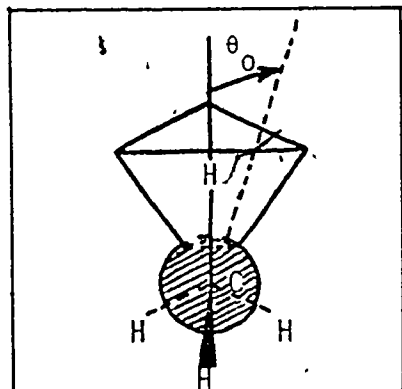
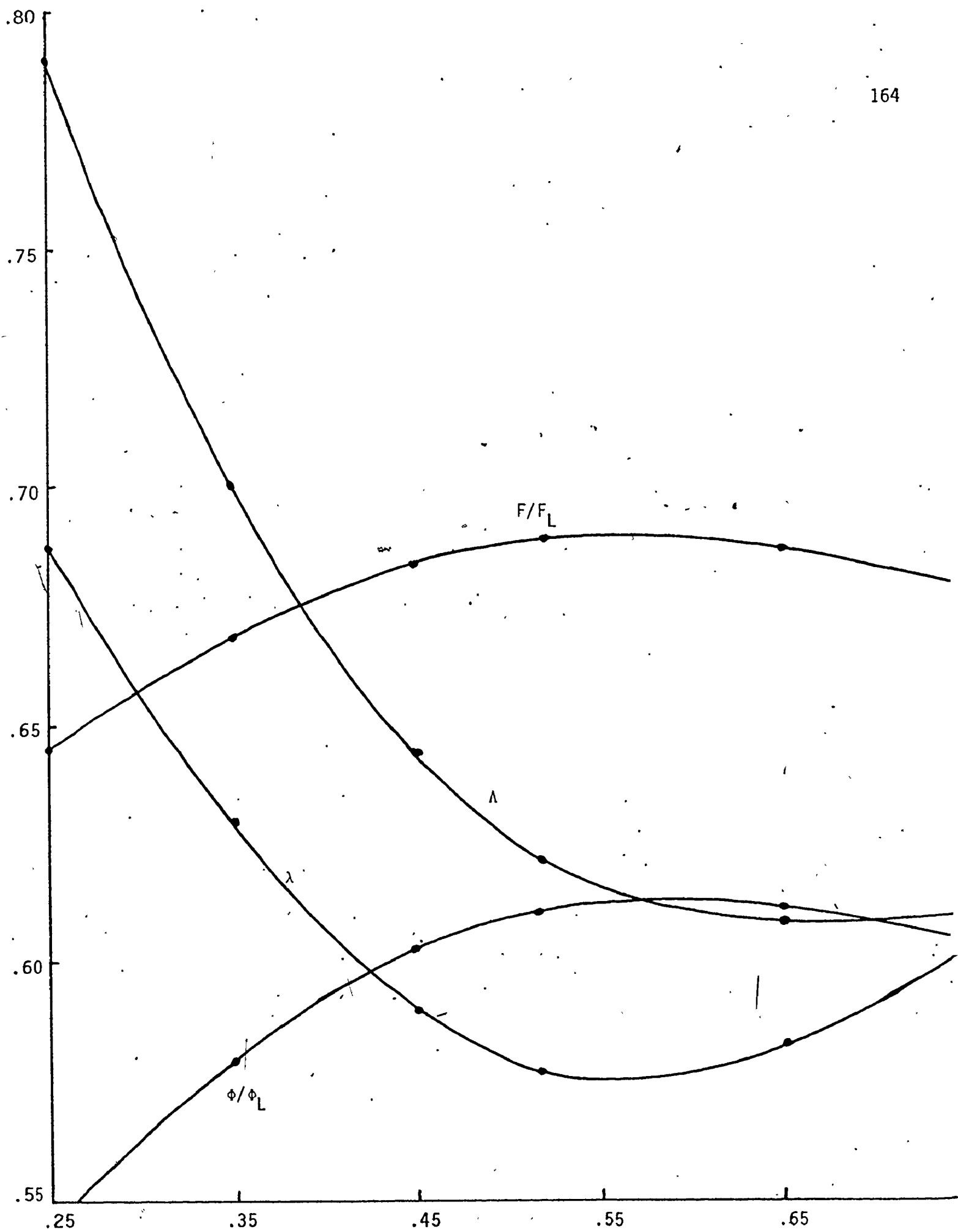


Figure 11. Fluctuation and Related Properties Versus R for CH_4
Tetrahedral Valence Fragments



one must define more than one θ_0 value for the three planes limiting the fragments, and fix two θ_0 values (one for each fragment) to sum to 109.47° (the tetrahedral angle). We chose the latter course, and in addition fixed both these θ_0 values to 54.7° .

For a set of four valence regions whose volumes sum to less than the full valence volume, then one must associate the omitted "slivers" with the core to create an "extended core" region.

Refining the orbital integration programmes to handle these variously shaped regions involved redefinition of the fragment boundaries and careful reoptimization of the choice of spatial grids for the gaussian quadrature numerical integration of orbital overlaps. The technical details are available from the author, but too lengthy and of insufficient import to include here.

The results of this study on CH_4 are reported in Table 9. Of all the partitionings, the one with lowest sum of fluctuations was found for $R = .53$ a.u. and $\theta_0 = 54.7^\circ$ and is thus a minimum with respect to both R and θ_0 . The orientation as well as shape of the fragment is important as shown by shifting the loges from being centred on bonds to being centred precisely between the bonds. The boundary of each fragment is then defined by three planes intersecting in rays along the bond directions themselves. This simple rotation of the loges increases the sum of fluctuations from 2.7258 to 5.282, respectively, the "best" and "worst" values obtained. This behaviour parallels that of the BeH_2 valence partition where bond-centred fragments were found preferable to semi-cylindrical fragments of identical population. The implications in terms of equivalent or localized orbitals are direct. The "best" parti-

TABLE 9

Total Partitionings of CH₄

H Fragment(s)		C Fragment		$\sum \Lambda_{\lambda}$	$\sum N_{\lambda}$
Shape	\bar{N}	Shape	\bar{N}		
R=.25, $\theta_0=45^\circ$	1.852	"extended core"	2.594	4.3594	10.000
R=.25, $\theta_0=50^\circ$	2.044	"extended core"	1.824	4.0326	10.000
R=.25, $\theta_0=54.7^\circ$	2.226	sphere	1.098	3.6631	10.001
R=.35, $\theta_0=45^\circ$	1.768	"extended core"	2.926	3.9330	10.000
R=.35, $\theta_0=50^\circ$	1.945	"extended core"	2.217	3.5784	10.000
R=.35, $\theta_0=54.7^\circ$	2.113	sphere	1.549	3.1932	10.001
R=.45, $\theta_0=45^\circ$	1.714	"extended core"	3.144	3.6500	10.000
R=.45, $\theta_0=50^\circ$	1.882	"extended core"	2.471	3.2627	10.000
R=.45, $\theta_0=54.7^\circ$	2.040	sphere	1.8400	2.8523	10.001
R=.53, $\theta_0=45^\circ$	1.683	"extended core"	3.2665	3.5366	10.000
R=.53, $\theta_0=50^\circ$	1.846	"extended core"	2.6152	3.1411	10.000
R=.53, $\theta_0=54.7^\circ$	1.999	sphere	2.005	2.7258 x	10.000
as immediately above, but fragment between bonds.					
R=.53, $\theta_0=60^\circ$ *	2.172/1.942	sphere	2.005	5.2892	10.001
R=.53, $\theta_0=65^\circ$ *	2.344/1.885	sphere	2.005	2.7431	10.002
R=.53, $\theta_0=60^\circ$ †	2.112/1.885	sphere	2.005	2.7944	10.005
		sphere	2.005	2.7468	9.998

TABLE 9 (Continued)

H Fragment(s)		C Fragment		$\sum \Lambda_{\lambda}$	$\sum \bar{N}_{\lambda}$ †
Shape	\bar{N}	Shape	Λ	Λ	\bar{N}
R=.65, $\theta_0=54.7^\circ$	1.947	sphere	0.6088	2.215	2.7303
R=.75, $\theta_0=54.7^\circ$	1.901	sphere	0.6099	2.398	2.8538
virial	1.063	virial	0.5597	5.749	4.1995
					10.001
					10.001
					10.000

* one large loge and three small loges; datum for both types separated by a slash (/) in each column (large loge listed first).

† two large loges (with θ_0 values between them set to 54.7° as mentioned in the text) and two small loges; datum for both given in each column separated by slash (large loge first).

‡ $\sum \bar{N}_{\lambda}$ should sum to precisely N; that it does not indicates the inaccuracy of the fragment integrations.

x minimum value found.

Figure 12.. Fluctuation Versus Population for "Bond" Fragments in 10-
Electron Molecules

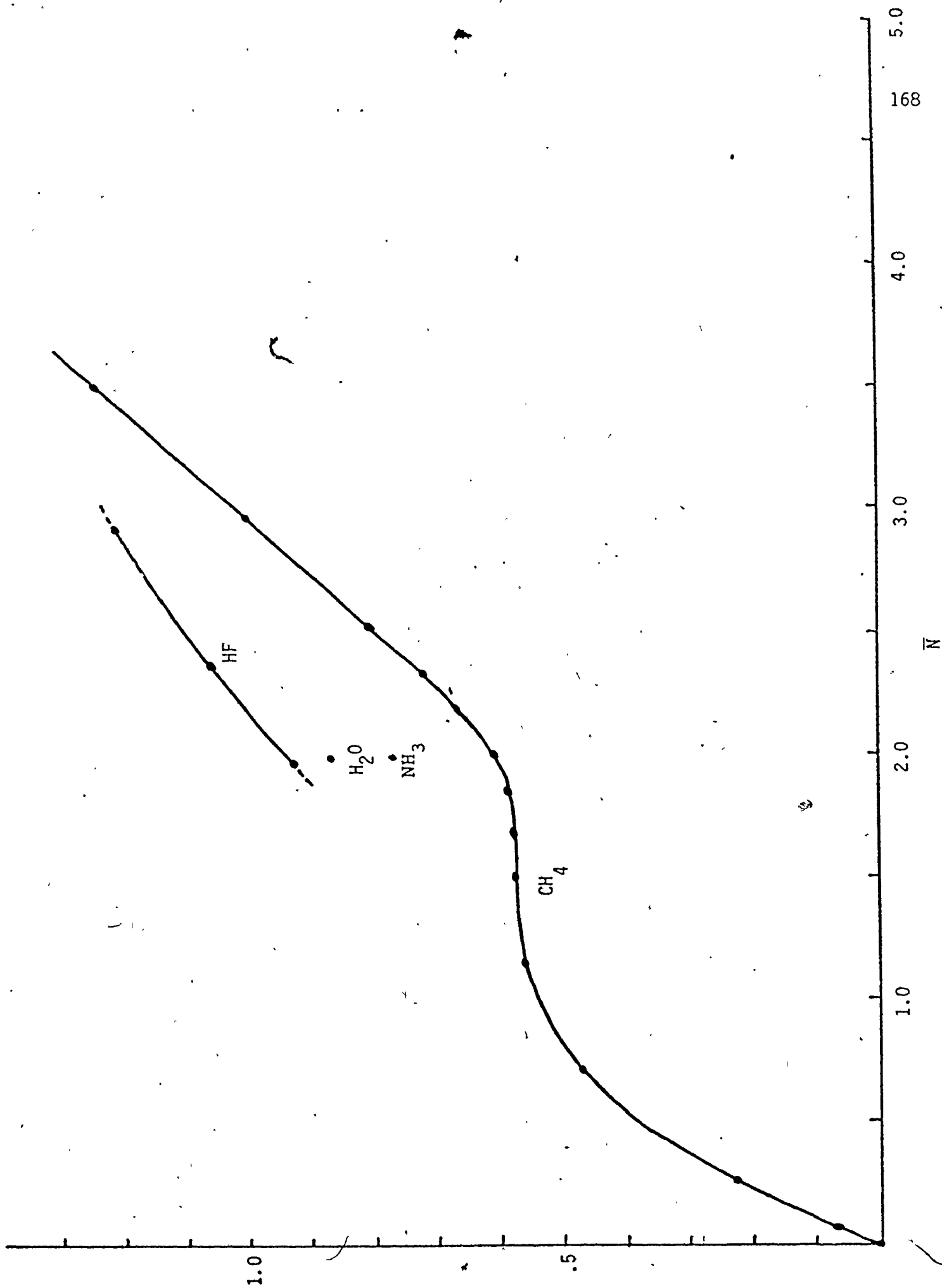
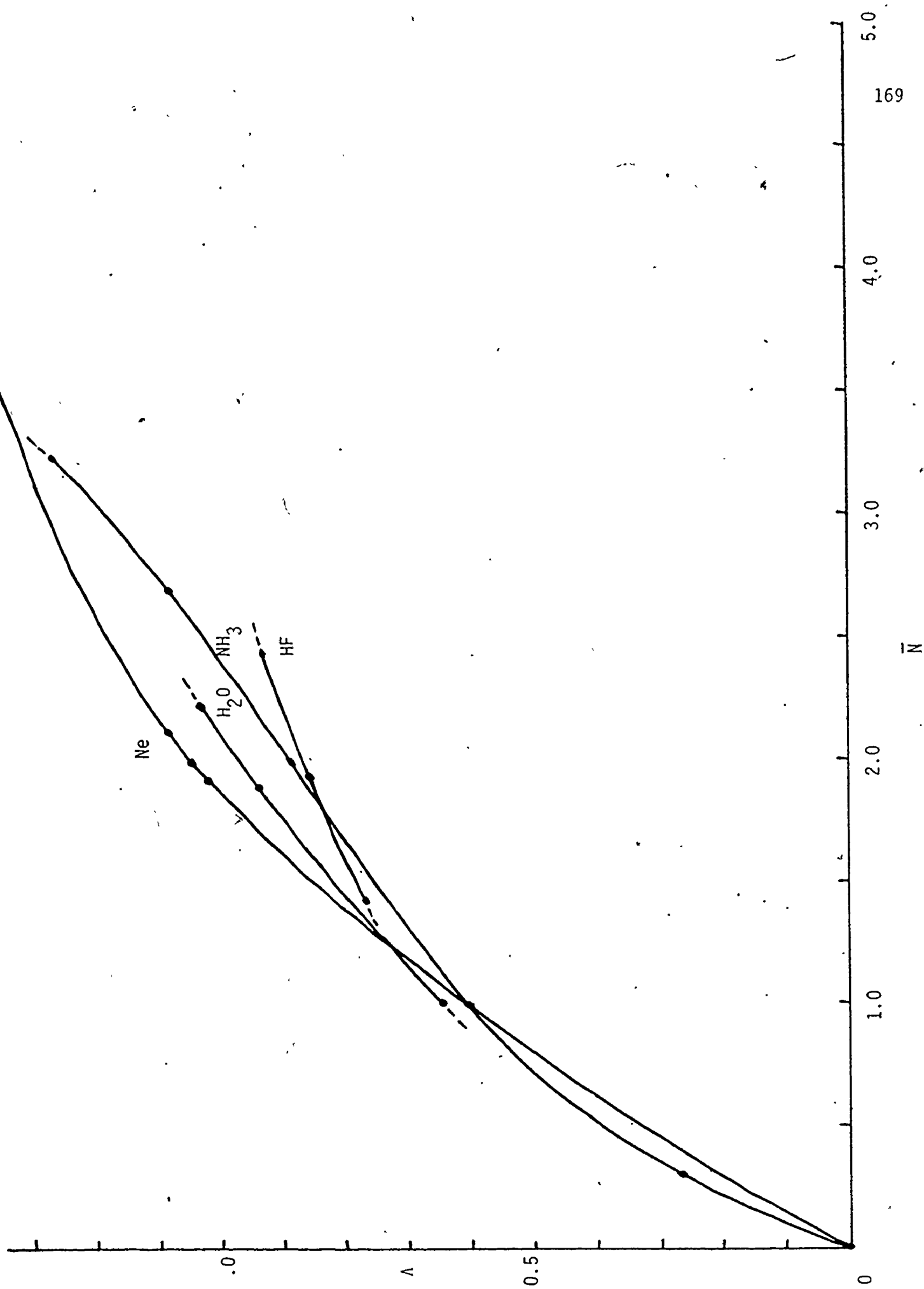


Figure 13. Fluctuation Versus Population for "Non-Bonded" Fragments in
10-Electron Molecules



tionings are those defined by surfaces lying between the localized orbitals. Virial partitioning of the molecule yields the second worst partitioning found. This is perhaps to be expected, as the hydrogen fragments have population of 1.063 and the carbon 5.749, far from any even population hence number of pairs.

Further, even for the most localized partition (as defined by $\sum \Lambda$) the "pure" correlation ratio (ϕ/ϕ_L) for the bond is only 61% of its limiting value for a totally intracorrelated loge. This agrees well with the conclusions of Sinanoglu and Skutnik⁵⁶ that inter-bond correlations contribute to the correlation energy as much as or more than the intra-bond correlations in CH_4 (and Ne).

Both Newton, Switkes and Lipscomb⁵⁷ (on the basis of a localized orbital analysis) and Sanchez and Ludeña⁵⁸ (on the basis of orbital overlaps) reach similar conclusions. As previously mentioned, the proper inclusion of the Coulomb correlation will tend to break up any localized groups. Hence our observation of almost equal inter- and intra-correlation for the Fermi-correlated Hartree-Fock wavefunction suggests that models based on localized electron pairs are strictly an oversimplification of the electron correlations in the molecules described here.

NH_3 , H_2O and HF

To complete this section, we surveyed valence partitionings of HF, H_2O and NH_3 into the conventional number of bond and lone valence pairs using the same sort of fragments as in the CH_4 valence partition, altering their orientation symmetrically to obtain all loge populations near 2.00.

The fragment fluctuations for bond pairs (Figure 12) and lone pairs (Figure 13) both indicate a trend of increasing delocalization (for fixed population) as one considers the series from CH_4 to Ne. The

non-bonded density on HF is the only exception, having a lower fluctuation than NH_3 and H_2O (for the same population) for $\bar{N} \geq 2.00$. At an intuitive level, one might explain the general trend as an increasing inter-correlation of bond and lone pairs as the heavy atom nuclear charge attracts the valence electron density into more compact distributions and the decreasing number of bonded protons decreases the number of regions of locally minimum potential along the bond directions (which, as previously noted, should tend to favour localization of pairs of electrons of opposite spin). Proceeding from CH_4 to Ne, we note (Table 10) that for the most symmetrical partitions into pairs the sum of fragment fluctuations increases from 2.726 to 4.549 and ratios of "fermi" and "pure" correlation, F/F_L and Φ/Φ_L , for bond and non-bonded density all decrease, providing further evidence of the increasing delocalization of population correlation.

Partitioning via the $\sum_{\lambda} \Lambda_{\lambda}$ criterion failed for NH_3 , as $\sum_{\lambda} \Lambda_{\lambda}$ was found to increase monotonically with θ_0 (defining the lone pair volume). H_2O , HF and Ne all contain more non-bonded density than NH_3 and doubtless the $\sum_{\lambda} \Lambda_{\lambda}$ criterion fails to localize four valence pairs in them as well.

In summary, by our various criteria, one can unambiguously define only a core loge for all these systems. The valence region in all cases is not well described by the picture of primarily intra-correlated electron pairs, methane being a borderline case (according to the Λ criterion), and the others containing more delocalized correlation.

LiH, BH, BeH₂

The high relative fragment inter-correlations found for the 10-electron series led to a reconsideration of the fragmentations claimed for the molecules studied in Chapter II. There we concluded that we had

TABLE 10

Fluctuation and Related Properties for Core and Valence Loges in Simple Hydrides

MOLECULE	Core Loge							Bond Loge						
	R	\bar{N}	Λ	F	F/F _L	ϕ	ϕ/ϕ_L	\bar{N}	Λ	F	F/F _L	ϕ	ϕ/ϕ_L	
LiH	1.42	1.999	.0908*	-1.9082	.9546	-.0758	.9092	2.001	.0908*	-1.9103	.9547	-.0758	.9092	
BeH ₂	0.95	2.012	.1363*	-1.8754	.9322	-.0400	.8981	1.994	.1444*	-1.8498	.9276	-.0396	.8915	
BH	0.70	2.002	.1582*	-1.8436	.9210	-.0392	.8814	1.998	.2648*	-1.7348	.8676	-.0356	.8014	
BH ₃	0.70	2.023	.1865*	-1.8362	.9078	-.0237	.8766	1.992	.3662*	-1.6263	.8162	-.0202	.7552	
BH ₄ ⁻	0.70	2.026	.2127*	-1.8135	.8950	-.0156	.8684	1.994	.4720*	-1.5221	.7633	-.0125	.7044	
CH ₄	0.53	2.005	.2388*	-1.7661	.8809	-.0152	.8510	1.999	.6216	-1.3774	.6890	-.0109	.6114	
NH ₃	0.43	2.002	.2762*	-1.7256	.8620	-.0147	.8275	1.997	.7715	-1.2259	.6138	-.0092	.5173	
H ₂ O	0.36	2.001	.3105*	-1.6905	.8448	-.0143	.8060	1.987	.8707	-1.1166	.5619	-.0080	.4532	
HF	0.30	1.966	.3450*	-1.6213	.8245	-.0137	.7816	2.037	.9559	-1.0807	.5306	-.0074	.4106	
Ne	0.261	1.963	.3769*	-1.5056	.8079	-.0133	.7610	---	---	---	---	---	---	
Ar	0.12	1.856	.5012*	-1.3549	.7300	-.0038	.6989	8.276	1.0522*	-7.2233	.8728	-.0112	.7646	

* indicates a local minimum (w.r.t. core radius, and bond angle variations where appropriate).

TABLE 10 (cont'd)

LECULE	Non-Bonded Loge						Cross-Correlations							
	\bar{N}	A	F	F/F _L	ϕ	ϕ/ϕ_L	2F _{CB}	2 ϕ_{CB}	2F _{CL}	2 ϕ_{CL}	2F _{BL}	2 ϕ_{BL}	2F _{BB'}	2 $\phi_{BB'}$
LiH	---	---	---	---	---	---	-.1815	.1515	---	---	---	---	---	---
BeH ₂	---	---	---	---	---	---	-.1363	.0400	---	---	---	---	-.1525	.0391
BH	2.000	.2950*	-1.7034	.8524	-.0346	.7786	-.1279	.0402	-.1884	.0382	-.4016	.0310	---	---
BH ₃	---	---	---	---	---	---	-.1243	.0202	---	---	---	---	-.3040	.0123
BH ₄ ⁺	---	---	---	---	---	---	-.1055	.0078	---	---	---	---	-.2794	.0057
CH ₄	---	---	---	---	---	---	-.1194	.0076	---	---	---	---	-.3744	.0047
NH ₃	2.005	.8984	-1.1062	.5518	-.0078	.4395	-.1292	.0075	-.1647	.0071	-.5438	.0029	-.4454	.0039
H ₂ O	2.005	.9675	-1.0370	.5173	-.0071	.3963	-.1381	.0073	-.1718	.0070	-.5582	.0027	-.4803	.0034
HF	1.999	1.0116	-0.9878	.4941	-.0065	.3676	-.1529	.0072	-.1790	.0067	-.5861	.0025	---	---
Ne	2.009	1.0429	-0.9665	.4810	-.0063	.3505	---	---	-.1885	.0067	---	---	---	---
Ar	7.868	.5818*	-7.2866	.8728	-.0126	.8686	-.9717	.0024	-.0307	.0052	-1.1328	.0199	---	---

TABLE 10 (cont'd)

LECULE	Cross- Correlations (cont'd)		Cross- to Intra-Correlation Ratios										$\frac{\sum N_{\lambda}}{\lambda}$	$\sum \lambda$
	$\frac{2F_{LL'}}{2\phi_{LL'}}$	$\frac{2\phi_{LL'}}{2\phi_{LL'}}$	$\frac{2F_{CB}}{F_C+F_B}$	$\frac{2\phi_{CB}}{\phi_C+\phi_B}$	$\frac{2F_{CL}}{F_C+F_L}$	$\frac{2\phi_{CL}}{\phi_C+\phi_L}$	$\frac{2F_{BL}}{F_B+F_L}$	$\frac{2\phi_{BL}}{\phi_B+\phi_L}$	$\frac{2F_{BB'}}{F_B+F_{B'}}$	$\frac{2\phi_{BB'}}{\phi_B+\phi_{B'}}$	$\frac{2F_{LL'}}{F_L+F_{L'}}$	$\frac{2\phi_{LL'}}{\phi_L+\phi_{L'}}$		
LiH	---	---	.0475	-1.000	---	---	---	---	---	---	---	---	4.000	.1816*
BeH ₂	---	---	.0366	-.5024	---	---	---	---	.0409	-.494	---	---	6.000	.4251*
BH	---	---	.0358	-.537	.0531	-.517	.117	-.442	---	---	---	---	6.000	.7180*
BH ₃	---	---	.0359	-.459	---	---	---	---	.0964	-.305	---	---	7.999	1.2851*
BH ₄	---	---	.0316	-.278	---	---	---	---	.0919	-.228	---	---	10.002	2.1007*
CH ₄	---	---	.0380	-.292	---	---	---	---	.1361	-.216	---	---	10.001	2.7252*
NH ₃	---	---	.0438	-.314	.0582	-.316	.233	-.171	.1820	-.212	---	---	9.998	3.4891
H ₂ O	-.6879	.0013	.0492	-.327	.0630	-.327	.259	-.179	.2150	-.213	.331	-.092	9.985	3.9869
HF	-.6287	.0019	.0566	-.341	.0686	-.332	.304	-.180	---	---	.318	-.146	10.000	4.3357
Ne	-.6324	.0019	---	---	.0739	-.342	---	---	---	---	.327	-.151	9.999	4.5485
Ar	---	---	.1134	-.160	.0035	-.317	.0782	-.836	---	---	---	---	18.000	2.1352

† $\sum \frac{N_{\lambda}}{\lambda}$ should equal N; deviation from that value measures inaccuracy of integrations.

isolated cores for the molecules $\text{LiH}^+(\text{X})$, $\text{LiH}(\text{X})$, $\text{BeH}(\text{H})$, $\text{BeH}(\text{A})$, $\text{BH}(\text{X})$, and $\text{BeH}_2(\text{X})$ of radius $R = 1.55, 1.42, 0.95, 1.00, 0.70$ and 0.95 a.u., respectively. The valence regions of $\text{BeH}(\text{X})$, $\text{BH}(\text{X})$ and $\text{BeH}_2(\text{X})$ each appeared to be further partitionable into two (conical) pairs, whereas $\text{LiH}^+(\text{X})$, $\text{LiH}(\text{X})$ and $\text{BeH}(\text{A})$ could not be further fragmented.

The molecules, $\text{LiH}(\text{X})$, $\text{BH}(\text{X})$ and $\text{BeH}_2(\text{X})$ were chosen for further perusal. We computed the variation in fluctuation and population for a spherical core on the heavy nucleus for each molecule. For the optimal core found in each case, an attempt was then made to further divide the valence region into (truncated) conical fragments. These were defined by the angle (α) between the internuclear axis and conical surface (see inserts on Figs. 14, 15 and 16).

The results for LiH are plotted in Figure 14. The core fluctuation has a clear minimum for a population of 2.00 and radius 1.42 a.u. between maxima for populations of 1.0 and 3.0 electrons. The fluctuation of the conical valence region has only a lone maximum between minima of 0 for zero volume and .0908 for the complete valence region. Thus, as in the previous analysis, we can distinguish a core but no valence partitionability for this molecule. Also, Λ for the 1.42 a.u. spherical core (0.0908) is lower than that for the virial (Li) fragment (0.0995).

The BH data are given in Figure 15. Again Λ_{core} has a minimum for a core population of 2.00, between maxima for populations of 1.0 and 4.0 (i.e., half the core, and the core plus half the valence region, respectively). The fluctuation for a valence lobe located on the non-bonded side of the B nucleus shows a clearly defined minimum for a population of 2.00 (and $\alpha = 73^\circ$) between maxima at 1.0 and 3.0 electrons. Clearly, the valence partitioning has been successful.

Figure 14. Fluctuation Versus R/\bar{N} for LiH Core/ Non-Bonded Fragments

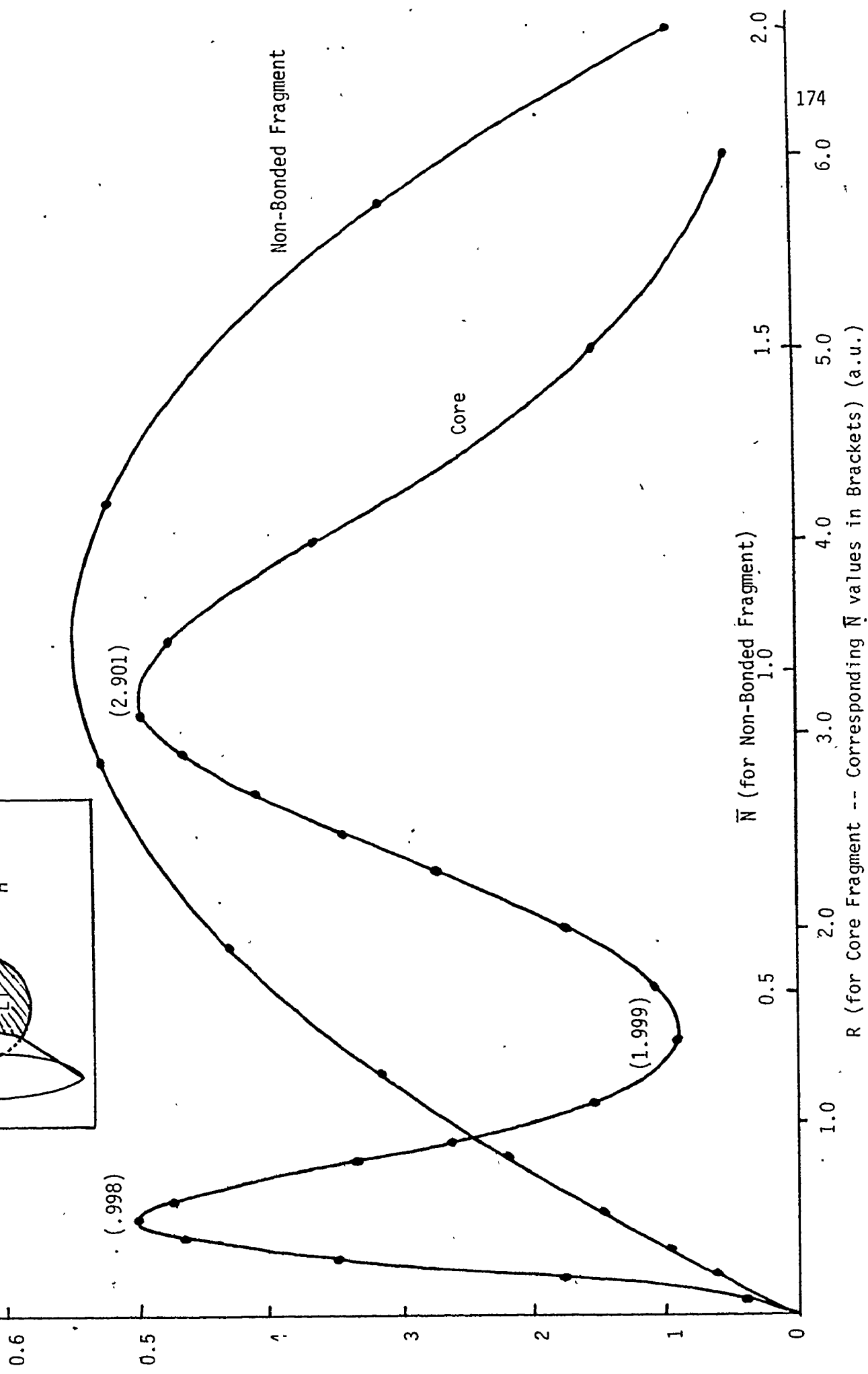
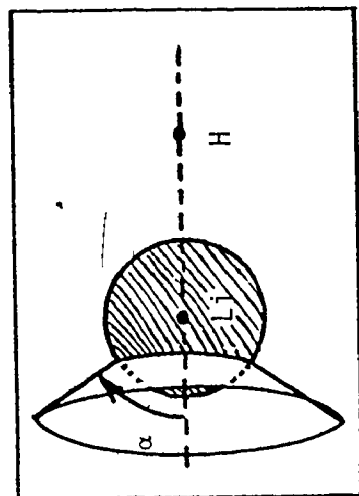
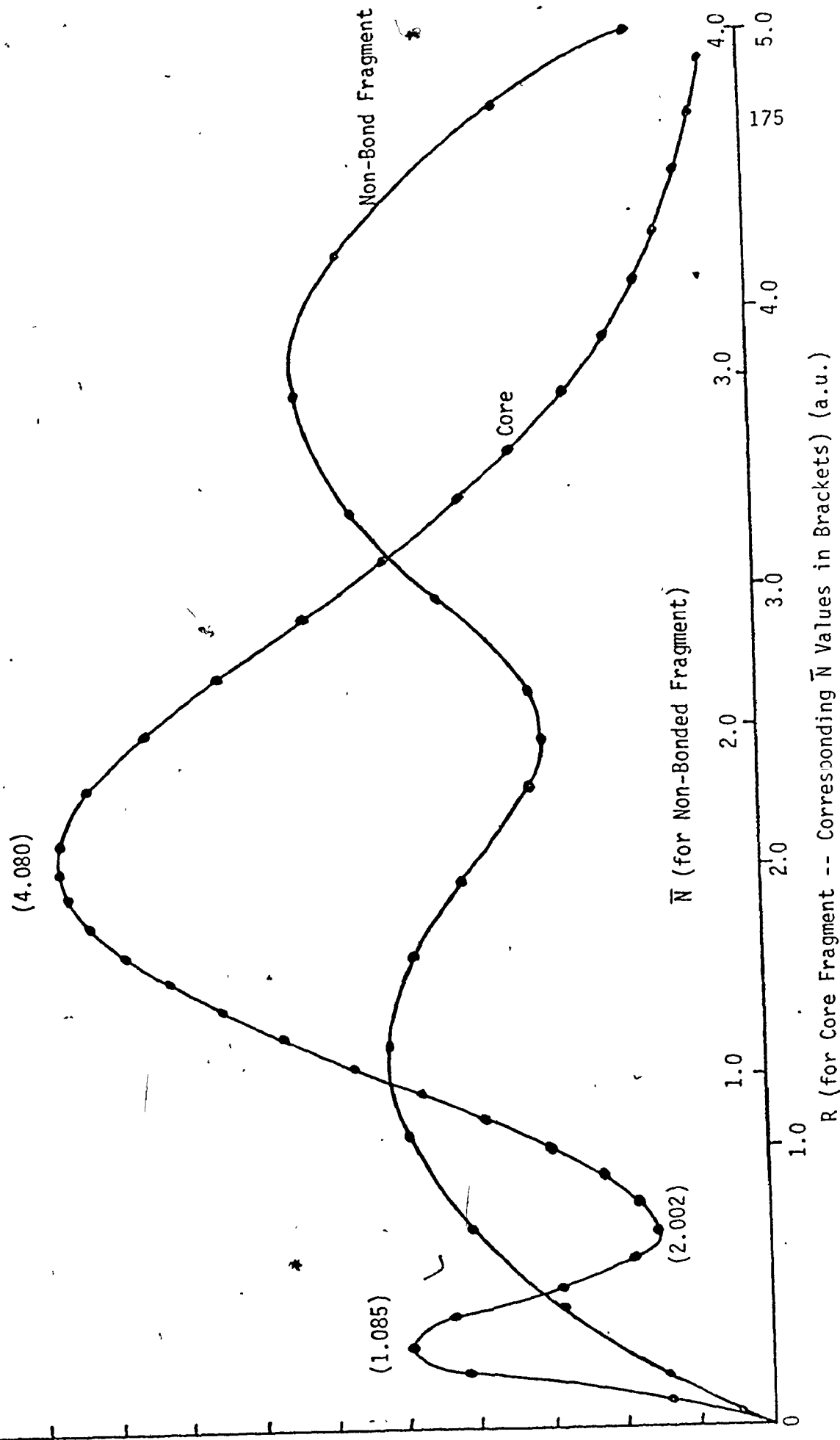
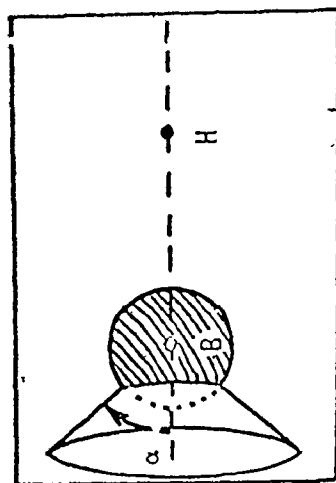


Figure 15. Fluctuation Versus R/\bar{N} for BH Core/ Non-Bonded Fragments



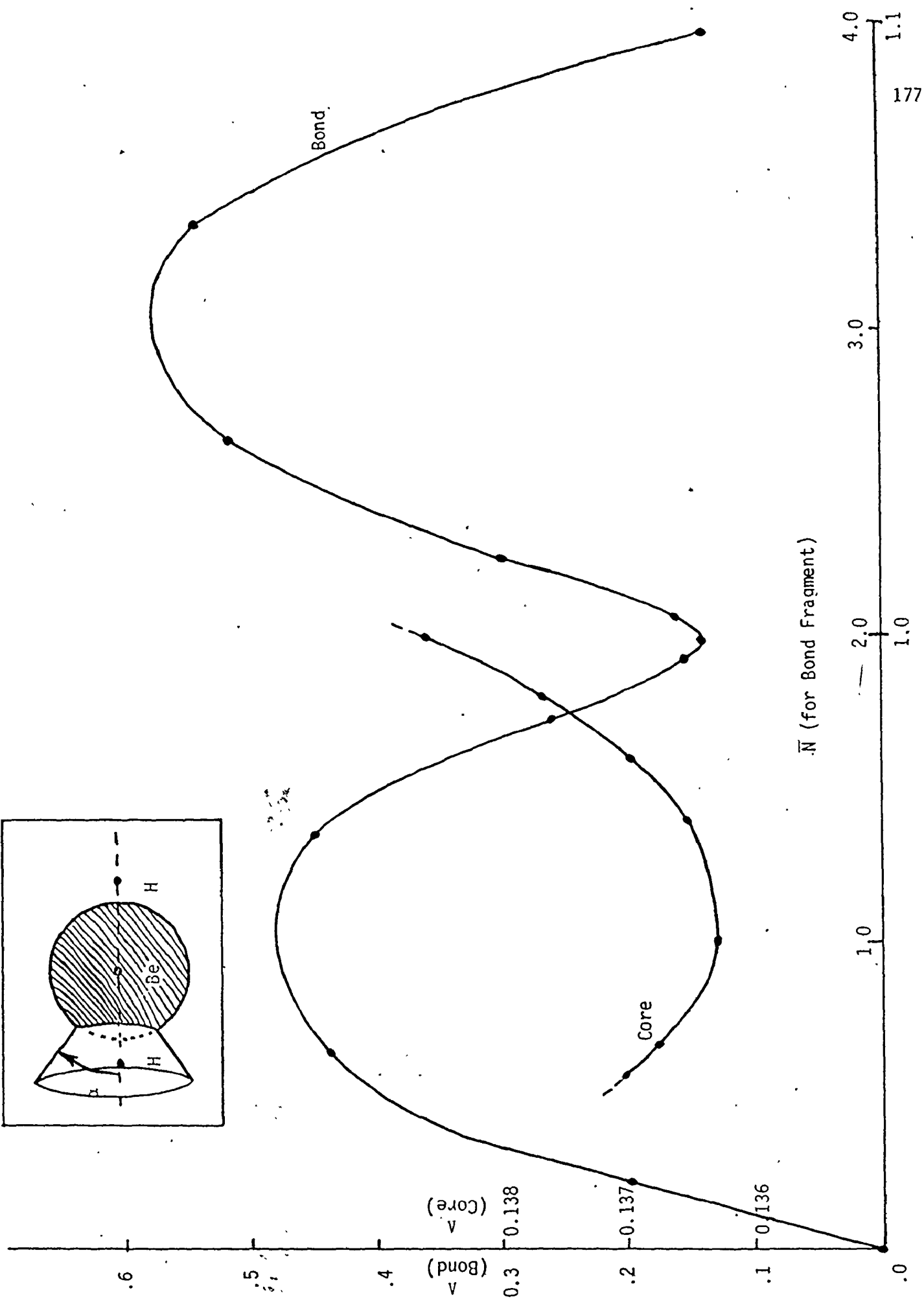
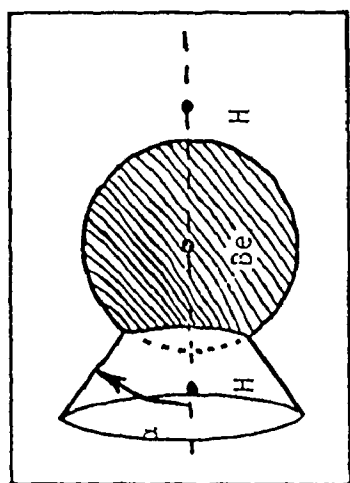
The BeH_2 plots are contained in Figure 16. A core of locally minimal Λ is clearly differentiable for $\bar{N} = 2.002$ and $R = 0.95$ a.u. The remaining valence region is partitionable into two equal loges ($\alpha = 90^\circ$) with population of 2.00 and locally minimum fluctuation ($= 0.1444$). The fluctuation for a conical valence region exhibits maxima for $\bar{N} \approx 1$ and 3. Thus, three localized pairs are identifiable.

The criteria developed in this chapter predict these molecules to be partitionable into the loges previously identified on the basis of the missing information function. The properties of these "best" partitionings of the molecules are listed in Table 10. The results further confirm the identification of primarily intra-correlated pairs. The sums of the loge fluctuations are very low (relative to the other systems studied).

The localization of correlation is more distinct in BeH_2 than that in BH , in agreement with the conclusions drawn about partitionability versus heavy nucleus charge in the 10-electron series. Specifically, for BeH_2 , the "bond" loge fluctuation is 0.1444, almost as low as that of the core (0.1363). The optimal BH bonded and non-bonded loge fluctuations (0.2648 and 0.2950) are both higher than the BeH_2 "bond" loge fluctuation. They are also higher than the boron core fluctuation (0.1582), which is itself higher than that for the beryllium core (0.1363).

In summary, all the molecules are partitionable, with the localization of pairs becoming less successful in the order LiH , BeH_2 and BH .

Figure 16. Fluctuation Versus R/\bar{N} for BeH_2 Core/Bond Fragments



R (for Core Fragment) -- Corresponding \bar{N} Values in Brackets (a.u.)

BH, BH₃, BH₄⁻

We next studied the variation in fragment localizability with the number of valence electrons and protons distributed around a given nucleus. The series of ground state molecules BH, BH₃, BH₄⁻ provided a convenient trial case.

The number of valence electrons around the B core increases from 4 to 6 to 8. With these molecules, we can also evaluate the variation in optimal boron core radius and fluctuation.

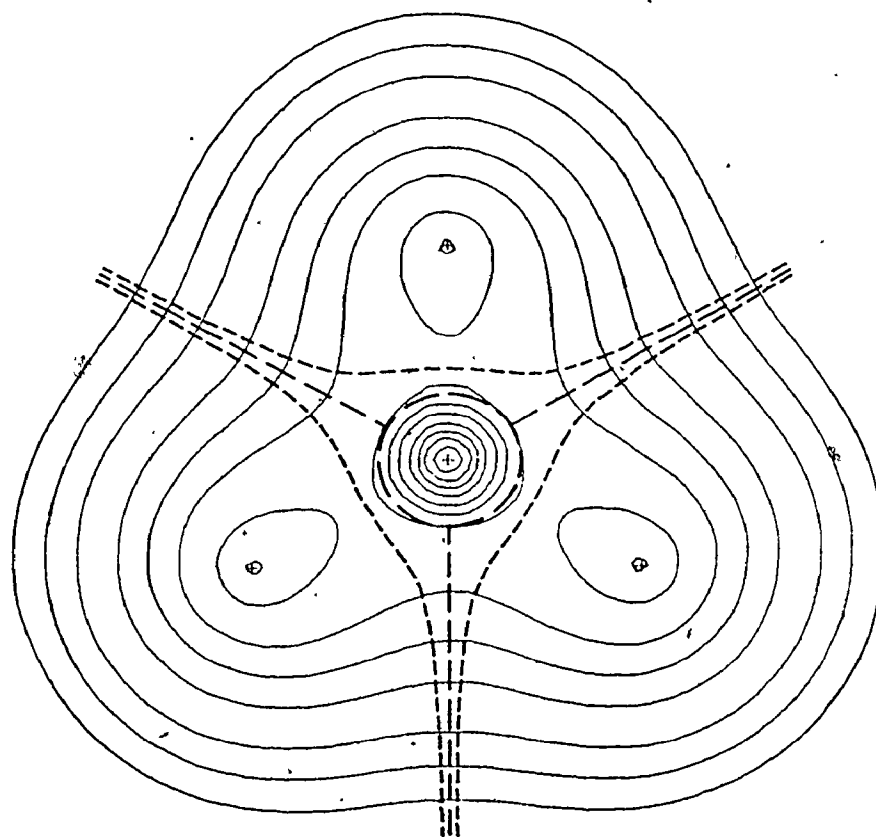
The BH results are derived (for convenient comparison with BH₃ and BH₄⁻) from those in the previous section. The BH₃ and BH₄⁻ results are based on wavefunctions which are expressed in an optimized Gaussian basis set including polarization functions,⁵⁹ yielding total energies near the Hartree-Fock limit. Figure 17 contains the charge density plots for BH₃ and BH₄⁻. The plot for BH is contained in Figure 3. The virial partitioning surfaces and optimal loge boundary surfaces (found below) are also included.

Figure 18 shows the variation in core fluctuation with radius for all three molecules. The optimal core radius remains almost unchanged for the three systems ($0.70 \pm .025$ a.u.). The corresponding core fluctuation increases from 0.1582 (BH) to 0.1865 (BH₃) to 0.2127 (BH₄⁻), as the increasing number of valence electrons increases the inter-correlation between core and valence regions.

The valence region of each of the three molecules was found to be partitionable into well-localized electron pairs.

The BH results (Figure 15) were briefly presented in a previous section. The two valence loges defined by $\alpha = 73^\circ$ each have a popu-

Figure 17. Contour maps of the electronic charge distributions for (top) $\text{BH}_3(X^1A_1)$ and (bottom) $\text{BH}_4^-(X^1A_1)$. In each diagram, the "best" loge boundaries are indicated by long dashed curves, and the virial partitioning surfaces by short dashed lines.



1 a.u.

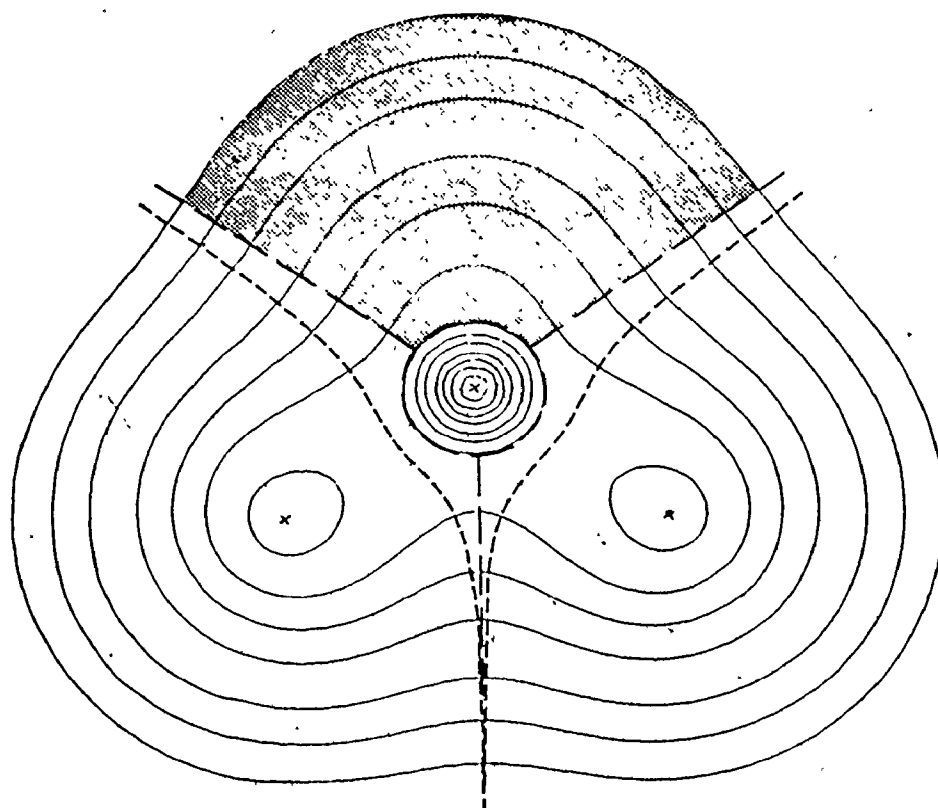
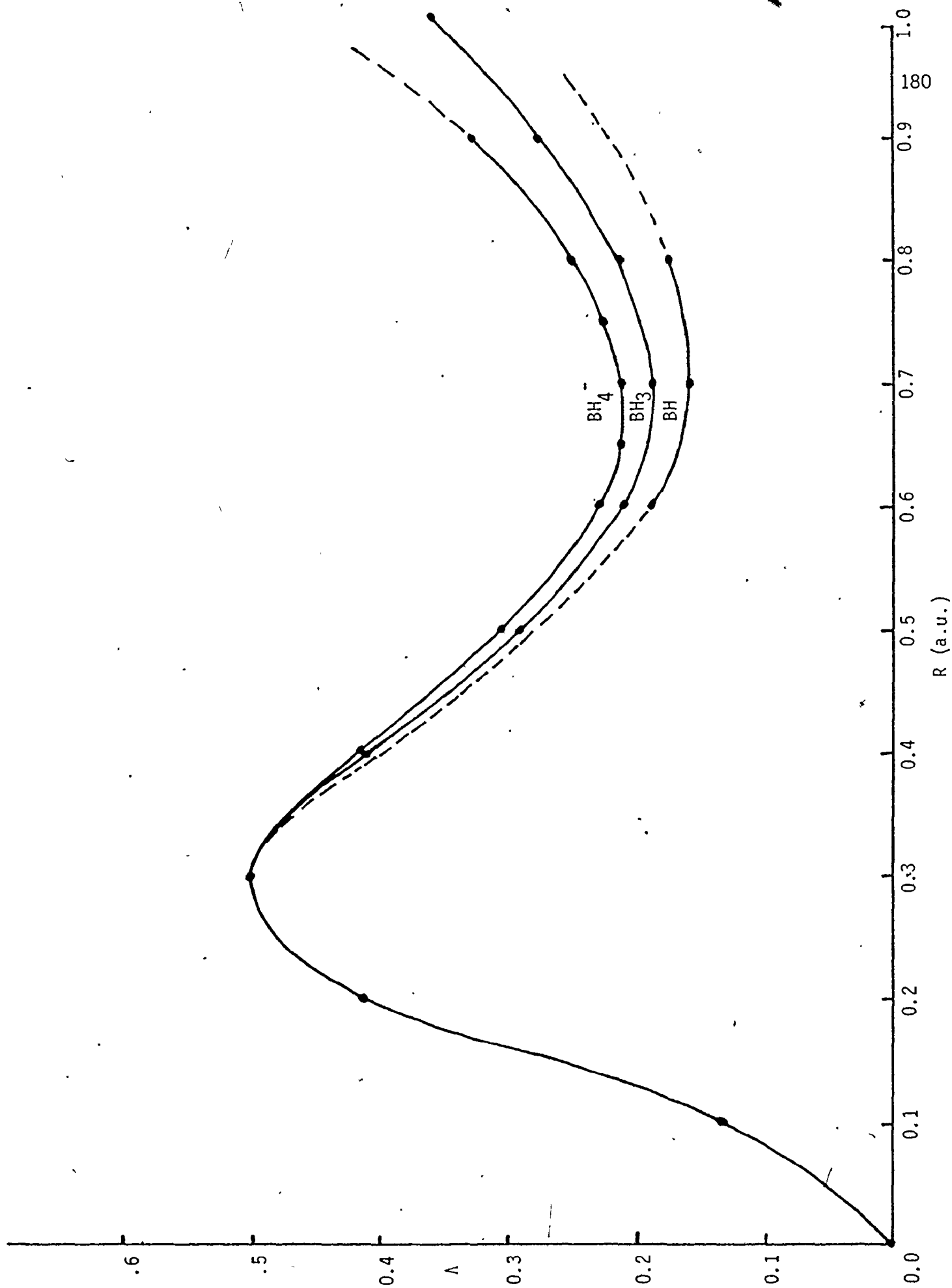


Figure 18. Fluctuation Versus R for BH , BH_3 , BH_4^- Spherical Cores



lation of 2.00. The non-bonded loge was found to have a fluctuation of 0.295 and the bonded loge to have a (lower) fluctuation of 0.265. Comparison of these values to the computed core fluctuation of 0.158 shows that the electron density is progressively more strongly localized for non-bonded, bonded and core loges. This conclusion agrees with our previous observation of the relative importance of core, bonding and non-bonding pairing reflected in the various event probabilities for $\text{BeH}(X)$ in Chapter II. The F/F_L and ϕ/ϕ_L ratios for the core, bonded and non-bonded loges (Table 10) are, respectively, 0.921, 0.868, 0.852, and 0.881, 0.801, and 0.779. The F/F_L and ϕ/ϕ_L ratios both also indicate a decreasing containment of the population correlation holes for the three types of region.

The $\text{BH}_3(X \ ^1A_1)$ valence region was found to be partitionable into three identical 120° wedge-shaped loges (c.f. insert in Figure 9 for similar Neon wedges) with a well-localized population of 2.00. For these loges, the fluctuation passed through a well-defined minimum value of 0.366 (Figure 19). The minimum value is larger than for BH, due to the extra two electrons in the valence region. The F/F_L ratios for the core and bond loges are 0.921 and 0.816; the ϕ/ϕ_L ratios are 0.877 and 0.755, respectively. Thus, again the correlation holes are predominantly loge-localized.

The $\text{BH}_4^-(X \ ^1A_1)$ valence region was found to be partitionable into four identical quadrant loges (c.f. insert in Figure 10 for similar CH_4 fragments). Each had a population of 2.00 and a fluctuation of 0.472 which was a local minimum to boundary angle variation (Figure 20). This minimum fluctuation is higher than in BH_3 , again showing the in-

Figure 19. Fluctuation and Related Properties Versus Population for
 BH_3 Valence Wedges

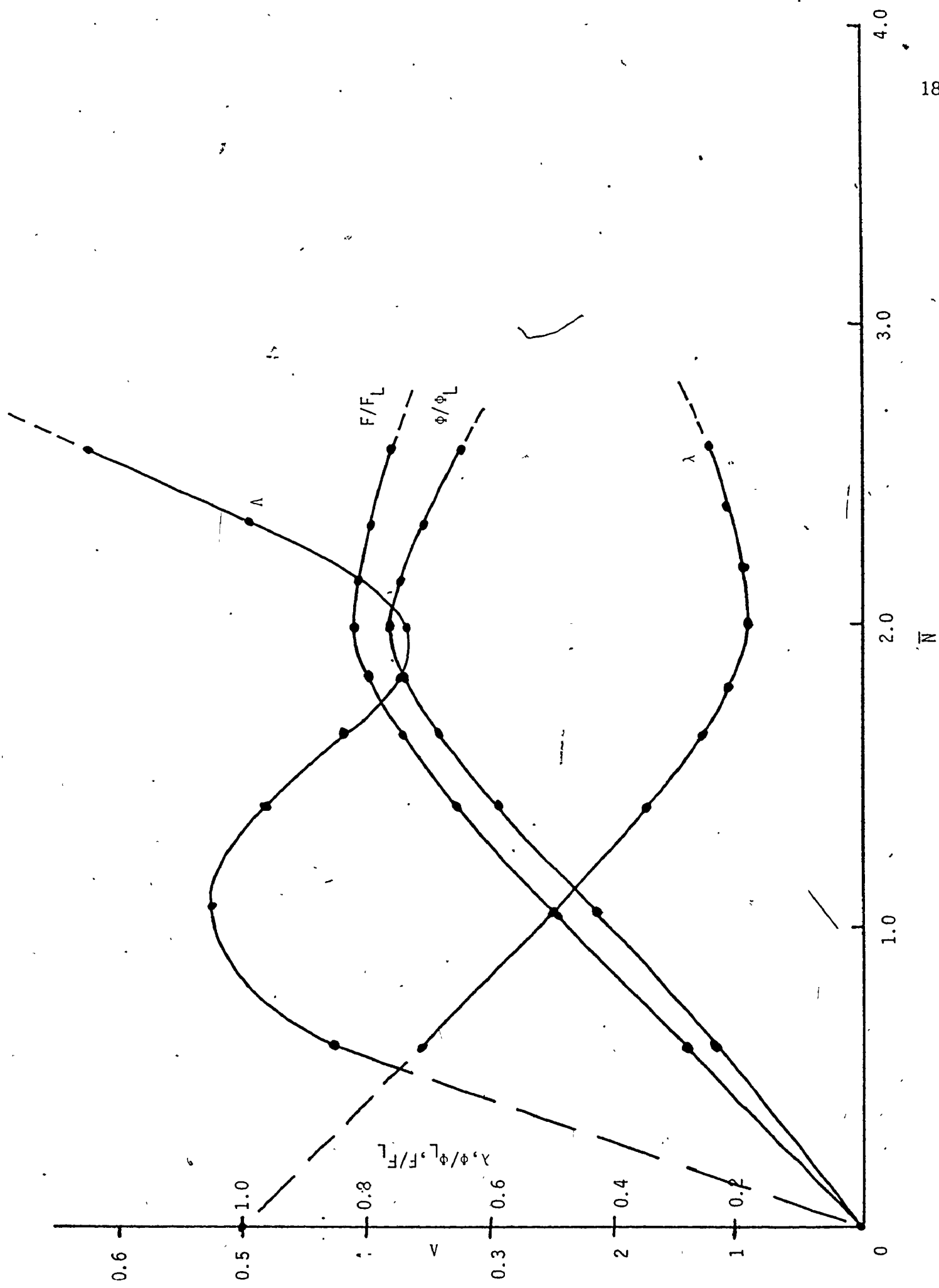
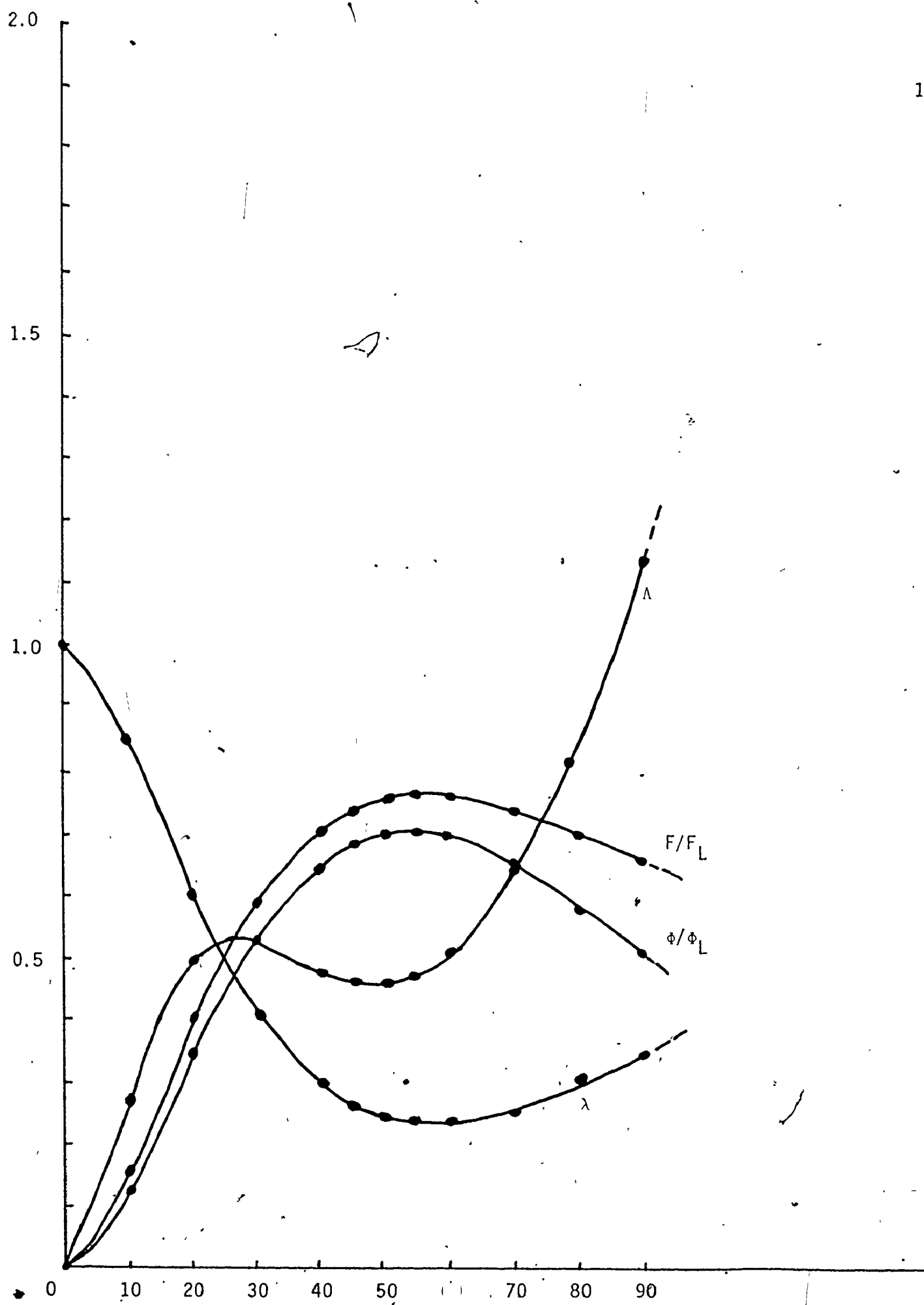
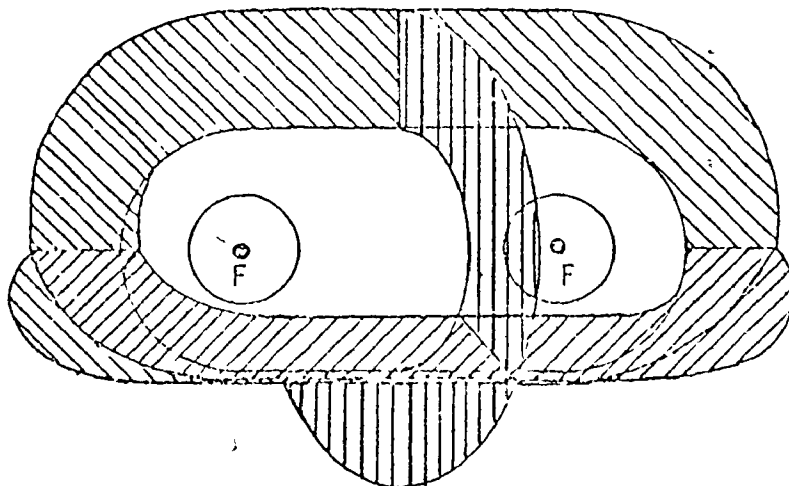
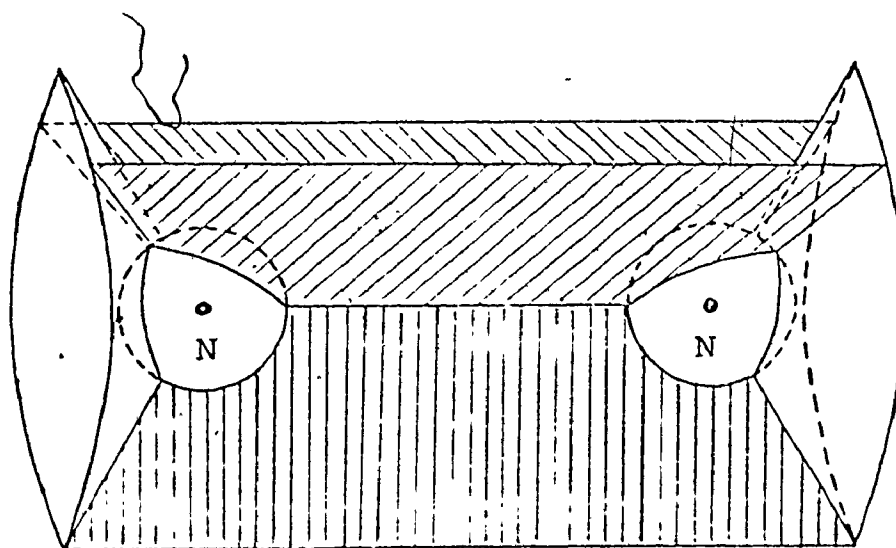


Figure 20. Fluctuation and Related Properties Versus θ_0 for BH_4^-
" C_{3v} " Valence Fragments





and



It is interesting to compare the observed variation in the partitionability of the molecules considered, with the predictions of the "tangent sphere model".^{8,61} In the latter, from the core radii and bond distances one can define a coordination number for each atom -- the number of electron pair "hard spheres" which can surround the core without "touching". One finds the following:

<u>Atom</u>	<u>Coordination Number</u>
Li	8
B,C	4
N,O	3
F,Ne	2

Thus, as we found, one predicts a "clean" partition of a valence octet density for C and B into relatively non-correlated pairs; however, this is not possible for N (in NH_3), O (in H_2O), F (in HF), or Ne.

CONCLUSIONS

We have applied the theory of the missing information function, $I(P_n, \Omega)$ and population fluctuation function, $\Lambda(\bar{N}, \Omega)$ to partitionings of the electronic charge density of molecules. We have established a direct correlation between the formal quantum description of event probability distributions to intuitive interpretations of electron pairing and group localizability in general.

In particular, we determined that the lowest non-trivial minimum in I corresponds to that partitioning of a molecular system which maximizes the remaining information on the distribution of electronic event probabilities in the coordinate space representation. Local minima in Λ define maximally intra-correlated quantum subsystems, and the minimum value of $\sum_{\lambda=1}^v \Lambda_{\lambda}$ for some maximum v defines that partition of a quantum system yielding the largest possible set of weakly inter-correlated quantum subsystems.

Partitionings of small molecules were studied to evaluate the effects of Fermi correlation on the localizability of groups of electrons in them. For all the molecules studied, a clear separation of spherical core pairs from valence loges was accomplished. For several molecules ($\text{BeH}(X)$, $\text{BH}(X)$, $\text{BeH}_2(X)$, $\text{BH}_3(X)$, $\text{BH}_4^-(X)$, $\text{CH}_4(X)$) unambiguous partitionings of the valence region into volumes containing well-localized pair populations were found. For several other molecules ($\text{LiH}^+(X)$, $\text{LiH}(X)$, $\text{BeH}(A)$, $\text{NH}_3(X)$, $\text{H}_2\text{O}(X)$, $\text{HF}(X)$, $\text{Ne}(X)$, $\text{Ar}(X)$, $\text{F}_2(X)$, $\text{N}_2(X)$), partitioning of the valence region into regions containing localized subgroups was found not possible.

Virial partitioning was found to yield the best partition as defined by $I(P, \Omega)$ in those molecules (LiH , LiH^+) which most closely approached the ionic bonding limit. However, by the Δ criterion, a spherical core yields a slightly better core for LiH than the virial fragment.

For covalently bonded systems, spherical heavy-atom cores of population approximately 2.00 were found to be better localized than virial fragments. Separability of valence pair groups was favoured by low heavy-atom nuclear charge (hence large core), few valence electrons, and the presence of bonded protons. Valence electron localizability was found more difficult for high heavy-atom nuclear charge (hence overall a more compact density distribution), a full octet of valence electrons, and few bonded protons. σ - π Valence separation was not found possible (for N_2).

FUTURE WORK

Given a system known to be partitionable when described by a Hartree-Fock wavefunction, will the system remain partitionable when Coulomb correlation is added? One could study this question by using a wavefunction incorporating Coulomb correlation via configuration interaction, for instance.

It has been shown³⁰ possible to rigorously define the expectation value of any observable property of a molecule in terms of a sum of loge contributions and of loge pair contributions. If the former predominate, then one may be able to simply construct accurate wavefunctions based on an antisymmetrized product of group functions each with well-

described intra-correlation of the various loge populations. The fluctuation criterion can be of use in selecting likely regions to attempt such localized subsystems.

Defining localizability with respect to the fluctuation in electron population is only one application of the fluctuation criterion. One might choose some other property, a kinetic energy density, for instance, and attempt to minimize the fluctuation of that quantity for partitions of momentum space.

One might consider further analysis to determine why it is that the best loge boundaries found (so far) mimic the "natural" partitioning provided by the zero flux surfaces in a molecule.

Given the interpretations noted to this point, one could study the actual localizability of the electronic population in various chemically interesting regions of molecules often treated as though localized, the aromatic sextet rings in benzene for instance, or valence "resonance structures" of an enol. The three-centre two-electron bond in borane dimer, B_2H_6 , would provide another interesting test of the electron pair idea.

We noted a difference in partitionability between two states of the same molecule $BeH(X)$ and $BeH(A^2\Pi_R)$. Can one perhaps find loge partitionings suitable for both states of an electronic excitation so that the electronic process can be described as a localized change in one of the largely intra-correlated subsystems?

APPENDIX B-1

PROGRAMME DIALØGE

CALCULATION OF P_μ AND $I(P)$ FOR ORBITAL WAVEFUNCTIONS

Evaluation of the P_μ and $I(P)$ for a molecular partitioning in general requires knowledge and use of the diagonal elements of the N^{th} order spinless density matrix kernel, $\Gamma^{(N)}$. Here we shall consider calculations for a two-logs partition of a pure system eigenstate, $\Psi(\{\underline{x}_n\})$, described by a single determinantal restricted Hartree-Fock LCAO-MO wavefunction. Given a set of real spatial molecular orbitals, $\{\phi_i(\underline{q})\}$, and the spin functions $\{\alpha(\sigma), \beta(\sigma)\}$, we then construct N spin orbitals $\psi_j(\underline{x})$ of the form

$$\psi_j(\underline{x}) = \phi_i(\underline{q})w(\sigma)$$

where

$$w(\sigma) = \alpha(\sigma) \text{ or } \beta(\sigma).$$

A short form indicating which spin function is used is to place a bar over the ϕ_i symbol to indicate $\beta(\sigma)$, $\alpha(\sigma)$ being assumed otherwise.

In the restricted H.-F. case, the spatial orbitals for α and β spin MO's are constrained to be chosen from the same set $\{\phi_i(\underline{q})\}$. The Pauli principle restricts us to placing at most two particles per spatial orbital, one of each spin. A typical state function thus takes the form of several doubly occupied spatial orbitals and possibly one or more MO's singly occupied by α -spin electrons. (We thereby define a wavefunction for the term level of maximum M_S value (spin projection for unique spin z-axis) consistent with the chosen electron MO configura-

tion.) Thus $\Psi(\{\underline{x}_n\})$ takes the general form:

$$\Psi(\{\underline{x}_n\}) = \frac{1}{\sqrt{N!}} \begin{vmatrix} \phi_1(q_1) & \overline{\phi_1}(q_1) & \phi_2(q_1) & \cdots & \phi_{N_\alpha}(q_1) \\ \phi_1(q_2) & \overline{\phi_1}(q_2) & \phi_2(q_2) & \cdots & \phi_{N_\alpha}(q_2) \\ \vdots & \vdots & \vdots & \ddots & \vdots \\ \phi_1(q_N) & \overline{\phi_1}(q_N) & \phi_2(q_N) & \cdots & \phi_{N_\alpha}(q_N) \end{vmatrix}$$

$$\equiv \frac{1}{\sqrt{N!}} | \phi_1(q_1) \overline{\phi_1}(q_2) \phi_2(q_3) \overline{\phi_2}(q_4) \cdots \phi_{N_\alpha}(q_N) |.$$

A more convenient form is obtained if we group the spatial orbitals associated with α -spin (N_α in number, say) separately from those associated with β -spin (N_β in number) and reorder particle labels to match the new order. Thus:

$$\Psi(\{\underline{x}_n\}) = \frac{1}{\sqrt{N!}} | \phi_1(q_1) \phi_2(q_2) \cdots \phi_{N_\alpha}(q_{N_\alpha}) \overline{\phi_1}(q_{N_\alpha+1}) \overline{\phi_2}(q_{N_\alpha+2}) \cdots \overline{\phi_{N_\beta}}(q_N) |.$$

Note that $N = N_\alpha + N_\beta$. This expression for $\Psi(\{\underline{x}_n\})$ is, of course, a summation of $N!$ products of the N spin orbitals, each term a permutation of the particle coordinate labels for the orbitals fixed in order (or equivalently, orbitals permuted for fixed label order).

We now evaluate $r^{(N)}(\{q_n\})$:

$$r^{(N)}(\{q_n\}) = \sum_{\{w\}_n} \Psi^*(\{\underline{x}_n\}) \Psi(\{\underline{x}_n\})$$

$$= \frac{1}{\sqrt{N!}} \sum_{\{w\}_n} | \phi_1(q_1) \phi_2(q_2) \cdots \phi_{N_\alpha}(q_{N_\alpha}) \overline{\phi_1}(q_{N_\alpha+1}) \overline{\phi_2}(q_{N_\alpha+2}) \cdots \overline{\phi_{N_\beta}}(q_N) |^2$$

Without the integration over particle spins, there are $(N!)^2$ terms in the square of the wavefunction expansions. However, the two

spin functions are orthonormal, i.e.:

$$\sum_w w_1(\sigma) w_2(\sigma) = \delta_{w_1 w_2}.$$

This results in only permutations within the N_α α -spin MO's and/or within β -spin MO's contributing non-zero cross terms after spin integration over all spin coordinates. The number of non-zero terms in $\Gamma^{(N)}$ is thereby reduced to $N!N_\alpha!N_\beta!$.

We are now finally in a position to evaluate the two-loge $P_n(\Omega)$, the probability of the event of localizing n electrons in the loge Ω and $(N-n)$ in Ω' (the remainder of R^3):

$$P_n(\Omega) = \frac{N!}{n!(N-n)!} \int_{\Omega} dq_1 \dots \int_{\Omega} dq_n \int_{\Omega'} dq_{n+1} \dots \int_{\Omega'} dq_N \Gamma^{(N)}$$

Given the $N!N_\alpha!N_\beta!$ terms we have found for $\Gamma^{(N)}$, we see that the actual computation of any $P_n(\Omega)$ requires that one multiply together N orbital overlaps (n integrals over the volume Ω , and $(N-n)$ over the volume Ω').

To make this clearer, consider a three-electron wavefunction:

$$\begin{aligned} \psi(x_1, x_2, x_3) &= \frac{1}{\sqrt{3!}} | \phi_1(q_1) \overline{\phi}_1(q_2) \phi_2(q_3) | \\ &= \frac{1}{\sqrt{3!}} | 1 \overline{1} 2 | \end{aligned}$$

(where the particle labels are assumed to be in the order 1, 2, 3 for all terms in the expansion of ψ).

$$\begin{aligned} \Gamma^{(N)}(q_1, q_2, q_3) &= \sum_{w_1} \sum_{w_2} \sum_{w_3} \psi^* \psi \\ &= \sum_{w_1} \sum_{w_2} \sum_{w_3} \frac{1}{3!} (1(\overline{1}2 + 2\overline{1}) - \overline{1}(12 + 21) + 2(1\overline{1} - \overline{1}1))^2 \end{aligned}$$

$$= \frac{1}{3!} [11 \ 11 \ 22 + 11 \ 22 \ 11 + 11 \ 11 \ 22 + 11 \ 22 \ 11 + 22 \ 11 \ 11 + 22 \ 11 \ 11 \\ - 12 \ 11 \ 21 - 12 \ 21 \ 11 + 11 \ 12 \ 21]$$

(where $11 \ 11 \ 22 \equiv \phi_1(q_1) \phi_1(q_1) \phi_1(q_2) \phi_1(q_2) \phi_2(q_3) \phi_2(q_3)$ for instance).

There are 4 $P_n(\Omega)$'s to be calculated: P_0, P_1, P_2, P_3 .

$$P_0(\Omega) = \frac{3!}{0!(3-0)!} \int_{\Omega'} dq_1 \int_{\Omega'} dq_2 \int_{\Omega'} dq_3 r^{(N)} \\ = \frac{1}{3!} [\langle 11 \rangle_{\Omega'} \langle 11 \rangle_{\Omega'} \langle 22 \rangle_{\Omega'} + \langle 11 \rangle_{\Omega'} \langle 22 \rangle_{\Omega'} \langle 11 \rangle_{\Omega'} + \langle 11 \rangle_{\Omega'} \langle 11 \rangle_{\Omega'} \langle 22 \rangle_{\Omega'} \\ + \langle 11 \rangle_{\Omega'} \langle 22 \rangle_{\Omega'} \langle 11 \rangle_{\Omega'} + \langle 22 \rangle_{\Omega'} \langle 11 \rangle_{\Omega'} \langle 11 \rangle_{\Omega'} + \langle 22 \rangle_{\Omega'} \langle 11 \rangle_{\Omega'} \langle 11 \rangle_{\Omega'} \\ - \langle 12 \rangle_{\Omega'} \langle 11 \rangle_{\Omega'} \langle 21 \rangle_{\Omega'} - \langle 12 \rangle_{\Omega'} \langle 21 \rangle_{\Omega'} \langle 11 \rangle_{\Omega'} + \langle 11 \rangle_{\Omega'} \langle 12 \rangle_{\Omega'} \langle 21 \rangle_{\Omega'}]$$

(where $\langle 11 \rangle_{\Omega'} \langle 11 \rangle_{\Omega'} \langle 22 \rangle_{\Omega'} \equiv \int \phi_1(q_1) \phi_1(q_1) dq_1 \int \phi_1(q_2) \phi_1(q_2) dq_2 \int \phi_2(q_3) \phi_2(q_3) dq_3$ for instance).

All of the other $P_n(\Omega)$'s follow the same pattern, the only change from the $P_0(\Omega)$ expression being the replacement of the degeneracy factor and the first n of the integral volume subscripts (Ω') by Ω . Given the set of P_n 's, $I(P)$ is easily calculated.

The 3-electron, 2-loge case considered above is about the simplest non-trivial one. The method rapidly "blows up" with increasing number of terms. For closed-shell wavefunctions ($N_\alpha = N_\beta$), one is faced with the following number of terms in $\psi(N!)$ and $r^{(N)}(N!N_\alpha!N_\beta!)$:

N	N!	$N!N_\alpha!N_\beta!$
2	2	2
4	24	96
6	720	25,920
8	40,320	23,224,320
10	3,628,800	52,254,720,000

Clearly, a significant degree of sophistication or approximation is required to evaluate the cross terms in $r^{(N)}$ for even a 10-electron case. Furthermore, the molecular spatial orbitals have non-zero overlaps over a subspace of R^3 , even if the orbitals belong to different irreducible representations of the nuclear point group. Orbital orthogonality permits significant simplification of usual Hartree-Fock calculations; its loss places a severe constraint on the size of systems for which $I(P)$ calculations can be made. Thus, for $N=5$, DIALØGE requires 12_{10} central processor (CP) seconds on the CDC-6400, but for $N=6$, 240_{10} CP secs. are needed.

Programme DIALØGE

For the small ($N \leq 6$) systems treated in this work, "brute force" computer programs sufficed to perform two- and three-loge partitionings. DIALØGE was written for the two-loge case. The mainline programme calls three subroutines.

Subroutine MAIN: This subroutine performs several functions:

- (a) calls subroutine PERMUT (which creates and permutes the list of orbital indices in the expansion of Ψ);
- (b) calls subroutine XTERM (which evaluates those permutations of the "standard" order of orbital indices $(1,2,\dots,N)$ giving non-zero contributions to $r^{(N)}$ (due to spin orthogonality));
- (c) reads the orbital overlap matrices (over loges Ω and Ω'); and,
- (d) generates the $P_n(\Omega)$ and $I(P)$, using the list of non-zero cross terms in $r^{(N)}$, the ordered lists of orbital indices for each permutation, plus the orbital overlap matrices.

Subroutine PERMUTE: This subroutine generates the $N!$ permutations

of the standard order of orbital indices in Ψ . Computer generation of the $N!$ permutations for variable N was found to be a non-trivial problem.⁴⁸ The following procedure was devised:

- (i) set $M = 2$;
- (ii) enter the "standard" order of integral indices $(1, 2, 3, \dots, N)$ in the first row of a storage array;
- (iii) "cycle" the last M indices (i.e., leaving the first $(N-M)$ indices untouched) yielding $(M-1)$ new permutations;
- (iv) determine the parity for each new permutation $(= (-1)^P)$ where P = the sum of the numbers of higher indices preceeding each index in the list of orbital indices);
- (v) add the new permuted orbital lists to the storage array; and,
- (vi) set $M = M+1$ and go to (iii), stopping the procedure for $M \rightarrow N$.

Consider the case of $N = 3$:

Permutation	Generated by	Orbital Indices	Parity
1	"standard" order	1 2 3	1
2	"cycle" last two indices of permutation 1	1 3 2	-1
3	"cycle" last three indices of permutation 1	3 1 2	1
4		2 3 1	-1
5	"cycle" last three indices of permutation 2	2 1 3	-1
6		3 2 1	-1

Subroutine XTERM: This subroutine compares the orbital lists for all the permutations in the expansion of Ψ to determine the $N!N_\alpha!N_\beta!$ non-zero cross terms in $r^{(N)}$. This is done simply by assuring that the k^{th} indices in both index lists belong to the α or β spin orbital list for $1 \leq k \leq N$.

REFERENCES

1. K. R. Symon, "Mechanics", Addison-Wesley, Reading, 1960, p. 185.
2. W. Kutzelnigg, Fortsch. Chem. Forsch. 41, 31 (1973).
3. O. Sinanoğlu, Advan. Chem. Phys. 14, 237 (1969).
4. F. L. Pilar, "Elementary Quantum Chemistry", McGraw-Hill, Toronto, 1968, p. 244.
5. P.-O. Löwdin, Phys. Rev. 97, 1474 (1955).
6. E. R. Davidson, Rev. Mod. Phys. 44, 451 (1972).
7. C. A. Russell, "The History of Valency", Humanities Press, New York, 1971.
8. R. J. Gillespie, "Molecular Geometry", Van Nostrand Reinhold Co., London, 1972.
9. G. N. Lewis, J. Am. Chem. Soc. 33, 762 (1916).
10. J. W. Linnett, "The Electronic Structure of Molecules -- A New Approach", Wiley, New York, 1964.
11. W. Pauli, Phys. Rev. 58, 716 (1940).
12. R. J. Gillespie, J. Chem. Educ. 51, 367 (1974).
13. N. V. Sidgwick and H. E. Powell, Proc. Roy. Soc. A176, 153 (1940).
14. R. J. Gillespie and R. S. Nyholm, Quart. Rev. Chem. Soc. 11, 339 (1957).
15. R. F. W. Bader and H. J. T. Preston, Can. J. Chem. 44, 1131 (1966).
16. R. S. Drago, J. Chem. Educ. 50, 244 (1973).
17. L. S. Bartell, "Pauli Mechanics", 1974, by private distribution.
18. L. C. Allen, Theoret. Chim. Acta. 24, 117 (1972).
19. A. D. Walsh, J. Chem. Soc. (Lond.) 2260, 2266, 2288, 2296, 2301 (1953); Prog. Stereochem. 1, 1 (1954).
20. R. S. Mulliken, Rev. Mod. Phys. 14, 204 (1942); J. Am. Chem. Soc. 11, 887 (1955).

21. M. A. Robb, W. J. Haines and I. G. Csizmadia, J. Am. Chem. Soc. 95, 42 (1973).
22. R. McWeeny and B. T. Sutcliffe, "Methods of Molecular Quantum Mechanics", Academic Press, New York, 1969, p. 77.
23. J. W. Linnett and A. J. Poë, Trans. Far. Soc. 47, 1033 (1951).
24. Reference 26, p. 107.
25. J. Odier, Thèse, Faculté des Sciences de L'Université de Paris, 1958.
26. R. Daudel, "The Fundamentals of Theoretical Chemistry", Pergamon Press, London, 1968.
27. C. Aslangul, C. R. Acad. Sci., Ser. B, 272, 1 (1971).
28. W. England, L. S. Salmon and K. Ruedenberg, Fortsch. Chem. Forsch. 23, 31 (1971).
29. M. Levy, J. Chem. Phys. 61, 1857 (1974).
30. C. Aslangul, R. Constanciel, R. Daudel, L. Esnault and E. V. Ludeña, Int. J. Quantum Chem. 8, 499 (1974).
31. R. E. Cristofferson, Advan. Quantum Chem., Ed. P.-O. Löwdin, Academic Press, New York, VI, 333 (1972).
32. R. F. W. Bader and P. M. Beddall, J. Am. Chem. Soc. 95, 305 (1973).
33. C. C. J. Roothaan, Rev. Mod. Phys. 23, 161 (1951).
34. A. Mazziotti, R. G. Parr and G. Simons, J. Chem. Phys. 59, 939 (1973).
35. S. Srebrenik and R. F. W. Bader, J. Chem. Phys. 61, 2536 (1974).
36. S. Srebrenik, H. Weinstein and R. Pauncz, Chem. Phys. Lett. (to be published).
37. R. F. W. Bader and G. R. Runtz, Mol. Phys. _____, 0000 (1975).
38. "The Virial Partitioning Method", R. F. W. Bader, G. R. Runtz and R. R. Messer, Sixth Jerusalem Symposium on Chemical and Biochemical Reactivity, B. Pullmann, Ed., Israeli Academy of Sciences and Humanities, 1974.

39. R. F. W. Bader, P. M. Beddall and J. Peslak Jr., J. Chem. Phys. 58, 557 (1973).
40. Reference 26, Chapter 8.
41. C. Aslangul, R. Constanciel, R. Daudel and P. Kottis, Advan. Quantum Chem. 6, 93 (1972).
42. R. Daudel, R. F. W. Bader, M. E. Stephens and D. S. Borrett, Can. J. Chem. 52, 1310 (1974); Erratum, Can. J. Chem. 52, 3077 (1974).
43. Reference 26, Chapter 3.
44. E. Shannon, Bell Sys. Tech. J. 27, 379 (1948).
45. P. E. Cade and W. M. Huo, J. Chem. Phys. 47, 614 (1967).
46. M. C. Goldberg and J. R. Ritter, J. Phys. Chem. 71, 3111 (1967).
47. R. F. W. Bader, "Comparison of Loge and Virial Methods of Partitioning Molecular Charge Distributions", "Localization and Delocalization in Chemistry", R. Daudel, Ed., Gauthier-Villars et Cie, Interscience, Pergamon Press.
48. S. M. Johnson, Math. of Comput. 17, 282 (1963).
49. G. Sperber, Intern. J. Quantum Chem. 5, 177 (1971).
50. R. McWeeny, Rev. Mod. Phys. 32, 335 (1960).
51. J. C. Slater, Phys. Rev. 81, 385 (1951).
52. Reference 22, p. 86.
53. E. Clementi, "Tables of Atomic Functions", IBM Corp., U. S. A., 1965.
54. E. V. Ludeña and M. Sanchez, J. Chem. Phys. 56, 3725 (1972).
55. G. Sperber, Int. J. Quantum Chem. 5, 189 (1971).
56. O. Sinanoglu and B. Skutnik, Chem. Phys. Lett. 1, 699 (1968).
57. M. D. Newton, E. Switkes and W. N. Lipscomb, J. Chem. Phys. 53, 2645 (1970).

58. M. Sanchez and E. V. Ludeña, Int. J. Quantum Chem. 6, 1113 (1972).
59. G. Runtz, Ph.D. Thesis, McMaster University, Hamilton, Ontario, 1974.
60. R. F. W. Bader and M. E. Stephens, Chem. Phys. Lett. 26, 445 (1974).
61. H. Bent, J. Chem. Ed.: 45, 768 (1968).